Karlsruher Institut für Technologie

Temperature dependence of the molecular composition and volatility of secondary organic aerosol

Zur Erlangung des akademischen Grades einer

DOKTORIN DER NATURWISSENSCHAFTEN (Dr. rer. nat.)

von der KIT Fakultät für

Bauingenieur-, Geo- und Umweltwissenschaften

des Karlsruher Instituts für Technologie (KIT)

genehmigte DISSERTATION von

Linyu Gao

Tag der mündlichen Prüfung: 11.07.2022

Referent: Prof. Stefan Norra

Korreferent: Prof. Thomas Leisner

Karlsruhe (2022)

Erklärung

Hiermit erkläre ich, dass ich die vorliegende Dissertation, abgesehen von der Benutzung der angegebenen Hilfsmittel, selbständig verfasst habe.

Alle Stellen, die gemäß Wortlaut oder Inhalt aus anderen Arbeiten entnommen sind, wurden durch Angabe der Quelle als Entlehnungen kenntlich gemacht.

Diese Dissertation liegt in gleicher oder ähnlicher Form keiner anderen Prüfungsbehörde vor.

Karlsruhe, im July 2022

Linyu Gao

Acknowledgments

This PhD has been a completely new adventure in my life, during which I discovered and learned lots of new things not only in the field of science. I would like to sincerely thank all colleagues and friends who I met during the four years!

I would like to thank my doctoral supervisors Prof. Dr. Stefan Norra and Prof. Dr. Thomas Leisner, for providing me the opportunities to be a PhD student and do research at IMK-AAF at KIT, and for the professional advice and support in proceeding with my PhD work. They are really kind and approachable.

I also would like to thank Dr. Harald Saathoff for being my direct supervisor, for guiding me in doing scientific research, and for professionally advising me to complete my PhD thesis. His office door was always open for any questions. Harald also provided and supported me to join summer schools, academic meetings, and scientific visits to other groups, with chances to communicate with other scientists. Harald is humous and amiable. He always did things to help me to release my stress. I really enjoy the time working with him, and sincerely appreciate his patience and kindness.

Many thanks also go to Dr. Wei Huang who helped me a lot, e.g., for guiding me to get familiar with instruments, and sharing her experience with science and life. Wei gave her suggestions whenever I faced troubles. She is really nice and trustworthy. I sincerely appreciate being a friend of hers, and daring to talk about everything to her without any concerns. Best wishes to her postdoc life in Helsinki and also in the future.

I also would like to kindly thank Assoc. Prof. Claudia Mohr and Dr. Angela Buchholz for hosting me during my aboard visits, and giving suggestions on data explanation. Thanks also go to the colleagues at Stockholm University (Dr. Cheng Wu) and University of Eastern Finland (Assoc. Prof. Siegfried Schobesberger and Zijun Li). I enjoy and appreciate the time working and talking with them all.

I also would like to thank all colleagues in the group of Atmospheric Chemistry, Aerosol Chemistry, and Trace Gases. Xiaoli helped me a lot, especially during my first year in Karlsruhe. She helped me to use HR-AMS, and shared with me lots of experience in work and life. I would also thank Lena for helping me to move house, and bringing humous always. Many thanks go to Hengheng for his kindness and friendliness. He helped me to survive from the hardest time during

my PhD period. I also learned a lot from Feng who maintained FIGAERO-CIMS together with me. Thanks for his help. Thanks also go to Tobias, Yuxuan, Yaqiong, and Yanxia for their kindness and humor. I would like to thank Georg, Frank, Rainer, Steffen, Jens, Tomasz, and all technicians in IMK-AAF, for helping with all my chamber experiments. Best wishes to all of them!

Thanks also go to Ms. Xu Li, my bestie, for accompanying me in my hard time despite the huge spatial distance and the time difference between China and Germany.

Furthermore, I would like to thank my parents and my sister for understanding and supporting me to do whatever I want to do. They are always at my side whenever I need them. Their encouragement makes me braver and more confident to surmount all difficulties. Mr. Zhaoxin Gao, Ms. Taoxiang Zou, and Ms. Zhan Gao, my heart will be with you forever. I miss my dad forever, and hope everything is fine in heaven.

Last but not least, special thanks go to my colleague and also my boyfriend, Junwei, for his love, trust, and support. Together, we took chamber campaigns, did field measurements, discussed data, wrote papers, and shared opinions on science. We also traveled to many places, did interesting and new things, and enjoyed our lives together. He is my perfect work & life cooperator. Thanks for all the tasty food that he cooked for me. Thanks for all the impressive memories we got in Germany.

I would also like to thank China Scholarship Council for funding me over my whole PhD period.

In the end, I would like to sincerely thank you all again for everything we experienced together! Best wishes to you all!

感谢那个在困境中没有放弃希望的自己。

高琳禹 Gao, Linyu

Karlsruhe, in July 2022

Abstract

Secondary organic aerosols (SOA) comprise a major fraction of the tropospheric aerosol smaller than 2.5 µm ($PM_{2.5}$) which have adverse effects on air quality, human health, and the climate. About 90% of them are formed by oxidation products from biogenic volatile organic compounds (BVOCs) mainly comprised of isoprene, monoterpenes, and sesquiterpenes. However, studies of the characteristic properties of biogenic SOA formed from single BVOC and their mixtures under conditions representative for the whole troposphere are still scarce.

Aim of this work is to achieve a better understanding of the impact of temperature and BVOC interaction on the formation pathways, chemical composition, volatility, and aging of SOA from the most abundant compounds of the three BVOC classes: isoprene, α-pinene, β-caryophyllene, and their mixtures. Therefore, I studied biogenic SOA from a) isoprene mixed with α-pinene, b) β-caryophyllene in the absence and c) the presence of NO_x, d) mixtures of isoprene and β-caryophyllene, e) mixtures of isoprene, α-pinene, and β-caryophyllene, in the atmospheric simulation chamber at KIT for conditions of the tropic boundary layer to the upper troposphere.

I observed distinct differences in SOA formed from α-pinene alone and its mixture with isoprene. In SOA from α-pinene and isoprene mixtures, intermediates of both formed new dimers. However, this did not significantly reduce the SOA yields nor the formation of typical dimers from α-pinene oxidation products alone. Formation of these dimers showed a minimum at 273K with 6±3% of the total oxidation products but increased to 12±4% and 9±3% at 243 and 313 K, respectively. The effective volatility of particulate organic compounds was reduced in the mixture compared to pure α-pinene SOA which enhances the atmospheric lifetime of these aerosol particles. The particle volatility decreased with increasing particle viscosity, corresponding to the lower temperature, and lower degree of oxidation. Oxidation products from isoprene as well as those formed by the interaction of α-pinene and isoprene intermediates, contributed to particle growth but had no significant contribution to new particle formation.

For the first time, the temperature dependence of the rate coefficient of β-caryophyllene reacting with O_3, which determines its atmospheric lifetime, was determined for the temperature range between 213-313K fitting to this Arrhenius equation: $k(243\text{-}313K) = (1.6\pm0.4)\times10^{-15} \times\exp((559\pm97)/T)$. SOA yields for the β-caryophyllene ozonolysis decreased at an organic mass loading of 10 µg m^{-3} from 37±11 to 17±5 % for the temperature increasing from 243 to 313 K,

respectively. For the β-caryophyllene ozonolysis in the absence of NO_x, higher temperatures favoured the formation of highly oxygenated molecules via autoxidation, while lower temperatures promoted the formation of less oxygenated dimers and oligomers. In presence of NO_3 radicals, increasing amounts of organic nitrates were formed with increasing temperature. At 313K, organic nitrates contributed (48.9±29.3)% of all $C_xH_yO_zN$ compounds detected, substantially higher than the (2.8±1.7)% formed at 213K. Most of the organic nitrates were monomers with a C_{15} skeleton with one nitrate group. Applying a new positive matrix factorization approach, I determined the effective volatility of SOA compounds distinguishing for the first time isomeric and thermally decomposed compounds. Based on the experimental data, I estimated the temperature dependent relative contributions of varying chemical oxidation pathways versus phase partitioning processes.

β-caryophyllene oxidation products could interact with those of α-pinene forming the dimers $C_{23}H_{36}O_{6\text{-}7}$ and $C_{24}H_{38}O_{6\text{-}8}$, which significantly reduced the formation of β-caryophyllene derived dimers $C_{27\text{-}30}$ and corresponding SOA yields. This suppression can be explained by the scavenging of corresponding monomers of β-caryophyllene by oxidation products of α-pinene and isoprene, resulting in the formation of $C_{17\text{-}25}$ dimers with lower molecular mass and volatility. The volatility of the particles in the ternary system was higher than in the isoprene β-caryophyllene system, mainly due to a higher contribution of products with smaller molecular mass from α-pinene and isoprene oxidation, and the reduced formation of lower volatile $C_{27\text{-}30}$ compounds.

These findings clearly demonstrate that it is not possible to predict SOA properties and yields based on the behaviour observed in single precursor systems alone. The temperature dependent interaction of intermediates of the oxidation of different precursor VOCs has a significant impact which was at least unravelled partially in this study on a molecular basis. Overall, this work demonstrates that ambient temperature has a strong impact on the chemical composition and volatility of SOA formed from individual biogenic VOC and their mixtures, via the interplay between chemical formation pathways and the partitioning of oxidation products.

Zusammenfassung

Sekundäre organische Aerosole (SOA) machen einen Großteil des troposphärischen Aerosols kleiner als 2,5 µm ($PM_{2,5}$) aus und haben negative Auswirkungen auf die Luftqualität, die menschliche Gesundheit und das Klima. Etwa 90 % von ihnen werden durch Oxidationsprodukte von biogenen flüchtigen organischen Verbindungen (BVOC) gebildet, die hauptsächlich aus Isopren, Monoterpenen und Sesquiterpenen bestehen. Studien zu den charakteristischen Eigenschaften biogener SOA, die aus einzelnen BVOC und ihren Mischungen unter für die gesamte Troposphäre repräsentativen Bedingungen gebildet werden, sind jedoch noch rar.

Ziel dieser Arbeit ist es, ein besseres Verständnis des Einflusses von Temperatur und BVOC-Wechselwirkungen auf die Bildungswege, chemische Zusammensetzung, Flüchtigkeit und Alterung von SOA aus den am häufigsten vorkommenden Verbindungen der drei BVOC-Klassen zu erreichen: Isopren, α-Pinen, und β-Caryophyllen sowie ihrer Mischungen. Daher untersuchte ich biogenes SOA aus a) Isopren gemischt mit α-Pinen, b) β-Caryophyllen in Abwesenheit und c) Anwesenheit von NO_x, d) Mischungen aus Isopren und β-Caryophyllen, e) Mischungen aus Isopren, α- Pinen und β-Caryophyllen in der atmosphärischen Simulationskammer am KIT für Bedingungen der tropischen planetaren Grenzschicht bis hin zur oberen Troposphäre.

Ich beobachtete deutliche Unterschiede in den SOA, die aus α-Pinen allein und seiner Mischung mit Isopren gebildet wurde. In SOA aus α-Pinen- und Isopren-Mischungen bilden Intermediate von beiden neue Dimere. Dies verringerte jedoch weder die SOA-Ausbeuten noch die Bildung typischer Dimere aus α-Pinen Oxidationsprodukten allein signifikant. Die Bildung dieser Dimere zeigt ein Minimum bei 273 K mit 6 ± 3 % der gesamten Oxidationsprodukte, steigt jedoch auf 12 ± 4 % und 9 ± 3 % bei 243 bzw. 313 K an. Die effektive Flüchtigkeit von partikulären organischen Verbindungen ist in der Mischung im Vergleich zu reinem α-Pinen SOA reduziert, was die atmosphärische Lebensdauer dieser Aerosolpartikel erhöht. Die Partikelflüchtigkeit nimmt mit zunehmender Partikelviskosität, entsprechend niedrigerer Temperatur und niedrigerem Oxidationsgrad ab. Oxidationsprodukte von Isopren sowie solche, die durch Wechselwirkung von α-Pinen- und Isopren-Zwischenprodukten gebildet werden, tragen zum Partikelwachstum bei, haben jedoch keinen signifikanten Beitrag zur Partikelneubildung.

Zum ersten Mal wurde die Temperaturabhängigkeit des Geschwindigkeitskoeffizienten von β-Caryophyllen bei der Reaktion mit Ozon, der seine atmosphärische Lebensdauer bestimmt, für

den Temperaturbereich zwischen 213-313 K gemäß dieser Arrhenius-Gleichung bestimmt: k (243-313K) = (1,6 ± 0,4) × 10–15 × exp ((559 ± 97)/T). Die SOA-Ausbeuten für die β-Caryophyllen Ozonolyse sanken bei einer organischen Partikelmasse von 10 µg m^{-3} von (37±11)% auf (17±5) % für die Temperaturerhöhung von 243 auf 313 K. Bei der Ozonolyse von β-Caryophyllen in Abwesenheit von NO_x begünstigen höhere Temperaturen die Bildung von stark sauerstoffreichen Molekülen durch Autoxidation, während niedrigere Temperaturen die Bildung von weniger sauerstoffreichen Dimeren und Oligomeren fördern. In Anwesenheit von NO_x- und NO_3-Radikalen wurden mit zunehmender Temperatur zunehmende Anteile an organischen Nitraten gebildet. Bei 313 K trugen organische Nitrate (48,9 ± 29,3) % aller nachgewiesenen $C_xH_yO_zN$-Verbindungen bei, wesentlich mehr als die (2,8 ± 1,7) %, die bei 213 K gebildet wurden. Die meisten organischen Nitrate waren Monomere mit einem C_{15}-Gerüst mit einer Nitratgruppe. Unter Anwendung eines neuen Ansatzes der positiven Matrix Faktorisierung (PMF) habe ich die effektive Flüchtigkeit von SOA-Verbindungen bestimmt, wobei ich zum ersten Mal zwischen Isomeren und thermisch zersetzten Verbindungen unterscheiden konnte. Basierend auf den experimentellen Daten habe ich die temperaturabhängigen relativen Beiträge verschiedener chemischer Oxidationswege gegenüber Phasenverteilungsprozessen abgeschätzt.

β-Caryophyllen-Oxidationsprodukte können mit denen von α-Pinen in Wechselwirkung treten, wobei die Dimere $C_{23}H_{36}O_{6\text{-}7}$ und $C_{24}H_{38}O_{6\text{-}8}$ gebildet werden, die die Bildung von allein aus β-Caryophyllen abgeleiteten Dimeren $C_{27\text{-}30}$ und entsprechende SOA-Ausbeuten signifikant reduzieren. Diese Reduktion kann durch Abfangen entsprechender Monomere von β-Caryophyllen durch Oxidationsprodukte von α-Pinen und Isopren erklärt werden, was zur Bildung von $C_{17\text{-}25}$-Dimeren mit geringerer Molekülmasse und Flüchtigkeit führt. Die Flüchtigkeit der Partikel im ternären System war höher als im Isopren-β-Caryophyllen-System, hauptsächlich aufgrund eines höheren Beitrags von Produkten mit kleinerer Molekülmasse aus der α-Pinen- und Isopren-Oxidation und der verringerten Bildung von weniger flüchtigen $C_{27\text{-}30}$ Verbindungen.

Diese Befunde zeigen deutlich, dass es nicht möglich ist, SOA-Eigenschaften und Ausbeuten allein auf der Grundlage des Verhaltens vorherzusagen, das in einzelnen Vorläufersystemen beobachtet wird. Die temperaturabhängige Interaktion von Zwischenprodukten der Oxidation verschiedener Vorläufer-VOC hat einen signifikanten Einfluss, der in dieser Studie zumindest teilweise auf molekularer Basis enträtselt wurde. Insgesamt zeigt diese Arbeit, dass die Umgebungstemperatur über das Zusammenspiel zwischen chemischen Bildungswegen und der

Phasenverteilung von Oxidationsprodukten einen starken Einfluss auf die chemische Zusammensetzung und Flüchtigkeit von SOA hat.

Contents

List of Figures

List of Tables

Abbreviations

AIDA	Aerosol Interaction and Dynamics in the Atmosphere
AMS	Aerosol Mass Spectrometer
AP	α-pinene
API	Atmospheric Pressure Interface
AVOCs	Anthropogenic Volatile Organic Compounds
BCA	β-caryophyllinic acid
BCP	β-caryophyllene
BG1	Background Factor 1
BVOCs	Biogenic Volatile Organic Compounds
C^*	Effective Saturation Concentration
C_{sat}	Saturation Concentration
C1	Cold Factor 1
C2	Cold Factor 2
C3	Cold Factor 3
C4	Cold Factor 4
C5	Cold Factor 5
C6	Cold Factor 6
$C_6H_6^+$	Benzene Cation
CCN	Cloud Condensation Nuclei
CE	Collection Efficiency
CHARON	Chemical Analysis of Aerosol Online
CI	Chemical Ionization
CI-API-TOF	Atmospheric Pressure Interface Time-Of-Flight Mass Spectrometer
CN_{error}	Constant Noise
CPC	Condensation Particle Counter
DHOC	Dimeric Highly Oxygenated Organic Compounds
DLOC	Dimeric Lowly Oxygenated Organic Compounds
d_m	Mobility Diameter
DMA	Differential Mobility Analyzer

d_{va}	Vacuum Aerodynamic Diameter
EESI-TOF-MS	Extractive Electrospray Ionization Time-of-Flight Mass Spectrometry
EI	Electron Ionization
ELVOC	Extremely Low Volatile Organic Compounds
ESI	Electrospray Ionization
FI	Field Ionization
FIGAERO	Filter Inlet for Gases and Aerosols
FT-ICR	Fourier Transform-Ion Cyclotron
GC	Gas Chromatography
H:C	Hydrogen to Carbon Ratio
HOM	Highly Oxidized Multifunctional
I^-	Iodide
I1	Intermediate Factor 1
I2	Intermediate Factor 2
IE	Ionization Efficiency
IMR	Ion Molecule Reactor
IN	Ice Nuclei
INP	Ice Nucleating Particles
ISO	Isoprene
I-TOF-CIMS	Iodide-Time-of-Flight-Chemical-Ionization-Mass-Spectrometry
LCU	Liquid Calibration Unit
LDI	Laser Ionization
LVOC	Low Volatile Organic Compounds
m/z	*Mass-to-Charge Ratio*
MCM	Master Chemical Mechanism
MCP	Multichannel Plate
MHOC	Monomeric Highly Oxidized Compounds
MLOC	Monomeric Lowly Oxygenated Organic Compounds
MOVI	Micro-Orifice Volatilization Impactor
MS	Mass Spectrometry
MW	Molecular Weight

ncps	Normalized Counts Per Second
NO_3	Nitrate Radicals
NPF	New Particle Formation
O:C	Oxygen to Carbon Ratio
O_3	Ozone
OA	Organic Aerosol
OH	Hydroxyl Radicals
org	Molecules without Nitrogen Atom
org-Ns	Organonitrates
OS_C	Carbon Oxidation State
PBL	Planetary Boundary Layer
PM	Particulate Matter
PMF	Positive Matrix Factorization
POA	Primary Organic Aerosol
PTFE	Polytetrafluorethylene
PTR-TOF-MS	Proton-Transfer-Reaction-Time-of-Flight-Mass-Spectrometer
Q	Quadrupole
Q_{exp}	Degree of Freedom of the Model Solution
S_{ij}	Solution Uncertainty
SMPS	Scanning Mobility Particle Sizer
SOA	Secondary Organic Aerosol
SVOC	Semi Volatile Organic Compounds
TDL	Tunable Diode Laser
T_g	Glass Transition Temperature
Thermogram	Thermal Desorption Profiles
T_{max}	Temperatures of Maximum Desorption
TME	Tetramethyl Ethylene
TOF	Time-of-Flight
TOF-AMS	Time-of-Flight Aerosol Mass Spectrometer
TOF-MS	Time-of-Flight Mass Spectrometers
ULVOC	Ultra-Low Volatile Organic Compounds

VOCs	Volatile Organic Compounds
V_p	Saturation Vapor Pressures
W1	Warm Factor 1
W2	Warm Factor 2
W3	Warm Factor 3
Y_{SOA}	SOA Yields
ΔH_{sub}	Enthalpy of Sublimation
ΔM_{org}	Particle Mass Concentration
1D-VBS	One Dimensional Volatility Basis Set

1 Introduction

Atmospheric aerosol is defined as a suspension of fine liquid or solid particles in a gas (Pöschl, 2005). The size of this particulate matter (PM) ranges over more than four orders of magnitude from several nanometers to several 10 µm (Prospero et al., 1983; Kolb and Worsnop, 2012). Major compounds present in atmospheric aerosol are mineral dust, sea-salt, organic aerosol (OA), inorganic salts (NH_4NO_3, $(NH_4)_2SO_4$), soot, pollen and several others. Over the past decades, atmospheric aerosol has been found to significantly influence atmospheric processes by directly scattering and absorbing solar radiation, providing condensation surfaces for the formation of cloud droplets and ice crystals, and being involved in heterogeneous chemical reactions (Ghan and Schwartz, 2007; Kolb and Worsnop, 2012; Zarnetske et al., 2021). As a result, they seriously adversely affect air pollution (Dockery et al., 1992; Law and Stohl, 2007), human health (Pöschl, 2005; Darquenne, 2012), visibility (Charlson, 1969; Appel et al., 1985), ecological integrity (Hu and Rao, 2009), and climate change (Aubry et al., 2021; Schmale et al., 2021). The largest fraction of fine atmospheric aerosol is organic aerosol which makes up 20-50% to the total fine aerosol mass at continental mid-latitudes and accounts for up to 90% in the tropical forested areas (Andreae and Crutzen, 1997; Roberts et al., 2001).

1.1 Organic aerosol

OA is a complex mixture comprising thousands of organic species (Goldstein and Galbally, 2007). It can be formed from a wide variety of sources. Primary organic aerosol (POA) is directly emitted from sources such as volcanic eruptions, plants, and biomass burning, whereas secondary organic aerosol (SOA) is formed from the oxidation of gaseous volatile organic compounds (VOCs) in the atmosphere, which is then followed by gas-to-particle partitioning. Some organic species are emitted to the atmosphere as vapors and subsequently condense on particles without undergoing chemical change. These aerosols can be classified also as POA (Kanakidou et al., 2005). The global OA burden is dominated by SOA (Hallquist et al., 2009; Shrivastava et al., 2015). For instance, about 50% of fine particles can be composed of organics in urban locations within the Northern Hemisphere (Zhang et al., 2007). After the emission or formation of OA, it ages via chemical and physical transformation, including cloud processing. Solid OA can be activated as ice nuclei (IN) forming ice crystals (Shiraiwa et al., 2011). The estimated OA lifetime

in the atmosphere has a large variability between several to up to ten days (Tsigaridis et al., 2014; Gliß et al., 2021).

1.2 Atmospheric volatile organic compounds

VOCs are typically termed as organic compounds with boiling points of up to 250 °C and vapor pressures greater than 10 Pa (at 25°C) at standard pressure (1013 hPa) (Koppmann, 2008; Cao et al., 2016). Methane is a dominant VOC but will not be discussed here since its contribution to aerosol formation is negligible. Atmospheric VOCs can be seen almost everywhere in the troposphere. The largest global VOC contributor is the natural ecosystem, such as terrestrial plants, fruits, grassland, and tropical woodlands, for which those VOCs are classified as biogenic VOCs (BVOCs, 760 TgC yr^{-1}) (Sindelarova et al., 2014). Besides, the VOCs emitted from human activities in urban areas, i.e. combustion process, transportation, and industrial activities, are assorted as anthropogenic VOCs (AVOCs, 110 TgC yr^{-1}) (Piccot et al., 1992). The BVOC emissions clearly dominate over other SOA precursors.

1.2.1 Biogenic volatile organic compounds

Hundreds of reactive BVOCs are produced and emitted into the atmosphere from the biosphere, depending on the location and meteorological conditions (Helmig et al., 2013). BVOCs comprises mainly hemiterpene (C_5H_8, ~70%), monoterpenes ($C_{10}H_{16}$, ~11%), and sesquiterpenes ($C_{15}H_{24}$, ~2.5%) (Owen et al., 2003; Keeling and Bohlmann, 2006; Sindelarova et al., 2014).

Isoprene (2-methyl-1,3-butadiene), the dominant hemiterpene, is also the strongest single BVOC contributor in the earth system. Isoprene is produced and emitted by several plants, such as oak trees (Sanadze and Kursanov, 1966; Langford et al., 2017) and its emission is found highly light and temperature dependent (Sanadze, 1969; Rinne et al., 2002). The global isoprene emission is estimated at a level of 500 Tg C yr^{-1}, which is roughly equal to the total emitted amount of methane, and is around four times higher than the sum of all anthropogenic VOCs, thus making isoprene the dominant hydrocarbon (Wang and Shallcross, 2000; Sharkey and Yeh, 2001; Sharkey et al., 2007; Guenther et al., 2012). In the atmosphere, isoprene is reactive to hydroxyl radicals (OH radicals), O_3, and nitrate radicals (NO_3 radicals) (Lin et al., 2013; Jenkin et al., 2015; Bates and Jacob, 2019). The lifetime of isoprene in the atmosphere is estimated to be 3 hours during daytime with 20 ppb of O_3 and 10^6 molecules/cm^3 of OH radicals, and 1.5 hours in the night with 20 ppb of O_3 and 10 ppt of NO_3 radicals under typical atmospheric conditions (Kesselmeier and

Staudt, 1999). However, although, the particle yield of isoprene oxidation products is estimated to be low (about 1%), it still has a large contribution to the global particles (e.g., 6 Tg yr^{-1}) due to its large abundance (Carlton et al., 2009).

α-pinene is a dominant monoterpene (155 Tg C yr^{-1} (Guenther et al., 2012)) comprising about 34% (Sindelarova et al., 2014) of all monoterpenes ($C_{10}H_{16}$), and is mainly emitted from plants, such as conifers, juniper, citrus trees, and in small amounts also from the fragrance and flavor industry (Allenspach and Steuer, 2021) due to its fresh pine scent and woody flavor (Vespermann et al., 2017). Unlike the high reactivity of isoprene to OH radicals, α-pinene has about 2 times lower reactivity to OH radicals, but is more reactive to O_3 and NO_3 radicals, making its lifetime at nighttime 5-30 min, significantly shorter than at daytime of 2-3 hours (Kesselmeier and Staudt, 1999). Considering their large emissions and high reactivities with atmospheric oxidants, as well as their relatively high SOA yields, monoterpenes like α-pinene are regarded as major source of SOA (Ehn et al., 2014; Zhang et al., 2018).

At last but very important, as a representor of sesquiterpenes ($C_{15}H_{24}$), β-caryophyllene is emitted from pine trees and agricultural fields, such as orange trees and potato plants (Ciccioli et al., 1999; Hansen and Seufert, 2003; Duhl et al., 2008; Kleist et al., 2012). The emissions of β-caryophyllene show temperature-dependent features, depending on period and season (Hansen and Seufert, 2003; Hakola et al., 2006). Because of the two carbon double bonds (endocyclic and exocyclic) inside its bicyclic structure, β-caryophyllene has the highest reactivity to the atmospheric oxidants (O_3, OH radicals, NO_3 radicals) compared to isoprene and α-pinene, and hence has the shortest lifetime (< 4 min at daytime, < 2 min at night) in the atmosphere (Kesselmeier and Staudt, 1999; Winterhalter et al., 2009b). The rate coefficient for O3 reacting with the endocyclic double bond was determined for 296K as $(1.2\pm 0.4) \times 10^{-14}$ cm^3 $molecule^{-1}$ s^{-1} (Shu and Atkinson, 1994a; Richters et al., 2015; Cox et al., 2020). It is estimated to be about 100 times larger than the rate coefficient of $(1.1 \pm 0.4) \times 10^{-16}$ cm^3 $molecule^{-1}$ s^{-1} for the exocyclic double bond (Shu and Atkinson, 1994a) of the first-generation products. Besides, the rate constant of β-caryophyllene reacting with OH radicals and NO_3 radicals are determined to be $(2.0\pm0.9) \times 10^{-10}$ cm^3 $molecule^{-1}$ s^{-1} (Shu and Atkinson, 1994b), and $(1.9\pm0.4) \times 10^{-11}$ cm^3 $molecule^{-1}$ s^{-1} (Atkinson, 1991), respectively. Due to its high reactivity and oxidation products with low vapor pressure, β-caryophyllene shows high SOA yields and can lead to new particle formation.

Thus, although it is not emitted in large quantities, β-caryophyllene still has a large aerosol formation potential and can even play a dominant role in specific periods and seasons (Geron and Arnts, 2010; Jardine et al., 2011).

1.2.2 Anthropogenic volatile organic compounds

AVOCs are chemically consisting mainly of aliphatic and aromatic hydrocarbons (e.g., benzene, toluene, naphthalene, xylene), and alcohols, various alkanes, glycol derivates, such as pentadecane (Theloke and Friedrich, 2007). Major AVOC sources are: biomass combustion, industrial processes, fuel evaporation, and solvent usage (Tuet et al., 2017).

Besides the anthropogenic organic emissions, some other anthropogenic pollutants (e.g., nitrogen oxides, NO_x) can react with BVOCs and hence effect on the SOA formation and composition (Calfapietra et al., 2013). The resulting organic nitrates or sulfates have a substantial impact on optical and health relevant properties of organic aerosol (Moise et al., 2015).

1.3 Secondary organic aerosol (SOA)

After emission into the atmosphere, VOCs are depleted mainly via oxidation by ozone (O_3), OH radicals, and NO_3 radicals generating thousands of different organic molecules. These components have higher oxidation states and most of them have also lower vapor pressures than their precursors. Hence, they have a potential to form SOA particles. The biogenic SOA formation is estimated to 88 TgC yr^{-1}, while the anthropogenic SOA contributes about 10 TgC yr^{-1} (Hallquist et al., 2009). After formation, SOA can be transported throughout the troposphere. On the one hand, the direct effect of BVOCs on climate is to reduce the amount of solar radiation. Biogenic SOAs can be effective scatters and have a potential for absorption (Shrivastava et al., 2017). On the other hand, hygroscopic biogenic SOAs can influence the cloud formation by acting as cloud condensation nuclei (CCN) and ice nucleating particles (INP).

In the following section, I will briefly introduce the SOA formation mechanisms and chemistry (1.3.1), physicochemical properties of SOA (1.3.2), the SOA from β-caryophyllene (1.3.3), and SOA from BVOC mixtures (1.3.4), and the impact of temperature on the SOA in the troposphere (1.3.5).

1.3.1 SOA formation mechanisms and chemistry

SOA is formed via gas phase reactions of biogenic or anthropogenic VOCs, followed by gas-to-particle conversion of low or semi volatile oxidation products. The VOCs degradation in the troposphere is initiated by atmospheric oxidants, such as O_3, OH radicals, NO_3 radicals. Chlorine or bromine radicals as well as Criegee radicals are also of some importance but only in special cases. As a result, first-generation products with diverse oxygenated functional groups can be formed, such as aldehydes (-CHO), alcohols (-OH), acids (-COOH), organic nitrates (-NO_2) etc. Those early-stage oxidation products can subsequently undergo further oxidation process, i.e. autoxidation via intramolecular hydrogen shift, to form lower volatile components with more complex functionalities, such as highly oxidized multifunctional (HOM) compounds (Bianchi et al., 2019), dimers, and other oligomers. Under atmospheric conditions, the oxidation reactions and chemical pathways are highly dependent on the metrological conditions, such as temperatures (Zhang et al., 2015; Quéléver et al., 2019), relative humidity (RH), and the solar radiation. For example, OH radicals play a key role in initialing VOC oxidation during daytime, while the nighttime chemistry is dominated by reactions of NO_3 radicals and O_3 with VOCs (Atkinson, 2000; Riemer et al., 2008).

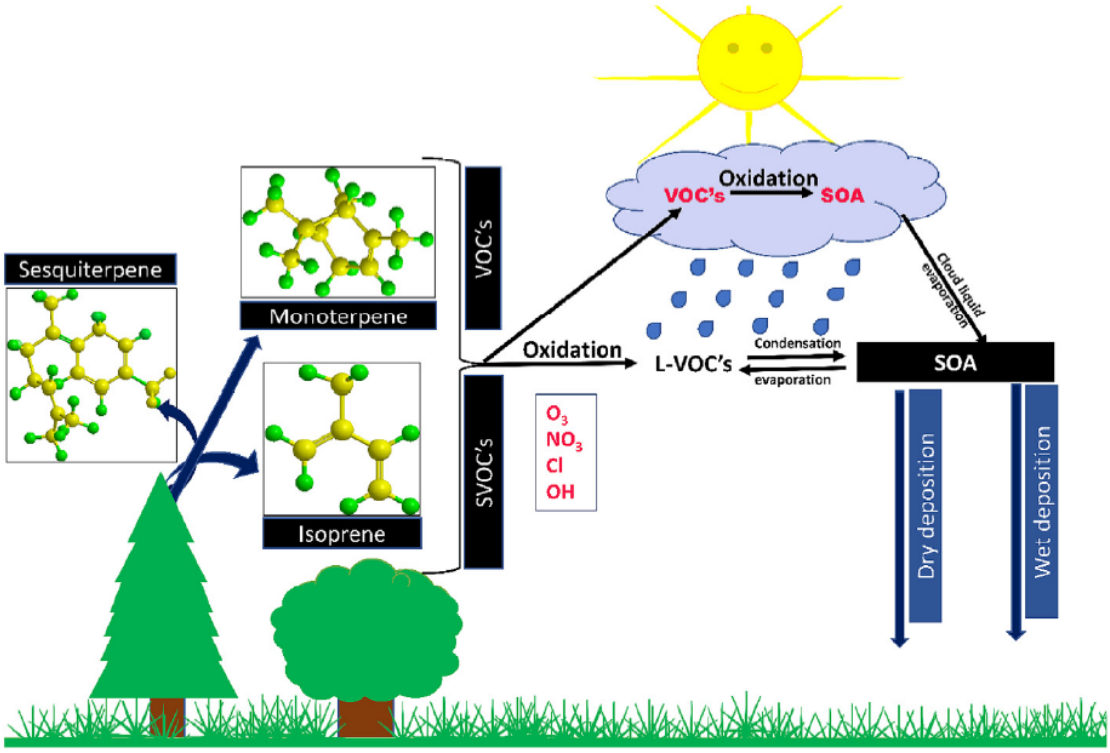

Figure 1. Schematic of SOA formation via BVOC oxidation (Mahilang et al., 2021).

OH and NO_3 radicals are able to abstract hydrogen from C-H and O-H bonds, and may add to C=C double bonds. In contrast, O_3 can only react with the C=C bonds of VOCs. This results in the formation of alkyl radicals, followed by the addition of oxygen, subsequently producing peroxy radicals (RO_2•). The rate coefficients of three biogenic terpenes (isoprene, α-pinene, β-caryophyllene) reacting with O_3 and OH radicals are already discussed in section 1.2. The schematic in Figure 2 (b) shows the reactions and functionality addition processes of the alkyl (R•), alkoxy (RO•) and peroxy (RO_2•) radicals, and the generation of closed-shell products, such as hydroperoxides (ROOH), carboxylic acids (RC(O)OH), peroxy acids (RC(O)OOH), alcohols (ROH), peroxynitrates ($ROONO_2$), organic nitrates ($RONO_2$), carbonyls (R(O)R') via decomposition, and hydroxycarbonyl via isomerization pathways (Ziemann and Atkinson, 2012). Recently, a new gas-phase pathway (so-called "autoxidation") involving consecutive intramolecular H-shifts in peroxy radicals followed by O_2 addition, has been recognized to form HOM compounds often with more than 6 oxygen atoms per molecule and low-volatility (Crounse et al., 2013; Bianchi et al., 2019). An example of HOM compound formation via an autoxidation pathway is presented in Figure 2 (a). As the fate of gas-phase oxidation products are determined largely by their saturation vapor pressures (hence volatilities) via partitioning between gas and condensed phases, the estimation of saturation vapor pressures of species is important in studying the particle formation. The SOA volatility will be discussed in section 1.3.2.

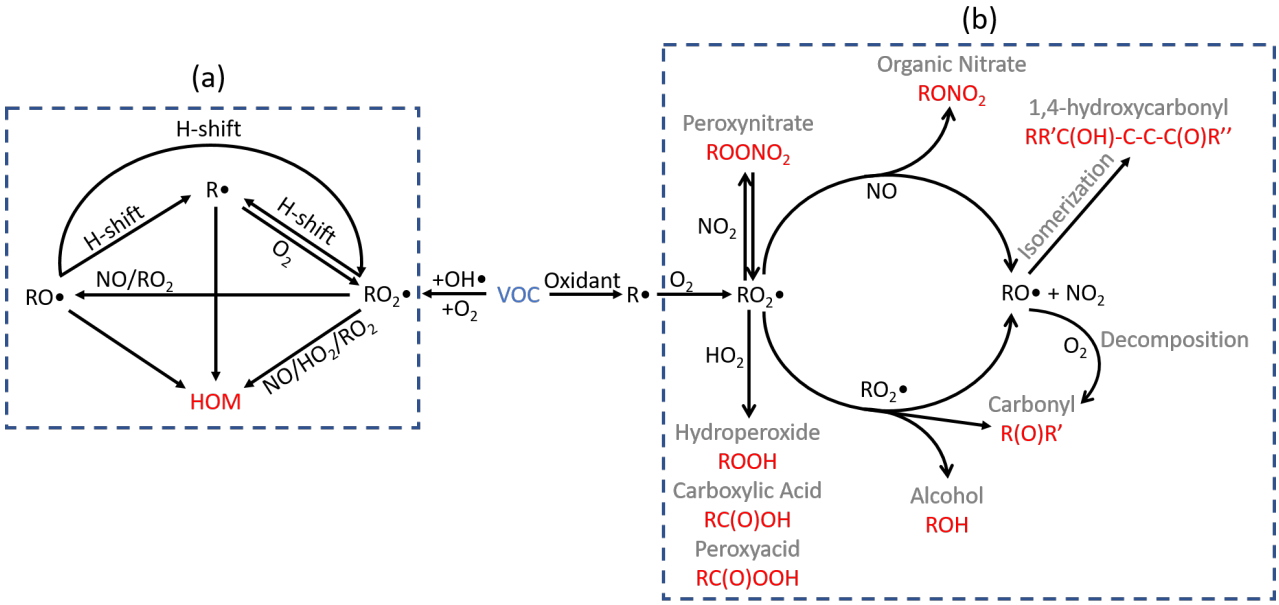

Figure 2. Schematic of VOC oxidation in the atmosphere. (a) typical autoxidation mechanisms to form HOM, adapted from Ehn et al. (2017); (b) other mechanisms through formation of alkyl or substituted alkyl radicals, adapted from Ziemann and Atkinson (2012).

The process with the addition of functional groups to a molecule is so-called functionalization, generating a more polar oxygenated and higher molecular weight product with substantially lower volatility (Pandis et al., 1992), as illustrated in Figure 3. Competing with functionalization is the fragmentation which typically leads to smaller molecules. Fragmentation principally leads to the scission of covalent C-C bonds, producing more volatile and less weight molecules that are less likely to condense. As another competing reaction, oligomerization results in the association of at least two molecules (monomeric precursors), generating a heavier molecule with substantially lower volatility (Kroll et al., 2011).

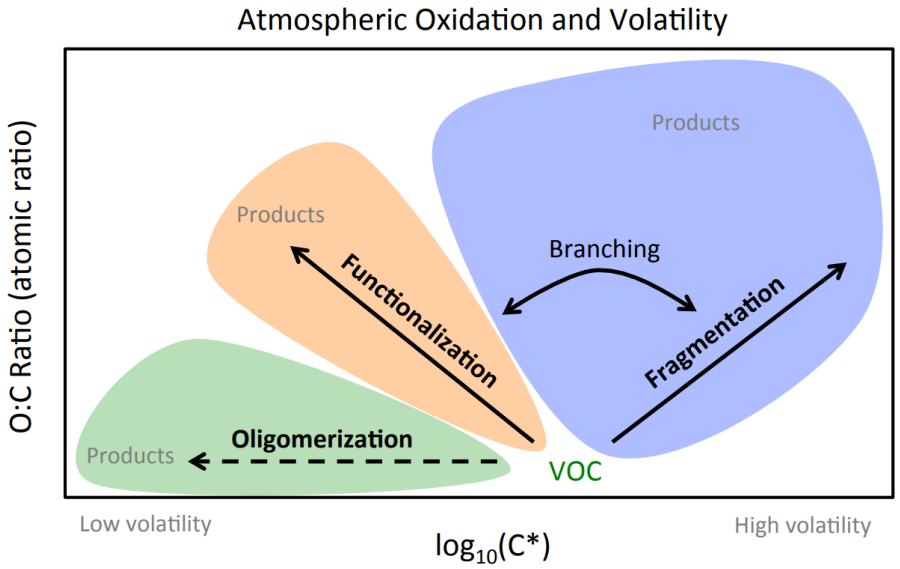

Figure 3. Three general atmospheric oxidation processes and their impact on volatility: fragmentation, oligomerization, and functionalization. They are categorized on basis of the decrease, increase, and no change of the molecular carbon numbers. The figure is adapted by Lopez-Hilfiker (2015) from Jimenez et al. (2009).

1.3.2 Physicochemical properties of SOA

Volatility and viscosity are two key physicochemical properties of SOA, and have profound effects on the gas-particle partitioning, particle formation and growth, heterogeneous reactions, ice nucleation pathways of SOA, and in turn air quality and climate (Bilde et al., 2015; Reid et al., 2018).

Volatility is important for the particle formation, because it can determine the fate of molecules by deciding whether components condense into or evaporate from the particle phase. As SOA is often complex and comprises of hundreds to thousands of components, there are several volatility classes needed to describe the compounds on basis of their effective saturation concentrations (C*, μg m^{-3}) (Donahue et al., 2009; Donahue et al., 2011; Donahue et al., 2012;

Schervish and Donahue, 2020): ultra-low volatile organic compounds (ULVOC, $\log_{10}C_{sat}$ <-8.5 μg m^{-3}), extremely low volatile organic compounds (ELVOC, -8.5< $\log_{10}C^*$ <-4.5 μg m^{-3}), low volatile organic compounds (LVOC, -4.5< $\log_{10}$ C* <-0.5 μg m^{-3}), semi volatile organic compounds (SVOC, -0.5< $\log_{10}$ C* <2.5 μg m^{-3}), intermediate volatile organic compounds (IVOC, 2.5< $\log_{10}$ C* <6.5 μg m^{-3}), and volatile organic compounds (VOC, $\log_{10}$ C* >6.5 μg m^{-3}).

At most atmospheric conditions, the compounds in the VOC/IVOC classes stay in the gas phase, while the semi-volatile components can partition between both gas and particle phases. Consequently, species in LVOC class stay mainly in the particle phase, while the ELVOC/ULVOC compounds are considered to be nonvolatile due to their extremely/ultra-low vapor pressures. Thus, the compounds with low and extreme/ultra-low volatilities have large potential to contribute to the formation and growth of SOA particles.

Volatility of a molecule highly depends on the molecular chemical properties, e.g., functional groups and structure. That is, isomers with the same formula may have varying magnitudes of volatilities (expressed as saturation vapor pressures) owing to their isomeric functionalities (Hyttinen et al., 2022). Furthermore, as the SOA particles are often composed by a handle of species, the effective volatility of a compound is convoluted not only by the pure compound volatility but also the interaction of each specific compound with the absorbing aerosol mixture (Pankow, 1994a; Donahue et al., 2006; Liu et al., 2021). Thus, the need to predict the effective volatilities of individual isomeric compounds from a complex SOA mixture is evident.

Particle viscosity is another important physicochemical property of SOA, and also affects the effective volatility. The SOA particles have been found to be viscous and can exist in liquid, semisolid or amorphous solid states (Shiraiwa et al., 2017; Reid et al., 2018), with low dynamic viscosity <10^2 Pa s, between 10^2 - 10^{12} Pa s, > 10^{12} Pa s, respectively, depending on temperature, humidity, and particle chemical composition (Reid et al., 2018). The substances in the particles with high viscosity may need more time to equilibrate with the gas phase, resulting the partitioning mechanism shift from absorptive to adsorptive (Shiraiwa and Seinfeld, 2012). The organic compounds in the solid particles react slower than in the liquid or semisolid phase due to diffusion limitation (Bastelberger et al., 2017). As a result, the particle formation and growth process are influenced, and in turn affecting cloud formation, visibility and climate (Shiraiwa et al., 2011; Maclean et al., 2017).

In recent studies, viscosity has been found to be sensitive on functional group addition, similar to the sensitivity of volatility (Rothfuss and Petters, 2017). A good correlation between particle viscosity and volatility reveals that decreasing viscosity leads to an increase of effective vapor pressure (Marshall et al., 2018; Champion et al., 2019; Zhang et al., 2019). A parameterization method to predict the glass transition temperature, which is related to the viscosity, on basis of effective volatility has been developed by Li et al. (2020).

1.3.3 SOA from β-caryophyllene ozonolysis

β-caryophyllene (BCP) is one of the most abundant sesquiterpenes, emitting from agricultural crops and pine trees, such as potato plants, cotton, and orange trees (Ciccioli et al., 1999; Agelopoulos et al., 2000; Rodriguez-Saona et al., 2001; Hansen and Seufert, 2003; Duhl et al., 2008). β-caryophyllene is a bicyclic compound with two carbon double bonds with different reactivities towards ozone, and enables to retain its long carbon chain throughout the oxidation process and thus have a strong contribution to SOA mass. At 296K, the rate constant for the endocyclic carbon double bond of β-caryophyllene reacting with ozone has been determined as $(1.2\pm 0.4) \times 10^{-14}$ cm^3 $molecule^{-1}$ s^{-1} (Shu and Atkinson, 1994a; Richters et al., 2015; Cox et al., 2020). It is larger (~100 times) than the rate constant of exocyclic carbon double bond reacting with ozone, which is determined to be $(1.1 \pm 0.4) \times 10^{-16}$ cm^3 $molecule^{-1}$ s^{-1} (Shu and Atkinson, 1994a). Therefore, at typical tropospheric conditions (e.g., 30 ppb of ozone), β-caryophyllene has life time of ~2 minutes, and its closed-shell first-generation products can exist ~3.5 hours (Winterhalter et al., 2009a).

The yields of SOA particles are thought to dependent on temperatures, organic particle mass concentration, and O_3 levels (Odum et al., 1996; Saathoff et al., 2009a; Chen et al., 2012a). For β-caryophyllene derived SOA, its yields vary span a large range between 5-70% with different conditions (e.g., temperature between 287-298K) conducted by previous studies (Jaoui et al., 2003b; Lee et al., 2006b; Winterhalter et al., 2009b; Chen et al., 2012c; Tasoglou and Pandis, 2015b). A comparison of the experimental conditions, particle mass concentration (ΔM_{org}), particle mass yields from these studies is given in the Table S1. For the ozonolysis of β-caryophyllene without OH scavenger, a SOA mass yield of 27% was observed at 293 K and an organic particle mass loading of 10 μg m^{-3} (Tasoglou and Pandis, 2015a). Winterhalter et al. (2009) measured yields ranging between 5 - 24% for particle mass loadings of 50 - 440 μg m^{-3} and no Criegee intermediate scavenger, with the yields increasing for higher concentrations of water vapour or

formic acid. Jaoui et al. (2003) measured a yield of 39.3 % without OH scavenger at 287-290 K and Lee et al. (2006a) observed a yield of 45% at 293K and a particle mass loading of 336 μg m^{-3} using cyclohexane as OH scavenger. Chen et al. (2012b) varied the O_3 levels and determined SOA yields between 8 - 46% for organic particle masses of 0.5-170 μg m^{-3}, 15.8-60% at 2.1 - 230 μg m^{-3}, and 14.6-69.5% at 19 - 77.4 μg m^{-3} for O_3 levels of 50 ppb, 100 ppb and 200 ppb, respectively. By using OH scavenger, Tasoglou and Pandis (2015) also quantified SOA mass yields at room temperature to be 64.4% at 17.6 μg m^{-3} for 300 ppb of O_3, 59.6% at 16.3 μg m^{-3} for 400 ppb of O_3, and 66.9% at 30.5 μg m^{-3} for 500 ppb of O_3.

Besides, the mechanisms for the formation of products derived from β-caryophyllene ozonolysis have been investigated extensively for room temperature (Jaoui et al., 2003a; Griffin et al., 1999; Lee et al., 2006a; Lee et al., 2006d; Winterhalter et al., 2009a; Nguyen et al., 2009; Jenkin et al., 2012; Richters et al., 2016b). Aldehydes, small acids, and acetone are the major oxidation products detected in the gas phase (Grosjean et al., 1993; Calogirou et al., 1999; Zhao et al., 2010; Larsen et al., 1998). On contrast, in the particle phase, the main oxidation products include ketones, aldehydes, alcohols and carboxylic acids (Dekermenjian, 1999; Lee et al., 2006a; Jaoui et al., 2003a; van Eijck et al., 2013; Jaoui et al., 2007; Li et al., 2011a; Alfarra et al., 2012). Some of them have been identified, including β-caryophyllonic acid ($C_{15}H_{24}O_3$), β-caryophyllinic acid ($C_{14}H_{22}O_4$, BCA), and β-hydroxycaryophyllonic acid ($C_{15}H_{24}O_4$) (Table S3). β-caryophyllinic acid is regarded as a tracer to estimate the emissions of β-caryophyllene in the real atmosphere (Jaoui et al., 2007; Hu et al., 2008; Parshintsev et al., 2008; Haque et al., 2016; Verma et al., 2021; Cheng et al., 2021). In addition, HOM molecules via autoxidation were studied from β-caryophyllene ozonolysis at 295 K by Richters et al. (2016a), with identification of major HOM molecules of $C_{14\text{-}15}H_{22}O_7$, $C_{14\text{-}15}H_{22}O_9$, and $C_{15}H_{22}O_{11,13}$ (Richters et al., 2016b).

As discussed above, as the oxidation products from β-caryophyllene enable to retain the long carbon skeletons, their saturation vapor pressures are expected to be low or extremely low, also owing to their multiple functional groups. For instance, the saturation vapor pressure of β-caryophyllinic acid was determined as 3.3×10^{-13} Pa (Li et al., 2011a), which is low enough to have high potential to condense into particle and lead to SOA formation. As a consequence, these β-caryophyllene derived oxidation products enable to play a key role in the new particle formation (NPF) (Kirkby et al., 2016; Kammer et al., 2020; Huang et al., 2021). During night-time, the reaction between unsaturated hydrocarbons and NO_3 radicals is substantially important and can

result in formation of SOA. With the high reactivity between β-caryophyllene and NO_3 radicals ($(1.93\pm0.35) \times 10^{-11}$ cm^3 $molecule^{-1}$ s^{-1}) (Shu and Atkinson, 1995; Winterhalter et al., 2009a; Calvert et al., 2008; Cox et al., 2020), the nighttime chemistry of degradation of β-caryophyllene is of importance on the SOA formation and growth. However, this has only been subject of few studies so far. The yields of SOA derived from dark reactions between β-caryophyllene and NO_3 were between 1.46 and 0.91 with SOA mass concentrations of 113.4 and 60.3 μg m^{-3}, respectively (Jaoui et al., 2013). Several organic nitrate products derived from β-caryophyllene were identified as $C_{15}H_{23,25}O_4N_1$ and $C_{15}H_{25}O_{6,7}N_1$, and their chemical formation pathways were included in Master Chemical Mechanism (MCM v3.2) by Jenkin et al. (2012).

1.3.4 SOA from BVOC mixtures

Recently, it was shown that the simultaneous presence of different VOCs can have an impact on the SOA formation from the individual VOC at a molecular level. For example, presence of the most abundant non-methane VOC, isoprene, can suppress the formation of new SOA particles e.g. by reducing the oxidant levels (Kiendler-Scharr et al., 2009). Furthermore, it can suppress the formation of the dimer products of α-pinene oxidation by terminating the C10 peroxy radicals (McFiggans et al., 2019; Heinritzi et al., 2020). The impact of isoprene on the new particle formation for α-pinene oxidation at lower temperatures (223 and 243K) was also investigated (Caudillo et al., 2021). However, the temperature dependence of the SOA formation from a binary mixture of α-pinene and isoprene for the whole range of troposphere conditions, and from a mixture of isoprene and β-caryophyllene with and without α-pinene have not been addressed yet.

1.3.5 The impact of temperature on the SOA in the troposphere

The troposphere covers a wide temperature range which dependents on the altitude from the planetary boundary layer (PBL) to the upper troposphere, latitude, and seasonal variations. Typically, the tropospheric temperatures range between 300 K to 200 K. In summer, some periods can even reach 318 K. Temperature influences not only the BVOC emissions, but also the transport of SOA. For example, BVOCs and their oxidation products are proposed to undergo transport from the PBL to the upper troposphere e.g. via convective systems typical for tropical periods, as shown in Figure 4 (Andreae et al., 2018). In this conceptual picture of a potential aerosol life cycle the temperature dependence of the different processes involved is quite important. On the one hand, the reduced temperatures lower the saturation vapor pressures of compounds according to the

Clausius-Clapeyron relation, which drives the organics to the particle phase. On the other hand, temperature has been shown to be a factor that affects the gas-phase reaction rate coefficients of synchronous pathways in different degrees, and hence constrains or promotes some of the pathways during the VOC oxidation. For example, the formation of HOM molecules via autoxidation is pointed out to be favored by higher temperatures (Quéléver et al., 2019; Bianchi et al., 2019). Hence, by influencing the production of oxidation components via gas-phase reactions, temperature can affect the chemical composition of the SOA particles. Thus, the temperature can have opposite impacts on condensing low oxidized compounds and promoting high oxidized components formation. Hence, the effect of temperature is balanced between these two aspects when the SOA is formed at varying temperatures. The interplay between these two aspects enhances the complexity of SOA formation and the volatility prediction during the cold and warm seasons and from the boundary layer to the upper troposphere (Ye et al., 2019).

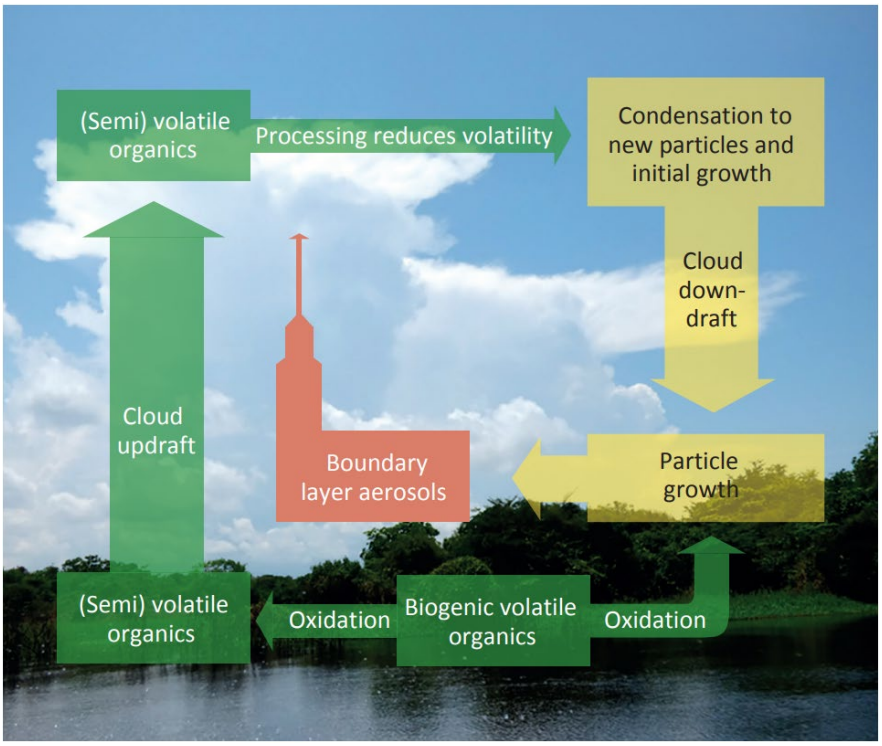

Figure 4. A conceptural schematic of the aerosol life cycle (formation and transport) over the Amazon Basin (Andreae et al., 2018).

As consequence of the overall impact of temperature on the SOA formation, multiple studies have shown that lower temperatures significantly increase the SOA yields, e.g. for α-pinene and limonene ozonolysis (Saathoff et al., 2009a), β-pinene ozonolysis (Von Hessberg et al., 2009), and isoprene ozonolysis (Clark et al., 2016). However, study of the impact of temperature on the SOA

from the oxidation of sole sesquiterpenes and BVOC mixtures are still scarce. Specifically, temperature dependence of condensable product formation and phase partitioning of the oxidation of sesquiterpenes and the BVOC mixtures still remain unclear. For β-caryophyllene, one of the most reactive sesquiterpenes with high SOA formation potential, only one model study is available for the temperature dependent kinetics (Nguyen et al., 2009), and no other molecular insight on the temperature dependent reaction exists.

1.4 Recent advances in online mass spectrometry

To get profound insights on the formation and aging of aerosols, it is important to measure their chemical composition and physicochemical properties, e.g., the molecular identification. Recent advances in the development and application of novel mass spectrometers lead to substantial progress especially for the characterization of organic aerosols (de Gouw, 2021).

This section will briefly summarize the major mass spectrometry techniques which have become available for online measurements for BVOCs (1.4.1) and SOA (1.4.2) in recent years.

1.4.1 Main units in mass spectrometers

The basic principle of mass spectrometry (MS) is to generate ions from either (in)organic compounds by suitable methods, to separate these ions by their *mass-to-charge ratio* (*m/z*) and to detect them qualitatively and quantitatively by their respective *m/z* and abundance (Gross, 2006). Basically, all mass spectrometers have three fundamental units: ion source, mass analyzer, and detector, which are under high vacuum conditions.

The initially neutral sample molecules can only be detected after they are charged. This process is called “ionization”. There are several ionization techniques, such as electron ionization (EI), chemical ionization (CI), field ionization (FI), electrospray ionization (ESI), and laser ionization (LDI). EI is the most widely used ionization method typically with 70 eV electrons. As one of the hard ionization techniques, EI is inherently quantitative but can also induce extensive fragmentation of the organic molecules. In contrast, as a softer ionization technique, CI allows to generate new ionized species by reaction between the uncharged analytes and reagent ions from an ion source. Depending on the reagent ion chosen, the breakage of the neutral analyte molecules and formation of fragments can be reduced or completely prevented.

Besides, there are different mass analyzers to separate the charged ions, including time-of-flight (TOF), quadrupole (Q), orbitrap, and Fourier transform-ion cyclotron (FT-ICR). To measure

the organics, some of them have been widely used for qualifying or quantifying the OA components. In the following sections, I will briefly review the main mass spectrometers for online measurements, their ionization methods, mass analyzer, and their applications in the biogenic organic aerosol field.

1.4.2 Gas phase measurements

For the measurement of volatile organic compounds, time-of-flight mass spectrometers (TOF-MS) using chemical ionization techniques have been recently developed. In advantage of TOF and CI techniques, TOF-CIMS is able to acquire mass spectra with a high time resolution, and enables the assignment of molecular formulas. These features make it possible for researchers to study the chemical composition of SOA at a molecular level.

As the organics differ in extensive functionality and polarities, several reagent ions have been considered for the ionization to cover the full range of organics from hydrocarbons to HOM molecules. For example, a TOF-MS using hydronium ions (H_3O^+) as reagent ion for the proton-transfer reactions (so-called "PTR-TOF-MS" or "H_3O^+-TOF-CIMS") has been developed to measure the species with proton affinity higher than H_2O (691 kJ mol^{-1}) , such as hydrocarbons (isoprene, terpenes, aromatics) and low oxidized organics (aldehydes, alcohol, acids, etc.) (Jordan et al., 2009; Blake et al., 2009). To identify the isomers that are behind the same mass, e.g. α-pinene and myrcene, a fast gas chromatography (GC) module can be coupled to a PTR-TOF-MS (so-called "GC-PTR-MS") to separate organic mixtures (Warneke et al., 2011; Koss et al., 2016).

For those organics of higher oxygenation and polarity, iodide (I^-) has been used for chemically ionizing the neutral compounds, and has been coupled to the TOF-MS (so-called "I^--TOF-CIMS") (Huey et al., 1995; Lopez-Hilfiker et al., 2016). Due to the high electronegativity of iodide ions, I^--TOF-CIMS is sensitive to the components with the addition of polar functional groups, like keto-, hydroxy-, and acid groups, but is completely insensitive to the nonoxygenated VOCs such as hydrocarbons (Lee et al., 2014). I^--TOF-CIMS has been demonstrated to enable to efficiently detect semi-volatile organic compounds, and can cover a substantial amount of the oxidized organics in SOA (Riva et al., 2017). For example, I^--TOF-CIMS explained at least half of the total organic mass of the atmosphere aerosols in Alabama and Finland (Lopez-Hilfiker et al., 2016).

In contrast to I^--TOF-CIMS, acetate-TOF-CIMS uses the acetate ions to selectively ionize acidic compounds such as carboxylic acids and nitrated phenols (Veres et al., 2008; Mohr et al., 2013). Besides, nitrate (NO_3^-) TOF-CIMS coupled a with an atmospheric pressure interface (API)

enables to detect the most highly oxidized species and low volatile compounds, e.g. highly oxygenated organic (O>5) molecules like HOM molecules (Riva et al., 2019), and even radicals such as peroxyl radicals. Additionally, using benzene cation ($C_6H_6^+$) as the reagent ion, benzene-TOF-CIMS enables to measure dimethyl sulfide and terpenes (Kim et al., 2016).

1.4.3 Organic aerosol particle measurement

Recently, numerous of volatilization inlets have been designed to evaporate the compounds from particle phase to gas phase, such as Filter Inlet for Gases and Aerosols (FIGAERO) (Lopez-Hilfiker et al., 2014), and Micro-Orifice Volatilization Impactor (MOVI) (Yatavelli et al., 2012). These inlets enable to evaporate the particles via a temperature increasing procedure, and enable to nearly simultaneously measure the species in the gas and particle phases when combining with a TOF-MS that couples a soft ionization technique such as I^--TOF-CIMS at downstream. As another advantage of these instruments, the thermal desorption profiles (hereafter 'thermograms') of the species can provide additional information on the volatilities (expressed as effective vapor pressures) of the detected components in SOA particles (Lopez-Hilfiker et al., 2015; D'Ambro et al., 2017).

The most widely used instrument to determine the size dependent concentration of aerosol particles is the so-called aerosol mass spectrometer (AMS). The time-of-flight aerosol mass spectrometer (TOF-AMS) is widely used to analyze non-refractory aerosol components including organics, sulfate, nitrate, and ammonium (Drewnick et al., 2005; DeCarlo et al., 2006; Canagaratna et al., 2007). Owing to the EI technique with high ionization energy (70eV), TOF-AMS is able to vaporize most organic species but induces extensive fragmentation. Thus, TOF-AMS provides the quantification of the concentration of bulk species, e.g., organics, nitrates, sulfates, but it cannot provide further insights into individual molecules. More recently, a Chemical Analysis of Aerosol Online (CHARON) has been designed for PTR-TOF-MS for the online measurement on the chemical composition of aerosol particles (Eichler et al., 2015). CHARON-PTR-TOF-MS hence allows a high time-resolution analysis on the SOA particles at a molecular level, although it also induces some fragmentation of the organic analytes due to its highly energetic proton transfer (Spanel and Smith, 1997; Blake et al., 2009). Besides, the limits to the online detection of highly oxidized compounds in the particles phase have been addressed by extractive electrospray ionization time-of-flight mass spectrometry (EESI-TOF-MS). EESI-TOF-MS allows the continuous measurement on the particles without pre-collection of particles (Lopez-Hilfiker et al.,

2019). However, the lack of thermal desorption makes it impossible to extract the effective volatilities of compounds from EESI-TOF-MS.

2 Research Questions

As outlined above, secondary organic aerosol (SOA) is of great importance in the whole troposphere, as it influences the air quality and the earth's climate. The formation of SOA always involves the gas-phase oxidation of volatile organic precursors and the condensation of the condensable oxidation products. Despite the large number of studies which have been done on SOA to date, at least two major questions are still unclear and remain to be addressed. One question is how does temperature influence the formation and physicochemical properties of the SOA particles. Tropospheric temperature varies spatially and seasonally, but molecular understanding on chemical composition and volatility of the SOA particles formed at a wide temperature range covering the typical atmospheric relevant conditions still remains unclear. For example, as a reactive bicyclic sesquiterpene, β-caryophyllene can have a strong contribution to SOA mass owing to the retention of its large carbon chain throughout the oxidation process. However, studies on the interplay of temperature between facilitating condensation of organics and changing the formation pathways of oxidation products on β-caryophyllene ozonolysis are still scarce. Another question is on the interaction effect of mixed VOCs on the SOA formation and the volatility of particles. It has long been realized that prediction of the SOA formation in the real troposphere requires knowledge of the emissions and the oxidation products of VOC mixtures. BVOCs show different ability to form SOA particles by sole BVOC oxidation leading to different chemical composition and varying volatility ranges. However, the chemical composition and volatility of SOA from VOC mixtures is still poorly understood. These existing knowledge gaps in atmospheric aerosol research lead to my following main research questions:

1) How does temperature (213-313K) influence the yields, chemical composition, and volatility of SOA derived from β-caryophyllene? Does the autoxidation of β-caryophyllene have a temperature dependence? How do isomers and thermal decomposition influence the volatility estimation? How to distinguish them?
2) Is there a temperature dependent interaction of oxidation products from isoprene and α-pinene? How is the temperature dependence of volatility of SOA from the oxidation of α-pinene and isoprene mixtures?
3) How does β-caryophyllene influence the chemical composition and volatility on the SOA derived from isoprene with and without the presence of α-pinene?

3 Methodology

To achieve my research objectives, I generated SOA in the aerosol and cloud simulation chamber AIDA. It allows me to study the oxidation of different VOCs, the formation of SOA as well as its aging over several hours or days and for a wide range of atmospheric conditions. During the SOA formation and aging period, I used several online instruments to measure the chemical composition of both aerosol phases, particle size distribution, and SOA volatilities. The major campaigns that I performed during my PhD study are summarized in Figure 5. In section 3.1 of this chapter, the techniques and calibration of the main instruments and research tools are described. Section 3.2 describes how I did the simulation chamber studies. The procedures to calculate SOA yields and SOA volatility are outlined in sections 3.3 and 3.4, respectively.

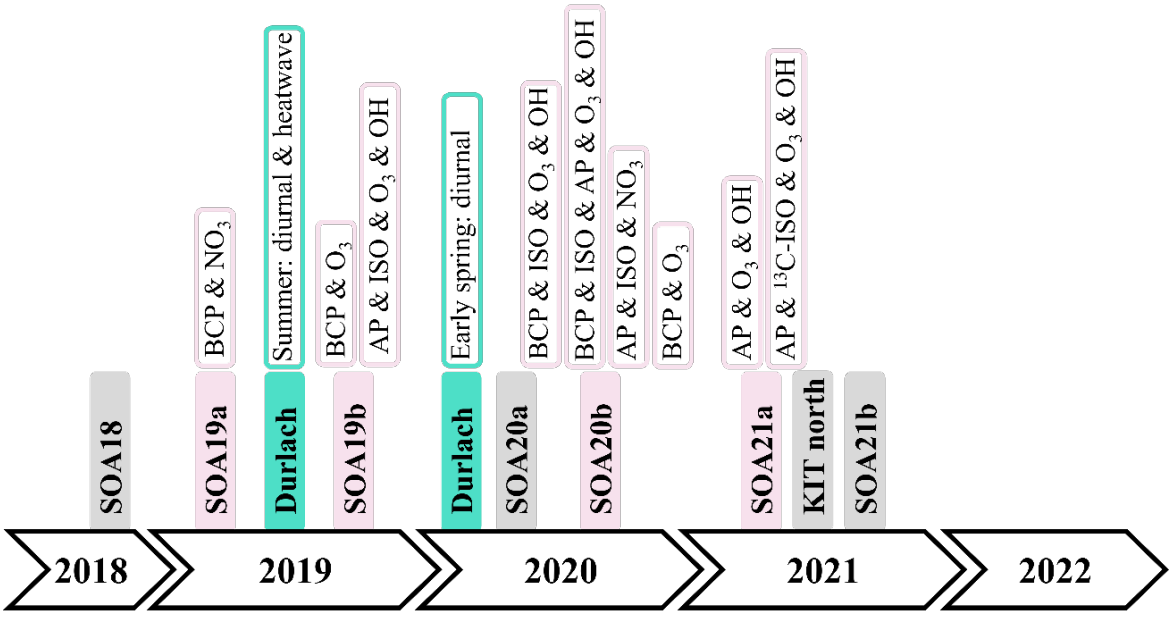

Figure 5. Timeline of major campaigns that I performed during my PhD study, and major dataset that is presented in this dissertation.

3.1 The AIDA simulation chamber and instrumentation

The chemical composition of oxidized components in the gas and particle phase, and the particle evaporation performance which was related to the molecular volatilities were measured by a Chemical Ionization Mass Spectrometer coupled with a FIGAERO inlet using iodide as the reagent ion (FIGAERO-CIMS, Aerodyne Research Inc.). The concentration of VOC precursors was detected by a Proton-Transfer-Reaction-Time-of-Flight-Mass-Spectrometer (PTR-ToF-MS

4000, Ionicon Analytic GmbH), while the particle concentration and size concentration were measured by a High Resolution-Time-of-Flight-Aerosol Mass Spectrometer (HR-ToF-AMS, Aerodyne Inc.) and a scanning mobility particle sizer (SMPS) utilizing a differential mobility analyzer (DMA, 3071 TSI Inc.) connected to a condensation particle counter (CPC, 3772, TSI Inc.).

3.1.1 AIDA simulation chamber

A schematic of the AIDA (Aerosol Interaction and Dynamics in the Atmosphere) simulation chamber at the Karlsruhe Institute of Technology and the main instrumentation used in this work are shown in Figure 6. The chamber is an 84.5 m^3 aluminum vessel equipped with a LED solar radiation simulator and with precisely controlled temperature, humidity, and gas mixtures. It is operated as a continuously stirred reactor with mixing times of 1-2 minutes achieved using a fan about 1 m above the bottom (Saathoff et al., 2009b). Wall and gas temperatures inside the chamber are controlled at ±0.3 K over a wide range of temperatures (313-183 K) (Wagner et al., 2006). The pressure inside the chamber can be varied from 0.01 to 1000 hPa and the relative humidity (RH) can be modified between close to zero to up to 100% and even supersaturated conditions (Möhler et al., 2003). Water vapor is measured in situ by a tuneable diode laser (TDL) hygrometer with an accuracy of ±5% and a calibrated reference dew point mirror hygrometer (MBW373LX, MBW Calibration Ltd.) with an accuracy of ±1% (Fahey et al., 2014). O_3 and NO_2 were measured with gas monitors ($O_3$41M and AS32M, both Environment SA). Particle size distributions and number concentrations were measured by a SMPS utilizing a DMA (3071 TSI Inc.) connected to a CPC. Particle number concentrations were measured by two CPCs (3022a and 3776, TSI Inc.). The particle number size distributions of the SMPS were corrected for the total number concentration measured by a calibrated CPC.

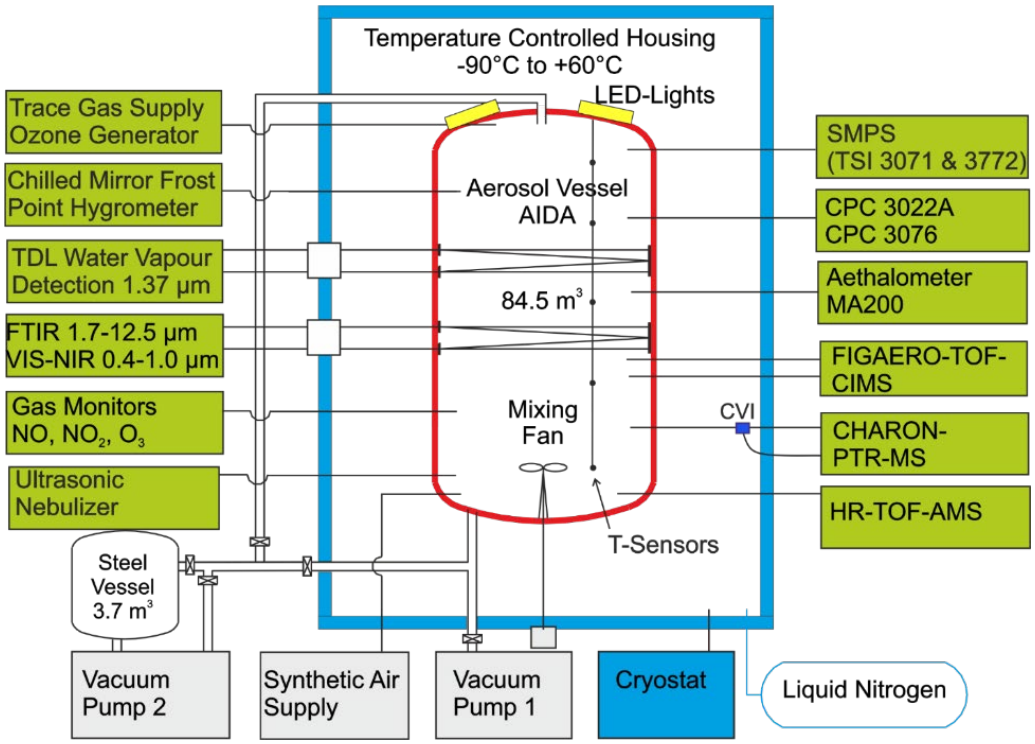

Figure 6. Schematic of the AIDA simulation chamber and its instrumentation used in this work.

3.1.2 FIGAERO-CIMS technique and calibration

As discussed in the section 1.4, as a novel mass spectrometry technique, FIGAERO-CIMS allows not only the measurement of both gas and particle composition in a molecular framework, but also the particle volatilization which can be related to the molecular effective vapor pressures avoiding substantial fragmentation (Hearn and Smith, 2004; McNeill et al., 2007; Aljawhary et al., 2013; Lopez-Hilfiker et al., 2014). FIGAERO-CIMS is a sensitive sensor for hundreds of oxidized compounds, and has a low detection limit of a few ppt for gaseous compounds, and some pg m^{-3} for particulate compounds. The schematics of the FIGAERO inlet and the CIMS are shown in Figure 7 and Figure 8, respectively.

In brief, FIGAERO-CIMS measures the gas phase compounds while collecting the particles on a Teflon filter (gas phase & collection mode in Figure 7 (b)). After the particle collection, the FIGAERO inlet switches to the heating mode (Figure 7 (c)). The particles are heated by a pure nitrogen as a carrier gas with a temperature ramp increasing linearly from room temperature to 200 °C within 15 minutes, and then soaks at 200 °C for 20 minutes to remove all detectable deposition compounds. The thermally desorbed compounds are then ionized by I^- ions in a following Ion Molecule Reactor (IMR), and measured downstream in a Time of Flight (TOF) mass

analyzer with a typical mass resolution of Δm/m = 4000. Please note that particle collection was also preformed independently, loaded Teflon filters were stored in a freezer, and analysed after the experiments by loading them into the Figaero inlet.

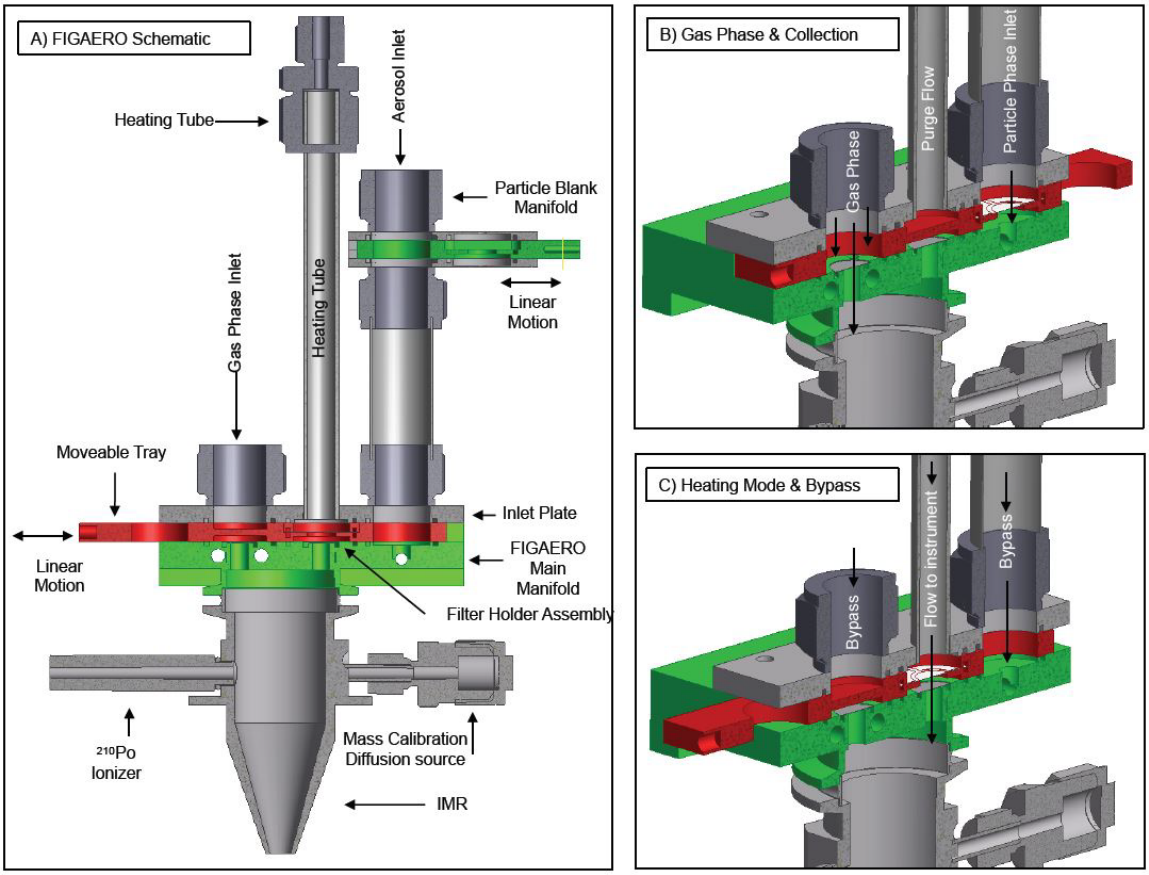

Figure 7. Schematic of FIGAERO inlet (A), with gas phase & particle collection mode (B), and heating mode (C).

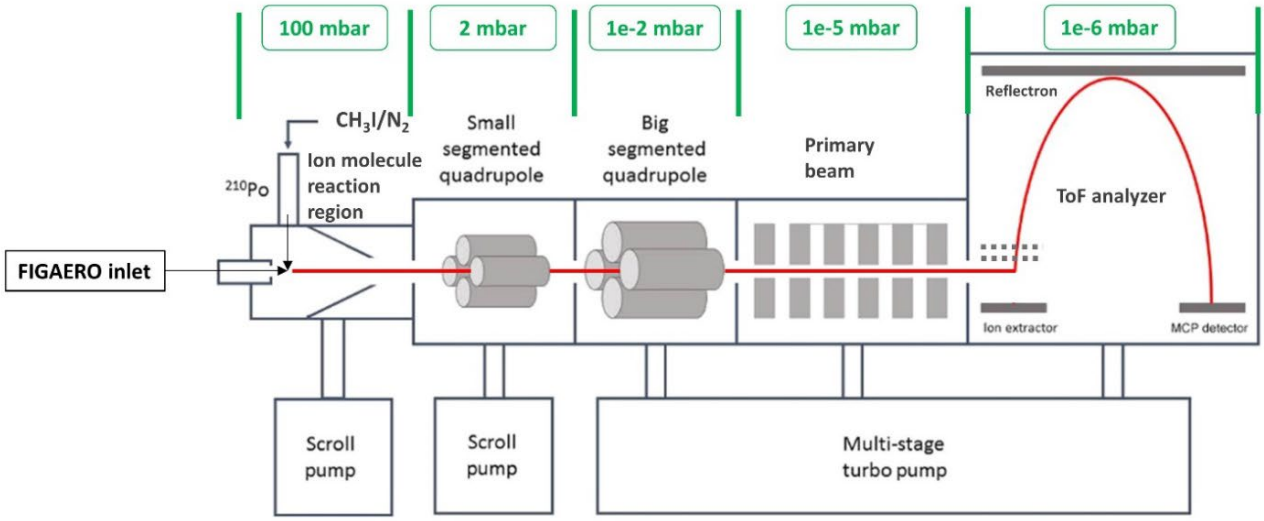

Figure 8. Schematic of FIGAERO-CIMS (Sanchez et al., 2016) with the different pressure zones.

The reagent ions (I^-) are generated by a flow of 2000 SLM of CH_3I (permeation tube) over a ^{210}Po alpha emitter. The reagent ions undergo ion molecule reactions, [Molecule] + I^- → $I(Molecule)^-$, with the sample molecules from VOCs or FIGAERO inlet, forming $I(Molecule)^-$ clusters with one negative charge in the IMR period at a total pressure of 100 mbar. The ion-molecule clusters are guided via segmented quadrupoles to form a primary ion beam which is injected into the TOF analyzer where they are reflected and detected by a multichannel plate (MCP) detector. Among all charged ions, the heavier ions need more time to fly over the whole acceleration period, while the ions with less mass travel faster. Thus, by recording their varying flying time, we can resolve and order all ions by their mass to charge ratios (*m/z*, Th).

The gas phase compounds are sampled online by FIGAERO-CIMS with a total flow rate of 5 SLM. A flow of 2 SLM enters the IMR of the instrument (controlled by an aperture), and a bypass flow of 3 SLM is added to lower the resident time of gas compounds in the ¼'' OD Teflon sampling tube. The particle phase compounds are collected online and offline (thereafter 'online filters' and 'offline filters'), and are thermally analyzed using the FIGAERO inlet as described above. Online filters are taken by FIGAERO when measuring the gaseous organics. Offline filters are collected manually using prebaked Teflon filters (Polytetrafluorethylene, PTFE, 1 μm, SKC Inc.) plated in a stainless-steel filter holder with a flow rate of 6 SLM for typically 5-10 min. After the particle deposition, the offline filters are stored in a freezer at -30 °C for subsequent analysis.

The sensitivity of the CIMS (I^-) can vary over about 4 orders of magnitude due to a wide range of ion molecule reaction rates, and substantial differences in transmission efficiency of hundreds of multifunctional organic molecules (Brophy and Farmer, 2015; Lopez-Hilfiker et al., 2016). The maximum sensitivity achievable, corresponding to the collision limit of the ion molecule reaction rates, is about 22 cps $pptv^{-1}$ (Lopez-Hilfiker et al., 2016). Generally, polarity and hydrogen bonding capability, molecular geometry, and steric factors control the sensitivities for compounds to be detected by iodide adduct CIMS. Components with polar functional groups, i.e. keto-, hydroxy-, and acid groups, show highest sensitivities. In contrast, low-oxidized compounds e.g., with only one functional group, such as monoaldehydes and mono-alcohols, can exhibit sensitivities below 0.1 cps $pptv^{-1}$ (Lee et al., 2014). The iodide adduct CIMS is insensitive to non-oxidized compounds.

Of course, calibrations with available authentic standards can be done to allow quantification of specific compounds. I calibrated the CIMS for β-caryophyllinic acid ($C_{14}H_{22}O_4$), which is

regarded as an atmospheric tracer for β-caryophyllene oxidation. β-caryophyllinic acid was dissolved in methanol to 2×10^{-13} g L^{-1} as a stand β-caryophyllinic acid solution, and then deposited on a PTFE filter in different volumes (1-10 µl) using a syringe. The sensitivity of β-caryophyllinic acid was calculated as $(2.4\ ^{+0.1}_{-0.6})$ cps ppt^{-1} (Figure S2).

Besides, a calibration (hereafter 'volatility calibration') which links the T_{max} (the desorption temperature with concentration peak in the thermogram) of the known organics to their vapor pressures was also done to relate vapor pressures (volatilities) of unidentified organics to their peak desorption rate temperatures T_{max}. The volatility calibration as a useful tool to estimate the individual vapor pressures has been developed in recent years (Lopez-Hilfiker et al., 2014; Stark et al., 2017; Bannan et al., 2019; Ylisirniö et al., 2021). As instrumentation setup can affect T_{max} for chemicals, I calibrated the FIGAERO-CIMS used in this work, with amounts of standard solutions which contain organic acids with different mixing ratios. The details and results will be presented in section 3.4.1.

The raw data from FIGAERO-CIMS is recorded with a frequency of 1 Hz and subsequently pre-averaged to 0.1 Hz. These data are analyzed using a software provided by the instrument manufacturer (Tofware version 3.1.2, TOFWERK). It is used to calibrate the ion time of flight using well detectable ions (I^-, I_3^-, I $(H_2O)^-$, I $(HNO_3)^-$), define the shapes of mass peaks, determine the mass resolution of the ions, and assign the molecular formulas. Post analysis, like converting signals to concentration, and calculating saturation vapor pressures, are done by specific MATLAB routines with scripts written by myself.

3.1.3 HR-TOF-AMS technique and calibration

A high-resolution time of flight aerosol mass spectrometer (HR-TOF-AMS), which can obtain the size-resolved real-time composition of non-refractory submicron aerosols (Jayne et al., 2000), is used in this work to measure the organic aerosol particles. The schematic of HR-TOF-AMS is showed in Figure 9. During the measurement, aerosol particles which have sizes typically ranging between 35nm to 1.5µm are sampled by a flow rate of 0.0008 m^3/min going into the instrument controlled by a 100 µm critical orifice (Zhang et al., 2004). In the aerodynamic lens, particles are gradually concentrated into a narrow beam at the exit of the lens using six apertures (Liu et al., 1995), and most sample gases are removed in the meanwhile. Subsequently, aerosol particles go into the aerodynamic particle sizing range (10^{-5} Torr) where the particle beam is

accelerated and cut by a mechanical chopper into a fixed length. In this period, particle sizes are defined in basis of different residence time from the time when particle beams go through the chopper to the time of the final detection by the subsequent TOF mass spectrometer. The nonrefractory species in the particles are thermally vaporized and ionized subsequently by 70 eV electron impact (EI) after impaction on a resistively heated surface (600 °C), followed by ion travels in TOF in V or W modes and detection by a MCP detector. Both 'V' and 'W' refer to the trajectories of the particles in TOF. The effective ion path length of particles in the V mode is 1.3 m, which has a higher sensitivity, while it in W mode is 2.9 m, which provides higher mass resolution. In this work, the HR-TOF-AMS was throughout operated in V mode. Hence, HR-TOF-AMS is unable to vaporize and measure the refractory species (e.g., crustal material, sea salt, and black carbon), and cannot offer the molecular information of individual compound, however, it is in advantage of measuring the absolute concentration of all nonrefractory organic species. As in my work, all the aerosol particles are within the detectable scope of HR-TOF-AMS, and hence it performs as a good complementary tool to FIGAERO-CIMS, and provides the additional information (e.g., total concentration, particles sizes) of the aerosol which I study on.

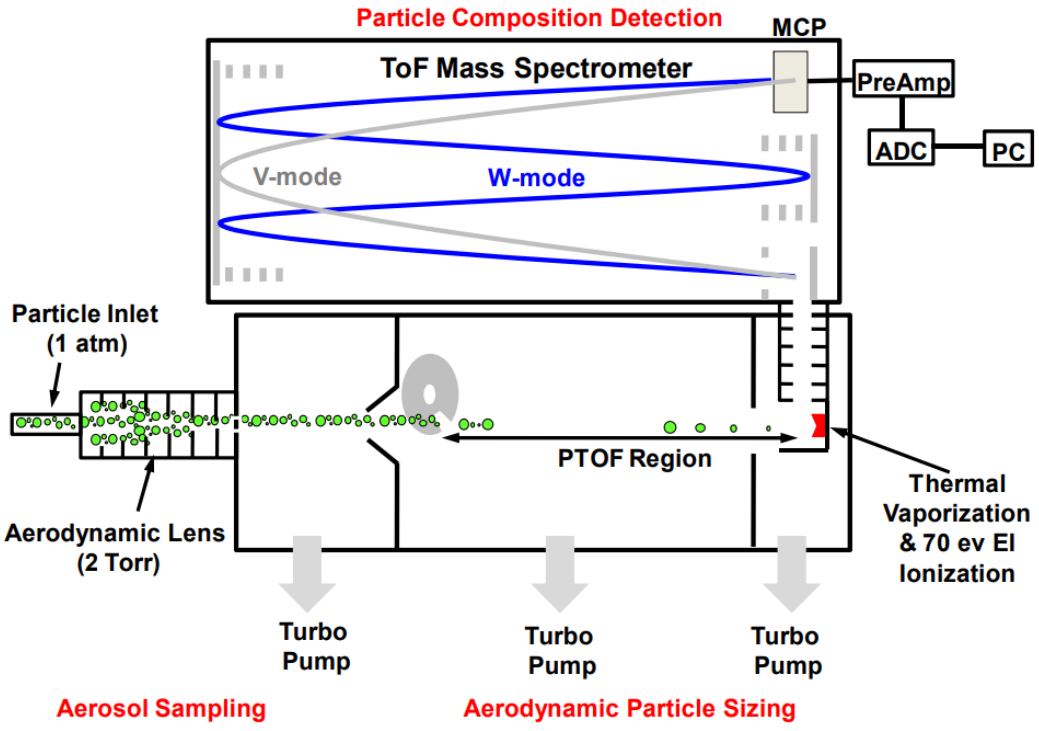

Figure 9. Schematic of the HR-TOF-AMS, adapted by Sun et al. (2009) from DeCarlo et al. (2006).

Given the above, the main information I focused on from HR-TOF-AMS includes: 1). Total concentration of organic species, and subsequent high resolution analyzed elemental oxygen to carbon ratio (O:C), hydrogen to carbon ratio (H:C) and average carbon oxygenation status ($\overline{OS_C}$) in bulk; 2.) particle aerodynamic size which is used to identify the SOA density. In my PhD work, all data from HR-TOF-AMS was analyzed by me using the TOF-AMS Analysis Toolkit (SQUIRREL v.1.6C, unit resolution analysis) and the TOF-AMS HR Analysis Toolkit (PIKA v. 1.2C, high resolution analysis) (http://cires1.colorado.edu/jimenez-group/ToFAMSResources/ToFSoftware/index.html).

To determine the concentration of total organic species, the data from HR-TOF-AMS is analyzed in the following steps: mass calibration, baseline determination, pre-process the raw data, parameter corrections (e.g., air beam, ionization efficiency (IE), collection efficiency (CE), and particle size), determination of peak width and peak shape, and peak identification. Parameters for IE correction and particle size correction are determined by IE calibration (using polystyrene latex, PSL) and size calibration (using ammoniate sulfate) (Jimenez et al., 2003; DeCarlo et al., 2006). CE values vary between 0.5 - 0.6 in this work due to the variation of RH in the sample air (Allan et al., 2004).

3.1.4 Proton transfer reaction mass spectrometer (PTR-MS)

The concentrations of BVOCs and low-oxygenated gaseous oxidation products were measured by a Proton-Transfer-Reaction-Time-of-Flight-Mass-Spectrometer (PTR-ToF-MS 4000, Ionicon Analytik GmbH). Data was analyzed using the software PTR viewer 3.3.12 (Ionicon). The PTR-ToF-MS is also interfaced with a particle inlet (CHARON), which allows to measure the semi-volatile particle components. A detailed description of the CHARON-PTR-MS has been provided elsewhere (Müller et al., 2017; Piel et al., 2021). During the period of BVOC injection and ozonolysis, the PTR-ToF-MS was operated for measuring gaseous volatile organic compounds (VOCs) only. After BVOCs were fully depleted, the PTR-ToF-MS was switched to an alternating measurement mode for detecting the low-oxygenated organic molecules in both gas and particle phases. This alternating measurement mode included 3-min HEPA filter measurement for the particle background, 5-min CHARON particle measurement, 1-min transition for instrument equilibration, 5-min of VOC measurement and another 1-min transition. The CHARON-PTR-MS measured the particle phase at a sampling flow of 500 SCCM via a 1/4” silcosteel tube, while the

gas phase was measured at a flowrate of 100 SCCM via a 1/16" PEEK tube taken from the particle measurement flow. Furthermore, a flowrate of 3.9 l/min was added to the total flow to minimize the residence time in the sampling tube. For measuring gases, the drift tube of the PTR-MS was kept at 393 K and 2.8 mbar leading to an electric field (E/N) of 127 Td. During alternating measurements, the drift tube was automatically optimized to 100 Td for particle measurement. BVOCs were calibrated using a liquid calibration unit (LCU-a, Ionicon Analytik GmbH). The PTR-ToF-MS operated at an E/N of 127 Td showed significant fragmentation of BVOCs, in agreement with previous studies (Kim et al., 2009; Kari et al., 2018).

Please note that the calibration, operation and data analysis of CHARON-PTR-MS were completely done by my colleague Junwei Song.

3.2 Experimental conditions and procedures

This section describes the experimental conditions, BVOC concentrations, SOA generation, and SOA aging procedures for all simulation chamber experiments.

3.2.1 α-pinene and isoprene mixture SOA generation and aging

The experiments on generation and aging of SOA from α-pinene ('AP') and isoprene ('iso') mixtures (hereafter '$SOA_{ap\text{-}iso}$') were conducted in a campaign in November and December 2019 (named 'SOA19b') covering 213K-298K. In another campaign conducted in April 2021 (named 'SOA21a'), another experiment on $SOA_{ap\text{-}iso}$ at 313K was done to complete the temperature range covering the conditions throughout the troposphere. In the SOA21a campaign, a reference SOA from sole α-pinene oxidation (hereafter 'SOA_{ap}') at 273K, and two experiments using isotopic carbon (^{13}C) labeled isoprene (hereafter '^{13}C-isoprene') to identify the interaction products from both α-pinene and isoprene at 273K and 298K were done, with the SOA generated in these two experiments as '$SOA_{ap\text{-}iso}$-^{13}C'. Those eight SOA types were generated and aged via similar processes. After the VOCs (α-pinene or mixture) were added into the AIDA chamber, O_3 was then injected to form stable SOA particles, followed by OH radical addition formed by reaction of tetramethyl ethylene (TME) with O_3. After the SOA concentration reached a stable level it was illuminated. Subsequently, the whole chamber temperature was slowly increased over night by a temperature increment of 15-30K. The detailed experimental conditions are listed in Table 1.

Except for Exp.6, the α-pinene: isoprene ratio is 1, and the total VOC: O_3 ratio is 1:10 with an excess of O_3. These experimental procedures are described in the following schematic:

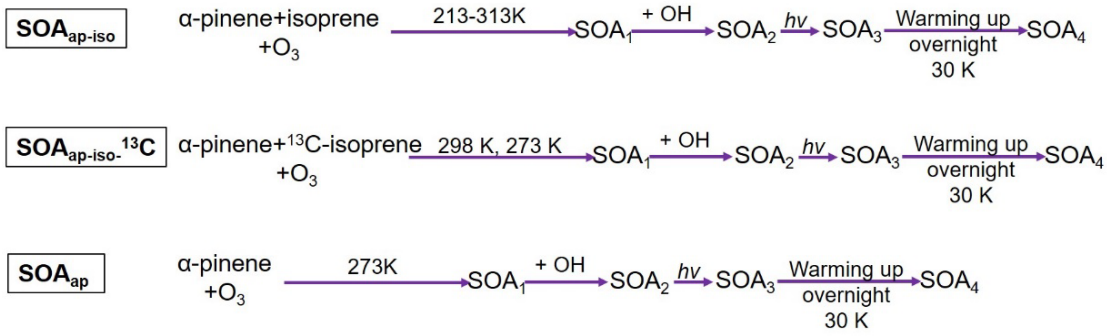

Typically, background measurements for both gas and particle phase are done before and after the addition of VOCs to identify any contamination inside the chamber. However, gas background levels were almost negligible for most experiments and most of the particle background signals were from filter matrix contaminations mainly due to fluorinated constituents of low relevance. Please note that the background in all experiments was measured in the same way.

Table 1. Experimental conditions for SOA from α-pinene and isoprene mixture.

Exp No.	SOA type	VOC [ppb]		O_3 [ppb]	Temp. before warming [K]	Temp. after warming [K]	RH [%]
		α-pinene	isoprene				
1	$SOA_{ap\text{-}iso}$	20.2	20.2	366	213	243	16
2	$SOA_{ap\text{-}iso}$	25	25	367	243	273	80
3	$SOA_{ap\text{-}iso}$	21.5	20.8	371	273	298	58
4	$SOA_{ap\text{-}iso}$	31.3	28.6	355	298	313	28
5	$SOA_{ap\text{-}iso}$	49.8	49.8	507	313	-	12
6	SOA_{ap}	20.5	-	345	273	-	63
7	$SOA_{ap\text{-}iso\text{-}}{}^{13}C$	20.8	23	353	273	298	61
8	$SOA_{ap\text{-}iso\text{-}}{}^{13}C$	28	31.1	357	298	313	12

3.2.2 β-caryophyllene SOA generation and aging

The different steps of the β-caryophyllene experiments with SOA from β-caryophyllene from a campaign in November and December 2019 (SOA19b) covering five different temperatures between 213 - 313 K are described in the following schematic:

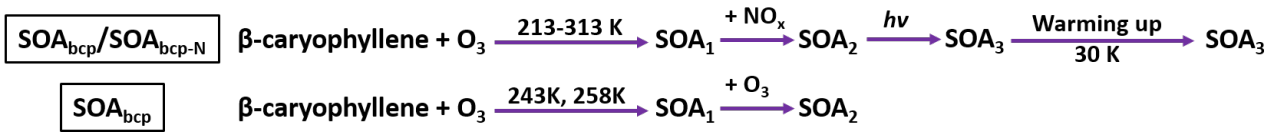

The experimental conditions are listed in Table 2. Two additional experiments were undertaken in March 2020 (SOA20a) to study the rate coefficients of β-caryophyllene reacting with O_3 at 243 K and 258 K. β-caryophyllene (98%, Carl Roth GmbH) was added to the AIDA chamber with a flow of 0.01 m3/min of synthetic air saturated with its vapor at 298K. Please note that the β-caryophyllene concentrations for the experiments at 213 K could not be measured due to the low vapor pressure and strong wall losses at lower temperatures. O_3 was in all experiments in excess and generated by a silent discharge generator (Semozon 030.2, Sorbios) in pure oxygen (99.9999%). The relative humidity ranged from 96% to 13% for experiments at 213 K and 313 K, respectively. This corresponds to water vapor concentrations of 1 Pa (3.4×10^{14} cm^{-3}) at 213 K and 952 Pa (2.2×10^{17} cm^{-3}) at 313 K, respectively, and reflects the variability of the water vapor concentrations throughout the troposphere. At the initial phase of each experiment, β-caryophyllene was depleted completely by ozonolysis and SOA was formed. Then a second addition of β-caryophyllene was done to generate more SOA mass. As the O_3 concentration was in large excess, during the second β-caryophyllene addition, the ratio of β-caryophyllene: O_3 still was similar to the initial β-caryophyllene addition. Thus, the chemistry between two rounds of β-caryophyllene addition was at the same concentration level. The total amount of β-caryophyllene consumed was the sum of these two additions. The corresponding conditions are marked as Exp.9-13 in Table 2. Subsequently, NO_2 (1000 ppm of 99.5% purity in nitrogen 99.999%, Basi Schöberl GmbH) was added to the reaction mixture still containing an excess of O_3. The step of SOA formation in the presence of NO_x was then initialized by adding more β-caryophyllene. This series of experiments is marked as Exp.16-20 in Table 2. Hence, the β-caryophyllene and O_3 concentrations listed in Table 2 for experiments Exp.16-20 include also the amounts which had been added in the previous experimental steps (Exp.9-13). O_3 was at nearly the same concentrations as for the initial experiments without NO_2, except for the experiments at 273 K. To get a slower decay of β-caryophyllene to better determine its rate coefficient at 273K, we added 73 ppb O_3 into the chamber first and then added more O_3 to the same concentration level (~300 ppb) as used for the other temperatures for comparison. All experiments were performed in the dark and no hydroxyl radical scavenger was used. Hence, the OH radicals generated in the

ozonolysis reaction with a yield of (8±3) % (Cox et al., 2020), (10.4 ± 2.3) % (Winterhalter et al., 2009b) or 6% (Shu and Atkinson, 1995) also contributed to SOA formation as will be detailed in chapter 4. Time zero in the plots refers to the first addition of O_3 to the reaction mixture.

Table 2. Compilation of experimental conditions for β-caryophyllene SOA formation and aging.

Exp. No.	SOA type	T [K]	RH [%]	β-caryophyllene [µg m^{-3}]	Total O_3 [ppb]	Total NO_2 [ppb]	NO_3· [ppb]
9	SOA_{BCP}	213	96	#	320	0	-
10	SOA_{BCP}	243	88	15.8±3.1 (15.6±3.1t)	317	0	-
11	SOA_{BCP}	273	67	109.5±21.9	73	0	-
12	SOA_{BCP}	298	27	65.0±13 (23.2±4.6 t)	325	0	-
13	SOA_{BCP}	313	13	78.6±15.7	290	0	-
14	SOA_{BCP}	243	59	65.0±13.0	6-505	0	-
15	SOA_{BCP}	258	50	94±19	13-419	0	-
16	SOA_{BCP-N}	213	96	#	320	27	-
17	SOA_{BCP-N}	243	88	14.2± 2.8t	317	32	0.8
18	SOA_{BCP-N}	273	67	109.5±21.9t	361	39	3.5
19	SOA_{BCP-N}	298	27	27.9± 5.6t	325	42	5.3
20	SOA_{BCP-N}	313	13	24.6±4.9t	290	46	5.6

[#]not detectable due to wall losses; [t] following β-caryophyllene addition calculated assuming a constant β-caryophyllene addition rate in each experiment;

3.2.3 α-pinene and isoprene and β-caryophyllene mixture SOA generation and aging

The experiments with SOA from mixtures of isoprene and β-caryophyllene in the absence and presence of α-pinene (hereafter '$SOA_{iso-BCP}$' and '$SOA_{iso-BCP-ap}$') were conducted in the campaign in November 2020 (named 'SOA20b') at 293K. The SOA generation process is similar to that described in the previous section (3.1.2), are illustrated in the following schematic:

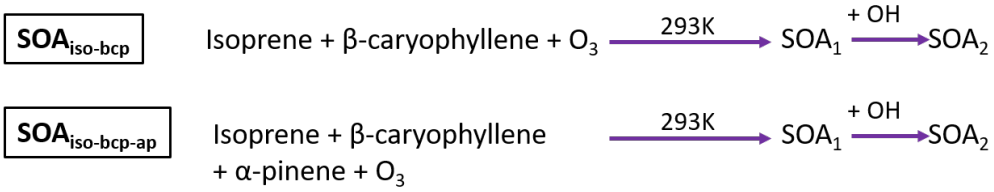

After the VOCs (two or three precursors) are added into the AIDA chamber, O_3 is added to form stable SOA particles, followed by OH radical addition from TME reacting with O_3. The detailed experimental conditions are listed in Table 3.

Table 3. Experimental conditions for SOA from α-pinene and isoprene mixture.

Exp No.	SOA type	VOCs conc. [ppb]			O_3 conc. [ppb]	RH [%]
		isoprene	β-caryophyllene	α-pinene		
1	$SOA_{iso\text{-}BCP}$	105±21	6.9±1.4	-	1082	39
2	$SOA_{iso\text{-}BCP\text{-}ap}$	108±22	5.5±1.1		946	39

3.3 Aerosol density and yield calculation

SOA yields (Y_{SOA}) were calculated as

$$Y_{SOA}=\Delta M_{org}/\Delta VOC, \quad \text{(Eq. 1)}$$

where ΔM_{org} is the SOA mass formed from the reacted mass of VOC precursors (ΔVOC). Similarly, the yields of specific products, e.g. β-caryophyllinic acid, a characteristic product of the β-caryophyllene ozonolysis, are calculated as $\Delta M_i/\Delta VOC$, where ΔM_i is the mass concentration of specific products formed from the reacted mass of VOC.

Based on the measured vacuum aerodynamic particle size distributions (d_{va}) (HR-TOF-AMS) and the mobility particle size distributions (d_m) simultaneously measured by a SMPS, the SOA density is calculated by the following equation (DeCarlo et al., 2004; Katrib et al., 2005; Saathoff et al., 2009b), assuming reference density of 1.0 g m^{-3} and spherical nonporous particles.

$$\rho = \frac{d_{va}}{d_m}, (g\ m^{-3}) \quad \text{(Eq. 2)}$$

3.4 Volatility determination

Volatility of the organics is a key property to determine their partitioning between gas and particle phase, which is usually expressed as the saturation vapor pressure (V_p, in Pa), and the effective saturation concentration (C^*, in μg m^{-3}) (Pankow, 1994b; Donahue et al., 2011):

$$C^* = \frac{V_p M_w}{RT}, \quad \text{(Eq. 3)}$$

M_w refers to the molecular weight of a compound, R is the molar gas constant, 8.314 J K^{-1} mol^{-1}, T is temperature in K.

SOA is usually a complex mixture composed of hundreds to thousands of mainly unknown organic compounds, and hence it is hard to evaluate the contribution of individual compounds to the bulk volatility. Thus, organics are treated by being classified into several volatility spaced bins (Donahue et al., 2009; Donahue et al., 2011; Donahue et al., 2012; Schervish and Donahue, 2020):

Volatility class	$\log_{10}C_{sat}$ (μg m^{-3})
ULVOC	< -8.5
ELVOC	(-8.5, -4.5)
LVOC	(-4.5, -0.5)
SVOC	(-0.5, 2.5)
IVOC	(2.5, 6.5)
VOC	> 6.5

In this work, I used two methods to estimate saturation concentration of individual molecules which may include one or more isomers. The volatility calibration method determines the effective saturation concentration, which is described in the following section 3.4.1. The formula method estimates the saturation concentration, and will be described in the section 3.4.2. Additionally, I applied thermogram PMF method to determine the effective saturation concentration of compounds, which will be illustrated in the section 3.4.3.

3.4.1 Volatility calibration

Heating aerosol particles collected on a filter in FIGAERO inlet of the CIMS, individual molecules with varying volatilities show different responses during the thermal desorption process. The temperature correspond to the concentration peak of a certain compound in the thermogram (T_{max}) correlates to the effective saturation vapor pressures of compounds in a complex mixture (Lopez-Hilfiker et al., 2014), i.e., SOA. By measuring the correlation between the T_{max} and the vapor pressure of known organic species, the C^*_{298K} of all the detected molecules can be quantified (Lopez-Hilfiker et al., 2014; Stark et al., 2017; Bannan et al., 2019; Ylisirniö et al., 2021).

In this work, volatility calibration is done with eight commercially available carboxylic acids and their vapor pressures from literature values (listed in Table 4). All eight organic acids are dissolved together in methanol, and then deposited on a Teflon filter using a syringe, followed by the same thermal desorption procedure used in the treatment of other particle samples in the

FIGAERO inlet. The concentration of organic acids differs to simulate the complex SOA particle mixtures studied in this work. For the FIGAERO-CIMS used in this work, the correlation between T_{max} and the known saturation vapor pressures of these organics was determined as $\log_{10}V_p = -0.48-0.04 \times T_{max}$, as shown in Figure 10.

Table 4. Summary on the chemicals used for volatility calibration, mixing ratios, T_{max}, and V_p.

Organic compound	Formula	Molecular weight (g mol^{-1})	Mixing ratio (10 solutions)										T_{max} (°C)	V_p (×10^{-4} Pa)	Ref. for V_p
			1	2	3	4	5	6	7	8	9	10			
Malonic acid	$C_3H_4O_4$	104	0.03	0.02	1	-	-	-	-	-	-	-	84^{+43}_{-22}	6.2	a
Succinic acid	$C_4H_6O_4$	118	0.02	0.07	-	1	-	-	-	-	-	-	70^{+21}_{-22}	13	a, b
Glutaric acid	$C_5H_8O_4$	132	0.02	0.13	-	-	1	-	-	-	-	-	65^{+26}_{-17}	$6.9^{+3.1}_{-2.9}$	a, b
Adipic acid	$C_6H_{10}O_4$	146	0.02	0.15	-	-	-	1	-	-	-	-	70^{+21}_{-0}	1.8	a, b
Pinonic acid	$C_{10}H_{16}O_3$	184	0.09	0.28	-	-	-	-	1	-	-	-	51^{+31}_{-16}	$102.8^{+197.2}_{-102.2}$	c, d, e
Azelaic acid	$C_9H_{16}O_4$	188	0.03	0.15	-	-	-	-	-	1	-	-	84^{+16}_{-0}	$0.067^{+0.007}_{-0.007}$	a, b
Tricarballylic acid	$C_6H_8O_6$	176	0.01	0.08	-	-	-	-	-	-	1	-	155^{+0}_{-23}	3.1×10^{-3}	f
β-caryophyllinic acid	$C_{14}H_{22}O_4$	254	0.78	0.04	-	-	-	-	-	-	-	1	89^{+52}_{-0}	3.3×10^{-9}	g

a, Bilde et al. (2015); b, Chattopadhyay and Ziemann (2005); c, Salo et al. (2010); d, Booth et al. (2011); e, Hartonen et al. (2013); f, Nannoolal et al. (2008); g, Li et al. (2011b).

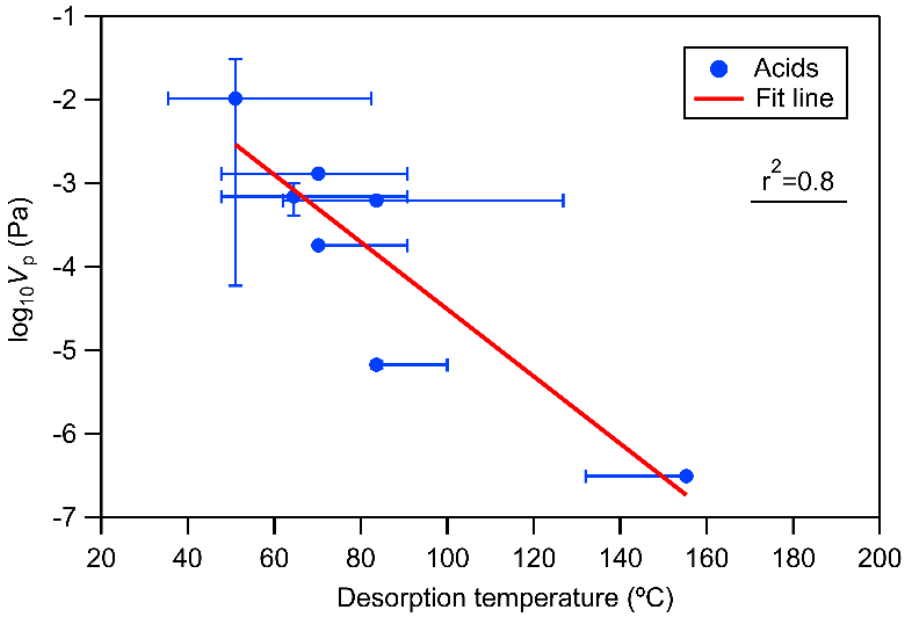

Figure 10. Correlation between temperatures of maximum desorption (T_{max}) and the known saturation vapor pressures (V_P) of seven carbocyclic acids.

3.4.2 Formula method

Considering the wide variety of functional groups in the molecular corridors, Donahue et al. (2011) and Li et al. (2016) put forward to a set of parameterization of volatility by characterizing the correlation between molecular weights and volatilities more than 30000 compounds, to allow prediction of the C_{sat} of unknown organic compounds from basic elemental information.

For the components containing only C, H, O, N:

$$\log_{10} C_{sat,298K} = (n_C^0 - n_C)\, b_C - n_O\, b_O - 2\, \frac{n_C n_O}{n_C + n_O}\, b_{CO} - n_N b_N \qquad \text{Eq. (4)}$$

where n_C^0, b_C, b_O, b_{CO}, and b_N are the included parameters (Table 5), n_C, n_O, n_N are the numbers of carbon, oxygen, and nitrogen, respectively (Li et al., 2016).

Table 5. Parameterization on volatility of molecules according to Li et al. (2016).

classes	n_C^0	b_C	b_O	b_{CO}	b_N
CHO	22.66	0.4481	1.656	-0.7790	
CHON	24.13	0.3667	0.7732	-0.0779	1.114

The saturation concentration at other temperatures can be estimated via the Clausius-Clapeyron equation (Donahue et al., 2006; Cappa and Jimenez, 2010):

$$\log_{10} C_{sat}(T) = \log_{10} C_{\mathrm{sat,298K}} + \frac{\Delta \mathrm{H}_{vap}}{R \ln(10)} \left(\frac{1}{298} - \frac{1}{\mathrm{T}}\right) \qquad \text{Eq. (5)}$$

The corresponding evaporation enthalpy ΔH_{vap} can be estimated according to Epstein et al. (2010) by

$$\Delta H_{vap}(kJ\ mol^{-1}) = -5.7 \times log_{10} C_{sat,298K} + 129 \qquad \text{Eq. (6)}$$

3.4.3 Thermogram positive matrix factorization (thermogram PMF)

Positive matrix factorization (PMF) has been developed to resolve the identities and contributions of components in a complex mixture (Paatero and Tapper, 1994; Lanz et al., 2007; Reff et al., 2007; Jimenez et al., 2009; Ulbrich et al., 2009), i.e., mass spectra with hundreds to thousands of compounds and their time series. In aerosol chemistry, PMF has been widely used to apportion the PM source in ambient measurements, especially for the dataset from the HR-TOF-AMS (Lee et al., 1999; Zhang et al., 2005; Ulbrich et al., 2009; Waked et al., 2014; Smith et al., 2022). Recently, PMF is also employed to analyze FIGAERO-CIMS data to deconvolute the

thermograms and to resolve different volatility factors to study the particle volatility at a molecular level (Buchholz et al., 2020; Tikkanen et al., 2020; Li et al., 2021).

As a bilinear model, PMF can be mathematically represented as

$$\mathbf{X} = \mathbf{GF} + \mathbf{E}\ , \qquad \text{(Eq. 7)}$$

When applying to the thermogram data from FIGAERO-CIMS, **X** refers to a $m \times n$ matrix which composed of normalized measured signal (ncps) with m rows of identified ions from the mass spectra, and n columns of time series of each ions over the thermal desorption period. **G** is a $m \times p$ matrix which contains the factor time series as columns and factor mass spectra as rows, and thus **F** accounts for the factor mass spectra as a $p \times n$ matrix. The $m \times n$ matrix **E** then contains the residuals of fitting output relative to the raw input data. The number of factors (p) has to be chosen by users due to no priori conditions are input. That is, the user can choose the best solution (i.e. number of factors) which fits the data best according to the solution uncertainty ($\mathbf{S}_{ij}$). The degree of freedom of the model solution Q_{exp}, is roughly equal to:

$$Q_{\text{exp}} \approx n \cdot m\ . \qquad \text{(Eq. 8)}$$

In parallel, a Q value for the solution is calculated as:

$$Q = \sum_{j=1}^{m} \sum_{i=1}^{n} \left(\frac{\mathbf{E}_{ij}}{\mathbf{S}_{ij}}\right)^2 \qquad \text{(Eq. 9)}$$

Q is calculated iteratively with a least square algorithm by constraining **G** and **F** values to be positive. The Q/Q_{exp} ratio is ideally equal to 1, which means the calculated modeled solution approaches the model degree of freedom.

$\mathbf{S}_{ij}$ is an important index because it can significantly influence the PMF output, and it can be altered by giving weight to data points that have fewer uncertainties (Paatero and Hopke, 2003).

$$S_{ij} = a \cdot \sqrt{\frac{\boldsymbol{X}_{ij}}{t_s}} + \delta_{noise,i}\ , \qquad \text{(Eq. 10)}$$

Where $\boldsymbol{X}_{ij}$ refers to the signal intensity of the ion i, t_s is the sampling time resolution in s, and $\delta_{noise,i}$ means the electronic noise of ion i. For my dataset of thermograms from FIGAERO-CIMS, I was mainly interest in the 'soak' and 'ramp' periods (section 3.3.1) where most organic species are desorbed to be within the main body of 'peaks' in their thermograms, but not in the start or the end of the thermograms. Thus, by weighting the data points that we are interested, a new error

scheme (so called 'CNerror') is introduced to emphasize on the thermogram peaks (Buchholz et al., 2020):

$$S_{ij} = \delta_{noise,i} , \quad \text{(Eq. 11)}$$

In my PhD work, all the PMF model related data is analyzed by me using a new established FIGAERO Thermogram PMF Evaluation Toolkit (PiT-PET, v.1.9, (Buchholz et al., 2020)) based on Igor 8 (Wave Metrics, Inc.). In brief, the analysis steps are as follows:

a). prepare data (input: mass spec data, mass error matrix, *m/z* values, ion names, desorption temperatures);

b). calculate and optimize the error (i.e. CNerror);

c). remove potential artificial ions (i.e. formic acid, lactic acid);

d). make a combined data set;

e). handle NaNs and choose downweigh factor (optional);

f). choose the range of number of factors, f_{peak} range;

g). run PMF model.

3.5 List of all chemicals used

chemical	formula	MW (g mol^{-1})	supplier	purity
Isoprene	C_5H_8	68.1	Sigma-Aldrich	95%
α-pinene	$C_{10}H_{16}$	136.2	Sigma-Aldrich	98%
^{13}C-isoprene	^{13}C-C_4H_8	69.1	Sigma-Aldrich	99%
β-caryophyllene	$C_{15}H_{24}$	204.4	Karlsruhe ROTH	98%
β-caryophyllinic	$C_{14}H_{22}O_4$	254.3	Toronto Research Chemicals	95%
Malonic acid	$C_3H_4O_4$	104.1	Merck	99%
Succinic acid	$C_4H_6O_4$	118.1	BDH Prolabo	100%
Glutaric acid	$C_5H_8O_4$	132.1	Merck	99%
Adipic acid	$C_6H_{10}O_4$	146.1	Merck	99%
Pinonic acid	$C_{10}H_{16}O_3$	184.2	Sigma-Aldrich	98%
Azelaic acid	$C_9H_{16}O_4$	188.2	Merck	88%
Tricarballylic acid	$C_6H_8O_6$	176.1	Sigma-Aldrich	99%

4 Results and Discussion

The characteristics of SOA formed from the oxidation of BVOC mixtures containing α-pinene and isoprene are presented in section 4.1. SOA formed by ozonolysis of β-caryophyllene is discussed in section 4.2 (no NO_x), and section 4.3 (with NO_x). Finally, I compare the chemical composition and volatility of SOA from the oxidation of BVOC mixtures of isoprene mixed with β-caryophyllene in the absence and presence of α-pinene (section 4.4).

4.1 SOA from oxidation of mixtures of isoprene and α-pinene

SOA from oxidation of mixtures of isoprene and α-pinene by O_3 and OH radicals was studied at 243K, 273K, 298K, and 313K with relative humidity ranging from 80-12%, respectively (Table 1). The mole ratios of VOCs : O_3 were fixed to ~0.2. The OH radicals were generated by the reaction of TME with O_3 with the same injection amount during all experiments. Reference experiments performed with α-pinene as the sole precursor were directly compared to the experiments with a mixture of α-pinene and isoprene.

Figure 11 compares the experiment with α-pinene alone and the mixture of both VOCs at 273K, showing the time evolution of precursors, oxidants, and particle concentrations for the two systems. The precursor VOC(s) were added first to the chamber, followed by the addition of O_3. The time zero is defined by the time point when O_3 was added for the first time. 7 minutes after O_3 addition (the end of period I), for the mixture experiment, ~28% of the initial α-pinene and ~7.5% of the initial isoprene were consumed. For comparison, ~37% of the initial α-pinene was reacted in the sole α-pinene system at the same time. Owing to the different rate constants with O_3 (Table 6) between these two precursors, ozonolysis of α-pinene is faster than isoprene, while OH radicals are more readily to react with isoprene. Specifically, OH radicals react about 2 times faster with isoprene (1.15×10^{-10}, IUPAC) than with α-pinene (5.84×10^{-11}, IUPAC) at 273K. As products of α-pinene reacting with O_3, OH radicals were found a yield of 79% at 273K (Tillmann et al., 2010). Thus, in the period I (Figure 11), VOCs underwent the reactions with both O_3 and OH radicals. In the period II, OH radicals were additionally added in substantial amounts. Thus, the ratio of OH radicals to O_3 was higher in the period II (OH radicals dominant) than the period I (O_3 dominant).

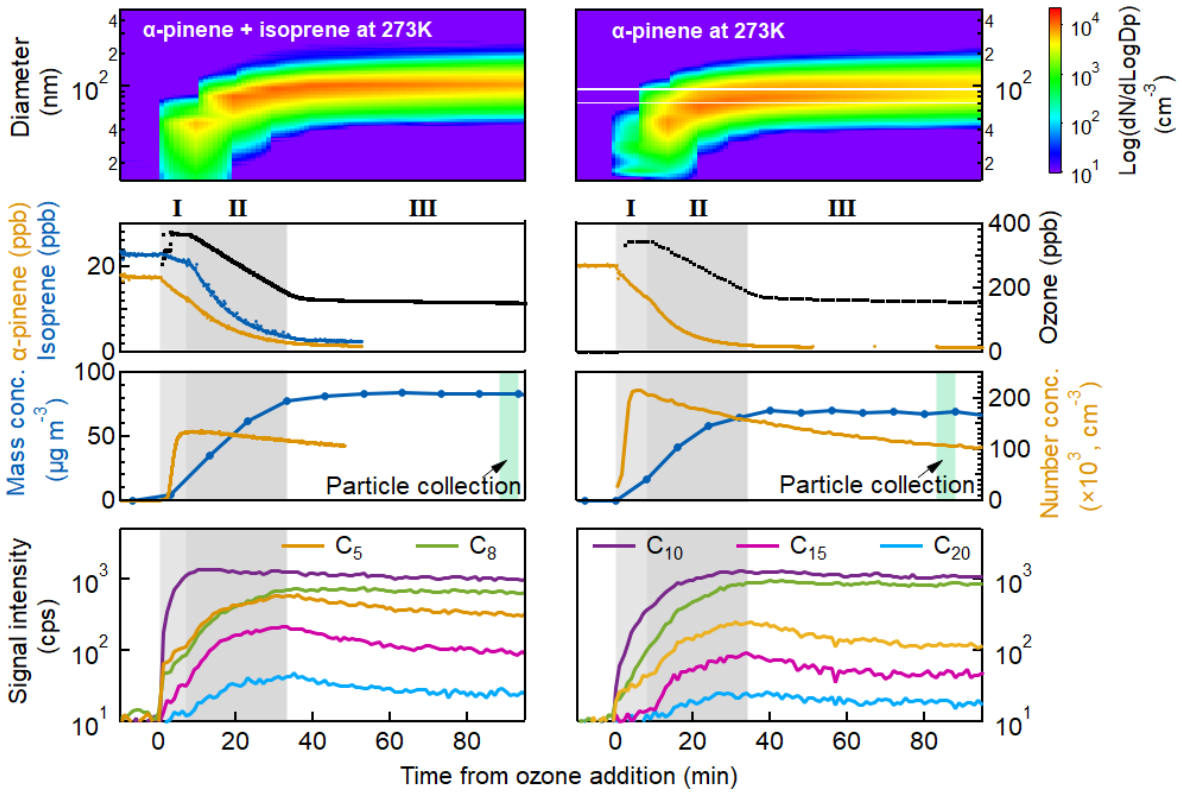

Figure 11. Experimental overview for the gas and particle phase at the experiments of mixture (left) and sole α-pinene (right) at 273K. First panel: particle size distribution. The color scale represents the log 10 of the normalized particle concentration in cubic centimeters (cm^{-3}). Second panel: mixing ratio in parts per billion by volume (ppbv) for α-pinene, isoprene, and O_3 concentrations. Third panel: particle mass concentration measured by SMPS using an assumed density of 1.3 g m^{-3}, and the number concentration for particles sized larger than 2.5 nm. The particles were collected during the time shown in the green shadow. Fourth panel: evolution of total signal intensities of C_5, C_8, C_{10}, C_{15}, and C_{20} carbon classes, measured in the gas phase by iodide-CIMS. The initial O_3 concentration at the sole α-pinene experiment is 345 ppb, and unfortunately the data for its evolution is unavailable due to an O_3 sensor defect. The time period (bright grey shaded) had only O_3 as oxidant, while period II (dark grey shaded) also had OH radicals formed by continuous addition of TME. The period III was after the TME addition.

As oxidation products, C_{10} compounds had the most rapid increase, followed by both the C_5 and C_8 classes in the experiment in presence of isoprene (Figure 11 left). However, the increase of C_8 class products was faster than C_5 compounds in the experiment without isoprene (Figure 11 right). As isoprene has a C_5 carbon skeleton, the higher contribution of C_5 compounds in the binary system is caused by monomeric oxidation products of isoprene, while the C_5 compounds in the sole α-pinene experiment are mainly fragments produced by the α-pinene ozonolysis. Furthermore, C_{15} products were formed in higher concentrations in presence of isoprene, which can be explained by the interaction of peroxy radicals derived from α-pinene and isoprene oxidation (Wang et al., 2021). In absence of pre-existing particles (seeds) in the chamber, new SOA particles nucleated shortly after adding O_3, shown in the top panel in the Figure 11, with mean diameters < 40 nm.

Without isoprene, a higher number concentration was observed, reaching ~2×10^5 cm^{-3}, compared to the binary system of 1.3×10^5 cm^{-3}. The suppression of the new particle formation by isoprene was found firstly by Kiendler-Scharr et al. (2009) with simulation experiments at 288K, and it was also observed in chamber studies conducted at 223K and 243K by Caudillo et al. (2021). This suppression of the new particle formation can be partially attributed to OH radical scavenging by isoprene Kiendler-Scharr et al. (2009).

Table 6. Preferred values of Rate coefficients of VOCs reacting with O_3, OH radical, and NO_3 radical from IUPAC (https://iupac-aeris.ipsl.fr/#).

VOC	oxidant	Rate coefficient (298K) cm^3 $molecule^{-1}$ s^{-1}	Rate coefficient (T) cm^3 $molecule^{-1}$ s^{-1}
α-pinene	O_3	9.6×10^{-17}	8.22×10^{-16} exp(-640/T), 240-370 K
α-pinene	OH radicals	5.3×10^{-11}	1.34×10^{-11} exp(410/T), 240-360 K
isoprene	O_3	1.28×10^{-17}	1.04×10^{-14} exp(-2000/T), 240-360 K
isoprene	OH radicals	1.0×10^{-10}	2.10×10^{-11} exp(465/T), 240-630 K
β-caryophyllene	O_3	1.2×10^{-14}	N/A
β-caryophyllene	OH radicals	2.0×10^{-10}	N/A
β-caryophyllene	NO_3 radicals	1.9×10^{-11}	N/A

Subsequently, after the OH radicals were generated (period II), the VOC precursors decreased faster in both experiments. Without isoprene, most oxidation product classes presented in Figure 11 continuously increased in the gas phase. In contrast, in the binary system, the C_{10} products seemed not to be formed anymore, even though the parent VOC α-pinene and isoprene still remained. There was no more formation of new particles larger than 2.5 nm, shown as the slight decrease of the particle number concentration in both systems. Hence, the oxidation products contributed to particle growth but not to new particle formation, visible by the increasing particle mass concentrations. The particles finally reached diameters of approximately 100 nm, which can act as ice nucleating particles or cloud condensation nuclei.

The TME injection and corresponding OH radical formation was stopped when isoprene and α-pinene were depleted. Afterward, the signal intensity of the gaseous oxidation products showed a slight decrease due to the partition of the particles and potentially owing to the wall losses, indicating there was no further formation of oxidation products in the gas phase. The particle mass concentrations reached stable levels of 66-83 μg m^{-3} as calculated from the measured size distribution assuming a constant particle density of 1.3 g/m^3 (Saathoff et al., 2009a). In the

following section, I will discuss the chemical composition and volatility of the relatively stable SOA present during the period (III).

4.1.1 Gas- and particle-phase chemical composition (273K)

To give an overview of the species measured in gas and particle phases for the two systems with and without isoprene at 273K, Figure 12 presents the carbon distribution and the oxygen content in the molecules. The products in the period II could be from the oxidation of the oxidized species formed in period I and the VOCs. Thus, the SOA present in the period III was a mixture of oxidation products from both time periods I and II and both oxidants.

The main oxidation products in both gas and particle phases, were $C_{8\text{-}10}H_yO_{4\text{-}6}$, followed by $C_5H_yO_{3\text{-}5}$ and $C_{11\text{-}16}H_yO_{2\text{-}8}$ which had larger fractions in the experiment with isoprene. Heinritzi et al. (2020) and Caudillo et al. (2021) have shown that the formation of C_{15} dimers can be enhanced due to the termination reaction between C_{10} peroxy radicals from α-pinene ozonolysis and C_5 peroxy radicals from isoprene oxidation with OH radicals, and hence preventing the formation of $C_{18\text{-}20}$ dimers from α-pinene ozonolysis. With the same explanation, Wang et al. (2021) reported that C_{11}, C_{12}, and C_{14} compounds may also be dimers originating from the interaction of oxidation products from both VOCs, and their formation may also be enhanced by the presence of isoprene. However, this work found no significant suppression effect of isoprene on the $C_{18\text{-}20}$ products, although the corresponding $C_{11\text{-}15}$ dimers were formed in significantly higher quantities in presence of isoprene (Figure 14). This may result from the difference for conditions with higher isoprene to α-pinene concentration ratios.

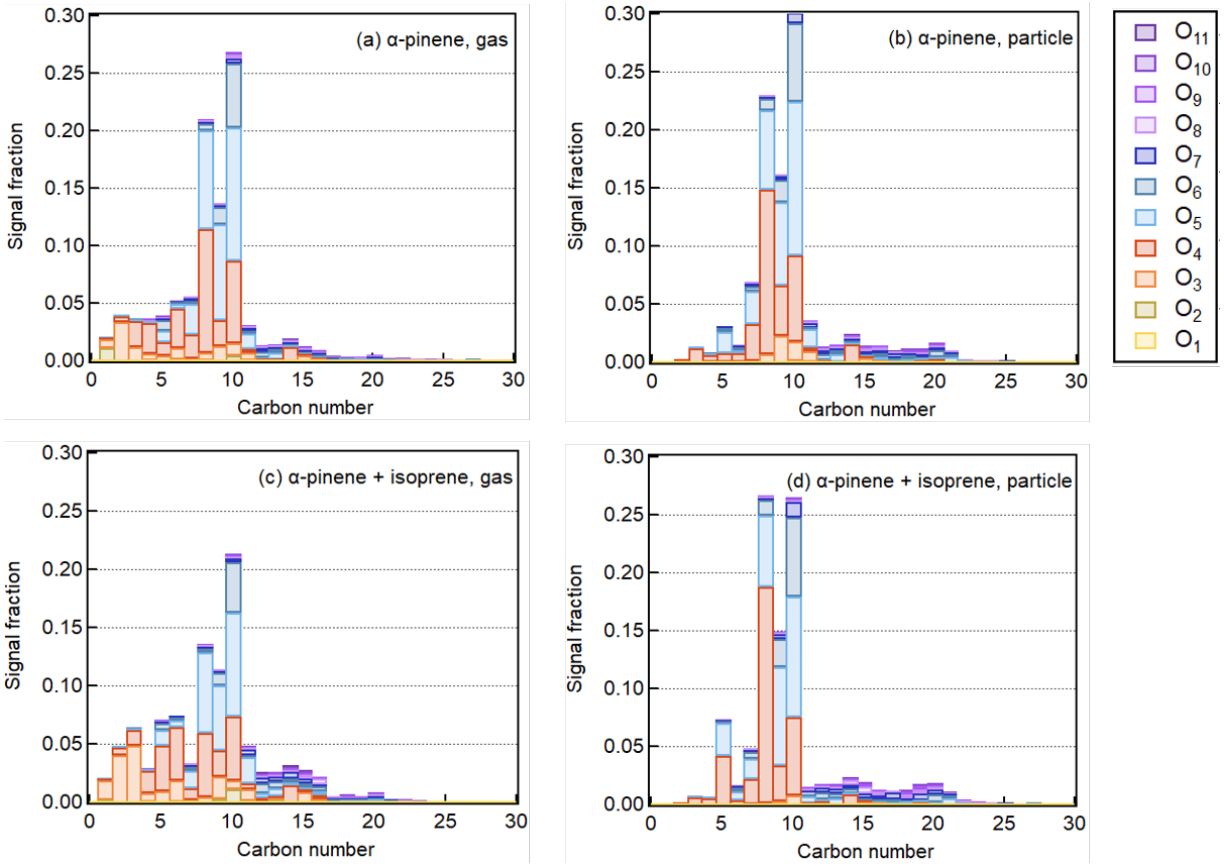

Figure 12. Carbon atom distribution and oxygen atom content in the molecules for the gas- and particle- phase oxidation products of α-pinene with and without the presence of isoprene at 273K. Both phases are measured with iodide-CIMS, while the FIGAERO is used for the particle-phase measurements. The signal intensities have been normalized to the total signals in each experiment and phase. Colors refer the specific number of oxygen atoms ranging between 1 and 11.

The $C_{8\text{-}10}H_yO_{4\text{-}7}$ compounds dominated the gas- and particle-phase composition in the sole α-pinene system, clearly identifying them as α-pinene derived oxidation products. This was consistent with the measurements conducted by Zhang et al. (2017), who firstly characterized the HOMs molecules from α-pinene oxidation as $C_{8\text{-}10}H_{12\text{-}18}O_{4\text{-}9}$. It was seen that $C_8H_yO_4$ had an larger signal fraction in the particle phase in presence of isoprene (18.4±0.6% in Figure 12 d), compared to that in the sole α-pinene experiment (14.1±1.5% in Figure 12 b). The increase of the signal fraction of the C_8 class was mainly contributed by $C_8H_{12}O_4$, as shown also in Figure 15 d. $C_8H_{12}O_4$ has been consistently identified as one of the major α-pinene derived products termed as norpinic acid (Jenkin, 2004; Lopez-Hilfiker et al., 2015) or its isomer terpenylic acid (Claeys et al., 2009; Gao et al., 2010). The terpenylic acid was suggested to be formed during the OH-initiated α-pinene oxidation after intramolecular isomerization via the norpinic acid channel (Claeys et al., 2009). Besides the $C_8H_{12}O_4$ iodide adduct ($C_8H_{12}O_4I^-$), the signal intensity of the ion after losing a

hydrogen iodide ($C_8H_{11}O_4^-$) was also significant. The left panel in Figure 16 shows the time evolution of $C_8H_{12}O_4I^-$ and $C_8H_{11}O_4^-$ in the two experiments at 273K. It was obvious that the molecules related to the $C_8H_{12}O_4I^-$ and $C_8H_{11}O_4^-$ were formed in the O_3 dominated period I of both experiments. However, the $C_8H_{11}O_4^-$ reached a stable level before the end of the OH radicals dominated period II, while the iodide adducts ($C_8H_{12}O_4I^-$) kept being formed over the whole period. The different responses to the high concentration of OH radicals indicate that $C_8H_{12}O_4I^-$ and $C_8H_{11}O_4^-$ correspond to isomers with different structures, e.g., norpinic acid and terpenylic acid. Due to their different molecular structures and functional groups, they have also different volatilities which affects their phase partitioning. This will be discussed in the next section in more details. However, it cannot be excluded that $C_8H_{12}O_4$ could be a fragment of the dimers which were formed from reaction of bimolecular peroxy radicals. A similar case was observed for $C_9H_{14}O_4I^-$ and $C_9H_{13}O_4^-$, which are likely to be pinic acid and are the potential block for dimer formation (Gao et al., 2010) (Lopez-Hilfiker et al., 2015).

Figure 13. Structures of two isomers of $C_8H_{12}O_4$: norpinic acid (left) identified by Kołodziejczyk et al. (2019), and terpenylic acid (right) determined by Claeys et al. (2009).

It was evident that HOM molecules containing at least 6 oxygen atoms per molecule contributed only a small fraction, potentially due to the low sensitivity of iodide adduct CIMS. Most of them had 8 carbon atoms per molecule. Compounds with O:C ratio above 0.6 contributed 22.7±0.2% to the total signals in the sole α-pinene system, slightly less compared with 24.5±1.6% in the mixture system.

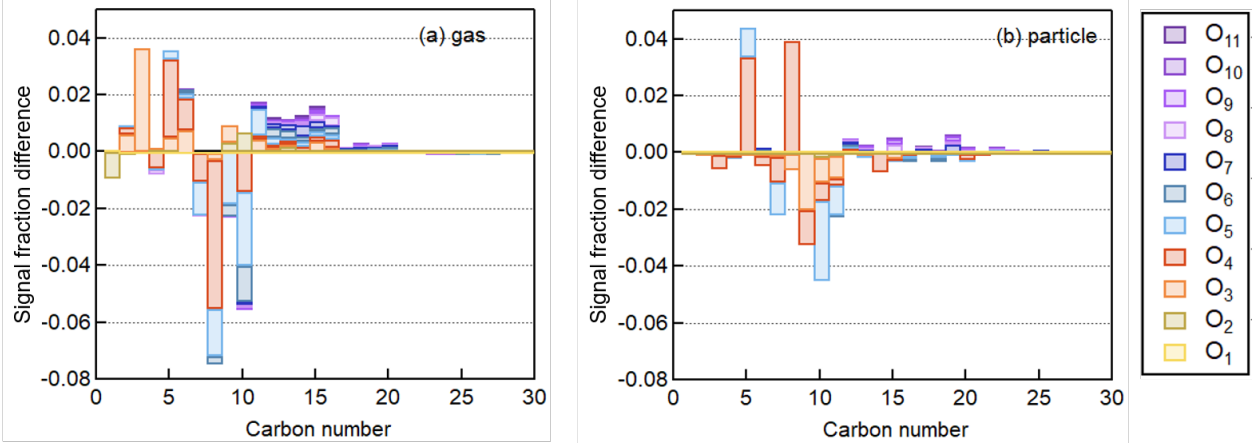

Figure 14. The signal fraction difference for gas (a) and particle phases (b) between two SOA formation experiments of α-pinene with and without isoprene present. The difference is indicated by the signal fraction of each product class from the binary system minus the reference system. The colors represent the oxygen atom per molecule.

Besides, also shown as Figure 14, The $C_{9\text{-}10}H_yO_{4\text{-}6}$ species have a substantially lower abundance in the binary system. This can be explained by a so-called termination reaction of peroxy radicals derived from α-pinene by the peroxy radicals from isoprene, resulting in the reduced formation of the closed-shell monomeric $C_{7\text{-}10}$ products compared with the experiment without isoprene. The increase of the signal fractions of all C_5 molecules results from the contribution of typical isoprene derived oxidation products, e.g., IEPOX (D'Ambro et al., 2019), including $C_5H_{12}O_4$ and $C_5H_{10}O_{3\text{-}5}$. It was seen that higher oxygenated molecules, e.g., the number of oxygen atoms per molecule > 6, contributed more in presence of isoprene.

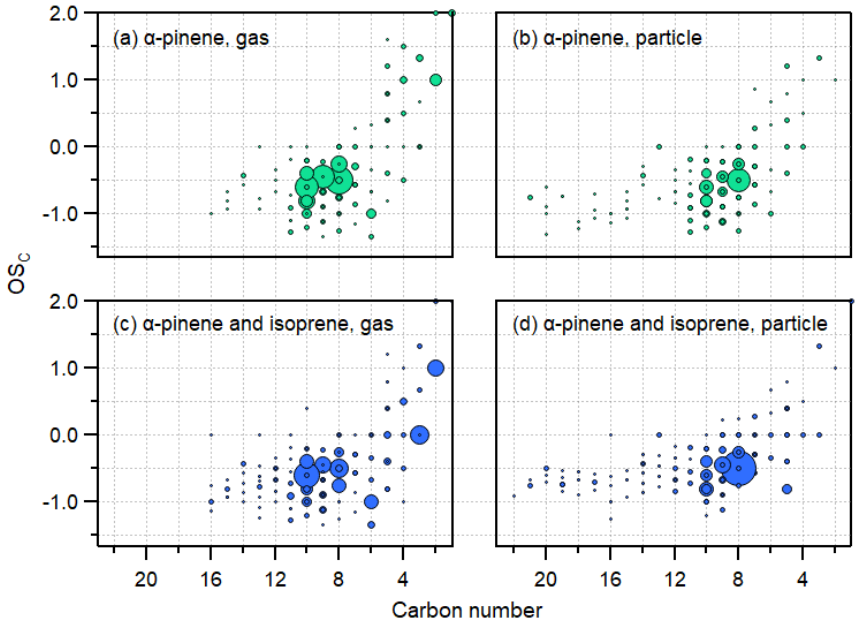

Figure 15. Chemical composition for both gas and particle phases for the sole α-pinene (a, b, green dots), and mixture (c, d, blue dots) SOA expressed as molecular carbon oxidation state (OS_C) corresponding to the number of carbons.

A comprehensive mapping of the molecular carbon oxidation state (OS_C) as a function of carbon number for both gas and particle phase molecules is shown in Figure 16 for both systems. As no nitrogen is involved, OS_C discussed in this chapter is defined as 2×O:C - H:C. The OS_C is supposed to have a strong correlation with volatility, and thus a useful parameter for studying the oxidation of organics that only includes elemental carbon, hydrogen, and oxygen (Kroll et al., 2011). SOA compounds with semi-/low volatility have OS_C values between -1 and +1 for molecules with less than 14 carbon atoms (Kroll et al., 2011). It was seen that the majority of signals in the sole α-pinene system comprised components at $C_{8\text{-}10}$ for the gas and particle phases, with signal-weighted averaged OS_C between -1 and -0.25. These results are comparable to the typical monoterpene ozonolysis SOA that has OS_C falling between -1.1 and 0.5. The overall mean OS_C value for the gas phase was -0.32 for sole and -0.38 for mixture systems, respectively. In the binary system, lower oxygenated $C_{8\text{-}10}$ species (e.g., $C_8H_{12}O_3$ with a molecular OS_C of -0.75) contributed more in the gas phase, resulting in a slightly lower overall OS_C, although the fraction of smaller and higher oxygenated molecules (C_2-C_6) was also higher. The OS_C value in the particle phase in the binary system was -0.49±0.02, a little higher than that for the sole precursor system (-0.52±0.00).

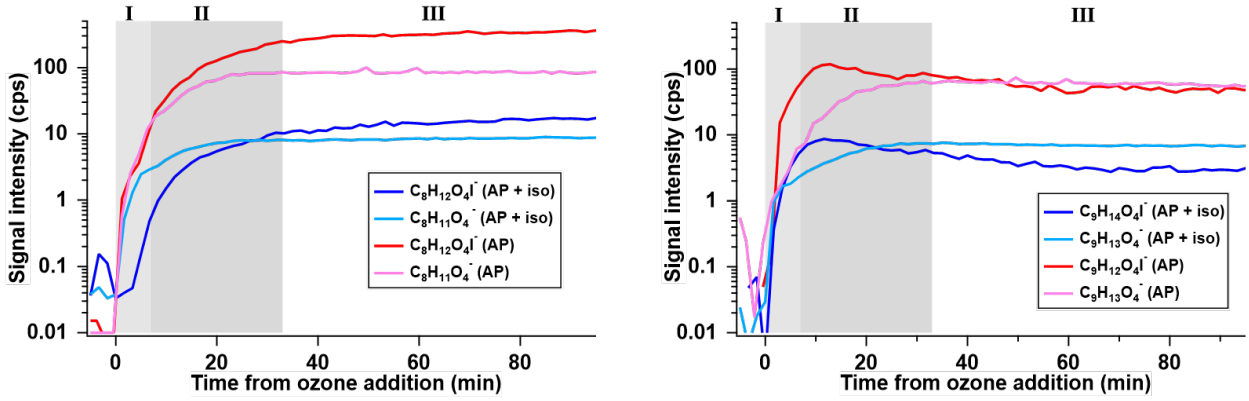

Figure 16. Gas phase evolution of $C_8H_{12}O_4I^-$, $C_8H_{11}O_4^-$, $C_9H_{14}O_4I^-$, and $C_9H_{13}O_4^-$ for the oxidation experiments with only α-pinene (red and pink lines) and a mixture of α-pinene and isoprene (light and dark blue lines). Period I was dominated by ozonolysis, while during period II OH radicals significantly contributed to oxidation of the VOC and their oxidation products

4.1.2 SOA volatility

Particles collected on Teflon filters and analysed by the thermal desorption in the FIGAERO inlet of the iodide-CIMS after the experiments. Volatility analysis of these organic compounds was based on the interpretation of the thermograms of corresponding ions as a function of

desorption temperatures. Total thermograms of major molecules in the sole α-pinene and the binary systems are presented in Figure 17 (a) for 273K. The total thermogram of the particle phase compounds formed in the binary system was signifcantly shifted to higher desorption tempeartures compared to the sole α-pinene system. This clearly shows that the particle phase compounds formed from the precursor mixture have lower effective volatilities and hence are less volatile than the compounds in the α-pinene SOA. Besides, it is shown in Figure 17 (b) that the T_{max} of individual molecule in the one precursor system is generally lower than that in the binary system. This can be explained by a higher viscosity of the particles from the binary system probably due to an increased abundance of higher molecular weight components, and in turn lower the particle volatility. This is somewhat counterintritive because sole isoprene SOA was found to have a lower viscosity than the sole α-pinene SOA at the same relative humidity (DeRieux et al., 2018).

It has been found that the viscosity generally increases with a decrease particle mass concentration (Champion et al., 2019). However, in this work, as the total normalised signals in mono-precursor system was $(4.2\pm0.1)\times10^7$ cps, comparable to that in the binary system of $(4.8\pm0.4)\times10^7$ cps, the potential impact of particle mass concentration could be excluded to change the particle viscosity. Besides, higher molecular weight and increased degree of functionalization of the organic species have also been found to lead to higher viscosity. As discussed previously, the OS_C for the particle phase compounds in the mono-precursor system was -0.52±0.00, reflecting lower oxygenation status than that in the mixture system (OS_C= -0.49±0.02). However, the particles in both systems had similar signal weighted mean molecular masses, with an average molecular formula of $C_{9.7}H_{15.4}O_{4.8}$ and $C_{9.7}H_{15.2}O_5$ in sole and binary systems, respectively. A larger fraction of heavier molecules, e.g., $C_{>10}H_yO_{>6}$, in the binary system enhanced the average molecular weight. Therefore, the higher viscosity in the binary system may be partially explained by oligomerization or other particle-phase processes that lead to higher molecular weight and lower O:C and OS_C (Yli-Juuti et al., 2017; Champion et al., 2019). For example, in this work, $C_{>10}H_yO_{>6}$ in the binary system contributed to (8.3±0.2)% of all compound signals, higher than that in the sole α-pinene system of (5.7±0.3)%.

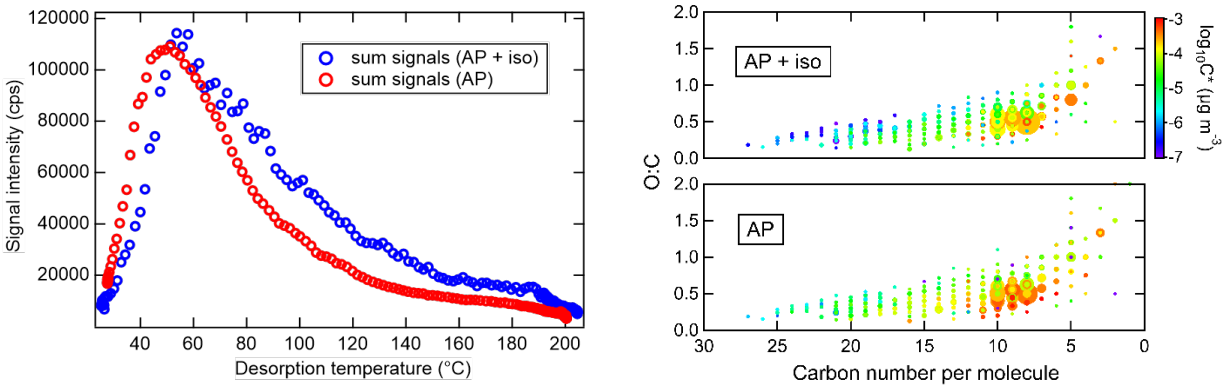

Figure 17. Sum thermograms of the particles from one and two VOC (left) and particulate molecular O:C ratio as a function of the carbon atom number per molecule (right). In the right panel, colors of the dots show the saturation concentration ($\log_{10}C^*$) of individual molecules, and the sizes are related to their abundance.

Despite of this, this work supports that the molecules with higher O:C ratios have plausibly lower volatilites for a fixed length of the carbon chain Figure 17 (b). For example, among all C_{10} molecules, an increase of number of oxygen atoms per molecule went along with lower saturation vapor pressures. Please note that this was not applicable to isomers. It can be seen that the saturation concentrations of all molecules were lower than 10^{-3} μg m^{-3}, with the voaltility prediction on basis of the calibrated correlation between vapor pressures and T_{max}. Figure 18 presents the volatility distribution mapped in a one dimensional volatility basis set (1D-VBS) framwork (Donahue et al., 2006) with signal fractions corresponding to logarithmic 298K effective saturation concentrations. Considering the particles formed at 273K, the ULVOC and ELVOC ranges at 273K were shifted to be with corresponding 298K $\log_{10}C^*$ lower than -5.8 μg m^{-3}, and between -5.8 and -1.8 μg m^{-3}, respectively. Briefly, in the sole α-pinene system, the majority (~98.6%) of species fell in the ELVOC range with $\log_{10}C^*$ between -5.5 to -2.5 μg m^{-3}. In the binary system, ~90.5% signals were in ELVOC bins, wherein ~9.5% species were ultra-low volatile. In detail, the relative abundance of components in the most volatile bins ($-3.5<\log_{10}C^*<-2.5$ μg m^{-3}) was reduced in the particles that are formed in presence of isoprene. The increase in the relative abundance of lower volatile classes ($\log_{10}C^*<-3.5$ μg m^{-3}) can result for two reasons. On the one hand, the T_{max} of a molecule in the binary system is higher than the T_{max} of the same molecule in the sole precursor system. This could be due to the increase in the viscosity of the particles formed in the binary system, as discussed above. On the other hand, the formation of species of lower volatility was promoted in presence of isoprene. For example, a higher abundance of $C_8H_{12}O_4$ and $C_5H_{12}O_4$ in the binary system was mapped into the bin between $\log_{10}C^*$ of -4.5

and -3.5. Lower volatile components that had higher relative abundance in the binary system, such as $C_{>10}H_yO_{>6,}$ leading to the higher signal fraction in the volatility bins ($log_{10}C^*$<-4.5).

It was clear that the particles formed in presence of isoprene were less volatile than the particles formed from the sole α-pinene oxidation. This suggested that, the particles from the binary system may have higher potential to act as cloud condensation nuclei or as ice nucleating particle. However, this finding seems to disagree with other studies that isoprene can suppress the formation of C_{20} components with lower volatiltiy, and enhance the formation of C_{15} species with relatively higher volatility (McFiggans et al., 2019; Wang et al., 2021). The discrepency could result from that, the potential suppressed HOM molecules (α-pinene derived dimers) detected by others, for example, using nitrate CIMS (Heinritzi et al., 2020), are not in a sensitive measurement range of iodide-CIMS in this work. Another reason is that, the suppression by isoprene can be higher resulting from a higher isoprene to α-pinene ratio, e.g., 3:1 and 15:1 (Wang et al., 2021; Caudillo et al., 2021). As shown in Figure 12, although the molecules with more than 6 oxygen atoms could be dectected, the majority of the signals in this work accounted for the median oxygenation species with 2-6 oxygen numbers.

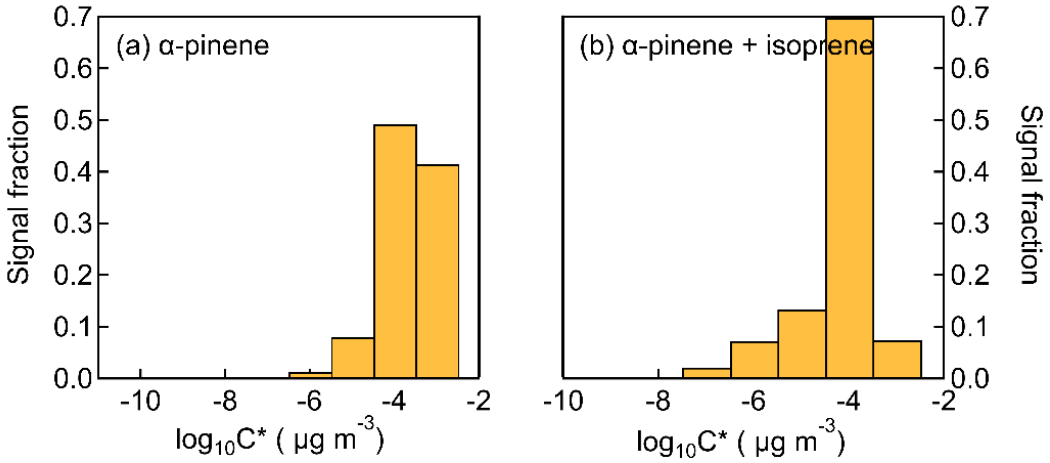

Figure 18. One-dimension volatility basis set (1D-VBS) with signal fraction as a function of logarithmic effective saturation concentration for the sole α-pinene system (a) and the isoprene α-pinene mixture system (b). The effective saturation concentration is estimated from calibrated T_{max} values.

4.1.3 The impact of temperature

Figure 19 shows the particulate signal distribution of major carbon groups: C_5, C_8, C_9, C_{10}, $C_{11\text{-}15}$, and $C_{16\text{-}20}$. It could be seen that the $C_{8\text{-}10}$ species dominated the particle phase compounds at 243K, 273K, 298K, and 313K, accounting for 49.5±1.0%, 67.5±0.4%, 52.6±0.4%, and

56.9±0.2%, respectively. Components in the dimer/trimer range (C_{11-20}) contributed 36.4±1.7%, 16.1±0.5%, 21.9±0.8%, 24.5±0.4%, repsectively. Specificly, the components with 10 carbon atoms were the most abundant group in the particles at 243K.The relative abundance of C_{10} increased with decreasing SOA formation temperatures. Among all species with 10 carbon atoms, the formation of the low oxygenated molecules ($C_{10}H_yO_{1-5}$) showed a negative monotonic correlation with SOA formation temperatures (Figure 19 (c)), suggesting that the fromation of early-stage oxidation products of α-pinene, such as pinonic acid ($C_{10}H_{16}O_3$), was significantly temperature dependent. However, the portion of high oxygenated species ($C_{10}H_yO_{6-9}$) increased from 243-298K, and had a slight decrease at 313K. This is consistent with the finding that α-pinene derived HOM formation is favoured by high temperatures (Bianchi et al., 2019). Besides, as $C_8H_yO_{1-3}$ only consisted of no more than 0.5% of the total signals for all temperatures, they will not be discussed in detail. It is seen in Figure 19 (e-g) that both $C_8H_yO_5$ and $C_8H_yO_{6-8}$ species had higher signal fractions with increasing temperatures.

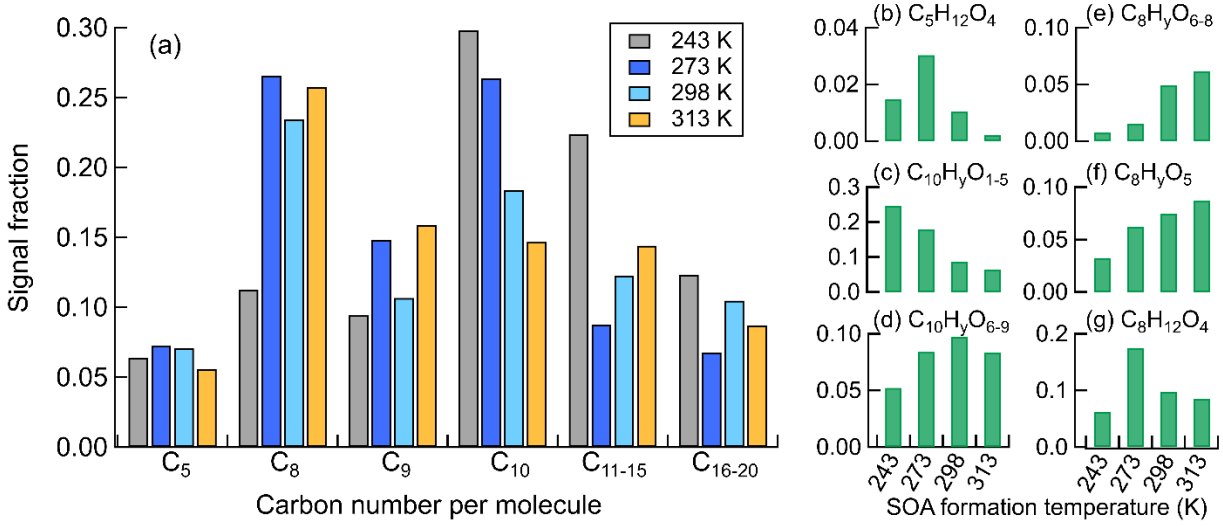

Figure 19. Carbon atom number per molecule distributions for C_5, C_8, C_9, C_{10}, C_{11-15}, C_{16-20} species in the particles formed at 243-313K (a). The signal fraction of $C_5H_{12}O_4$, $C_{10}H_yO_{1-5}$, $C_{10}H_yO_{6-9}$, $C_8H_yO_{6-8}$, $C_8H_yO_5$, and $C_8H_yO_4$ as a function of temperature is shown as (b)-(g).

As an identified block for formation of α-pinene derived dimers (like $C_{17}H_{26}O_6$ (Zhang et al., 2015)), $C_8H_{12}O_4$ was abundant but has nonmonotonic correlation with SOA formation temperatures, contributing 6.1±0.0%, 17.1±0.6%, 10.0±0.3%, and 9.5±0.4% from 243K to 313K. The lowest relative abundance of $C_8H_{12}O_4$ at 243K could be explained by the fact that the formation of $C_8H_{12}O_4$ via C-C bond cleavage is reduced at lower temperatures as the case of other C8 species shown in Figure 19 (e) and (f). Another explanation could be the enhanced formation

of dimers from C_8 compounds at lower temperatures. One explanation of the decrease of $C_8H_{12}O_4$ above 273K is that, more dimers were formed with $C_8H_{12}O_4$ as one of the parent via e.g., accreation reaction. This is in agreement with the strong thermal decomposition at higher desorption temperatures leading to $C_8H_{12}O_4I^-$ ion in from particles formed at the temperatures above 273K, as shown in Figure 20 (a). A second mode in the thermograms of $C_8H_{12}O_4I^-$ for particles formed at 298K and dominated most for signal aera of the $C_8H_{12}O_4I^-$ ions detected. For particles formed at 313K, $C_8H_{12}O_4I^-$ ions had a T_{max} of ~120 °C, indicating a thermal decomposition from heavier molecules such as dimers. To compare, there was no significant second peak existing in the $C_8H_{12}O_4I$- thermograms detected from the particles formed at 243K and 273K. This indicates that formation of the related thermal unstable dimers (or oligomers) is favoured at higher temperatures. Using the parameterization approach for the glass transition temperature prediction by DeRieux et al. (2018), the glass transition temperature (T_g) was estimated to be 289K and 278K, higher than the particle formation temperatures of 243K and 273K, respectively. This suggests that the particles formed below 273K are likely to be in a semi-solid or glassy state. In contrast, the T_g for the particles at 298K and 313K were calculated to be 283K and 285K, indicating those particles to be liquid. This supports the possibility that the formation of dimers (or oligomers) related to $C_8H_{12}O_4$ could take place in the condensed phase.

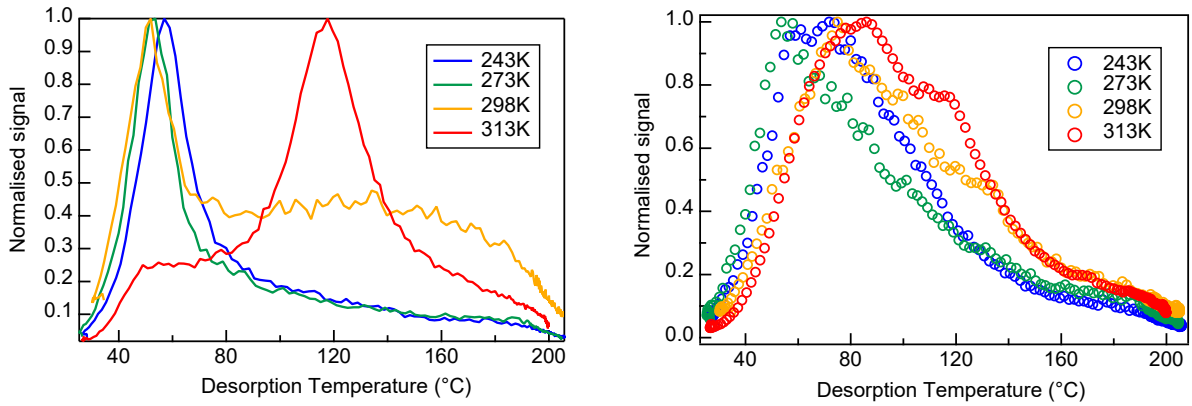

Figure 20. The thermograms of total ions (left) and $C_8H_{12}O_4$ (right) for the particles formed at 243K (blue), 273K (green), 298K (yellow), and 313K (red).

Additionally, the potential interaction of products from α-pinene and isoprene oxidation are expected to have carbon skeleton between $C_{11\text{-}15}$. The relative abundance of the $C_{11\text{-}15}$ compounds was higher at increasing SOA formation temperatures, potentially resulting from stronger interaction reactions. However, the signal fraction $C_{16\text{-}20}$ group showed a non monotonic correaltion with temperatures, which was expected to contain the potential α-pinene derived

dimers. This suggests that the formation of low oxidized α-pinene derived dimers might include by other mechanisms, e.g., heterogeneous reactions.

The total thermograms of all detected ions from the particles formed at 243K, 273K, 298K, and 313K are presented in Figure 20 (b). A significant decrease of the T_{max} was exhibited with reduced SOA formation temperatures from 313K to 273K. This could be related to the oxygenation of the particle phase compounds. The signal-weighted averaged O:C ratio of the particle formed at 313K was 0.57±0.01, while that at 298K, 273K, and 243K were 0.57±0.01, 0.52±0.01, and 0.47±0.01, respectively. It was seen that lower SOA formation temperature led to less oxygenated particles, resulting in higher volatilites and hence lower overall T_{max}. In contrast, the T_{max} for the particle phase compounds formed at 243K was found higher than that at 273K, indicating a lower particle volatility. This may be explained by the potential enhancement of particle viscosity at 243K, where the ambient temperature was estimated to be 46 K lower than the glass transition temperature. In addition, the thermal decomposition of dimers (or oligomers) gives rise to the second mode of the total thermograms for the particles formed at 313K and 298K, and may also induce higher T_{max} of the first peak.

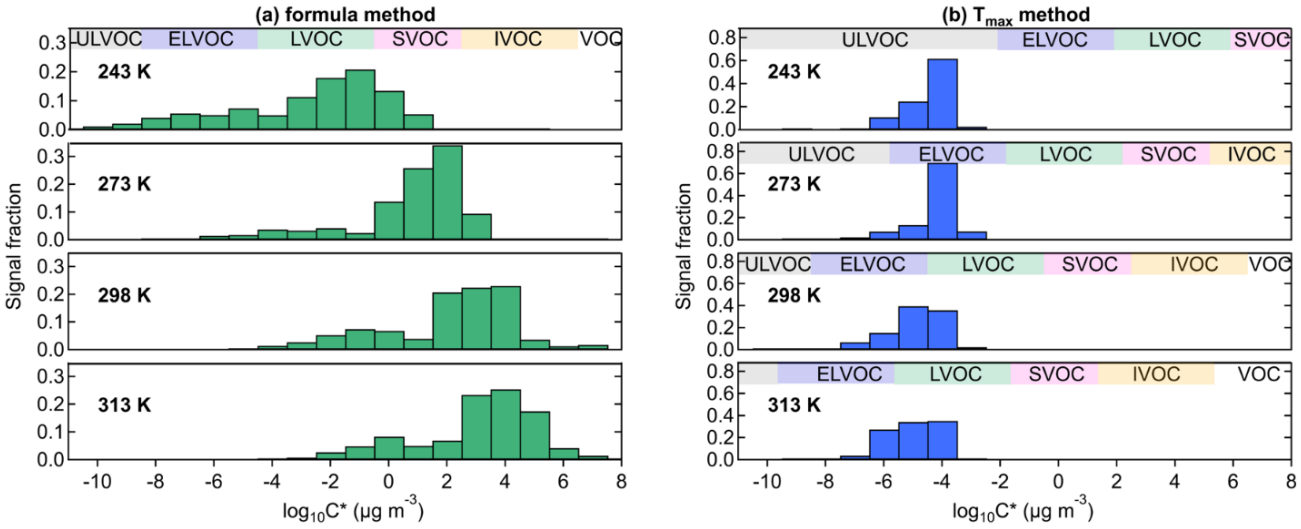

Figure 21. One-dimension volatility basis set for the particles formed at 243K, 273K, 298K, and 313K. The saturation concentration is estimated via (a) formula method, and (b) T_{max} approach. The different volatility classes are indicated as well.

Volatility distributions for the particles formed at 243K-313K are mapped into a one-dimensional volatility basis set framwork in Figure 21. The saturation concentration C^* was predicted by two approaches: a parameterization method on basis of element composition (Li et al., 2016), and the T_{max} method using a calibrated correlation between C^* and T_{max} for known

compounds as explained in the method section (Stark et al., 2017). As the *C** estimated from the T_{max} method assumes a temperature of 298K, to be comparable with the formula method. Therefore, the volatility class border at other temperatures was converted to be comparable to 298K. The *C** from the prediction via the formula method was substantially higher than that from the T_{max} method, with about six orders of magnititude for the α-pinene and isoprene particles. Nevertheless, the impact of temperature was still clearly visible on the volatility of the particles formed at varying conditions. Using the formula method, the components in the particles at 243K spaned widely ULVOC to SVOC classes, while the majority of species in the particle at 313K distributed in the IVOC range. However, according to the T_{max} approach, the particles formed at 243K contained compounds with effective saturation concentrations lower than 0.01 μg m^{-3}, and all remained in the ULVOC bin. As temperature increased, a larger fraction of molecules fell in the volatility range between C^* $10^{-6.5}$ and $10^{-4.5}$ μg m^{-3}, and the relative abundance of higher volatile bins ($10^{-4.5} < C^* < 10^{-3.5}$) decreased. This could result from either the increase of the fraction of C_{11-20} molecules or the thermal decomposition species from dimers (or oligomers) which have higher T_{max} and lower volatility. This is not consistent with the obversation from Ye et al. (2019), who presented a progressive shift of the sole α-pinene derived products toward higher (300 K) C^* due to reduced formation of HOM molecules at lower temperatures. The discrepency may result from the reduction of HOM formation in presenceof isoprene. Hence, this work highlights the impact of dimer (or oligomer) formation on the particle volatility distribution, especially at high ambient temperatures.

4.1.4 Summary

In this chapter, I have compared the chemical composition and volatility of the SOA formed from the oxidation of a BVOC mixture of α-pinene and isoprene with the SOA derived from sole α-pinene oxidation under atmospheric relevant conditions at 273K. Besides, I have also explored the temperature dependent chemical characteristics and volatility of the SOA from the mixture of isoprene and α-pinene using iodide adduct FIGAERO-CIMS.

In comparison between the SOA particles derived from α-pinene with and without isoprene at 273 K, the majority of gas and particle signals in both systems mainly comprised $C_{8-10}H_yO_{4-7}$, indicating α-pinene derived oxidation products still dominated the SOA from a mixture of α-pinene and isoprene. With similar signal fraction of C_{11-15} species, $C_{11-15}H_yO_{1-6}$ in the binary system

(6.0±1.2%) was lower than the sole α-pinene system (7.5±0.7%), while $C_{11\text{-}15}H_yO_{>6}$ consisted of higher fraction in the binary system (3.8±0.2%) than the sole α-pinene system (2.4±0.4%). Besides, the relative abundance of $C_{16\text{-}20}$ molecules in both systems accounted for 5.9±0.3% in the sole system, slightly lower than in the binary system (6.6±0.1%). This indicates that the presence of isoprene does not substantially reduce the α-pinene derived $C_{16\text{-}20}$ dimers or total SOA mass under experimental condition in this work with an isoprene to α-pinene concentration ratio of 1:1.

Besides, the 273K SOA derived from the mixture of α-pinene and isoprene had a lower volatility, with a higher T_{max} of the total thermogram. The majority of components in the particles from the sole α-pinene was with lgC^* between -4.5 to -2.5 μg m^{-3}. In contrast, most species in the particles from the mixture spanned lower volatility bins with saturation concertation between $10^{-6.5}$ to $10^{-3.5}$ μg m^{-3}. The systematic increase in T_{max} of individual molecules indicates that the particle in the binary system is more viscous probably due to higher abundance of the components in larger molecular weights, and in turn lower the volatility. This suggests that the SOA particles from a mixture of α-pinene and isoprene have a higher potential to react as cloud condensation nuclei or ice nucleating particles.

The particles from mixtures of α-pinene and isoprene at 243K, 273K, 298K, and 313K comprised mainly $C_{8\text{-}10}$ species (> 50% signals). A significant impact of temperature on the chemical composition was found. The formation of C_{10} group was favored at lower temperatures, which was the most abundant group in the particle formed at 243K. however, with temperature rising, the signal fraction of C_{10} went down and C_8 increases to be the most abundant fraction. Besides, $C_8H_yO_{5\text{-}8}$ had positive temperature dependent signal fraction, suggesting there was less C-C bond cleavage in the reduced temperatures. As the most abundant molecule, $C_8H_{12}O_4$ was found a thermal fragmentation of larger molecules (e.g., dimers) in the particles between 298K and 313K. This indicated the formation of related thermal unstable dimers (or oligomers) was favored at higher temperatures. To explain, based on the estimation of glass transition temperature, the particles formed at 243K and 273K are likely to be semi-solid, and the particles formed at 298K and 313K could be liquid. This highlights the need to consider condensed-phase chemistry as one of the sources of the dimer or oligomer formation at 298-313K.

In addition, higher particle volatility was suggested by increased T_{max} of the total thermograms of particles formed from 273K to 313K, being explained by the higher particle oxygenation at

rising SOA formation temperatures. However, at 243K, the particle had a higher T_{max}, suggesting a lower volatility compared to the particle generated at 273K. This could be interpreted that the volatility of the particle at 243K is affected more by the high viscosity but less by the low oxygenated molecules.

4.2 SOA from β-caryophyllene ozonolysis at different temperatures

This section will present an overview of the experiments (section 4.2.1), kinetics (4.2.2), SOA yields (4.2.3), molecular composition (4.2.4), and SOA volatility (4.2.5) from β-caryophyllene ozonolysis over a wide temperature range of 213-313K. Please note that parts of section 4.2.1, 4.2.2, 4.2.3, and 4.2.4 are reprinted with permission from the journal of Atmospheric Chemistry and Physics corresponding to my publication: Gao, L., Song, J., Mohr, C., Huang, W., Vallon, M., Jiang, F., Leisner, T., and Saathoff, H.: Kinetics, SOA yields, and chemical composition of secondary organic aerosol from β-caryophyllene ozonolysis with and without nitrogen oxides between 213 and 313 K, Atmos. Chem. Phys., 22, 6001–6020, https://doi.org/10.5194/acp-22-6001-2022, 2022.

4.2.1 Overview of the experiments

Figure 22 shows the time evolution of the β-caryophyllene, trace gases (O_3, NO_2), particle mass, and size distribution for the β-caryophyllene ozonolysis at 298K. Five full experiments including subsequent illumination and warming up periods at all temperatures are shown in Figure S4. After SOA formation from the β-caryophyllene ozonolysis, NO_2 was added leading to formation of N_2O_5 and NO_3 radicals due to reactions with an excess of O_3, subsequent addition of β-caryophyllene in the presence of NO_x resulted in the pre-existing SOA particles but also induced the new particle formation. In the next step the SOA was aged by illumination with a solar simulator to mimic atmospheric photochemical aging processes. In a final step, the whole chamber was warmed by 30 K over a time of 10 hours to study the phase partitioning of SOA. To make it clearer, as an example, at 298K (Figure 22 (d)), after the nucleation, the diameters of particles grew to 36 nm and increased further to 57 nm and 69 nm after subsequent O_3 and β-caryophyllene additions, and finally to 122 nm after the NO_2 addition. At the low initial O_3 concentration of 25 ppb, the particle mass started to increase. It reached stable within 20 minutes after the O_3 level was increased to above 300 ppb, stabilizing at 13.3 μg m^{-3}. A further particle mass increase was found after a second β-caryophyllene addition, reaching at 17.0 μg m^{-3}. To this SOA, 42 ppb of NO_2 was

added, which reacted with the excess of O_3 forming NO_3 radicals and consequently led to a small increase in particle size and mass (1.9 nm and 0.9 µg m^{-3}, respectively) due to their reaction with β-caryophyllene oxidation products. Following the third addition of β-caryophyllene to the reaction mixture, the particle mass concentration reached to 50.6 µg m^{-3}. During the third addition of β-caryophyllene, I observed quick growth of the existing particles and formation of new particles. Table 7 summarizes the SOA mass, particle diameters, O:C, density, and yields for the experiments at all temperatures. During the following illumination, the mass concentration had a slight increase, and then decreased subsequently in the final warming period.

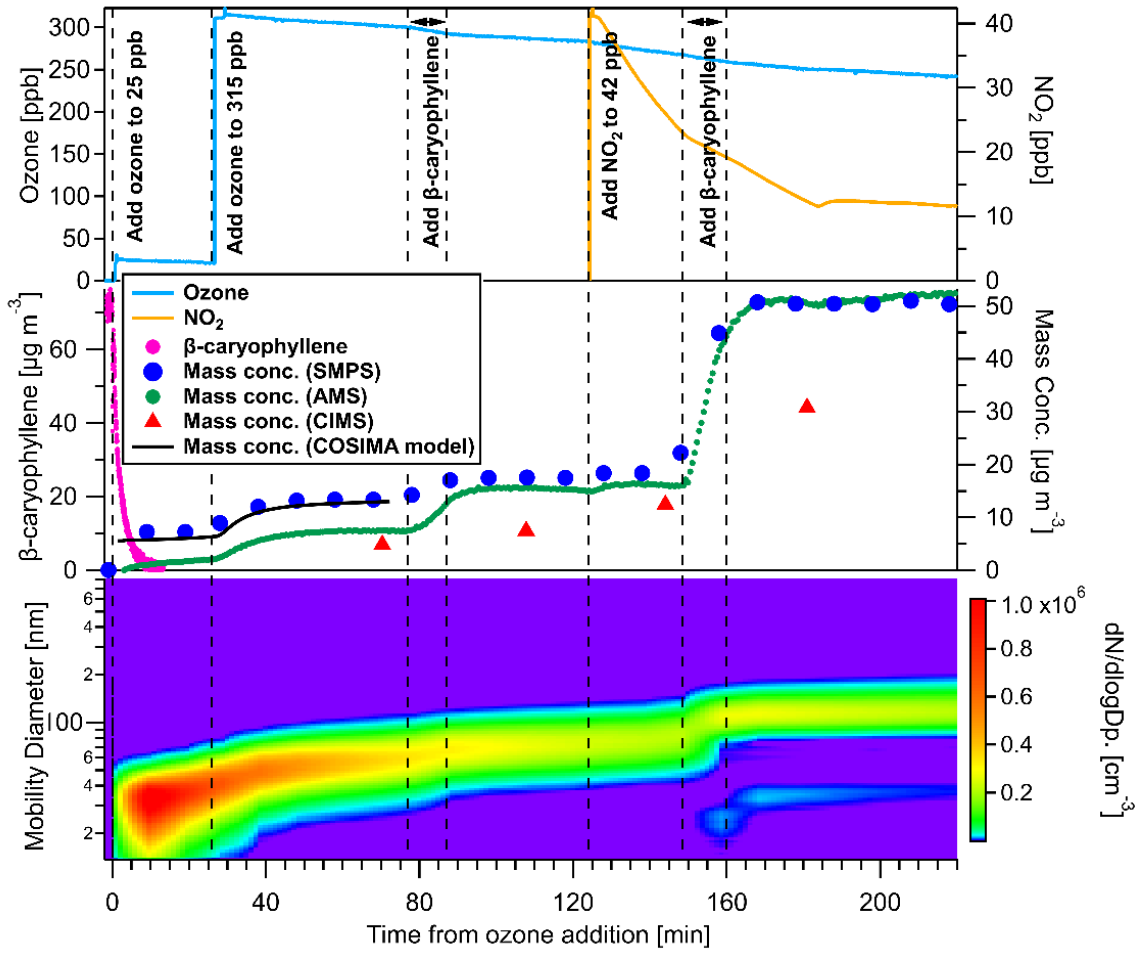

Figure 22. Time evolution of trace gases, particle mass, and particle size for β-caryophyllene ozonolysis at 298K first without and then in presence of NO_2. The time axis is relative to the first addition of O_3. Top panel shows the concentration of O_3 (blue) and NO_2 (yellow) as well as the experiment steps; middle panel shows the change of β-caryophyllene (pink), particle concentration from SMPS (blue dots) and COSIMA model (black line), AMS (green dots) and CIMS (red triangle); bottom panel shows the particle size distribution over the course of the whole experiment.

In the initial phase of the experiment, the discrepancy in particle mass concentrations measured from HR-TOF-AMS and SMPS is owing to the fact that HR-TOF-AMS has lower transmission of sub-100 nm particles in the aerodynamic lens, and hence it poorly detects small particles with diameters below 70 nm (Liu et al., 2007; Williams et al., 2013). After he particle diameters reached to 122 nm (160 minutes in Figure 22), the mass concentrations from SMPS agreed well with HR-TOF-AMS assuming CE of 0.6. As FIGAERO-CIMS is sensitive to polar oxidized compounds, the sum of all compounds detected by FIGAERO-CIMS can only be a fraction of the total organic aerosol compounds measured by HR-TOF-AMS. By applying the maximum sensitivity of 22 cps/ppt for all organic species, FIGAERO-CIMS explains around 36-61 % of the total organic particle mass from HR-TOF-AMS.

Table 7. Compilation of SOA mass, diameter, O:C, density, and yields.

Exp. No.	SOA mass^{+} (SMPS) [μg m^{-3}]	geo. mean diameter (nm)	O:C (CIMS)	SOA density [g cm^{-3}]	SOA Yield [%]	BCA Yield [%]
9	14.4±3.6	67.3±1.2	0.26	0.75±0.06	-	-
10	4.5±1.1	73.3±1.1	0.32	0.86±0.14	28.5±8	11.1±7.3
11	31.5±7.9	73.5±1.9	0.38	1.0±0.08	29.7±8	4.1±2.7
12	13.6±3.4	68.5±1.5	0.41	1.09±0.12	20.9±6	0.8 ± 0.5 (4*)
13	13.7±3.4	52.9±3.6	0.42	1.09±0.16^{ass}	17.4±5	0.6±0.4

$^{+}$ SOA mass wall loss corrected; * measured by (Jaoui et al., 2003a); ^{ass} assumed to have the same density as at 298K due to its large measurement uncertainty; BCA, β-caryophyllinic acid, regarded as a tracer of β-caryophyllene in the atmosphere.

4.2.2 Kinetics of the β-caryophyllene reacting with O_3

After the first addition of an excess of O_3, β-caryophyllene was depleted within less than 5 minutes. To investigate the kinetics of β-caryophyllene reacting with ozone, I used a kinetic model to resolve the initial β-caryophyllene decay. Figure S5 shows an example of the comparison between measured data for the experiment at 313 K with the kinetic model results. Three main reactions were considered in the kinetic analysis to fit the observation:

$Rection\ 1\text{:}\ BCP + O_3 \rightarrow product\ 1 + OH\cdot, k_1;$

$Rection\ 2\text{:}\ BCP + O_3 \rightarrow product\ 2 + OH\cdot, k_2;$

$Rection\ 3\text{:}\ BCP + OH\cdot \rightarrow product\ 3, k_3;$

where BCP is the β-caryophyllene; $product\ 1$, $product\ 2$, $product\ 3$ represent different classes of the reaction products; k_1, k_2, k_3 are the correspond reaction rate coefficients.

All kinetic parameters fitted are summarized in Table S2. The yields of OH radicals produced from β-caryophyllene ozonolysis increased from (5±2) % at 243 K to (15±2) % at 313K. Around 91-92% of the β-caryophyllene were calculated to react with O_3 under 243-313K.

Temperature dependent rate coefficients for β-caryophyllene ozonolysis are shown in Figure 23. I determined the rate coefficient for 298 K as (1.09±0.21) × 10^{-14} cm^3 $molecule^{-1}$ s^{-1}, agreeing very well with Shu and Atkinson (1994b) of (1.16 ± 0.43) × 10^{-14} cm^3 $molecule^{-1}$ s^{-1}, and Richters et al. (2016a) of (1.1± 0.3) × 10^{-14} cm^3 $molecule^{-1}$ s^{-1} for 296 K. Furthermore, the rate coefficient increased at reduced temperatures, in an agreement with the density-functional theory (DFT) quantum chemical calculations by Nguyen et al. (2009), but with a slightly higher slope in this work. I determined the temperature dependent rate coefficients as k = (1.6±0.4) ×10^{-15} ×exp((559±97)/T), corresponding to a reaction enthalpy of (5.6±1.0) kJ mol^{-1}.

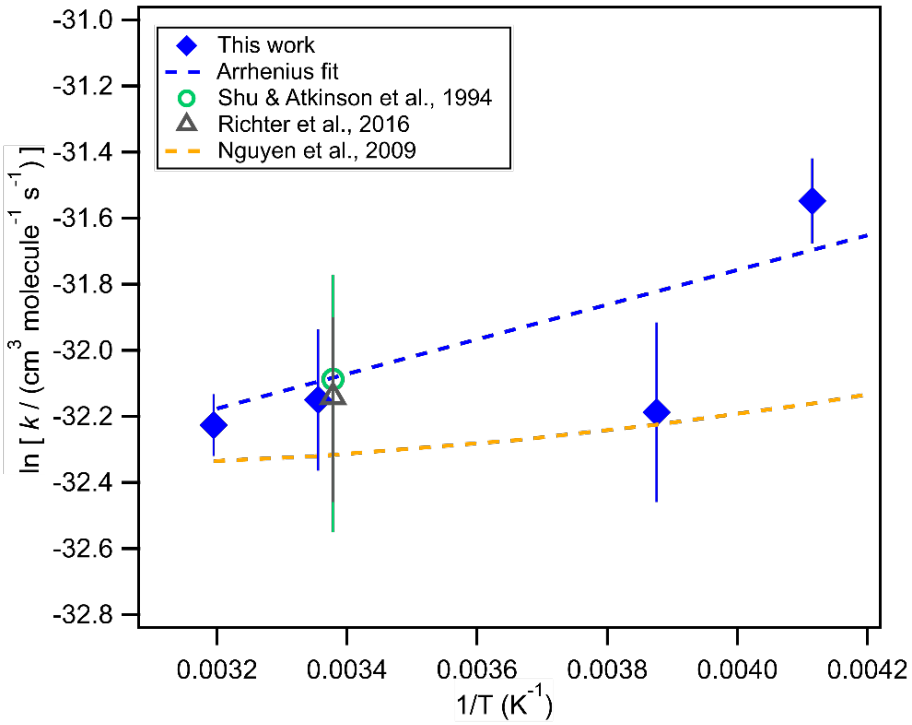

Figure 23. Arrhenius plot of the rate coefficients determined for the reaction of O_3 with the endocyclic double bond of β-caryophyllene (blue diamonds) compared to the values measured by Shu and Atkinson (1994b) (green circle) and Richters et al. (2016a) at 296 K (grey triangle) as well as model calculations by Nguyen et al. (2009) (yellow dashed line). The blue dashed line is a fit to the rate coefficients determined in this work.

4.2.3 SOA yields

With a constant organic particle mass concentration of 10 μg m^{-3}, the yields of β-caryophyllene ozonolysis without NO_2 as a function of temperatures are presented in Figure 24. It is seen that the SOA yields increased with reduced temperatures from 313K to 243K. With organic particle mass concentration of 10 μg m^{-3}, I determined a SOA yield at 298K as (19.4±6) %. The yields at 298K in this work was lower by around 55% and 40% than other studies from Chen et al. (2012c) and Tasoglou and Pandis (2015b), which used OH radical scavengers. The lower yields in this work could be explained by that OH radicals may oxidize potentially more VOCs causing lower SOA yields. The temperature dependence in this work for β-caryophyllene is significantly weaker than α-pinene (Saathoff et al., 2009b), reflecting lower vapor pressures of β-caryophyllene derived condensable oxidation products. Besides, in this study, the SOA formation time of about 90 minutes was longer than the typical lifetime of the first-generation products from β-caryophyllene ozonolysis (20 minutes) at an O_3 level of 300 ppb, thus the difference cannot be explained by potential incomplete reactions. Different initial O_3 levels may also contribute to the higher yields reported by Chen et al. (2012c) and Tasoglou and Pandis (2015b). For my study the wall losses and corresponding corrections were relatively small and cannot explain deviations of 40-55%. Typically, the losses of acidic gases are larger in an aluminium chamber compared to a Teflon chamber and it may be vice versa for particle losses. This depends on the age of the chamber walls, potential electrostatic losses, and the volume to surface ratio of the chamber. It is therefore not easy to determine the impact of the different wall losses and the wall loss corrections. We can only speculate it to high wall loss corrections for the studies in the Teflon chamber contribute to the different yields.

An overview of the SOA yields determined by other researchers is given in Figure S6 in comparison with our results in the temperature range between 243 and 313 K. The formed SOA masses reflected the different oxidation products of differing volatilities (Chan et al., 2007) formed at low and high temperatures, which will be discussed in the following section.

Please note that the wall loss correction was done by calculations with aerosol dynamic model COSIMA supported by Dr. Harald Saathoff.

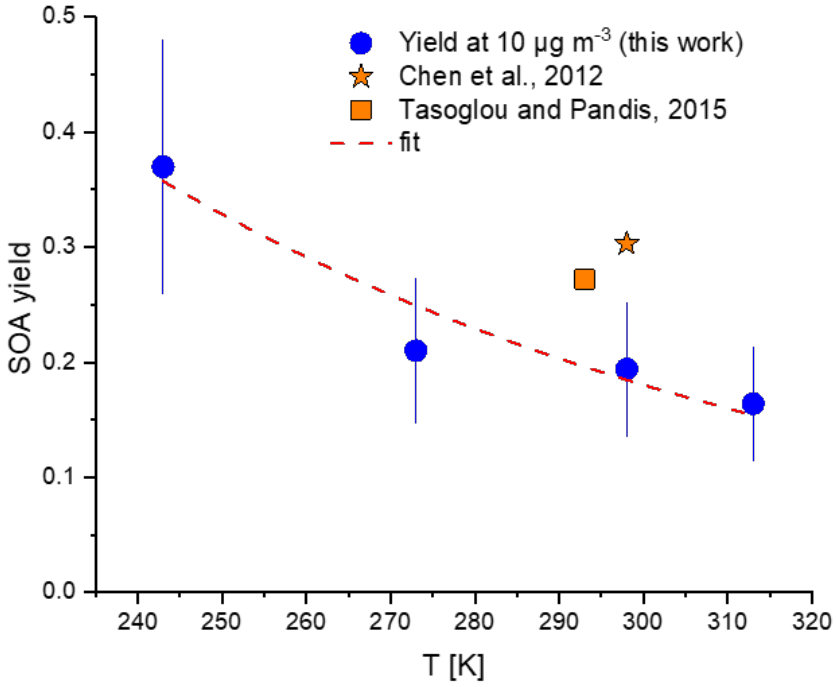

Figure 24. SOA mass yield from β-caryophyllene ozonolysis at a constant total organic aerosol mass (M_{org}) of 10 µg m^{-3} for temperatures between 243 – 313 K from this study in comparison with literature data. The dashed line represents a single exponential fit to the data. Chen et al. (2012c) used OH/CI scavenger and ammonium sulfate as seeds; Tasoglou and Pandis (2015b) used OH/Cl scavenger.

4.2.4 Molecular composition

Figure 25 presents the mean gas-phase mass spectra for all five temperatures between 213-313K, showing the gas-phase chemical composition without NO_2 after the system reached steady stable. It was seen that compounds with *m/z* below 400 Th were detected significantly in the gas phase by FIGAERO-CIMS. The signals were normalized to the total gas-phase $C_xH_yO_z$ compounds at each temperature. Between 213K and 273K, the most dominant monomeric compounds in the gas phase were $C_{15}H_{24}O_3$ (likely β-caryophyllonic acid), $C_{15}H_{24}O_4$ (likely β-hydroxycaryophyllonic acid), $C_{15}H_{26}O_4$ (not identified yet), and $C_{14}H_{22}O_4$ (β-nocaryophyllonic acid or β-caryophyllinic acid). They have been identified as oxidation products of β-caryophyllene ozonolysis at room temperature in previous studies (Jaoui et al., 2003a; Winterhalter et al., 2009a; Chan et al., 2011a; Li et al., 2011a). Other lower oxidized molecules, such as $C_{14}H_{20}O_2$, $C_{15}H_{22}O_2$ and $C_{14}H_{20}O_3$, were detected by PTR-MS as a complement to the chemical composition for gas phase (Figure S7, plotted by my colleague Junwei Song). Combined with FIGAERO-CIMS measurement, the $C_{15}H_{22}O_2$ is interpreted as the fragmentation compound from $C_{15}H_{24}O_3$ by losing H_2O, which could be tentatively identified as β-caryophyllene aldehyde (Li et al., 2011a).

Measurement from PTR-MS illustrates that the low oxygenated monomeric species with less than 5 oxygen atoms, which contributed abundantly at low temperatures (213-243K), could also be formed at higher temperatures (273-313K) but reacted subsequently to form higher oxygenated components with lower volatilities (Figure S10). Similar process cannot be excluded for the small molecules, like $C_2H_4O_3$ and $C_4H_6O_4$.

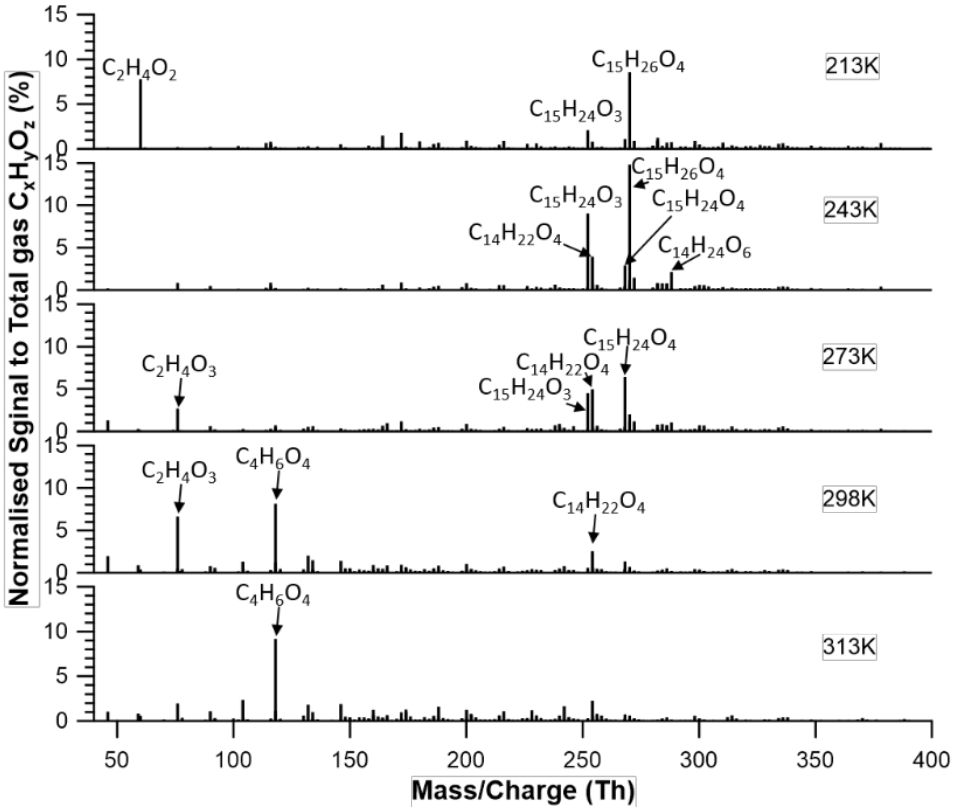

Figure 25. Averaged CIMS gas phase mass spectra (background subtracted) for all temperatures, indicating the gas information when the SOA got stable in the absence of nitrogen oxides. The particle information sampled at the same time is given in Figure 26 and Figure 27.

For clear comparison, I present the mass spectra and molecular assignment for the particle phase from β-caryophyllene ozonolysis at 213K and 313K in Figure 26. For both lowest and highest temperatures, several oxidation products, some of the oxidation products have been identified in previous studies, were observed. For example, $C_{14}H_{22}O_4$ is likely to be β-caryophyllinic acid or β-hydroxynocaryophyllon aldehyde, while $C_{15}H_{24}O_3$ could be β-hydroxycaryophyllon aldehyde or β-caryophyllonic acid, and $C_{14}H_{22}O_7$ is likely to be 2,3-dihydroxy-4-[2-(4-hydroxy-3-oxobutyl)-3,3-dimethylcyclobutyl]-4-oxobutanoic acid (Jaoui et al., 2007; Li et al., 2011a; Winterhalter et al., 2009a; Chan et al., 2011a; Jaoui et al., 2003a; Griffin et al., 1999; Lee et al., 2006a; Lee et al., 2006d; Nguyen et al., 2009; Jenkin et al., 2012; Richters et

al., 2016b). The major oxidation products detected in this work are listed in Table S3. Furthermore, from the measurement of CHARON-PTR-MS, lower oxidized molecules, such as $C_{14}H_{20}O_{2\text{-}3}$, $C_{14\text{-}15}H_{22}O_3$, and $C_{15}H_{22}O_2$ were observed (Figure S9). Taking fragmentation by losing one H_2O molecule into account (Gkatzelis et al., 2018), $C_{14}H_{20}O_{2\text{-}3}$ and $C_{15}H_{22}O_{2\text{-}3}$ could be fragmented from $C_{14}H_{22}O_{3\text{-}4}$ and $C_{15}H_{24}O_{3\text{-}4}$, respectively, which were the most abundant molecules detected by FIGAERO-CIMS, as shown in Figure 26.

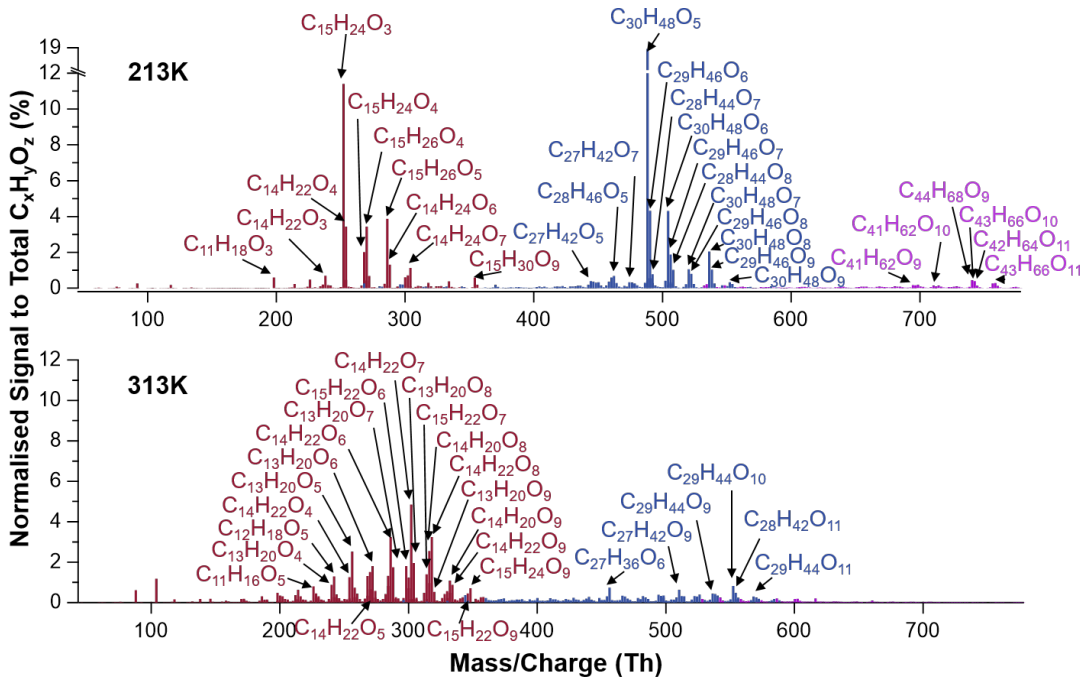

Figure 26. CIMS mass spectra of particle phase compounds obtained from ozonolysis of β-caryophyllene without NO_2 at 213K (upper panel) and 313K (lower panel). Colours refer to monomeric (brown), dimeric (blue) and trimeric (purple) compounds, labels represent the assignment of individual molecules.

For the particle formed at 213K, the most abundant molecules were $C_{15}H_{24}O_3$, $C_{30}H_{48}O_5$ and $C_{44}H_{68}O_9$, for monomers ($C_{1\text{-}15}$), dimers ($C_{16\text{-}30}$) and trimers ($C_{>30}$), respectively, which were clearly visible. In contrast, at 313K, the monomers dominated the particle and only a few dimers were detected, with the most abundant signals in $C_{14}H_{22}O_7$ and $C_{29}H_{44}O_{10}$, respectively. Trimers were not significantly formed at 313K. It was evidently seen that the monomeric species formed at 313K were more oxygenated and had higher elemental O:C ratios (Figure 26), with major signals of $C_{14\text{-}15}H_{22\text{-}24}O_{6\text{-}9}$, compared with $C_{14\text{-}15}H_{22\text{-}24}O_{3\text{-}7}$ for the monomer class in the particle formed at 213K. This could be explained that, at higher temperatures, after the formation of early-stage oxidation products, those remaining in the gas phase (e.g., semi-volatile compounds) enable to undergo further oxidation reactions between their unsaturated exocyclic double bonds and the

excess of O_3, finally forming higher oxygenated products. The substantially lower V_p of organics at 213K than at 313K according to Clausius-Clapeyron equation leads to the rapid condensation of low oxidized molecules at 213K. For example, HOM molecules such as e.g. $C_{14}H_{22}O_7$ could be formed via simple or extended autoxidation (Richters et al. (2016)). In addition to $C_{14}H_{22}O_7$, I also detected five compounds, such as $C_{14}H_{22}O_9$ and $C_{15}H_{22\text{-}24}O_{7,9}$, which were also likely formed from autoxidation reactions (Jokinen et al., 2016). At 313K, monomeric highly oxidized compounds (MHOC), consisting of $C_{14\text{-}15}H_{22\text{-}24}O_{6\text{-}9}$, contributed 42.5% of total organic signals, exceeding the contribution of monomeric low oxygenated organic compounds (MLOC) of $C_{14\text{-}15}H_{22\text{-}24}O_{3\text{-}7}$ with a signal fraction of 24.9%. On contrast, at 213K, signal fraction of MHOC and MLOC was 6.9% and 30.5%, respectively. Furthermore, six confirmed HOM molecules consisted of nearly zero at 213K and 9.2% at 313K (Figure 28), indicating that autoxidation pathway had a strongly positive temperature dependence on temperatures.

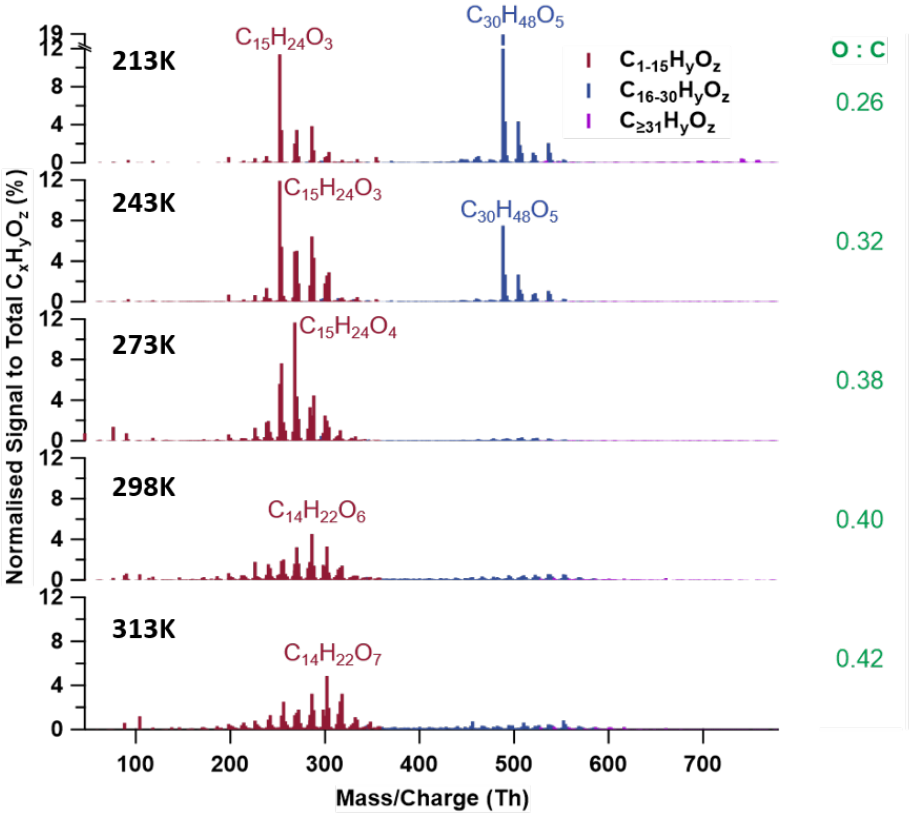

Figure 27. CIMS mass spectra for particle phase compounds for all five temperatures (213 - 313K). Colours refer to monomeric (brown), dimeric (blue) and trimeric (purple) compounds. The table lists the signal-weighted bulk O:C ratios for each temperature. The mass to charge ratios in x-axis are subtracted by I^- (m/z = 126.9).

The dimer patterns were completely different between the particles formed at 213K and 313K. The majority of dimers formed at 213K consisted of lowly oxygenated organic compounds (DLOC) with $C_{28\text{-}30}H_{44\text{-}48}O_{5\text{-}9}$, accounting for 53.7% to total particle-phase signals. On contrast, dimers formed at 313K contained mainly higher oxidized compounds (DHOC), e.g., $C_{27\text{-}29}H_{42\text{-}44}O_{9\text{-}11}$, making up 27.6% to total particle-phase signals. Here, to explain the potential formation pathway (see Figure S11) for the most abundant dimers at the coldest and warmest temperatures, I put forward esterification reactions which are similar to monoterpenes reported by Yasmeen et al. (2010) and Müller et al. (2008). For example, $C_{30}H_{48}O_5$ might be potentially esterified at 213K by two abundant monomers, $C_{15}H_{26}O_3$ and $C_{15}H_{24}O_3$. Similarly, $C_{14}H_{22}O_7$ and $C_{15}H_{24}O_3$ are potentially blocks for the formation of $C_{29}H_{44}O_9$ at 313K. Their molecular structures and reactions are presented in Figure S11. However, it cannot be excluded that the reaction between a β-caryophyllene derived stabilized Criegee intermediate and an organic acid to form $C_{30}H_{48}O_5$, which is similar to the mechanisms for α-pinene (Lee and Kamens, 2005; Witkowski and Gierczak, 2014; Kristensen et al., 2016).

Trimers ($C_{41\text{-}43}H_{62\text{-}68}O_{9\text{-}11}$) were only observed from the particles formed at 213K, accounting for 8.6% to total particle-phase signals. The potential pathway for the formation of $C_{44}H_{68}O_9$ is presented in Figure S11. Note that the assignment of those high weight (>700 Th) molecules has relative high uncertainties as for smaller mass peaks.

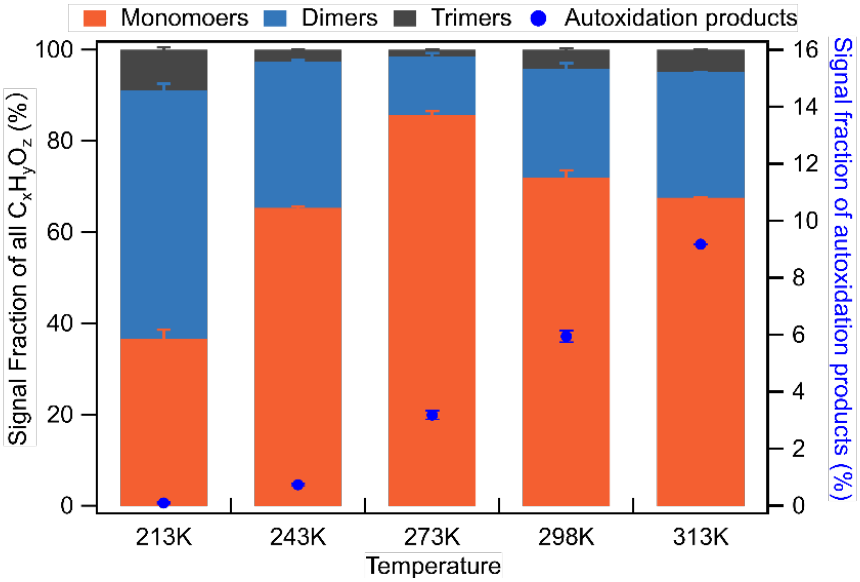

Figure 28. Product groups contributing to SOA from ozonolysis of β-caryophyllene without NO_2 at temperatures between 213 – 313 K. Autoxidation-products calculation includes $C_{14}H_{22}O_{7,9}$, $C_{15}H_{22}O_{7,9}$ and $C_{15}H_{24}O_{7,9}$ identified in previous studies (Jokinen et al., 2016; Richters et al., 2016b).

The mass spectra for the particles formed from β-caryophyllene ozonolysis without the presence of NO_3 radicals at 213K, 243K, 273K, 298K, and 313K are presented in Figure 27. With temperature increased, the most abundant monomer was higher oxygenated and with higher molecular mass, from $C_{15}H_{24}O_3$ (213-243K), $C_{15}H_{24}O_4$ (273K) to $C_{14}H_{22}O_6$ (298K) and $C_{14}H_{22}O_7$ (313K). This illustrates that high temperature favours the formation of higher oxygenated products, such as HOM molecules, while reduced temperature facilitates the condensation of early-stage oxidation products before their further oxidation reactions.

Figure 28 presents the contribution of monomers, dimers, trimers, and HOM molecules formed at different temperatures. The contribution of monomers was 67.5%, 68.9%, 85.3%, 64.7%, and 39.2% at reduced temperatures, respectively, wherein a decrease was found for the contribution of HOM molecules from 9.2% to 0.1%. This indicates β-caryophyllene derived HOM formation is positively monotonically temperature dependent, which is similar to α-pinene system (Bianchi et al., 2019).

Two different dimeric patterns were observed at varying temperatures. A dimeric pattern for low temperatures (213-243 K) was represented by $C_{28\text{-}30}H_{42\text{-}48}O_{5\text{-}8}$ (LT-group), while the other pattern for high temperature (273-313K) consisted mainly of $C_{28\text{-}30}H_{36\text{-}44}O_{9\text{-}11}$ (HT-group). The contribution of LT-group was negatively temperature dependent, with 53.7% and 32.8% at 213K and 243K, respectively. On contrast, the HT-group had slightly positive temperature dependence, accounting for 13.8% to 27.6% from 273K to 313K (Figure 28), indicating the dimer formation (HT-group) was favoured with increasing temperatures. Furthermore, the contribution of major products in both gas and particle phases are presented in Figure S12. The signal fractions of $C_{15}H_{26}O_4$ and $C_{15}H_{24}O_3$ (likely β-caryophyllonic acid) were higher at lower temperature (213-243K), while $C_{14}H_{22}O_4$ was measured at all temperatures with a low contribution of 0.05% to the SOA. $C_{15}H_{24}O_4$ (likely β-hydroxycaryophyllonic acid) existed at all temperatures but with the highest contribution at 273K. The two most abundant HOM molecules, $C_{14}H_{22}O_6$ (likely hydrated β-oxocaryophyllonic acid) and $C_{14}H_{22}O_7$ (not yet identified) were also observed at all temperatures but their signal fractions were significantly positively temperature dependent, accounting for 0.08% to 2.3% and 0.01% to 3.6% from 213K to 313K, respectively.

4.2.5 SOA volatility

The average oxidation state of carbon (OS_C) is an ideal metric for the degree of oxidation of organic species and serves as a key index to describe the chemical complexity of organic aerosols (Kroll et al., 2011). This quantity increases with the overall degree of oxidation. Since the SOA in this part of my study was formed in the absence of NOx and nitrate radicals, only C, H, and O atoms were relevant, and the OS_C was calculated as $OS_C = 2 \times O{:}C - H{:}C$ (Kroll et al., 2011), with O:C and H:C being the ratio of oxygen and hydrogen to carbon.

To have an overview of the SOA bulk composition at all temperatures and facilitate the comparison with other studies, the bulk O:C, H:C, and OS_C are summarized in Table 8. The bulk O:C increased from 0.21 to 0.45 with enhanced temperatures from 213K to 313K, indicating the higher degree of oxidation of SOA particles formed at increased temperatures. Besides, the bulk OS_C at 213K to 273K was below -1, and distributed in the period between the slope of -2 to -1 in the Van-Krevelen diagram, suggesting the oxygenation of the functional groups in these SOA particles were between ketone/aldehyde and carboxylic acids. Comparably, the particles formed at 298K and 313K were with OS_C higher than -1, indicating their functionalities were more oxidized than the carboxylic acids. This can be supported by the molecular chemical composition of the particle phase, where the monomers (carbon atoms ≤15) were detected with higher oxygen content at 298-313K, and as lower oxidized species between 213-273K, shown in Figure 30 (a). Dimers (15 < carbon atoms ≤30) were only abundant at 213-243K.

Table 8. Compilation of experimental conditions, O:C ratios, H:C ratios, OS_C, and the Tmax of total thermograms.

Exp .No.	T [K]	BCP conc. [ppb]	O_3 initial conc. [ppb]	SOA particle type	O:C	H:C	OS_C	T_{max} of total thermogram [°C]
1	213	-	320	SOA_{213K}	0.21	1.64	-1.22	101
2	243	1.55	317	SOA_{243K}	0.25	1.67	-1.17	99
3	273	9.09	73	SOA_{273K}	0.29	1.70	-1.12	69
4	298	8.02	325	SOA_{298K}	0.42	1.71	-0.87	88
5	313	10.34	290	SOA_{313K}	0.45	1.66	-0.76	96

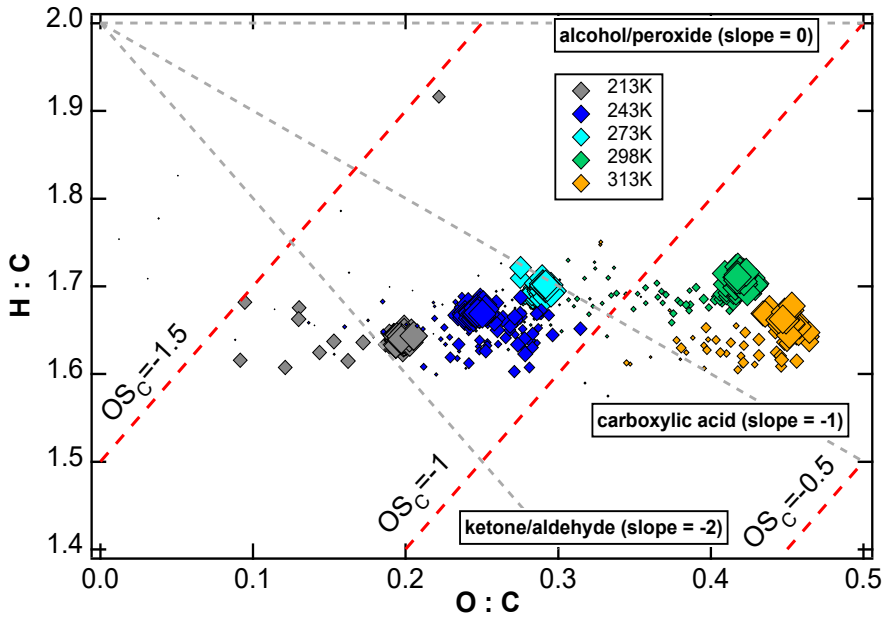

Figure 29. Bulk into Van-Krevelen diagram over the SOA generation period at all temperatures. Symbols are coloured by temperature and sized by the time from the first O_3 addition. The carbon oxidation states (OS_C) are shown with grey dotted lines. (OS_C= 2 O:C – H:C).

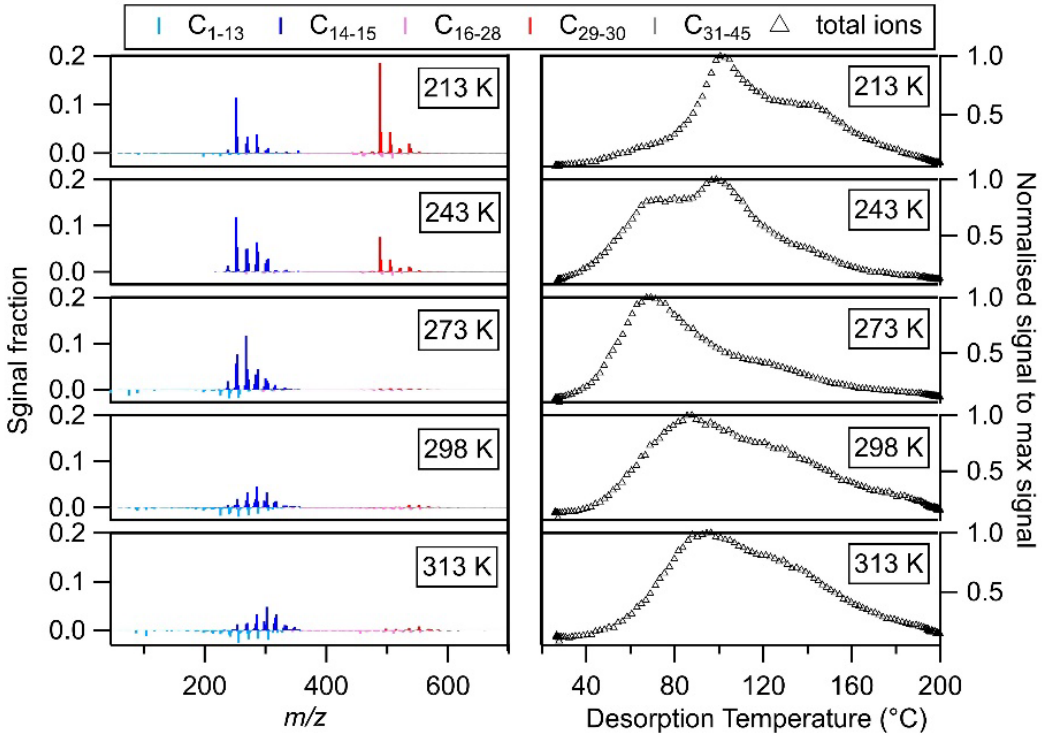

Figure 30. Mass spectra (left) and total thermogram (right) of SOA (up to bottom) at 213K, 243K, 273K, 298K, and 313K.In the left panel, compounds with different carbon numbers were colored. Monomers with 14-15 carbons were in positive stick, and dimers with 29-30 carbon atoms were in negative sticks.

In the Figure 30(b), the total thermograms of all detected molecules differed in their shapes and T_{max} for all SOA particles formed at varying temperatures. The T_{max} first decreased and then increased when the formation temperature reduced from 313K to 213K, as shown in Table 8. The multi-modal thermograms of SOA_{213K} and SOA_{243K}, and the broad thermogram shapes of SOA_{273K}, SOA_{298K}, and SOA_{313K} emphasize the complexity of the composition of β-caryophyllene SOA as a function of formation temperatures. This complexity made the determination of the particle volatility challenging, i.e., the T_{max} value of each total thermogram was not necessarily representative of the overall particle volatility. Hence PMF analysis was used to resolve the sum thermograms into multiple groups of compounds based on their desorption behaviour.

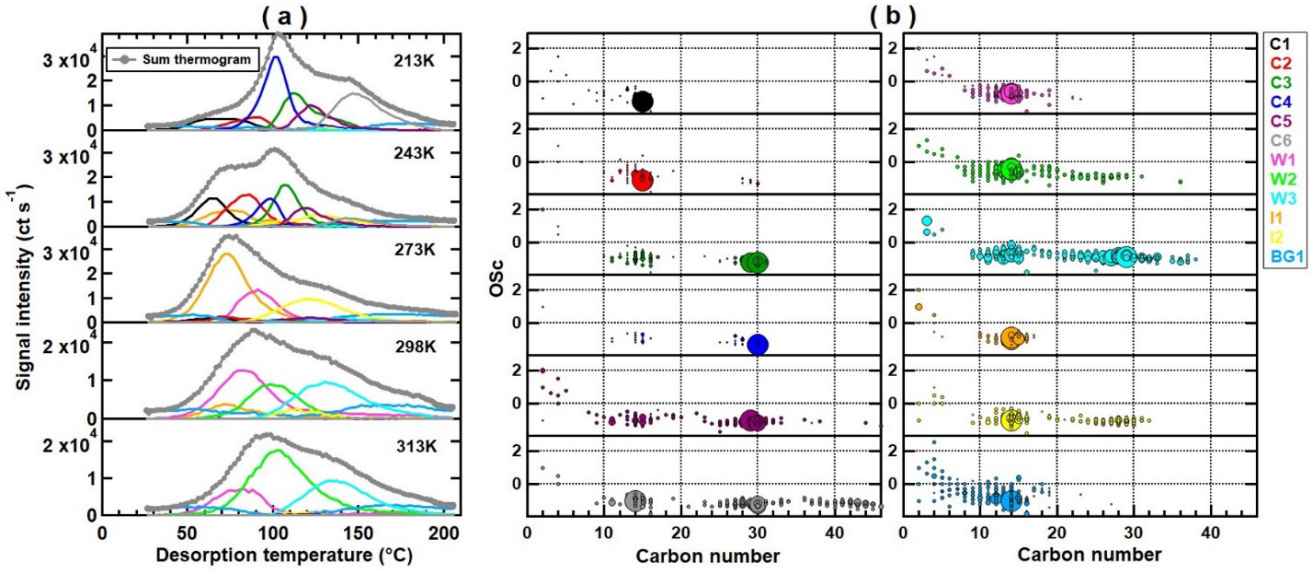

Figure 31. A 12-factor PMF solution for β-caryophyllene SOA particles at five temperatures. (a) sum thermograms (grey lines and points) and the factor thermograms for each sample; (b) the averaged chemical composition of each factor, with the averaged carbon oxidation state (OS_C) corresponding to the averaged carbon number. Colors are the same in all panels and indicate the individual factors in (a) and (b).

A 12-factor PMF solution was chosen as the optimal solution to explain the desorption behaviour of the data set with the particle samples at five formation temperatures (Figure 31), the solution residual and the evaluation of different solutions are shown in Figure S13 and Figure 32, respectively. The contribution of each factor to the total thermogram of each SOA type is shown in Figure 33. The signal-weighted mean molecular composition, O:C, and OS_C are summarized in

Table 9. One background factor was identified (BG1) which covered the remaining instrument background which is not captured by the chamber blank measurement. The factor composition differs between the experiments and could be divided into three groups: cold case factors (occurring at 213K, 243K), intermediate temperature factors (occurring at 243K, 273K, and 298K), and warm case factors (occurring at 298K, 313K). The cold case factors are dominated by monomers (C1, C2), dimers (C3, C4, C5), and thermal decomposition compounds from oligomers (C6) based on their thermal desorption behaviour and factor mass spectra (i.e., the presence of $C_{>15}$ compounds). The three warm case factors were classified in the same way as mainly monomers (W1, W2) and dimers and/or oligomers with some thermal decomposition products (W3). The difference in factor composition between the warm and cold cases indicates the diversity of the chemical pathways and condensing process involved in the SOA formation process in the different temperature regimes.

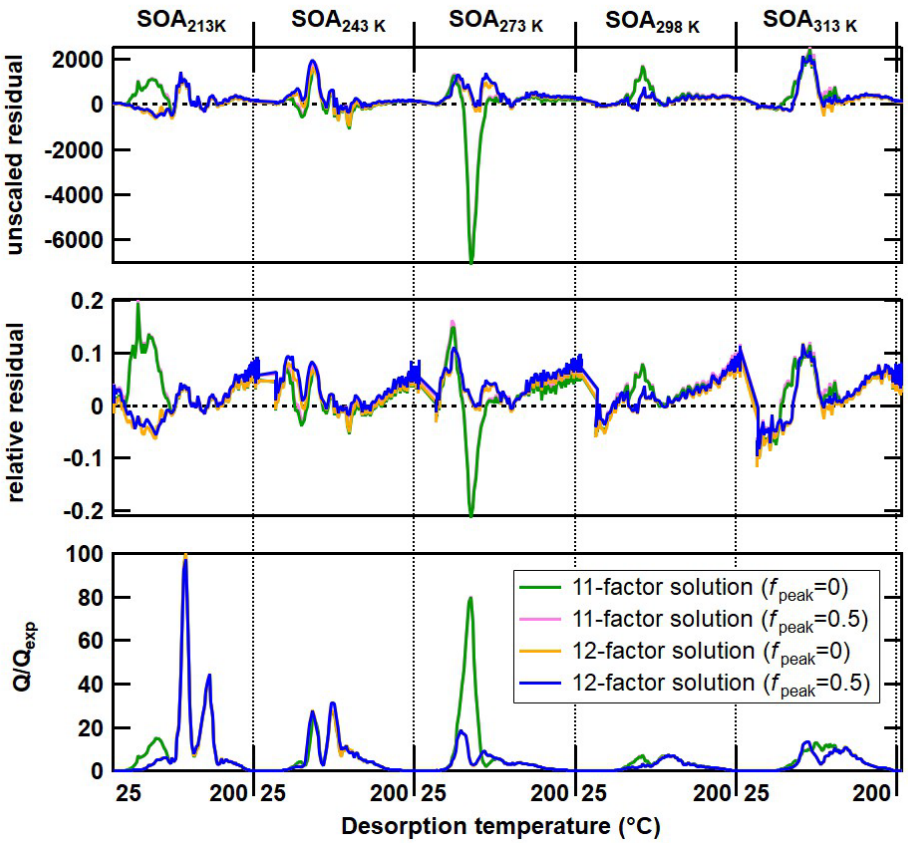

Figure 32. Residual, relative residual, and Q/Q_{exp} change for all samples (SOA formed at 213K, 243K, 273K, 298K, and 313K) when varying the number of factors and f_{peak} values.

Table 9. Summary on the molecule formula, O:C and OS_C of 12 PMF factors.

	Factor number	Molecule formula	MW (g mol^{-1})	O:C	OS_C	T_{max} (°C)
cold	C1	$C_{14.2}H_{24.0}O_{4.5}$	266	0.35	-0.99	60
	C2	$C_{14.9}H_{25.0}O_{5.6}$	293	0.41	-0.85	85
	C3	$C_{24.7}H_{39.4}O_{6.1}$	433	0.30	-1.00	105
	C4	$C_{27.3}H_{43.6}O_{5.4}$	458	0.22	-1.16	95
	C5	$C_{24.8}H_{39.4}O_{7.0}$	449	0.34	-0.93	120
	C6	$C_{28.4}H_{44.9}O_{6.5}$	490	0.26	-1.08	145
warm	W1	$C_{13.8}H_{21.4}O_{5.8}$	280	0.45	-0.66	85
	W2	$C_{15.0}H_{22.6}O_{6.8}$	311	0.49	-0.53	100
	W3	$C_{22.9}H_{34.0}O_{7.8}$	434	0.38	-0.74	135
intermediate	I1	$C_{13.5}H_{22.1}O_{5.1}$	266	0.43	-0.80	70
	I2	$C_{19.8}H_{31.0}O_{6.1}$	366	0.34	-0.9	125
background	BG1	$C_{14.3}H_{21.7}O_{5.3}$	278	0.46	-0.61	N/A

The two SOA samples in the cold case are resolved by a similar factor pattern, indicating similar SOA formation processes at 213K and 243K. Factor C1 (factor T_{max} of 60 °C) and C2 (factor T_{max} of 85 °C) are dominated by $C_{15}H_{26}O_4$ and $C_{15}H_{26}O_5$, respectively, which are the most abundant monomers except for $C_{15}H_{24}O_3$ and $C_{15}H_{24}O_4$ (discussed in section 3.4) in the cold case. C4 is dominated by the dimer $C_{30}H_{48}O_5$. As another dimer factor for the cold case, C3 has larger contributions of dimers with higher oxidation states (signal weighted averaged OS_C of -1.0) and correspondingly has lower volatility as indicated by the higher factor T_{max} (105 °C) than C4 (OS_C = -1.2, factor T_{max} = 95 °C). The T_{max} of the dimer factors is higher than the monomer factors as expected due to the longer carbon chain and much higher molecular weight despite their lower mean factor OS_C. In the higher Tmax period, C5 (T_{max} = 120 °C) shows contributions of both dimeric and apparently monomeric compounds. These apparent monomers could be either thermal decomposition products from larger oligomers (e.g., trimers), or the less volatile dimers due to their similar averaged carbon and hydrogen number with the dimer factor C3 ($C_{24.7}H_{39.4}O_{6.1}$), but with higher oxygen number. C6 has the highest T_{max} (145 °C) among all cold factors, comprising of apparently monomeric, dimeric, and trimeric compounds, and is more likely a representation of the mixture of thermal decomposition compounds from large oligomers.

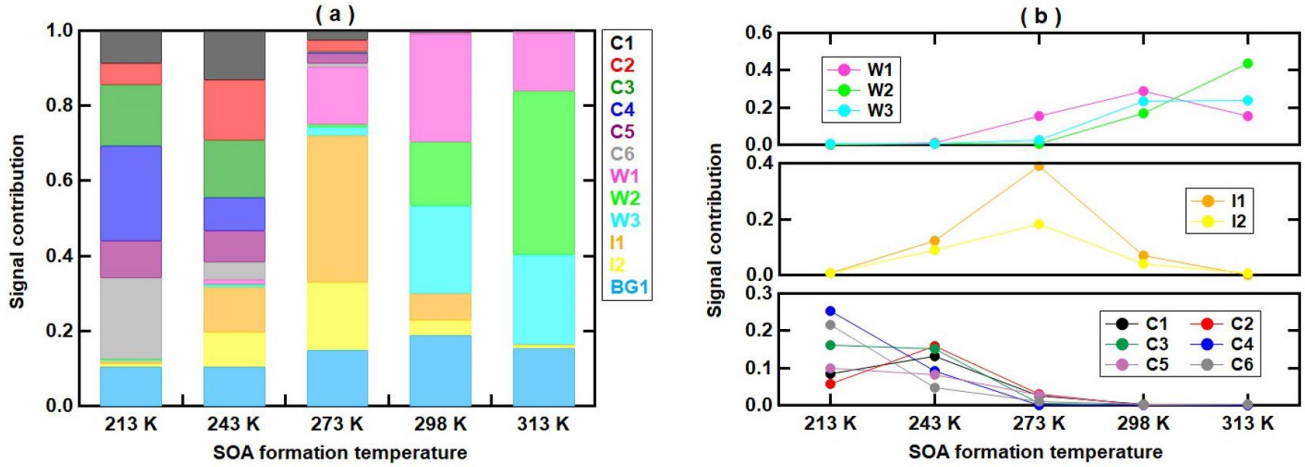

Figure 33. Factor contribution to β-caryophyllene SOA at five temperatures. The total detected deposited signals are $(3.0 \pm 0.9) \times 10^4$ counts s^{-1} for the five samples.

Different from the cold case, the two SOA samples in the warm case are resolved completely by a totally disparate factor pattern with two monomeric factors (W1, W2) and a dimeric factor (W3). The chemical composition shows that W2 mainly consists of HOM molecules, with a signal-weighted average elemental composition of $C_{15.0}H_{22.6}O_{6.8}$, the highest observed OS_C and O:C ratio (-0.53 and 0.49) among all factors, and the highest monomer factor T_{max} (100 °C). Thus, W2 is categorized as the least volatile monomer factor. In parallel, as the other monomer factor at the warm case, W1 has the second-highest OS_C and O:C ratio (-0.66 and 0.45) among all sample factors. Although some molecules with the same formulas can contribute to both W1 and W2, e.g., $C_{14}H_{22}O_{6\text{-}7}$, the PMF analysis identifies those molecules to be isomers with different structures due to a large T_{max} difference of 25 °C between W1 and W2. It signifies that those isomeric monomers belong to different volatility ranges. In addition, the only dimer factor in the warm case, W3, has a high T_{max} of 135 °C and is actually a mix of dimers and again either extremely low-volatile monomers or thermal decomposition products from oligomers.

In addition, I1 and I2 are labelled as the intermediate temperature factors, consisting of the monomers and/or with small amount of dimers, and differ 50 °C in T_{max} to each other. More than 60% of signals at SOA_{273K} are resolved by I1 and I2, suggesting the intermediate factors contribute mostly to the SOA formation temperature at about 273K.

$C_{15}H_{24}O_3I^-$ was the most abundant ion detected by FIGAERO-CIMS for low- and intermediate temperature experiments. The ion thermograms are depicted in Figure 34. The thermogram PMF analysis was unable to reconstruct the desorption behaviour of this ion even

with 15 factors. This may be caused by the rather unique thermal desorption behaviour of this ion and its distinct changes between experiments. Two trends are visible: The contribution of $C_{15}H_{24}O_3I^-$ in both the particle and the gas phase decrease with increasing formation temperature (see Supporting Information) and the shape of the thermograms change significantly.

For the higher formation temperatures, the fitted main part of the thermogram is in the SVOC or upper LVOC range, and their partition into the particle phase is expected to be affected by the increasing formation temperature. However, the overall concentration of $C_{15}H_{24}O_3$ in the gas phase also decreases with increasing formation temperatures (Supporting Information), which suggests that the lower particle phase concentration of $C_{15}H_{24}O_3$ results mainly from the decrease of the formation pathway of $C_{15}H_{24}O_3$. It is also possible that $C_{15}H_{24}O_3$ is still formed at higher temperature but is then consumed by consecutive reactions.

Careful inspection of the ion thermograms shows that for each experiment at least two peaks are clearly visible in the ion thermogram and that the T_{max} of these two peaks varies between experiments. From the comparison of the thermograms of all experiments we derived, that most likely up to six compounds (isomers and/or decomposition products) contribute to the signal with this elemental composition. Hence, a set of six Gaussian peaks with manually chosen peak positions was used to fit the thermograms of $C_{15}H_{24}O_3I^-$ in all SOA samples (Figure 34). Not all thermograms are composed of six modes, for example, for SOA_{213K}, compound 2 (T_{max} = 61 °C) was set to zero by the fitting algorithm and does not contribute to the fitted total thermogram. It indicates that the real compound represented by compound 2 does not exist in SOA_{213K}. We acknowledge that the T_{max} values chosen for these 6 compounds will impact the fitting result. However, comparing multiple solutions with different T_{max} values showed that the overall interpretation presented below was not affected.

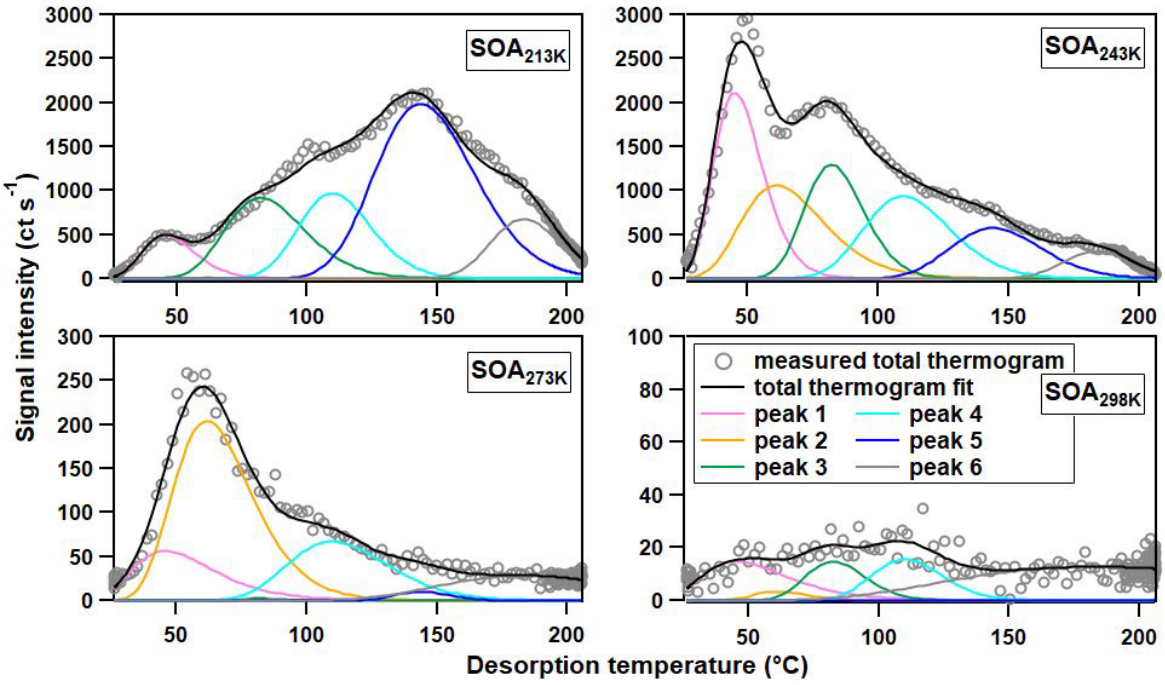

Figure 34. Fixed-peak gaussian fit for $C_{15}H_{24}O_3I^-$ at the temperature (from top to bottom) of 213K, 243K, 273K, and 298K. Grey circles refer to the measured data from FIGAERO-CIMS, while the black solid lines are the fitted total thermogram. Other colored solid lines show the individual fitted gaussian peaks.

For this molecule, compounds fitted with T_{max} below 100 °C are assumed to be monomers since 100 °C is roughly the threshold temperature where thermal decomposition may start to be relevant for carboxylic acid systems based on their estimated enthalpy of sublimation (ΔH_{sub})(Salo et al., 2010). In this monomer range, at least two compounds contribute significantly to the total thermogram (compound 1 (T_{max} = 45 °C), compound 2 (T_{max} = 60 °C), and compound 3 (T_{max} = 82 °C) in SOA_{213K} and SOA_{243K}). The observed change in the ratio between these three compounds cannot be explained with a shift towards lower volatility compounds with increasing formation temperature. Therefore, it can be concluded that the formation pathway of the dominating isomer behind $C_{15}H_{24}O_3$ changes at varying SOA formation temperatures.

In a previous study, two isomeric compounds (β-hydroxycaryophyllon aldehyde and β-caryophyllonic acid) were identified for this sum formula as early-stage oxidation products from β-caryophyllene ozonolysis(Jaoui et al., 2003b; Winterhalter et al., 2009b; Li et al., 2011b; Chan et al., 2011b). While it is not clear if these two compounds were indeed detected in our study, we can us these known molecular structures as examples for the types of compounds that may be produced in our study. As the molecular structure is known for these two compounds, the expected saturation vapor pressure can be calculated with a group contribution method(Moller et al., 2008;

Nannoolal et al., 2004). Saturation vapor pressure of 1.4×10^{-4} Pa for the aldehyde and 3.8×10^{-5} Pa for the acid were estimatedI.e., the C^*_{298K} of these two isomers are over one order of magnitude different which shows that isomeric compounds can have distinctly different volatility and thus occur at different T_{max} values in the thermogram.

In the higher desorption temperature period, a mode is dominating (compound 5 (T_{max} = 144 °C) especially for SOA_{213K}, while it contributes less to the SOA formed at high temperatures, i.e. >273K. Considering its high T_{max}, it is more likely a decomposition product of thermally unstable larger molecular weight compounds, e.g. dimers, or other oligomers. This suggests that the formation of dimer/oligomers which can be thermally fragmented to be $C_{15}H_{24}O_3$ is favored at lower SOA formation temperatures. Thermal decomposition has been found to be a significant contributor to the total ion signal in monoterpene SOA(Docherty et al., 2005; Stark et al., 2017), and here we suggest it is also important in β-caryophyllene SOA. By the calibrated correlation between the saturation vapor pressure and T_{max}, we estimate the $\log_{10}C^*_{298K}$ for these six compounds as 3.3, -3.9, -4.8, -5.9, -7.2, and -8.8 μg m^{-3} in order of compound number. Thus, the $C_{15}H_{24}O_3$ isomers span the ULVOC range at 213-243K, and the ELVOC range at 273K, while the potential decomposed oligomers are all in the ULVOC range at all SOA formation temperatures, revealing a high condensing potential for β-caryophyllene oxidation products to contributing to the particle formation.

The conversion of volatility bins is apparent with the temperature change as shown in Figure 35 (a) and (b). Using the PMF factor method (Figure 35 (b)), for SOA_{298K} and SOA_{313K}, all factors including the HOM factor (W1), fall in the LVOC and ELVOC range (based on C^*_T), with C^*_{298K} of most compounds being below 10^{-4} μg m^{-3}. For the cold case (213-243K), the volatility class shifts to the ULVOC range (based on C^*_T) for both monomer and dimer factors. It indicates that the particles formed at colder temperatures are less volatile and less oxygenated than at warmer temperatures which agrees with the HR-AMS measurement in Table 8 and Figure 29. The oxidation state of the monomers in SOA_{213K} and SOA_{243K} is significantly lower than the those detected in SOA_{298K} and SOA_{313K}, and hence the monomer factors (C1, C2) have higher $\log_{10}C^*_{298K}$ than the HOM factor (W1) as expected. But due to the significantly lower ambient temperatures which control the effective volatility more than the differences in chemical

composition., C1 and C2 in SOA_{213K} and SOA_{243K} are still less volatile than W1 in SOA_{298K} and SOA_{313K}.

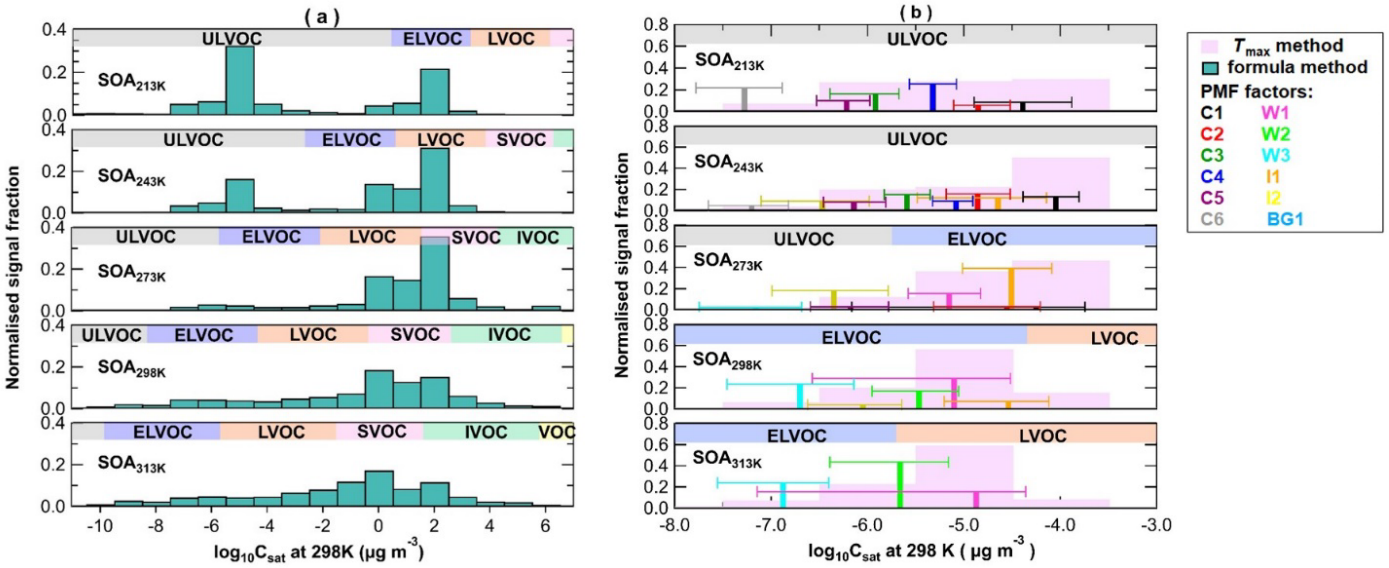

Figure 35. One-dimension volatility basis set (1D-VBS) in basis of formula method (a), and volatility calibration(b) for SOA formed at temperatures (from top to bottom) of 213K, 243K, 273K, 298K, and 313K. (b): purple wide bars are 1D-VBS from the T_{max} method on basis of the molecular volatility calibration, and narrow bars are from thermogram PMF method. The colored boxes along the x-axis in (a) and (b) indicate the volatility classes: ULVOC, ELVOC, LVOC, SVOC, IVOC, and VOC. These boundaries of the volatility classes defined at 298K and are shifted to the reaction temperatures using the Clausius-Clapeyron relation. The detailed calculations are presented in the Appendix1.

For comparison, the molecular volatility distribution on basis of the formula method(Li et al., 2016; Donahue et al., 2011) (Figure 35 (a)) and the T_{max} method (pink shadow in Figure 35 (b)) are presented as well. From the formula method, for SOA_{298K} and SOA_{313K}, compounds span a wide volatility period between ELVOC and IVOC range, with $-10 < \log_{10}C^*_{298K} < 6$, with mainly monomers falling in the bins in SVOC and IVOC ranges. This range extends to much higher volatilities than the volatility bins estimated from thermogram PMF factors ($-8 < \log_{10}C^*_{298K} < -4$). On the contrary, the two relevant volatility groups are in the SOA_{243K} and SOA_{213K}, with monomeric contribution mainly in LVOC and/or ELVOC classes, and dimeric contribution in the ULVOC class, which describes quantitatively higher volatilities of monomers and similar volatilities of dimers compared to the estimation from the thermogram PMF method. The molecular volatility calibration method is more similar to the thermogram PMF method. However, the thermal decomposed compounds which have a relatively shorter carbon backbone and higher molecular T_{max}, i.e., compounds in factor C6 (Figure 35 (b)) bias the derived volatility leading to an overestimation of the molecular volatility when using the T_{max} method.

Given the above, the lower overall volatility of β-caryophyllene SOA is observed using the thermogram PMF method compared to the estimation from the formula method and T_{max} method over a wide SOA formation temperature range of 213K-313K. This discrepancy highlights not only again the effect of chemical environments on the volatility distributions (e.g., activity coefficient changes) (Stark et al., 2017) in complex chemical mixtures, i.e., SOA particles, but also the impact of compounds thermally decomposed from larger oligomers, especially for mixtures arising from compounds with long carbon chains and containing a large fraction thermally unstable of oligomers.

Both, the PMF analysis with most ion thermograms showing contributions of multiple factors and the analysis of the single ion in section 3.3, show that the single ion thermogram may be formed by multiple isomers and products of thermal decomposition with a range of volatilities spanning multiple orders of magnitude in C*. Selecting a single T_{max} value to represent the volatility of this group of compounds can work well if the group is dominated by one or a few compounds with similar volatility and the tailing/fronting of the thermogram is not too pronounced. This volatility estimation method will capture changes of the dominant compound which determines the T_{max} position, e.g., depending on the SOA formation conditions. But it does not take other changes in the ratio between the isomers/decomposition product into account and may thus overestimate the volatility of the sample.

With varying SOA formation temperature, factors showed different responses, as shown in Figure 33 (b). We grouped the factors according to the behaviour of their signal contribution with increasing formation temperature. ‘Decreasing factors’ (C4, C6) showed lower contributions with increasing formation temperature. ‘Increasing factors’ (W2, W3) increased their contribution with formation temperature. ‘Peak factors’ (C1, C2, W1, I1, I2) exhibited first increasing and then decreasing contributions. ‘Trapezoid factors’ (C3, C5) did not change their contribution between the two lowest formation temperatures, but at higher formation temperatures their contribution decreased.

How much a factor contributes to the measured particle phase composition depends on how much of the compounds grouped into this factor are produced in each experiment in relation to the other reaction products. The importance of individual chemical reaction pathways is temperature dependent. For example, the degree of autooxidation increases with temperature (Bianchi et al.,

2019)while dimer formation generally decreases with higher temperatures. Changes in the contribution of factors can also be cause by the temperature dependent partitioning. With higher formation temperatures, the C_T^* values of the factors increase, and the gas-to-particle phase partitioning will adjust accordingly. For example, the compounds grouped into a factor may become too volatile to stay in the particle phase. Thus, the contribution of this factor will decrease with increasing formation temperature. Note that an increase in C_T^* will only be relevant if this leads to a shift into the upper LVOC or SVOC range. For the experimental conditions, the ELVOC and ULVOC category can be considered to be non-volatile and such compounds will partition almost completely into the particle phase.

The decreasing factors only exist at 213-243K where all compounds are estimated to be in the ULVOC range. Thus, they will not change their gas-to-particle partitioning and only be affected by the formation chemistry. The formation of the compounds grouped into the decreasing factors seem to be favoured by lower temperatures (i.e. 213K). The major compound in C4, $C_{30}H_{48}O_5$, has a larger signal contribution in the gas phase at 243K than at 213K. With the same reasoning, trapezoid factors also seem to be mostly governed by the formation chemistry but with a higher optimal temperature (i.e., between 213K and 243K). Since the peak factors occur over the whole formation temperature range, both mechanisms (temperature dependent gas-to-particle partitioning and temperature dependent chemistry) need to be considered. As the partitioning process is expected to have a minor impact on the factors in the ULVOC range, C1, C2 and I2 are mainly controlled by the formation chemistry with an optimal temperature of 243K. W1 falls into the ELVOC (at 273-298K) and SVOC range (at 313K) thus the partitioning to the particle phase will be reduced at the highest formation temperature. This counteracts the expected increase of production of compounds grouped into W1 (i.e., HOM molecules) leading to a peak of the contribution at 298K..The other factors relevant in the warm cases all have a lower volatility (ELVOC to LVOC range at all formation temperatures). They are increasing factors as the increase in production with increasing temperature is not affected by changes in partitioning.

4.2.6 Summary

In this chapter, different types of SOA were performed to investigate the yields, kinetics, chemical composition, and volatility of particles from β-caryophyllene oxidation. The rate coefficient of β-caryophyllene reacting with O_3 was determined between 243 and 313K, showing

decreasing values with increasing temperatures. Its reaction enthalpy of (5.6±1.0) KJ mol^{-1} and OH radical yields increasing from (5±2) % at 243K to (15±2) % at 313K were determined.

The variation of the ozonolysis temperatures revealed substantial impact on the abundance of individual organic molecules. In the first generated SOA, monomers (mainly $C_{14-15}H_{22-24}O_{3-7}$) and dimers (mainly $C_{28-30}H_{44-48}O_{5-9}$) were abundant, wherein minor signals of trimers (mainly $C_{41-44}H_{62-66}O_{9-11}$) were mainly detected at 213K. Potential dimer and trimer formation pathways are proposed. With temperature increasing to 313K, monomers and dimers ($C_{14-15}H_{22-24}O_{6-9}$ and $C_{27-29}H_{42-44}O_{9-11}$, respectively) became more oxidized, and no significant trimeric signals were detected.

In addition, a counterbalancing effects of oxidation product formation chemistry and the temperature was observed. The particle measurements found a counter-intuitive behaviour of the T_{max} of the sum thermograms from FIGAERO-CIMS, which indicates the particle volatility increased first and then decreased with the ambient temperatures from 213K to 313K. I used PMF to deconvolute thermograms and distinguish the isomers and thermal decomposition compounds in figuring out the temperature dependence on SOA particle formation and volatility from β-caryophyllene ozonolysis.

Three volatility estimation methods were applied to determine the volatility of β-caryophyllene SOA particle formed at 213-313K. All detected species formed at 213K-243K are in the ULVOC range, and compounds formed at 298K-313K were more volatile to span ELVOC and SVOC bins. As more HOM compounds that were in larger oxygenation were formed at higher temperatures, the volatilities of those particles on one hand decreased with the higher contribution of HOM molecules, and on the other hand increased with the higher ambient temperatures. As a result, HOM monomers were in the SVOC range at 313K, and can evaporate to the gas phase via the partitioning process. Hence, compounds remaining in the particles were contributed more from dimers with lower volatilities.

4.3 SOA from β-caryophyllene ozonolysis in the presence of NO_x

After the SOA formation from β-caryophyllene ozonolysis additional SOA was formed in presence of NO_2, N_2O_5, and NO_3 radicals, mainly condensing on the pre-existing particles but partially also forming new particles, shown as the time period between 118-220 min in Figure 22.

In this section, I will present the molecular composition (4.3.1), and SOA volatility (4.3.2) of the SOA formed in the presence of NO_x. Please note that part of section 4.3.1 is reprinted with permission from the journal of Atmospheric Chemistry and Physics corresponding to my publication: Gao, L., Song, J., Mohr, C., Huang, W., Vallon, M., Jiang, F., Leisner, T., and Saathoff, H.: Kinetics, SOA yields, and chemical composition of secondary organic aerosol from β-caryophyllene ozonolysis with and without nitrogen oxides between 213 and 313 K, Atmos. Chem. Phys., 22, 6001–6020, https://doi.org/10.5194/acp-22-6001-2022, 2022.

The particle mass formed in the presence of NO_3 corresponded to 49%, 34%, 49%, 65%, and 63% to the total particle mass at 213K-313K, respectively. As β-caryophyllene could also be oxidized by NO_3 radicals, organonitrates (org-Ns) were formed as the major products (Kiendler-Scharr et al., 2016; Wu et al., 2021). I used a kinetic box model to estimate the concentration of NO_3 radicals before the final addition of β-caryophyllene, as shown in Figure S10, Figure S12, and Table 7. Besides, the maximum contribution of NO_3 radicals to the β-caryophyllene oxidation was estimated to be 72%, 90%, and 84% for 313K, 298K, and 273K based on the concentration of O_3 and NO_3 radicals and reaction rates.

4.3.1 Molecular composition

The averaged mass spectra for gas phase at all temperatures are presented in Figure 36, illustrating the corresponding chemical composition with a stable SOA concentration after the last addition of β-caryophyllene, e.g., time period after 160 minutes in Figure 22. Orgnonitrates (org-Ns) in the gas phase had decreasing signal fractions of 48.9%, 46.5%, 38.3%, 26.0% and 20.7% from 313K to 213K, respectively. Org-Ns comprised mainly three carbon groups, $C_5H_7O_6N$, $C_{10}H_{15}O_{5\text{-}7}N$ and $C_{15}H_{23,25}O_{6\text{-}8}N$. Figure 36 shows the time series of gas-phase signals of $C_5H_7O_6N$, $C_{10}H_{15}O_6N$, and $C_{15}H_{25}O_7N$. It was seen that $C_5H_7O_6N$ and $C_{10}H_{15}O_6N$ was formed immediately after the NO_2 addition, suggesting their formation was corresponded to products derived from β-caryophyllene ozonolysis and NO_3 radicals. On contrast, $C_{15}H_{25}O_7N$ was formed only after the addition of β-caryophyllene, indicating that it was a product of β-caryophyllene reacting with NO_3 radicals.

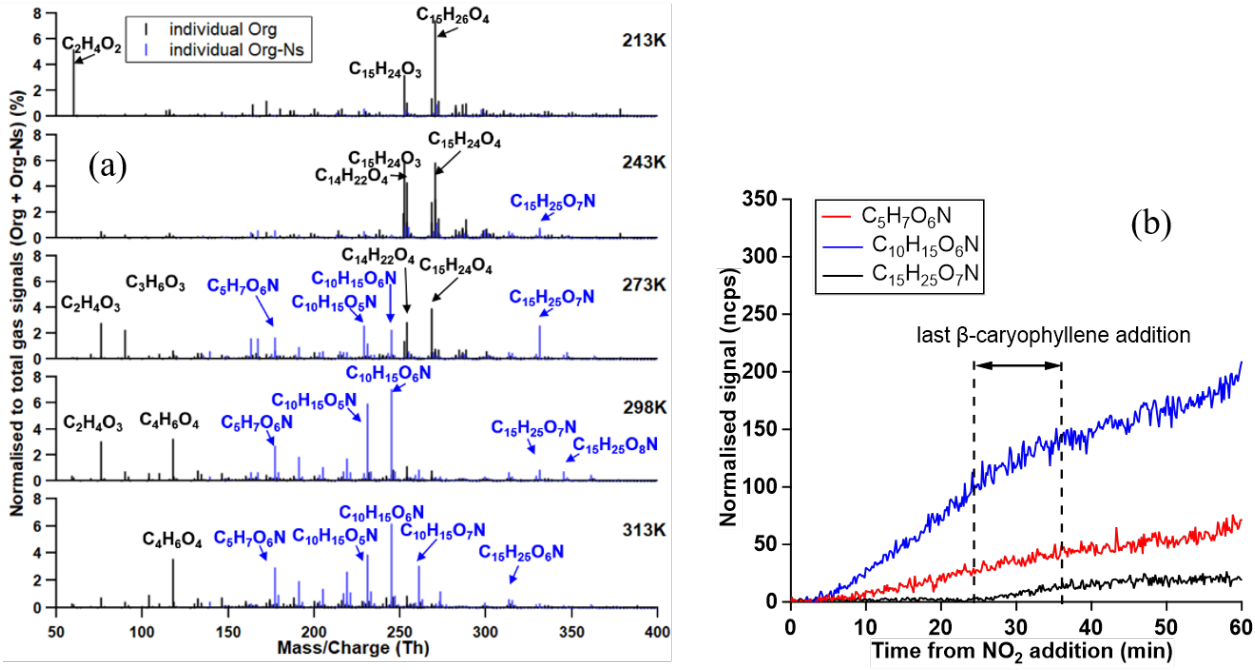

Figure 36. CIMS gas phase mass spectra for all temperatures in the presence of NO_2 (a). These spectra correspond to the same time as the particle phase spectra shown in Figure 38. Colours refer to compounds without nitrogen atoms (black) and compounds with one nitrogen atom (blue). The I^- (*m/z* =126.9) was subtracted and here the mass/charge refers to the weight of the molecules. The panel (b) shows the FIGAERO-CIMS measurement for the signal change of three typical organonitrate molecules for C_5 ($C_5H_7O_6N$, red line), C_{10} ($C_{10}H_{15}O_6N$, blue line) and C_{15} ($C_{15}H_{25}O_7N$, black line) corresponding to the evolution starting after NO_2 addition at 298K.

Chemical composition for the particle phase from β-caryophyllene ozonolysis in the presence of NO_2 at 213K and 313K is showed in Figure 37. At 213K, the particle was dominated by the no nitrogen-containing organic compounds (org), with signal fraction of 97.1%. Its mass spectrum was similar to the particle without presence of NO_3, consisting of monomers (41.2%), dimers (48.2%), and trimers (7.4%), with the most abundant molecules of $C_{15}H_{24}O_3$, $C_{30}H_{48}O_5$ and $C_{44}H_{68}O_9$, respectively. Besides, org-Ns only accounted for 2.8% to the particle at 213K measured by FIGAERO-CIMS, and 8% detected by HR-AMS (Figure S15), with $C_{15}H_{25}O_7N$ as the major org-N molecule.

On contrast, at 313K, the chemical composition was substantially different with that at 213K. Around 48.9% signals were explained by org-Ns. Monomeric org-Ns composed of $C_{15}H_{23,25}O_{6\text{-}10}N$, accounting for 35.5% to total signals. This is agreed with the organonitrates of $C_{15}H_{23\text{-}25}O_{7\text{-}9}N$ reported by Wu et al. (2021). Besides, 51.1% total signals were explained by org species, consisting for 28.3% monomeric orgs ($C_{13\text{-}15}H_{20\text{-}24}O_{4\text{-}8}$), 16.6% of dimeric orgs ($C_{20}H_{22\text{-}24}O_{7\text{-}9}$) and 6.3% of trimeric orgs ($C_{35}H_{48}O_{10\text{-}13}$).

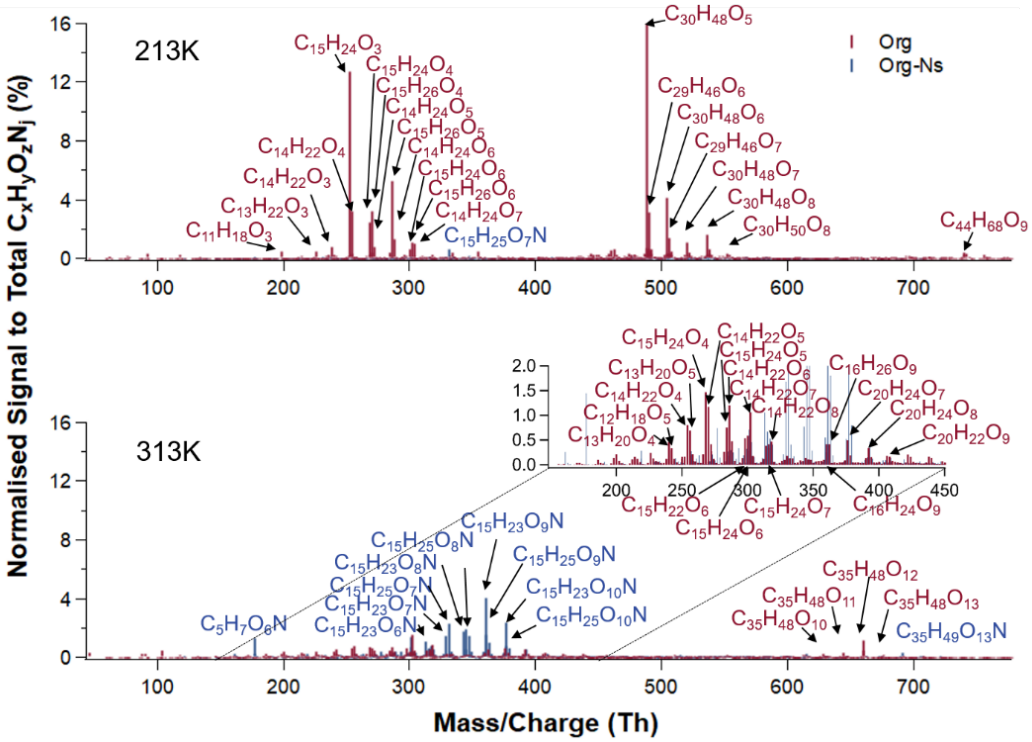

Figure 37. CIMS mass spectra of particle phase compounds obtained from ozonolysis of β-caryophyllene in presence of nitrogen oxides at 213K (upper panel) and 313K (lower panel). Colours refer to compounds without nitrogen atoms (red) and compounds with one nitrogen atom (blue).

Figure 38 shows the mass spectra and the assignment of molecules for particle phases formed at all temperatures. For 298K and 313K, $C_{15}H_{24}O_4$ exhibited with the highest signal fraction among all orgs while $C_{14}H_{22}O_7$ was not the most abundant product. This is attributed to the addition formation of pure MLOCs after the addition of NO_2, being confirmed by the comparison of the signal intensities of $C_{15}H_{24}O_4$ and $C_{14}H_{22}O_7$ before and after the addition of last β-caryophyllene (Figure S16).

Furthermore, I observed dimeric molecules with skeletons containing 20 carbon atoms, such as $C_{20}H_{24}O_{7\text{-}8}$, as shown in the insertion of Figure 37, and trimeric components with skeletons containing 35 carbon atoms, such as $C_{35}H_{48}O_{12}$, as presented in Figure 37 and Figure 38. Those C_{20} and C_{35} species were newly formed after the presence of NO_3 radicals, observed only in the particles formed at temperatures above 273K. However, the oxidation products of β-caryophyllene ozonolysis reacting with NO_2 and NO_3 radicals cannot be excluded as the source of the formation of C_{20} and C_{35} species. On contrast, no substantial changes were observed on the chemical composition of pure organic molecules formed at 213-243K, compared with that from β-caryophyllene ozonolysis without NO_3 present Figure 27. This could be resulted from the lower

concentrations of NO_3 radicals at lower temperatures. The potential lower activity of the reaction pathway involving NO_3 radicals may also play a role.

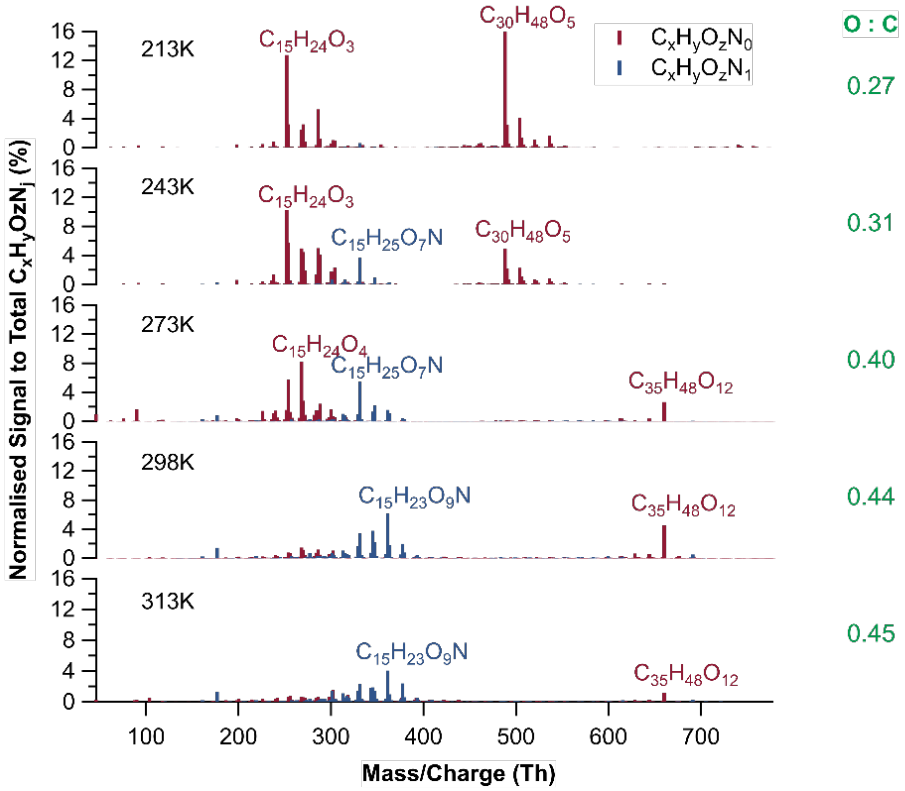

Figure 38. CIMS mass spectra for particle phase compounds for all five temperatures (213 – 313 K). Colors refer to $C_xH_yO_zN_0$ (brown) and $C_xH_yO_zN_1$ (blue) compounds. The table lists the average O:C ratios for each temperature.

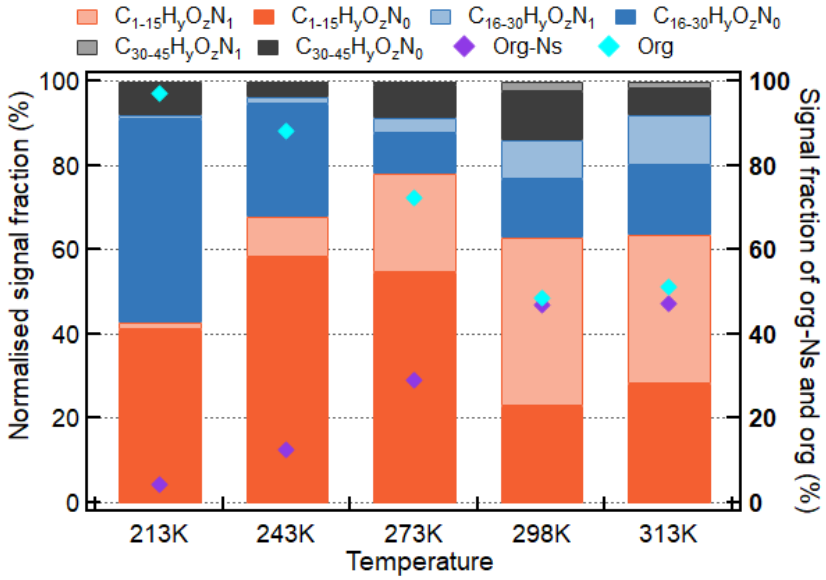

Figure 39. Product groups (monomeric org, dimeric org, trimeric org, monomeric org-Ns, dimeric org-Ns, and trimeric org-Ns) contributing to SOA from ozonolysis of β-caryophyllene in presence of nitrogen oxides at temperatures between 213 – 313 K.

In addition, with temperature increasing, the signal fraction of organonitrates was higher, accounting from 2.8% to 51.5% from 213K to 298K, and 48.9% for 313K, dominated by $C_{15}H_{23,25}O_{6\text{-}10}N_1$. The monomeric org-Ns contributed from 1.7% to 40.1% from 213K to 298K, and 35.5% at 313K (Figure 39), with an obvious shift of the most abundant org-N from $C_{15}H_{25}O_7N_1$ at 243-273K to $C_{15}H_{23}O_9N_1$ at 298-313K. A monotonic increase in the signal-weighted mean O:C ratio of org-Ns from 0.41 to 0.51 from 213K to 298K, and 0.50 at 313K was observed. I assume that the positive temperature dependence on the formation and oxygenation of org-Ns may also be corresponding to the highest temperature (313K). The decrease of signal fraction of org-Ns could be explained by that the oxidation products at 313K was too oxygenated (e.g., O:C ratio > 0.51) to be detected by FIGAERO-CIMS. This is supported by the measurement from HR-TOF-AMS that the mass fraction of organonitrates had a monotonic increase from 8% to 61% from 213K to 313K (Figure S15). Furthermore, thermal instability of some org-N species, such as peroxy nitrates (Francisco and Krylowski, 2005; Lee et al., 2016), resulting in thermally fragments (e.g., $C_5H_7O_6N_1$), could also result in the weaker increase of total org-Ns at 313K. Major products in both gas and particle phases are presented in Figure S17. Compared with the SOA formed with NO_2 absence, the signal fraction of $C_{15}H_{24}O_{3\text{-}4}$ in the SOA decreased in the SOA formed in the presence of NO_2. $C_{30}H_{48}O_5$ had higher signal intensity at 213-243K. On contrast, $C_{35}H_{48}O_{12}$ contributed more at higher temperatures (273K-313K), while $C_{15}H_{25}O_7N$ showed the largest signal fraction only at 273K.

4.3.2 SOA volatility

To compare with the SOA formed from β-caryophyllene ozonolysis (already discussed in section 4.2), a 11-factor PMF solution was conducted to resolve the total thermograms of all no-nitrogen-containing products that were generated in the presence of NO_x at five temperatures. Figure 40 shows the total thermograms from the measurement, the resolved thermograms of individual factors, and the averaged chemical composition of factors by showing the molecular OS_C corresponding to the numbers of carbon. For the SOA particles formed at cold temperatures (213K and 243K, hereafter 'cold case'), six factors were retrieved to consist of ~95% signals of the measured thermograms (Figure S18). The evaluation of different solutions is presented in Figure 41. Comparing Figure 40 with Figure 31 and Table 9 with Table 10, the O:C, OS_C, chemical composition, and T_{max} of the six cold factors in both groups of SOA particles at the cold cases kept similar. As no additional factors for the particles at the cold case were generated, the volatility of

the no-nitrogen-containing components corresponding to the six cold factors were indicated to be similar to that of the particles from β-caryophyllene oxidation without NO_x (discussed in section 4.2.2).

Besides, there were two warm factors abundantly contributed to the particles formed only at high temperatures (298K and 313K, hereafter 'warm case'). Shown in Figure 40, W1 comprised abundantly C_{14} and C_{20} molecules, while W2 consisted of a wide range of compounds of C_3 and C_{10}-C_{40}. As presented in Figure 37 and Figure 38, the newly formed C_{20} and C_{35} no-nitrogen-containing components were classified in the two warm factors, with T_{max} of 95 and 145 °C, as shown in Table 10, respectively.

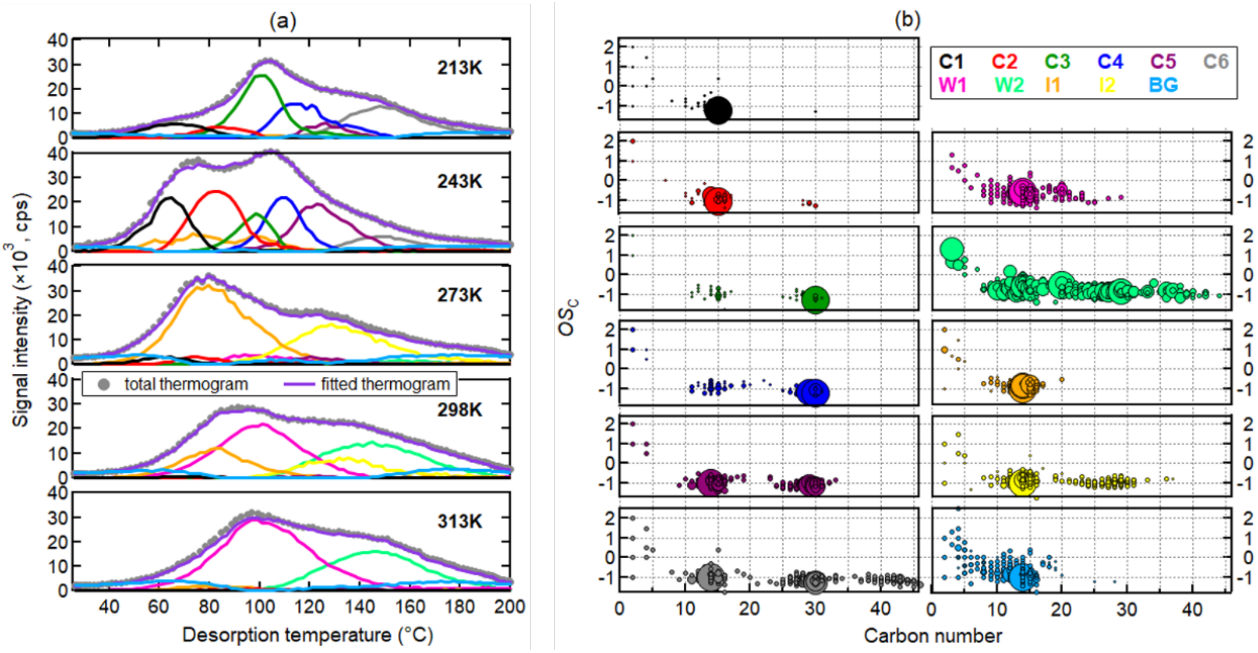

Figure 40. A 11-factor PMF solution for all no-N-containing organics in the β-caryophyllene SOA particles at five temperatures. (a) the measured total thermograms of all no-N-containing organics (grey point), the fitted total thermograms (purple line), and the factor thermograms for each sample; (b) the averaged chemical composition of each factor, with the averaged carbon oxidation state (OS_C) corresponding to the averaged carbon number. Colors are the same in all panels and indicate the individual factors in (a) and (b).

Table 10. List of 11 PMF factors and their properties like atomic composition, MW, O:C ratio, OS_C, and peak desorption temperature.

	Factor number	Molecule formula	MW (g mol^{-1})	O:C	OS_C	T_{max} (°C)
Cold	C1	$C_{14.3}H_{24.1}O_{4.6}$	266	0.35	-0.99	60
	C2	$C_{14.8}H_{24.8}O_{5.5}$	293	0.40	-0.87	80
	C3	$C_{25.7}H_{41.3}O_{5.3}$	433	0.25	-1.11	95
	C4	$C_{25.5}H_{40.6}O_{6.3}$	458	0.30	-1.00	110
	C5	$C_{22.2}H_{35.6}O_{6.3}$	449	0.30	-0.97	120
	C6	$C_{26.5}H_{41.8}O_{6.4}$	490	0.29	-1.02	145
Warm	W1	$C_{14.9}H_{22.4}O_{6.5}$	280	0.46	-0.59	95
	W2	$C_{21.9}H_{32.3}O_{7.5}$	311	0.39	-0.70	145
Intermediate	I1	$C_{13.6}H_{21.8}O_{5.2}$	266	0.42	-0.77	80
	I2	$C_{18.6}H_{28.7}O_{6.2}$	366	0.37	-0.81	130
Background	BG1	$C_{14.0}H_{21.5}O_{5.1}$	278	0.46	-0.64	N/A

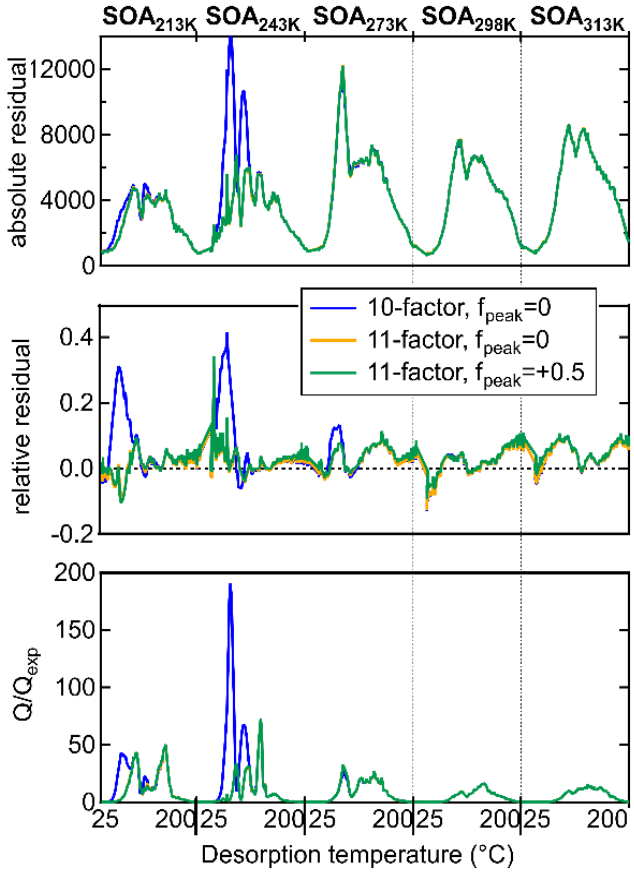

Figure 41. Residual, relative residual, and Q/Q_{exp} change for no-nitrogen-containing molecules in all samples (SOA formed at 213K, 243K, 273K, 298K, and 313K) when varying the number of factors and fpeak values.

In addition, it was seen in Figure 42 (a) that the total thermograms of all nitrogen-containing molecules were also multimodal, indicating the potential thermal decomposition on organic nitrates. The thermogram of all nitrogen-containing products formed at 213K was excluded, as the organic nitrates at 213K were not significantly formed. All nitrogen-containing products were categorized with eight factors, including four warm factors (W1-W4), three intermediate factors (I1-I3), and one background factor (BG) (Figure 42 b). W1 and W2 consisted of mainly C_{15} compounds, and they were thus regarded as monomeric factors, with high O:C ratio of 0.54 and 0.58, and T_{max} of 85 and 95 °C , respectively. W3 included C_{19} compounds followed by C_{15} species, with O:C ratio of 0.5 and T_{max} of 115 °C, whereas W4 had the lowest O:C of 0.47 but the highest T_{max} of 135 °C among all the warm factors. The abundance of W1 and W3 had a monotonic correlation with SOA formation temperatures, indicating the formation of the compounds corresponding to W1 and W3 was favoured by higher temperatures. However, W2 and W4 had peak contribution at 298K. The decrease of W2 and W4 at 313K could result from two reasons. On one hand, either the components related to W2 and W4 were formed less at higher temperature above 298K, or they were corresponding to other factors at 313K, e.g., factor W1. One the other hand, the related compounds may evaporate more at 313K and remain less in the particle phase. For the three intermediate factors, I1 and I2 had averaged molecular formula of $C_{14.3}H_{22.8}O_{6.8}N_1$ and $C_{14.4}H_{22.4}O_{8.0}N_1$, suggesting them to be monomeric factors, whereas I3 consisted of an averaged carbon chain of $C_{21.3}$, with O:C ratio of 0.42. I1 and I3 has negative monotonic correlation with the particle formation temperatures, indicating the related compounds were either formed more at lower temperature below 273K or evaporated more at higher temperatures. I2 had a peak contribution at 273K, indicating the species included in I2 were formed most at 273K.

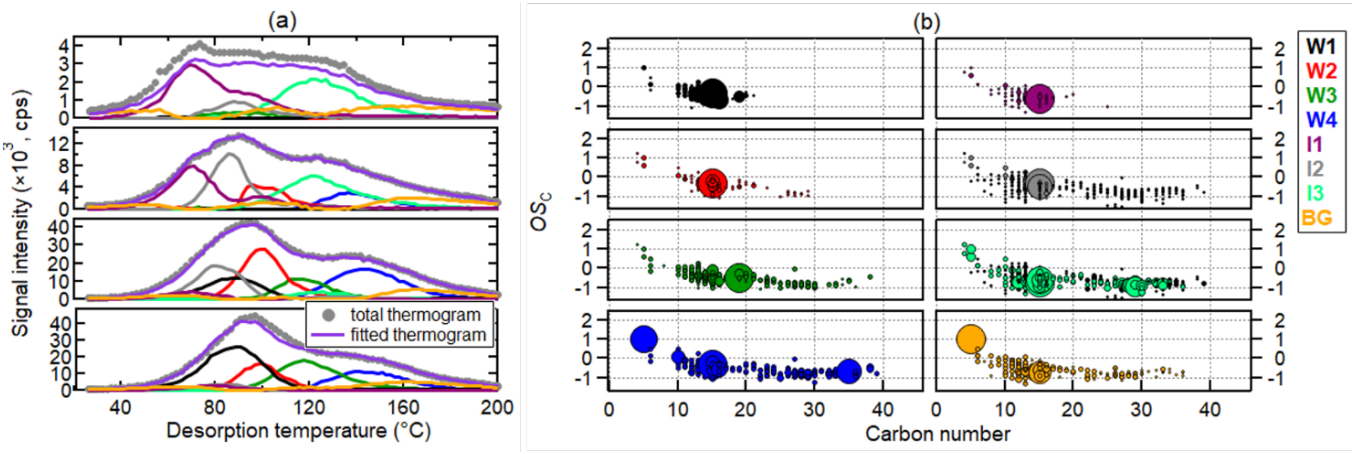

Figure 42. An 8-factor PMF solution for all N-containing organics in the β-caryophyllene SOA particles at five temperatures. (a) the measured total thermograms of all no-N-containing organics (grey point), the fitted total thermograms (purple line), and the factor thermograms for each sample; (b) the averaged chemical composition of each factor, with the averaged carbon oxidation state corresponding to the averaged carbon number. Colors are the same in all panels and indicate the individual factors in (a) and (b).

Table 11. List of 8 PMF factors and their properties like atomic composition, MW, O:C ratio, OS_C, and peak desorption temperature.

	Factor number	Molecule formula	MW (g mol^{-1})	O:C	OSC	T_{max} (°C)
Warm	W1	$C_{14.5}H_{21.6}O_{7.7}$	319	0.54	-0.41	85
	W2	$C_{15.2}H_{23.2}O_{8.6}$	343	0.58	-0.36	95
	W3	$C_{17.7}H_{25.4}O_{8.1}$	367	0.50	-1.46	115
	W4	$C_{21.8}H_{31.3}O_{8.7}$	432	0.47	-0.51	135
Intermediate	I1	$C_{14.3}H_{22.8}O_{6.8}$	303	0.49	-0.62	70
	I2	$C_{14.4}H_{22.4}O_{8.0}$	323	0.57	-0.42	85
	I3	$C_{21.3}H_{32.2}O_{8.1}$	417	0.42	-0.68	120
Background	BG1	$C_{14.4}H_{21.3}O_{6.4}$	297	0.54	-0.41	N/A

By converting the calibrated T_{max} to the saturation vapor pressures, Figure 43 showed the retrieved volatility distributions from either the molecules identified in FIGAERO-CIMS or the factors generated in thermogram PMF method. For both no-nitrogen-containing compounds and organic nitrates, the volatility bins (C^*_T) shifted with the SOA formation temperatures. At the cold case, all factors fell in ULVOC bins. The volatility bins shifted to be ULVOC and ELVOC at 273K, and to be ELVOC and LVOC at 298 and 313K. This was consistent with the volatility distribution using the T_{max} calibration approach. Specifically, more compounds were estimated via PMF method to be with saturation concentrations between 10^{-8} to 10^{-6} μg m^{-3} at the same ambient temperature of 298K, which were overestimated by the molecular T_{max} calibration method. Those

compounds were principally either lower volatile isomers or the thermal decomposed components. In this work, most of those compounds were at the case of thermal decomposition.

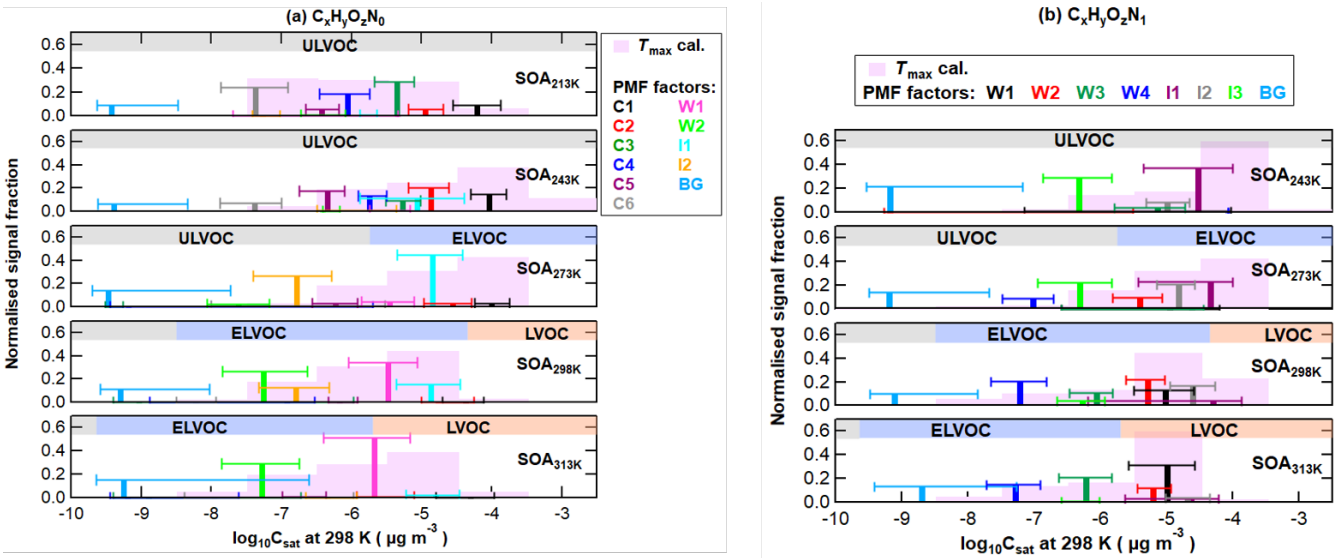

Figure 43. One-dimension volatility basis set (1D-VBS) from the T_{max} method and the PMF approach for the no-nitrogen-containing species(a), and nitrogen-containing components(b) for SOA aged with NO_x at temperatures (from top to bottom) of 213K, 243K, 273K, 298K, and 313K.

4.3.3 Summary

This chapter describes the chemical composition of the SOA from β-caryophyllene oxidation in the presence of NO_x for both gas and particle phases, and determines the volatility of the pure organics and organic nitrates in the β-caryophyllene SOA particles at 213-313K. Higher temperature resulted in higher oxygenated β-caryophyllene related organic nitrates. The gas phase organic nitrates showed an increasing abundance with increasing temperature from 20.7% to 48.9% at 213K to 313K, respectively. These organic nitrates mainly comprise three groups in different carbon numbers: $C_5H_7O_6N$, $C_{10}H_{15}O_{5\text{-}7}N$, and $C_{15}H_{23,25}O_{6\text{-}8}N$.

In the particle phase, higher signal contribution of organic nitrates was observed at higher temperatures. At 313K, organic nitrates consisted of 48.9% signals, substantially higher than that formed at 213K (only 2.8%). Most of the organic nitrates were found as monomers with a C_{15} skeleton with one nitrate group, assigned as $C_{15}H_{23,25}O_{6\text{-}10}N$, with their signal-weighted O:C ratio increasing from 0.41 to 0.51 for temperatures from 213K to 313K. Besides, reduced signal fraction of HOM species formed at 298-313K indicated the formation of organic nitrates was favored compared with the formation of autoxidation products. In addition, dimeric and trimeric pure organic species without nitrogen atoms (C_{20}, C_{35}) were newly formed in the presence of nitrogen

oxides at 298-313K, which substantially changed the chemical composition of pure organic components and indicates more termination ways might exist.

In addition, the effective volatility of pure organic products at 213-243K showed similar volatility compared to that of the compounds in the SOA particle from the β-caryophyllene ozonolysis. At 273-313K, the pure organic products (including newly formed C_{20} compounds) fell in the LVOC and ELVOC ranges. Volatility of organic nitrates increased from ULVOC range at 243K to ELVOC and LVOC bins.

4.4 SOA from oxidation of isoprene, α-pinene, and β-caryophyllene mixtures

In this chapter, I will present the comparison of the chemical composition (section 4.4.1) and volatility (section 4.4.2) of the SOA particles from mixtures of isoprene and β-caryophyllene with/without α-pinene at 294±1 K, with initial O_3 at lower (20-40 ppb) and higher (>500 ppb) levels, separately.

4.4.1 Chemical composition

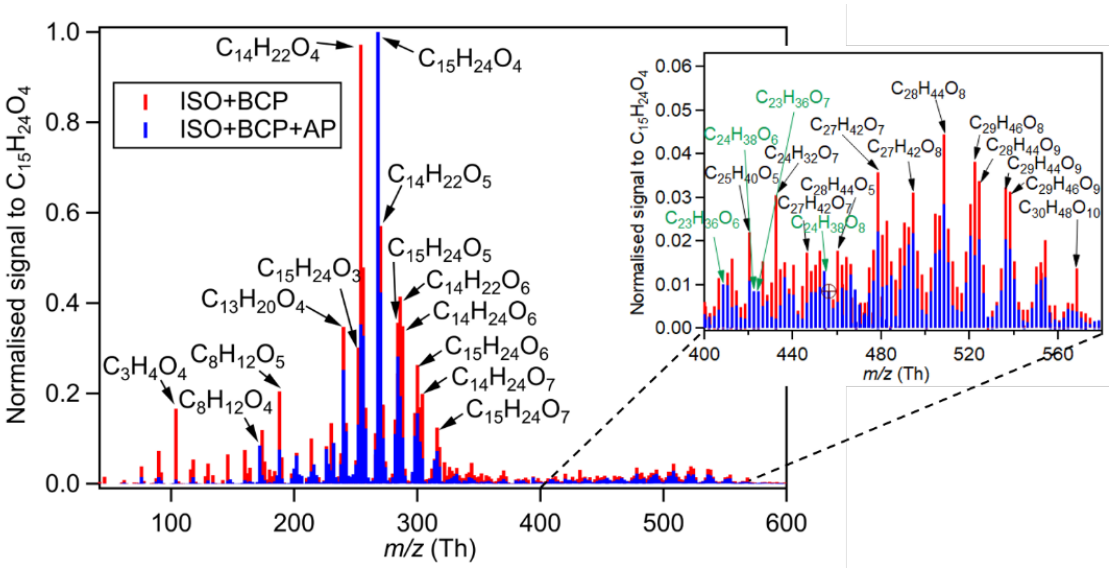

Figure 44. Mass spectra of the particles formed from binary (isoprene + β-caryophyllene) and ternary (isoprene + β-caryophyllene + α-pinene) system at low O_3 levels. The signals are normalized to the most abundant molecule ($C_{15}H_{24}O_4$) in each mass spectrum. The legends label the assigned molecular formulas. The insertion shows the mass spectra of the high weight mass range between 400 to 580 Th, wherein the green labels refer to the molecules with higher intensities in ternary system.

To provide the comparison for the chemical context of different systems, Figure 44 shows the chemical composition of the particles formed from the oxidation of a mixture of isoprene and β-caryophyllene in the absence and presence of α-pinene at low initial O_3 levels. The particles were formed after the initial reaction with 20-36 ppb O_3. The mass spectra were normalized to the $C_{15}H_{24}O_4$, which was detected to be the strongest signal intensity in both systems. It was seen that the oxidation products in the particle phases in both systems were dominated by the molecules with 13-15 carbon atoms, with significant signals of $C_{24\text{-}30}H_{40\text{-}48}O_{5\text{-}10}$ components. In the two-precursor system, the most abundant signals were $C_{15}H_{24}O_4$ and $C_{14}H_{22}O_4$ which were expected to be the early-stage oxidation products from β-caryophyllene which was discussed in the section 4.2. This is unsurprising, given the known high reactivity of O_3 reaction with β-caryophyllene ((1.2 ±0.4) × 10^{-14} cm^3 $molecule^{-1}s^{-1}$) compared to that with isoprene (1.28 × 10^{-17} cm^3 $molecule^{-1}$ s^{-1}) (Atkinson et al., 1982; Ren et al., 2017). Hence, the isoprene is expected to be initialled by the produced OH radicals. However, two of the representative closed-shell products $C_5H_8O_3$ (HPALDs) (Berndt et al., 2019) and $C_5H_8O_4$ which are sensitive enough to be detected by FIGAERO-CIMS, and the $C_{19\text{-}20}$ compounds that are the potential candidates of the interaction dimers from two precursors, had week signals in the binary and ternary systems, indicating the contribution of isoprene derived components to the particle mass was limited. Considering the rate coefficient of OH radicals reacting with isoprene (1×10^{-10} cm^3 $molecule^{-1}$ s^{-1}) is at the same level of that with β-caryophyllene (2×10^{-10} cm^3 $molecule^{-1}$ s^{-1}), the OH radical yield from the β-caryophyllene ozonolysis was indicated to be low, constant with the results from section 4.2. Additionally, as the oxidation products from β-caryophyllene, the monomers with 14-15 carbon atoms produced in the binary system were less oxidized than those from the ozonolysis of sole β-caryophyllene at 298K. This is potentially due to the low initial O_3 level of the binary system, leading to less oxidation products terminated via the autoxidation pathway.

The quantification of all oxidized molecule was nevertheless not accurate due to the lack of mass calibration, the detected signal of individual component was still comparable between two experiments due to the unchanged sensitivity of FIGAERO-CIMS as expected. As a typical α-pinene derived oxidation product which was sensitive enough to be detected by our FIGAERO-CIMS as discussed in the section 4.1, there was a significant enhancement of the relative signal intensity of $C_8H_{12}O_4$ and $C_{15}H_{24}O_4$ in the ternary system. This suggested the contribution of the products from α-pinene cannot be neglected, although the rate constant of O_3 reacting with α-

pinene is 100 times lower than it with β-caryophyllene (Atkinson et al., 1982; Khamaganov and Hites, 2001; Stewart et al., 2013). In addition, in the high weight range between 400-480 Th, several molecules, such as $C_{23}H_{36}O_{6\text{-}7}$ and $C_{24}H_{38}O_{6\text{-}8}$, had higher intensities in the ternary system (Figure 44). This indicated these molecules to be the interacted dimeric products from α-pinene and β-caryophyllene. Besides, unlike the highly oxygenated molecules ($C_{14\text{-}15}H_{22\text{-}24}O_{6\text{-}9}$) found as the major monomeric products in the single β-caryophyllene ozonolysis at 298K, the $C_{14\text{-}15}$ molecules formed in the ternary mixture systems were also lower oxidized with 3-8 oxygen atoms owing to the lower O_3 level. It is not excluded that the $C_{14\text{-}15}$ products could also be the dimers interacted between α-pinene and isoprene derived compounds.

Attributing of the elemental composition in the high resolution FIGAERO-CIMS analysis, Figure 45 (a, b) illustrates the particulate molecular carbon oxidation status corresponding to the number of carbons for the binary (isoprene + β-caryophyllene) system and the ternary (isoprene + β-caryophyllene + α-pinene) system at low O_3 levels. In both systems, the majority of signals was contributed by $C_{14\text{-}15}$ molecules, with OS_C between -1.3 to -0.2. The signal-weighted O:C ratio of the particle was 0.44 for binary system, slightly higher than that in the ternary system, because the contribution of the low mass weight molecules with $C_{<6}$ which have higher OS_C values than the major $C_{14\text{-}15}$ products. Note that the bulk O:C could be higher, and might be underestimated by this work, because the possibility that the higher oxidized oligomers may exceed the detection range of FIGAERO-CIMS cannot be excluded.

Subsequently, with the addition of excessive amount of O_3, the remaining VOC precursors were reacted, such as isoprene. The particulate chemical composition in both mixture systems are presented in the Figure 45 (c, d). For the binary system, it was seen that the majority of the signal increase was contributed by the $C_{13\text{-}15}$ and $C_{25\text{-}30}$ components, but not in the C_5 and C_{20} molecules. This indicates that the formation of potential dimers from isoprene and β-caryophyllene is not the major interactive way to derive the interacted oxidation products in the binary system. The signal-weighted O:C ratio was slightly decreased mainly due to the lower signal fraction of high oxygenated compounds in low weights with $C_{<5}$. The differences of the particulate chemical composition between initial low and subsequent high O_3 levels in the binary system can be seen in the Figure 46 (a). It was seen that the most of the $C_{14\text{-}15}H_yO_{\geq 6}$ compounds had an increase in signal fraction compared to that at the low O_3 level, wherein the relative signal abundance of $C_{14\text{-}15}H_yO_{<6}$ compounds were reduced, resulting from the subsequent oxidation of the carbon double

bond of unsaturated β-caryophyllene products. However, unlike the ozonolysis of the sole β-caryophyllene, the products from the autoxidation, $C_{14}H_{22}O_{7,9}$ and $C_{15}H_{22\text{-}24}O_{7\text{-}9}$, consisted only 2.5% of the total signals even with an access of O_3 of ~1000 ppb. This could result from that the β-caryophyllene was almost depleted before the addition of 1000 ppb O_3, thus, the reaction involved by the O_3 attack to the first double bond was not the dominating pathway. As the α-pinene and isoprene were depleted after the addition of ~1000 ppb O_3, the $C_{14\text{-}15}H_yO_{\geq 6}$ could also be their interaction products. Besides, after the large addition of O_3, the contribution of β-caryophyllene dimers ($C_{29\text{-}30}$) also increased, shown as Figure 45 (c) and Figure 46 (a).

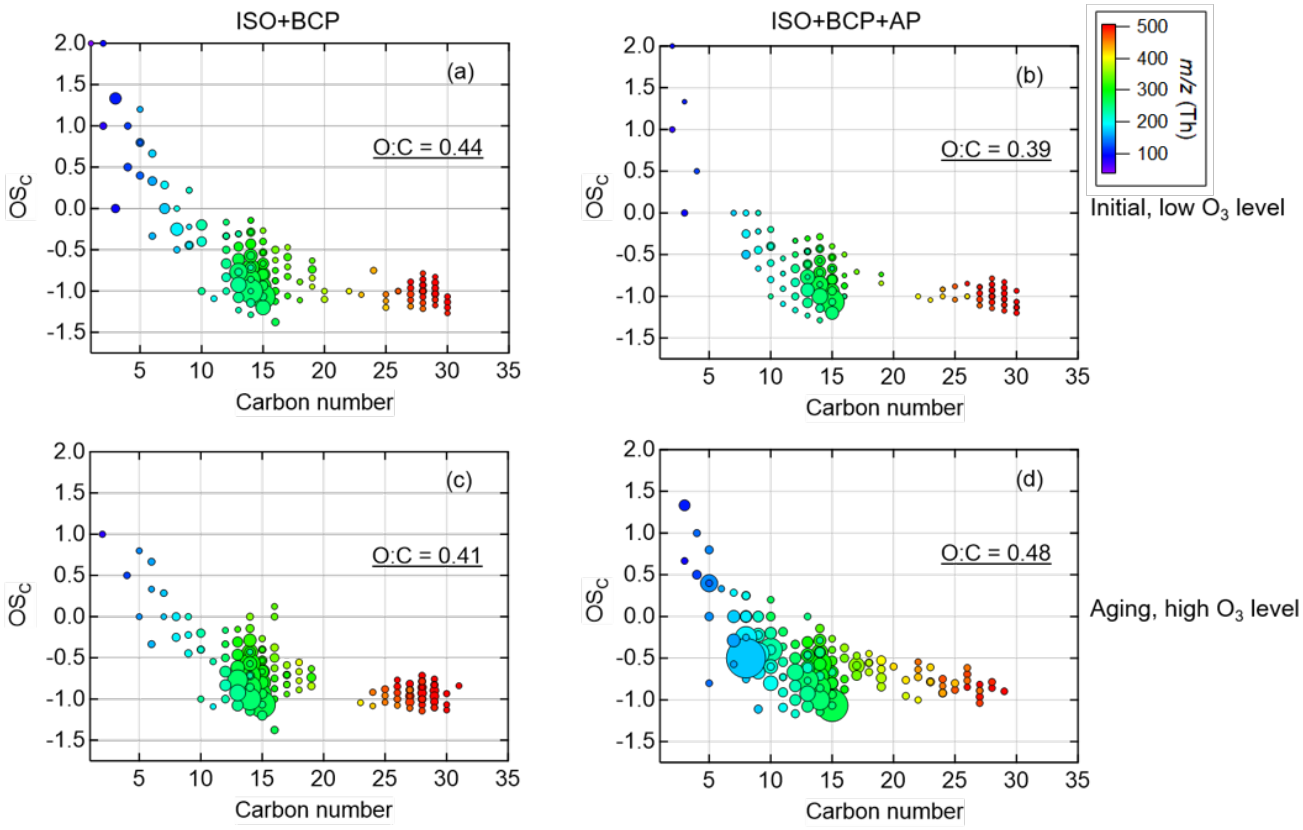

Figure 45. Particulate molecular carbon oxidation status (OS_C) corresponding to the number of carbon atoms per molecule at low and high O_3 levels. (a) binary isoprene/β-caryophyllene system at initially low O_3 level; (b) ternary isoprene/β-caryophyllene/α-pinene system at initially low O_3 level; (c) binary isoprene/ β-caryophyllene system aged at a higher O_3 level; (d) ternary isoprene/β-caryophyllene/α-pinene system aged by a higher O_3 level. The sizes of the dots relate to the root signal intensity of molecules, and the colors refer to the molecular mass weights. The insert gives a signal-weighted O:C ratio calculated on basis of the detected molecules from FIGAERO-CIMS. Only the components with the signal fraction higher than 0.1% were counted.

However, with the presence of α-pinene, the particle composition at the high O_3 level was substantially different, complexed with the interaction products among the oxidation of the parent precursors. A lot of $C_{5\text{-}10}$ molecules in relative higher oxygenation with OS_C between -0.8 to 0.5

were formed, showed in Figure 45 (b), with dominant signals of $C_8H_{12}O_4$ and $C_5H_8O_5$. They were suggested to be the oxidation products from either α-pinene or isoprene. Isoprene is expected to be initialled by the OH radicals yielded mainly from the α-pinene ozonolysis. As a result, the particle signal-weighted O:C ratio increased to be 0.48. Besides, the signals of $C_{14\text{-}15}$ molecules also increased abundantly, resulting from the oxidation of the second carbon double of the unsaturated β-caryophyllene derived products that remained in the gas phase. However, the highly oxygenated molecules of $C_{14\text{-}15}H_{22\text{-}24}O_{6\text{-}9}$ that were the major monomers of sole β-caryophyllene ozonolysis at 298K were not formed significantly in the ternary system with subsequent addition of ~950 ppb O_3. However, unlike the formation of highly oxidized oligomers in the binary, with the presence of α-pinene, the signal fraction of $C_{27\text{-}30}$ compounds decreased, whereas the species with 17-25 carbon atoms contributed more at the subsequent high O_3 level. It indicated the β-caryophyllene dimers ($C_{27\text{-}30}$) were suppressed by the α-pinene and isoprene derived products, resulting in the formation of shorter chain molecules ($C_{17\text{-}25}$). Additionally, the signal intensity of $C_{15}H_{24}O_4$ increased more than other $C_{14\text{-}15}$ molecules, even though its signal fraction reduced, compared to that at the low O_3 level previously, shown as Figure 46 (b). It indicated that the $C_{15}H_{24}O_4$ was likely to be produced not only as the β-caryophyllene derived early-stage oxidized product but also the potential interaction molecule from α-pinene and isoprene oxidation.

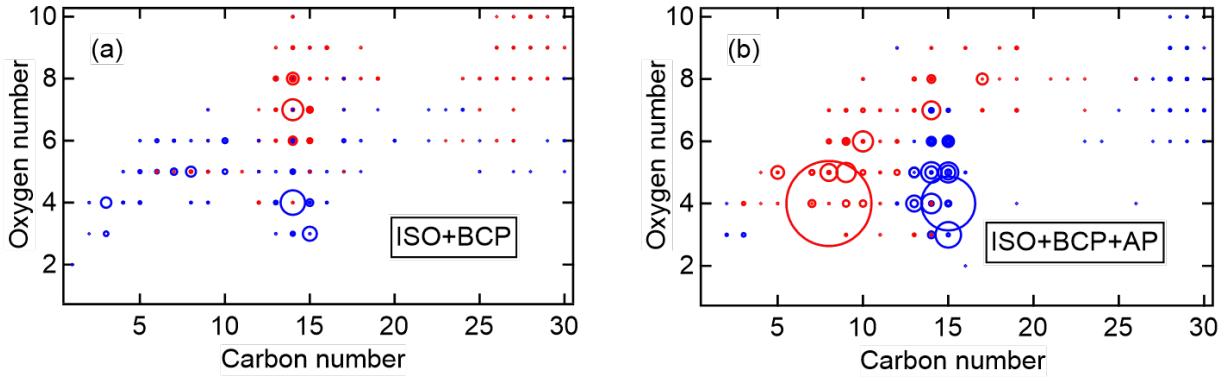

Figure 46. Oxygen number corresponding to the carbon atom number per molecule for those molecules that show changes between low and high O_3 levels in the binary (a) and ternary system (b). Red circles refer to the molecules that have higher signal fractions in the high O_3 level, while blue circles refer to molecules that contribute more in the low O_3 level. The symbol sizes are related to the amount of signal change.

Figure 47 shows the carbon distribution of the particulate signals in the binary and ternary precursor systems at the low initial and high subsequent O_3 levels. The signals of individual molecule were normalised to the same reagent ion concentration. In the binary system, after the

subsequent aging with the excessive amount of O_3, the relative abundance of the groups with more than 13 carbon numbers was similar as discussed above. In contrast, in the ternary system, the evident increase of signal intensities of C_{4-5} and C_{8-10} was associated with their parent precursors of isoprene and α-pinene, respectively, after the aging by O_3 of ~950 ppb. Besides, C_{13-15} had an increase of 111% in the ternary system compared to that of 38% for the binary system, indicating that some of the C_{13-15} species were contributed by the interaction products from α-pinene and isoprene, e.g., $C_{15}H_{24}O_4$ as discussed above, except for the oxidation products from the unsaturated β-caryophyllene derived compounds reacting with additional O_3. The larger increase of the signal abundance of C_{17-20} and C_{21-25} compounds in the ternary system indicated them to be formed from the interaction of β-caryophyllene with isoprene and α-pinene, respectively. As the potential dimers from β-caryophyllene, C_{27-30} species had a less increase of 44% compared to that in the binary system (68%), suggesting that part of the β-caryophyllene derived C_{14-15} radicals were terminated by the C_{4-5} or C_{7-10} radicals from the oxidation of isoprene or α-pinene.

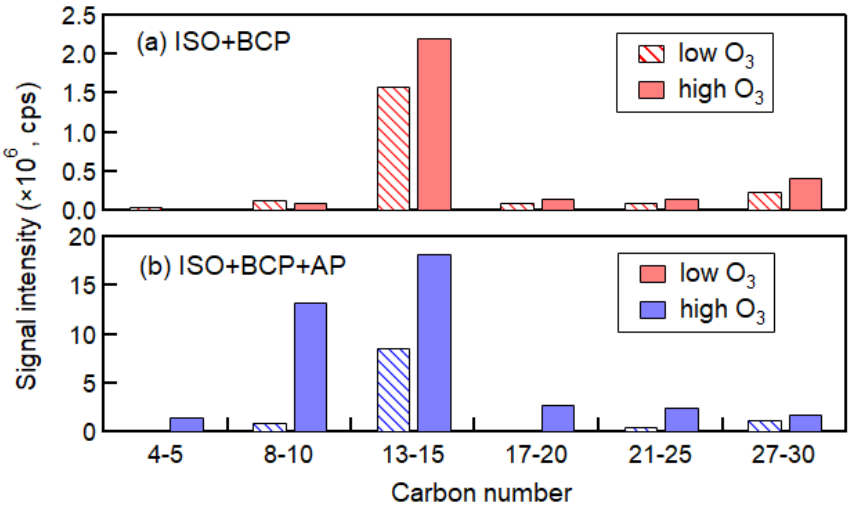

Figure 47. Carbon distribution of the particles formed at binary (a) and ternary (b) systems. The bars are marked with colors according to the different types of particles.

4.4.2 Volatility comparison

Figure 48 shows the volatility distributions from the species identified by the FIGAERO-CIMS in both precursor systems at initial low and subsequent high O_3 concentrations. The volatilities (expressed as C^*_T, μg m^{-3}) of the products were estimated using two methods for comparison: the elemental parameterisation method (hereafter 'formula method') and the calibrated T_{max} approach.

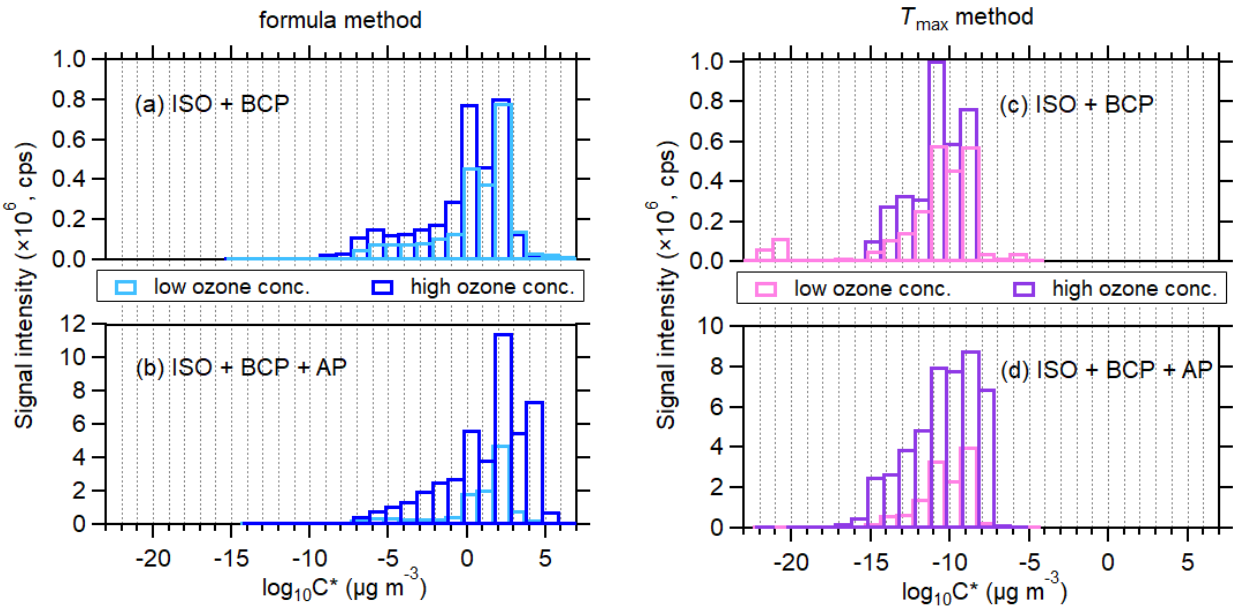

Figure 48. Volatility distributions expressed as effective saturation concentration (C^*) in the volatility basis set framework of all the products identified by the FIGAERO-idodie-CIMS as a function of the particle signal fraction in all systems at low (a) and high (b) O_3 levels with the C^* calculated by the T_{max} method and the formula method.

In the binary systems at the low initial O_3 level (Figure 48a), the SOA particle volatility estimated via the calibrated T_{max} method showed that the signals of most products were in ULVOCs range (~97%), whereas from the formula approach Figure 48c. The majority of the signals was attributed to the wide volatility ranges varying ELVOCs to IVOCs, characteristically splitting with ELVOCs (7.6%), LVOCs (42.6%), SVOCs (44.2%), and IVOCs (4.7%). In contrast, for the ternary system (Figure 48b), almost all detected products were in the ULVOCs range, determined by the T_{max} method. However, using the formula method (Figure 48d), the species distributed mainly among ELVOCs (12%), LVOCs (24.9%), SVOCs (58.2%), and IVOCs (3.7%). The volatility estimated by the T_{max} method was apparently lower than that of the formula method as expected, which was consistent with the prior studies from other groups (Stark et al., 2017). Despite of the difference of two different estimation approaches, the volatility bins of the particles formed in the presence α-pinene tended to be centred in more volatile ranges, compared that in the binary system. This is in the expectation that more α-pinene and isoprene derived products in higher volatilities are formed in the ternary system by the completion of O_3 among α-pinene and β-caryophyllene and initiation of isoprene with the produced OH radicals, compared to the dominating β-caryophyllene ozonolysis in the binary system.

Subsequently, the volatility distribution of the particles formed after the aging with additional O_3 changed, shown as Figure 48. In the two-precursor system, almost all detected species spanned in the ULVOC range according to the T_{max} approach (Figure 48 a), wherein there was a broader distribution from the formula method (Figure 48 b), with signals of 15.5% in ELVOCs, 40.2% in LVOCs, and 40.1% in SVOCs. The newly formed products contributed to the less volatile bins in the subsequent particle aging stage. In contrast, in the three-precursor system, the products had evident shifts to be in more volatile bins calculated via both approaches, owing to the higher signal fractions of α-pinene and isoprene derived and interacted species produced in the high ambient O_3 concentrations (shown in the Figure 45 and Figure 46).From the formula method (Figure 48d), 17.9% signals were characterised to be in the IVOCs, 44.6% in SVOCs, and 28% in the LVOCs bins. There was a sharp increase of the signal intensity of products in the most volatile bins ($\log_{10}C^*$ = 4.5 in Figure 48 b, and $\log_{10}C^*$ = -7.5 in Figure 48 d), consisting of mainly the α-pinene and isoprene derived products, such as $C_8H_{12}O_4$, $C_9H_{14}O_5$, $C_{10}H_{16}O_4$, $C_5H_{10}O_5$, and the early-stage oxidation products of β-caryophyllene, like $C_{11}H_{18}O_3$ and $C_{15}H_{24}O_3$.

The volatility of individual molecule estimated from T_{max} method was with several orders of magnitudes different with that from the formula method. One explanation is that the formula method biases the vapor pressure estimation with long carbon organics, such as the β-caryophyllene oxidation system detailly discussed in the section 4.2. On the other hand, the T_{max}-V_p calibrations are conducted using the syringe method which was recently pointed to potentially enable to shift the T_{max} (Ylisirniö et al., 2021).

However, although substantial discrepancies were found between the two approaches, it was clearly seen that the volatility distribution of the particles in the ternary system was shifted to be more volatile bins than the binary system at high O_3 concentrations. It has three reasons. One explanation is that α-pinene is competitive with β-caryophyllene to react with O_3, and produces the lighter molecules that have higher volatilities as expected. The second justification is that isoprene is initialled by the OH radicals produced from the α-pinene ozonolysis with a yield of ~85%, and derives even more volatile compounds with less weights. The isoprene is expected to act as unreactive VOC in the binary system because its reactivity with O_3 is more than 1000 times lower than β-caryophyllene, and the OH radical from β-caryophyllene ozonolysis has a low yield of ~15% (more details in section 4.2). Thus, the contribution of isoprene derived monomers was diminished in the binary system. The last reason for the volatility enhancement in the ternary

system is that the formation of β-caryophyllene derived low volatile C_{27-30} dimers can be suppressed, potentially because of the termination of peroxy radicals arising from β-caryophyllene by those from the α-pinene and isoprene to form the relative more volatile C_{17-20} and C_{21-25} compounds.

4.4.3 Summary

In this chapter, I have compared the chemical composition and volatility of the particles from two VOC mixtures systems: isoprene mixed with β-caryophyllene, isoprene mixed with β-caryophyllene and α-pinene, at low and high O_3 levels.

At low O_3 level (20-40 ppb), the particles in both systems were dominated by the C_{13-15} molecules, followed by $C_{24-30}H_{40-48}O_{5-10}$ components. In the two-precursor system, the most abundant signals were $C_{15}H_{24}O_4$ and $C_{14}H_{22}O_4$ which were likely to be the early-stage oxidation products from β-caryophyllene. Week signals for isoprene derived products (e.g., $C_5H_8O_{3-4}$) and the potential candidates of the interaction dimers from two precursors (C_{19-20}), indicated the contribution of isoprene to the total particle mass was limited. This confirmed the low OH radical yields from β-caryophyllene ozonolysis, e.g., ~15% as discussed in section 4.2. Besides, the autoxidation products only consisted of minority of the signals in the binary system, potentially resulting from the low initial O_3 level.

In comparison, in the three-precursor system, a higher relative signal fraction of $C_8H_{12}O_4$ was observed, which was expected to be the oxidation products from α-pinene oxidation, even though the reactivity of the ozonolysis of α-pinene was ~100 times lower than β-caryophyllene. Furthermore, $C_{23}H_{36}O_{6-7}$ and $C_{24}H_{38}O_{6-8}$ were found in higher abundance in the ternary system, suggesting them to be dimers products from interaction of α-pinene and β-caryophyllene oxidation products.

Subsequently, at high O_3 level (~1000 ppb), all the remaining VOC precursors were depleted. In the two-precursor system, C_5 and C_{19-20} molecules were still with low signal intensity, suggesting the major chemistry was the oxidation of unsaturated β-caryophyllene derived products and dimer formation, but not the oxidation of isoprene. This was supported by a higher signal fraction of $C_{14-15}H_yO_{\geq 6}$ and lower contribution from $C_{14-15}H_yO_{<6}$ compounds.

In the ternary system, the particle composition at the high O_3 level was substantially different, showing more interaction products from different parent precursors. The dominant signals were $C_8H_{12}O_4$ and $C_5H_8O_5$, which were likely to be the oxidation products from α-pinene and isoprene, respectively. The signal fraction of $C_{14\text{-}15}$ molecules also increased, resulting from either the oxidation of the unsaturated β-caryophyllene derived components, or the interaction of products from the oxidation of α-pinene and isoprene. Furthermore, the signal fraction of $C_{27\text{-}30}$ compounds decreased, whereas the $C_{17\text{-}25}$ species contributed more than at lower O_3 level. This may be explained by suppression of formation of β-caryophyllene dimers ($C_{27\text{-}30}$) by scavenging of corresponding monomers by oxidation products of α-pinene and isoprene, resulting in the formation of the smaller weighted interaction $C_{17\text{-}25}$ dimers. The volatility of the particle in the ternary system was more volatile than the binary system, mainly due to the higher contribution of lower weighted products from α-pinene and isoprene oxidation, and the suppressed fraction of lower volatile $C_{27\text{-}30}$ compounds.

5 Conclusion and Outlook

Secondary organic aerosol (SOA) is of great importance in the whole troposphere, as it influences the air quality and the earth's climate. However, the impact of temperature as relevant to the atmospheric conditions over the whole troposphere on the SOA chemical composition and physicochemical properties still remains unclear. Besides, current studies fail to address the complexity of SOA from mixtures of biogenic volatile organic compounds. Thus, I have generated and aged SOA in an atmospheric simulation chamber to characterize the SOA derived from six types of VOC precursors under varying temperatures. Based on the scientific results of this dissertation, the major conclusion and the atmospheric implications are summarized in section 5.1, and the results leading to new scientific questions will be discussed in section 5.2.

5.1 Conclusions and atmospheric implications

In this dissertation, the chemical composition and physicochemical properties of six types of SOA were investigated in the atmospheric simulation chamber (AIDA) at KIT. They were derived from different VOC precursors, including 1) β-caryophyllene, 2) β-caryophyllene mixed with NO_x, 3) α-pinene, 4) α-pinene mixed with isoprene, 5) isoprene mixed with β-caryophyllene, and 6) isoprene mixed with α-pinene as well as β-caryophyllene. Studies on the temperature dependence covering the range 213-313K were performed for the first time on β-caryophyllene ozonolysis in the absence and presence of NO_x, and on the oxidation of α-pinene mixed with isoprene. With the application of two advanced online mass spectrometric techniques of FIGAERO-CIMS and HR-AMS, I characterized the gaseous and particulate chemical composition of all six types of SOA. By the deployment of a newly extended PMF approach coupled with thermal desorption profiles of particulate molecules, I characterized the effective volatility of SOA particles.

By the comparison of SOA from the oxidation of α-pinene with and without isoprene at 273K, the majority of gas and particle signals in both systems comprised of $C_{8\text{-}10}H_yO_{4\text{-}7}$, indicating α-pinene derived oxidation products still dominated the SOA from a mixture of α-pinene and isoprene with a concentration ratio of 1:1. The relative abundance of $C_{16\text{-}20}$ molecules (dimers) in both systems was similar, accounting for 5.8±0.2% (sole system) and 6.7±0.1% (binary system). This indicates that the presence of isoprene in a similar concentration as α-pinene does not impact the $C_{16\text{-}20}$ dimers significantly at 273K. This can be different if isoprene concentrations are

significantly higher e.g. as in tropical rain forests (McFiggans et al., 2019). Besides, the majority of the species in the SOA derived from α-pinene and isoprene mixtures have saturation concentrations (C^*) between $10^{-6.5}$ and $10^{-3.5}$ μg m^{-3}. Hence significantly lower volatile than the sole α-pinene derived SOA that had C^* values between $10^{-4.5}$ and $10^{-2.5}$ μg m^{-3}. Higher T_{max} of individual molecules in the binary system indicates that the SOA derived from α-pinene and isoprene mixtures may be more viscous than the sole α-pinene derived SOA, probably resulting from the larger contribution of high molecular weight molecules, i.e., C_{15-20}. The lower volatility and potential higher viscosity of SOA derived from α-pinene and isoprene mixtures may have a higher potential to act as cloud condensation nuclei or ice nucleating particles than the sole α-pinene derived SOA and should have a longer atmospheric lifetime in terms of evaporation. Furthermore, more oxidation products with a C_{10} skeleton and less like $C_8H_yO_{5-8}$ were observed at lower temperatures, suggesting less C-C bond cleavage at reduced temperatures. Analysis of thermograms of one of the most abundant molecules, $C_8H_{12}O_4$, showed stronger thermal decomposition in the total signal of $C_8H_{12}O_4$ formed at temperatures above 273K. This allows the conclusion that the formation of corresponding thermal unstable dimers (or oligomers) is favored at higher temperatures. The SOA particles formed at 313K and 298K were in a liquid phase state, according to their glass transition temperatures of 283K and 285K, respectively, estimated from the parameterization method. In contrast, the SOA particles formed at 273K and 243K were likely to be in a semi-solid state, corresponding to higher glass transition temperatures of 289K and 278K, respectively. This highlights the need to consider condensed-phase chemistry as one of the sources of the dimer or oligomer formation (DePalma et al., 2013; Chen et al., 2019) at 298-313K. It can be concluded, that it is not possible to predict SOA properties and yields based on the behaviour observed in single precursor systems alone. The temperature dependent interaction of intermediates of the oxidation of different precursor VOC has a significant impact that needs to be studied on a molecular basis.

As one of the most reactive sesquiterpenes, β-caryophyllene has two carbon double bonds and is expected to have a high potential to form SOA particles. In this work, the temperature-dependent rate coefficient of the endocyclic double bond in β-caryophyllene reacting with O_3 was determined to have a negative dependence on temperature: k (243-313K) = (1.6±0.4) × 10^{-15} × exp((559±97)/T). Besides, the variation of the ozonolysis temperature revealed a substantial impact on the abundance of individual organic molecules. There are two major chemical

composition patterns for the β-caryophyllene derived SOA particles formed above and below 273K, differing in the monomers, dimers, and trimers, and revealing that the formation pathway of β-caryophyllene derived oxidation products changes from lower to higher ambient temperatures. Higher temperatures favour the formation of highly oxygenated monomeric molecules ($C_{14\text{-}15}H_{22\text{-}24}O_{6\text{-}9}$), while early-oxidation products ($C_{14\text{-}15}H_{22\text{-}24}O_{3\text{-}7}$) dominated at lower temperatures. Lower temperatures led to substantially more dimer ($C_{28\text{-}30}H_{44\text{-}48}O_{5\text{-}9}$) formation, while the dimers ($C_{27\text{-}29}H_{42\text{-}44}O_{9\text{-}11}$) formed at higher temperatures were more oxygenated but with substantially less contribution. This leads to the conclusion that the formation pathways of β-caryophyllene derived monomers are strongly temperature-dependent, with more HOM molecule formation at higher temperatures and more early-stage or first-generation oxidation products at reduced temperatures. In addition, large molecular weight trimers or oligomers ($C_{41\text{-}44}H_{62\text{-}66}O_{9\text{-}11}$) with very low volatility were found in significant quantities at 213K. While for the dimer formation, mechanisms could be suggested, the oligomer formation requires more studies to clarify their formation mechanism e.g. potential condensed phase reactions including hydroperoxides ((DePalma et al., 2013; Chen et al., 2019)).

Additionally, an interplay between oxidation product formation chemistry and the partitioning process was observed on the β-caryophyllene SOA between 213-313K. The particle analysis shows a counter-intuitive behavior of the T_{max} of the sum desorption thermograms from FIGAERO-CIMS, which indicates that the particle volatility increases first and then decreases with the ambient temperatures increasing from 213K to 313K. To estimate the effective volatility of β-caryophyllene derived SOA particles, I distinguished isomers and thermal decomposition compounds using a newly extended positive matrix factorization approach to deconvolute the thermal profiles of all detected oxygenated products. All detected species formed at 213-243K were in the ULVOC range, revealing that gas to particle partitioning was not the major process controlling the temperature dependence in this temperature range. On the contrary, the volatility of compounds formed at 298-313K span from ELVOC to SOVC volatilities where the partitioning altered the particulate chemical composition significantly. Compared with the volatility estimated from a parameterization approach based on molecular elemental composition (Li et al., 2016), and calibration of T_{max} values based on peak desorption temperatures of thermograms of individual molecules of known saturation vapor pressure, for the first time, I could show an improved

volatility determination for organic mixtures including isomers and thermal decomposition of some compounds.

In the presence of NO_x, the formation of β-caryophyllene derived organic nitrates showed a positive temperature dependence. Most of the organic nitrates were found as monomers with a C_{15} skeleton with one nitrate group, assigned as $C_{15}H_{23,25}O_{6\text{-}10}N$, with their O:C ratio increasing with temperatures between 213K and 313K. In presence of NO_3 radicals, the fraction of HOM species was significantly reduced compared to the pure β-caryophyllene ozonolysis at 298-313K. This indicates some competition between autooxidation and reactions with NO_x or NO_3 radicals leading to organic nitrates. Hence, the interaction of anthropogenic oxidants like NO_3 with β-caryophyllene oxidation significantly alters the oxidation state, composition, and volatility of the resulting SOA. The volatility analysis shows that the nitrogen-containing products are in the LVOC and ELVOC ranges for ambient temperatures of 298-313K.

In all systems with mixed VOC that I studied, always reaction products from the interaction of intermediates of the oxidation of the different VOC were formed altering the chemical composition and volatility of the resulting SOA. Generally, the presence of VOC with lower molecular weight can lead to the formation of a larger fraction of dimers (oligomers) with lower molecular weight and higher volatility. Depending on VOC ratios this can significantly reduce SOA yields (McFiggans et al., 2019) but has also a large impact on the new particle formation potential (Caudillo et al., 2021). However, the potential interactions can be complex and besides VOC ratios also levels of different oxidants and their reaction rates with the VOC need to be accounted for.

In SOA derived from ozonolysis of an isoprene β-caryophyllene mixture, oxidation products consisting of $C_{13\text{-}15}$ and $C_{24\text{-}30}H_{40\text{-}48}O_{5\text{-}10}$ molecules dominated the particles. The lower signal intensities of C_5 and $C_{19\text{-}20}$ molecules confirmed the limited impact of OH radicals generated from β-caryophyllene ozonolysis at 298K and follows the lower reactivity of isoprene with O_3 compared to β-caryophyllene. Even with relatively high O_3 concentrations, isoprene derived oxidation products contributed less than 10.2% to total particulate signals. However, with the presence of α-pinene, the chemical composition was substantially different for the SOA particles from the oxidation of isoprene mixed with β-caryophyllene. At a low O_3 level (20-40 ppb), the α-pinene derived product $C_8H_{12}O_4$ was detected as a major particulate compound, but also the β-

caryophyllene derived oxidation products substantially contributed to the particle phase mass, suggesting the ozonolysis of α-pinene is competitive to that of β-caryophyllene in forming condensable oxidation products. From the interaction of intermediate oxidation products of α-pinene and β-caryophyllene the following dimers were identified, $C_{23}H_{36}O_{6\text{-}7}$ and $C_{24}H_{38}O_{6\text{-}8}$. At relatively high O_3 levels (~1000 ppb), isoprene was also depleted substantially also by the OH radicals produced from the α-pinene ozonolysis. Hence, the SOA particles comprised oxidation products derived from β-caryophyllene, α-pinene, isoprene, and their interaction products. For example, $C_{14\text{-}15}$ molecules were abundant, which result from the oxidation of β-caryophyllene directly but also from the interaction of oxidation products from α-pinene and isoprene. A decrease in $C_{27\text{-}30}$ species and an increase in $C_{17\text{-}25}$ components suggests that the β-caryophyllene derived dimer formation was suppressed by the α-pinene or isoprene derived oxidation products. Due to the higher contribution of molecules with less molecular weight, e.g., oxidation products of isoprene, the volatility of the three-precursor SOA particles at high O_3 levels was higher than at low O_3 levels as well as for the two-precursor SOA particles. These experimental results illustrate the complexity of the interactions of the different SOA precursors. However, it should be possible to implement the findings, especially for the temperature dependent formation of the different types of dimers, which dominate new particle formation and SOA yields, into detailed chemical kinetic models like the MCM (Jenkin et al., 2004, 2012, 2015) to improve the prediction of SOA formation for more realistic scenarios.

Based on the results presented it can be concluded that this dissertation answers all major research questions that were put forward in the beginning. This work demonstrates that temperature (213-313K) has a strong impact on the chemical composition and physicochemical properties of the SOA from the oxidation of BVOC mixtures and sole β-caryophyllene in the absence and presence of NO_x, respectively. This work helps to get a better understanding of the interplay of temperature between facilitating condensation of organics and changing the chemical reaction pathways leading to different oxidation products of BVOCs. This work reveals the formation and volatility distribution of those SOA particles over a so-far unprecedented temperature range of 213-313K, covering the conditions from the planetary boundary layer to the upper troposphere, by carefully distinguishing the impact of isomers and thermal decomposition of some compounds. Besides, this work also demonstrates that the mixture of BVOC precursors can enhance the complexity of SOA by yielding interaction products, compared with the SOA

derived from a single BVOC precursor. The study of the chemical composition and volatility of the SOA from different BVOC mixtures under low and high O_3 levels with molecular insight helps to get a better understanding of the complex real atmospheric aerosols.

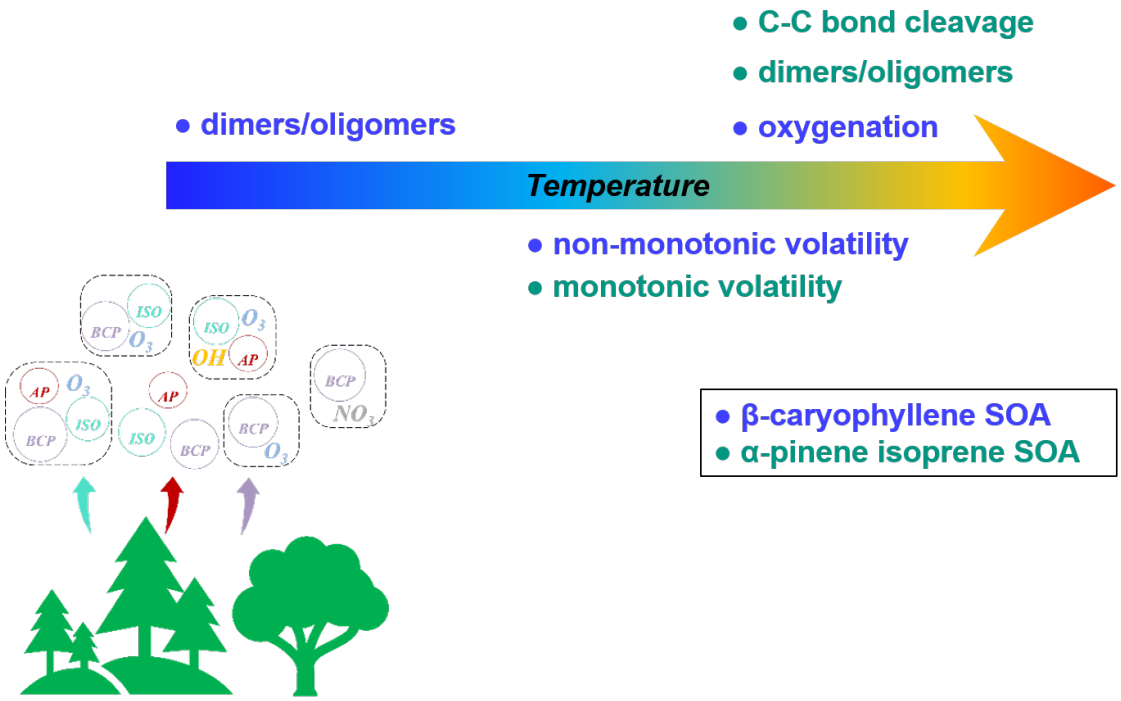

Figure 49. Individual biogenic emissions and their mixtures react with atmospheric oxidants, followed by gas-to-particle partitioning of oxidation products, resulting in the formation of secondary organic aerosol with different chemical compositions and physicochemical properties. The resulting SOA properties are associated mainly with the precursor VOC and ambient temperatures.

5.2 Outlook

This work also leads to new scientific questions, some of which could be the research focus for future studies:

a) β-caryophyllene derived $C_{14\text{-}15}$ molecules were observed as dominant in the SOA particles formed from the oxidation of BVOC mixtures of α-pinene, isoprene, and β-caryophyllene. Owing to the high reactivity of β-caryophyllene, the emissions of β-caryophyllene are currently mainly estimated based on its oxidation products (atmospheric tracers, e.g., $C_{14\text{-}15}$). However, the $C_{14\text{-}15}$ species can also be interaction products from isoprene and monoterpenes. Thus, the identification of $C_{14\text{-}15}$ molecules in the real atmosphere is needed

to substantiate the estimated emissions and contribution from different BVOCs in different areas, e.g., forests, and wetlands.

b) Temperature dependent volatility of particles derived from the BVOC mixture of α-pinene and isoprene was observed. Based on a parameterization approach, the phase states of the particles were estimated. The correlation of chemical composition, volatility, and viscosity of particles derived from a mixture of α-pinene and isoprene is still scarce. Thus, direct measurement of the viscosity, and studies of the correlations are required.

c) Different chemical composition patterns of β-caryophyllene derived SOA were observed at different temperatures. The temperatures for which the chemical mechanisms changed most significantly were between 243K and 273K. More detailed studies are required to clarify the exact tipping temperatures.

d) For SOA particles formed in the boundary layer, their volatility is suggested to change during transport or processing in convective clouds. Thus, further studies on the particle volatility change upon SOA aging e.g. with the variation of atmospheric conditions (e.g., temperature, RH) is required for different SOA derived from mixtures of major VOCs.

References

Agelopoulos, N. G., Chamberlain, K., and Pickett, J. A.: Factors Affecting Volatile Emissions of Intact Potato Plants, Solanum tuberosum: Variability of Quantities and Stability of Ratios, Journal of Chemical Ecology, 26, 497-511, 10.1023/A:1005473825335, 2000.

Alfarra, M., Hamilton, J., Wyche, K., Good, N., Ward, M., Carr, T., Barley, M., Monks, P., Jenkin, M., and Lewis, A.: The effect of photochemical ageing and initial precursor concentration on the composition and hygroscopic properties of β-caryophyllene secondary organic aerosol, Atmospheric Chemistry and Physics, 12, 6417-6436, 2012.

Aljawhary, D., Lee, A. K. Y., and Abbatt, J. P. D.: High-resolution chemical ionization mass spectrometry (ToF-CIMS): application to study SOA composition and processing, Atmos. Meas. Tech., 6, 3211-3224, 10.5194/amt-6-3211-2013, 2013.

Allan, J. D., Bower, K. N., Coe, H., Boudries, H., Jayne, J. T., Canagaratna, M. R., Millet, D. B., Goldstein, A. H., Quinn, P. K., Weber, R. J., and Worsnop, D. R.: Submicron aerosol composition at Trinidad Head, California, during ITCT 2K2: Its relationship with gas phase volatile organic carbon and assessment of instrument performance, Journal of Geophysical Research: Atmospheres, 109, https://doi.org/10.1029/2003JD004208, 2004.

Allenspach, M., and Steuer, C.: α-Pinene: A never-ending story, Phytochemistry, 190, 112857, https://doi.org/10.1016/j.phytochem.2021.112857, 2021.

Andreae, M. O., and Crutzen, P. J.: Atmospheric Aerosols: Biogeochemical Sources and Role in Atmospheric Chemistry, Science, 276, 1052-1058, doi:10.1126/science.276.5315.1052, 1997.

Andreae, M. O., Afchine, A., Albrecht, R., Holanda, B. A., Artaxo, P., Barbosa, H. M. J., Borrmann, S., Cecchini, M. A., Costa, A., Dollner, M., Fütterer, D., Järvinen, E., Jurkat, T., Klimach, T., Konemann, T., Knote, C., Krämer, M., Krisna, T., Machado, L. A. T., Mertes, S., Minikin, A., Pöhlker, C., Pöhlker, M. L., Pöschl, U., Rosenfeld, D., Sauer, D., Schlager, H., Schnaiter, M., Schneider, J., Schulz, C., Spanu, A., Sperling, V. B., Voigt, C., Walser, A., Wang, J., Weinzierl, B., Wendisch, M., and Ziereis, H.: Aerosol characteristics and particle production in the upper troposphere over the Amazon Basin, Atmos. Chem. Phys., 18, 921-961, 10.5194/acp-18-921-2018, 2018.

Appel, B. R., Tokiwa, Y., Hsu, J., Kothny, E. L., and Hahn, E.: Visibility as related to atmospheric aerosol constituents, Atmospheric Environment (1967), 19, 1525-1534, https://doi.org/10.1016/0004-6981(85)90290-2, 1985.

Atkinson, R., Winer, A. M., and Pitts, J. N.: Rate constants for the gas phase reactions of O3 with the natural hydrocarbons isoprene and α- and β-pinene, Atmospheric Environment (1967), 16, 1017-1020, https://doi.org/10.1016/0004-6981(82)90187-1, 1982.

Atkinson, R.: Kinetics and Mechanisms of the Gas-Phase Reactions of the NO3 Radical with Organic Compounds, Journal of Physical and Chemical Reference Data, 20, 459-507, 10.1063/1.555887, 1991.

Atkinson, R.: Atmospheric chemistry of VOCs and NOx, Atmospheric Environment, 34, 2063-2101, https://doi.org/10.1016/S1352-2310(99)00460-4, 2000.

Aubry, T. J., Staunton-Sykes, J., Marshall, L. R., Haywood, J., Abraham, N. L., and Schmidt, A.: Climate change modulates the stratospheric volcanic sulfate aerosol lifecycle and radiative forcing from tropical eruptions, Nature Communications, 12, 4708, 10.1038/s41467-021-24943-7, 2021.

Bannan, T. J., Le Breton, M., Priestley, M., Worrall, S. D., Bacak, A., Marsden, N. A., Mehra, A., Hammes, J., Hallquist, M., Alfarra, M. R., Krieger, U. K., Reid, J. P., Jayne, J., Robinson, W., McFiggans, G., Coe, H., Percival, C. J., and Topping, D.: A method for extracting calibrated volatility information from the FIGAERO-HR-ToF-CIMS and its experimental application, Atmos. Meas. Tech., 12, 1429-1439, 10.5194/amt-12-1429-2019, 2019.

Bastelberger, S., Krieger, U. K., Luo, B., and Peter, T.: Diffusivity measurements of volatile organics in levitated viscous aerosol particles, Atmos. Chem. Phys., 17, 8453-8471, 10.5194/acp-17-8453-2017, 2017.

Bates, K. H., and Jacob, D. J.: A new model mechanism for atmospheric oxidation of isoprene: global effects on oxidants, nitrogen oxides, organic products, and secondary organic aerosol, Atmos. Chem. Phys., 19, 9613-9640, 10.5194/acp-19-9613-2019, 2019.

Berndt, T., Hyttinen, N., Herrmann, H., and Hansel, A.: First oxidation products from the reaction of hydroxyl radicals with isoprene for pristine environmental conditions, Communications Chemistry, 2, 21, 10.1038/s42004-019-0120-9, 2019.

Bianchi, F., Kurtén, T., Riva, M., Mohr, C., Rissanen, M. P., Roldin, P., Berndt, T., Crounse, J. D., Wennberg, P. O., Mentel, T. F., Wildt, J., Junninen, H., Jokinen, T., Kulmala, M., Worsnop, D. R., Thornton, J. A., Donahue, N., Kjaergaard, H. G., and Ehn, M.: Highly Oxygenated Organic Molecules (HOM) from Gas-Phase Autoxidation Involving Peroxy Radicals: A Key Contributor to Atmospheric Aerosol, Chemical reviews, 119, 3472-3509, 10.1021/acs.chemrev.8b00395, 2019.

Bilde, M., Barsanti, K., Booth, M., Cappa, C. D., Donahue, N. M., Emanuelsson, E. U., McFiggans, G., Krieger, U. K., Marcolli, C., Topping, D., Ziemann, P., Barley, M., Clegg, S., Dennis-Smither, B., Hallquist, M., Hallquist, Å. M., Khlystov, A., Kulmala, M., Mogensen, D., Percival, C. J., Pope, F., Reid, J. P., Ribeiro da Silva, M. A. V., Rosenoern, T., Salo, K., Soonsin, V. P., Yli-Juuti, T., Prisle, N. L., Pagels, J., Rarey, J., Zardini, A. A., and Riipinen, I.: Saturation Vapor Pressures and Transition Enthalpies of Low-Volatility Organic Molecules of Atmospheric Relevance: From Dicarboxylic Acids to Complex Mixtures, Chemical reviews, 115, 4115-4156, 10.1021/cr5005502, 2015.

Blake, R. S., Monks, P. S., and Ellis, A. M.: Proton-Transfer Reaction Mass Spectrometry, Chemical reviews, 109, 861-896, 10.1021/cr800364q, 2009.

Booth, A. M., Montague, W. J., Barley, M. H., Topping, D. O., McFiggans, G., Garforth, A., and Percival, C. J.: Solid state and sub-cooled liquid vapour pressures of cyclic aliphatic dicarboxylic acids, Atmos. Chem. Phys., 11, 655-665, 10.5194/acp-11-655-2011, 2011.

Brophy, P., and Farmer, D. K.: A switchable reagent ion high resolution time-of-flight chemical ionization mass spectrometer for real-time measurement of gas phase oxidized species: characterization from the 2013 southern oxidant and aerosol study, Atmos. Meas. Tech., 8, 2945-2959, 10.5194/amt-8-2945-2015, 2015.

Buchholz, A., Ylisirniö, A., Huang, W., Mohr, C., Canagaratna, M., Worsnop, D. R., Schobesberger, S., and Virtanen, A.: Deconvolution of FIGAERO–CIMS thermal desorption profiles using positive matrix factorisation to identify chemical and physical processes during particle evaporation, Atmos. Chem. Phys., 20, 7693-7716, 10.5194/acp-20-7693-2020, 2020.

Calfapietra, C., Fares, S., Manes, F., Morani, A., Sgrigna, G., and Loreto, F.: Role of Biogenic Volatile Organic Compounds (BVOC) emitted by urban trees on ozone concentration in cities: A review, Environmental Pollution, 183, 71-80, https://doi.org/10.1016/j.envpol.2013.03.012, 2013.

Calogirou, A., Larsen, B., and Kotzias, D.: Gas-phase terpene oxidation products: a review, Atmospheric Environment, 33, 1423-1439, 1999.

Calvert, J. G., Derwent, R. G., Orlando, J. J., Wallington, T. J., and Tyndall, G. S.: Mechanisms of atmospheric oxidation of the alkanes, 2008.

Canagaratna, M. R., Jayne, J. T., Jimenez, J. L., Allan, J. D., Alfarra, M. R., Zhang, Q., Onasch, T. B., Drewnick, F., Coe, H., Middlebrook, A., Delia, A., Williams, L. R., Trimborn, A. M., Northway, M. J., DeCarlo, P. F., Kolb, C. E., Davidovits, P., and Worsnop, D. R.: Chemical and microphysical characterization of ambient aerosols with the aerodyne aerosol mass spectrometer, Mass Spectrometry Reviews, 26, 185-222, https://doi.org/10.1002/mas.20115, 2007.

Cao, X.-L., Sparling, M., and Dabeka, R.: Occurrence of 13 volatile organic compounds in foods from the Canadian total diet study, Food Additives & Contaminants: Part A, 33, 373-382, 10.1080/19440049.2015.1129072, 2016.

Cappa, C. D., and Jimenez, J. L.: Quantitative estimates of the volatility of ambient organic aerosol, Atmos. Chem. Phys., 10, 5409-5424, 10.5194/acp-10-5409-2010, 2010.

Carlton, A. G., Wiedinmyer, C., and Kroll, J. H.: A review of Secondary Organic Aerosol (SOA) formation from isoprene, Atmos. Chem. Phys., 9, 4987-5005, 10.5194/acp-9-4987-2009, 2009.

Caudillo, L., Rörup, B., Heinritzi, M., Marie, G., Simon, M., Wagner, A. C., Müller, T., Granzin, M., Amorim, A., Ataei, F., Baalbaki, R., Bertozzi, B., Brasseur, Z., Chiu, R., Chu, B., Dada, L., Duplissy, J., Finkenzeller, H., Gonzalez Carracedo, L., He, X. C., Hofbauer, V., Kong, W., Lamkaddam, H., Lee, C. P., Lopez, B., Mahfouz, N. G. A., Makhmutov, V., Manninen, H. E., Marten, R., Massabò, D., Mauldin, R. L., Mentler, B., Molteni, U., Onnela, A., Pfeifer, J., Philippov, M., Piedehierro, A. A., Schervish, M., Scholz, W., Schulze, B., Shen, J., Stolzenburg, D., Stozhkov, Y., Surdu, M., Tauber, C., Tham, Y. J., Tian, P., Tomé, A., Vogt, S., Wang, M., Wang, D. S., Weber, S. K., Welti, A., Yonghong, W., Yusheng, W., Zauner-Wieczorek, M., Baltensperger, U., El Haddad, I., Flagan, R. C., Hansel, A., Höhler, K., Kirkby, J., Kulmala, M., Lehtipalo, K., Möhler, O., Saathoff, H., Volkamer, R., Winkler, P. M., Donahue, N. M., Kürten, A., and Curtius, J.: Chemical composition of nanoparticles from α-pinene nucleation and the influence of isoprene and relative humidity at low temperature, Atmos. Chem. Phys., 21, 17099-17114, 10.5194/acp-21-17099-2021, 2021.

Champion, W. M., Rothfuss, N. E., Petters, M. D., and Grieshop, A. P.: Volatility and Viscosity Are Correlated in Terpene Secondary Organic Aerosol Formed in a Flow Reactor, Environmental Science & Technology Letters, 6, 513-519, 10.1021/acs.estlett.9b00412, 2019.

Chan, A., Kroll, J., Ng, N., and Seinfeld, J.: Kinetic modeling of secondary organic aerosol formation: effects of particle-and gas-phase reactions of semivolatile products, Atmospheric Chemistry and Physics, 7, 4135-4147, 2007.

Chan, M., Surratt, J., Chan, A., Schilling, K., Offenberg, J., Lewandowski, M., Edney, E., Kleindienst, T., Jaoui, M., and Edgerton, E.: Influence of aerosol acidity on the chemical composition of secondary organic aerosol from β-caryophyllene, Atmospheric Chemistry and Physics, 11, 1735-1751, 2011a.

Chan, M. N., Surratt, J. D., Chan, A. W. H., Schilling, K., Offenberg, J. H., Lewandowski, M., Edney, E. O., Kleindienst, T. E., Jaoui, M., Edgerton, E. S., Tanner, R. L., Shaw, S. L., Zheng, M., Knipping, E. M., and Seinfeld, J. H.: Influence of aerosol acidity on the chemical composition of secondary organic aerosol from β-caryophyllene, Atmos. Chem. Phys., 11, 1735-1751, 10.5194/acp-11-1735-2011, 2011b.

Charlson, R. J.: Atmospheric visibility related to aerosol mass concentration, Environmental science & technology, 3, 913-918, 1969.

Chattopadhyay, S., and Ziemann, P. J.: Vapor Pressures of Substituted and Unsubstituted Monocarboxylic and Dicarboxylic Acids Measured Using an Improved Thermal Desorption Particle Beam Mass Spectrometry Method, Aerosol Science and Technology, 39, 1085-1100, 10.1080/02786820500421547, 2005.

Chen, L., Huang, Y., Xue, Y., Shen, Z., Cao, J., and Wang, W.: Mechanistic and kinetics investigations of oligomer formation from Criegee intermediate reactions with hydroxyalkyl hydroperoxides, Atmos. Chem. Phys., 19, 4075-4091, 10.5194/acp-19-4075-2019, 2019.

Chen, Q., Li, Y., McKinney, K., Kuwata, M., and Martin, S.: Particle mass yield from beta-caryophyllene ozonolysis, Atmospheric Chemistry and Physics, 12, 3165-3179, 2012a.

Chen, Q., Li, Y. L., McKinney, K. A., Kuwata, M., and Martin, S. T.: Particle mass yield from β-caryophyllene ozonolysis, Atmos. Chem. Phys., 12, 3165-3179, 10.5194/acp-12-3165-2012, 2012b.

Chen, Q., Li, Y. L., McKinney, K. A., Kuwata, M., and Martin, S. T.: Particle mass yield from beta-caryophyllene ozonolysis, Atmospheric Chemistry and Physics, 12, 3165-3179, 10.5194/acp-12-3165-2012, 2012c.

Cheng, Y., Ma, Y., and Hu, D.: Tracer-based source apportioning of atmospheric organic carbon and the influence of anthropogenic emissions on secondary organic aerosol formation in Hong Kong, Atmos. Chem. Phys., 21, 10589-10608, 10.5194/acp-21-10589-2021, 2021.

Ciccioli, P., Brancaleoni, E., Frattoni, M., Di Palo, V., Valentini, R., Tirone, G., Seufert, G., Bertin, N., Hansen, U., Csiky, O., Lenz, R., and Sharma, M.: Emission of reactive terpene compounds from orange orchards and their removal by within-canopy processes, Journal of Geophysical Research: Atmospheres, 104, 8077-8094, https://doi.org/10.1029/1998JD100026, 1999.

Claeys, M., Iinuma, Y., Szmigielski, R., Surratt, J. D., Blockhuys, F., Van Alsenoy, C., Böge, O., Sierau, B., Gómez-González, Y., Vermeylen, R., Van der Veken, P., Shahgholi, M., Chan, A. W. H., Herrmann, H., Seinfeld, J. H., and Maenhaut, W.: Terpenylic Acid and Related Compounds from the Oxidation of α-Pinene: Implications for New Particle Formation and Growth above Forests, Environmental Science & Technology, 43, 6976-6982, 10.1021/es9007596, 2009.

Clark, C. H., Kacarab, M., Nakao, S., Asa-Awuku, A., Sato, K., and Cocker III, D. R.: Temperature effects on secondary organic aerosol (SOA) from the dark ozonolysis and photo-oxidation of isoprene, Environmental Science & Technology, 50, 5564-5571, 2016.

Cox, R. A., Ammann, M., Crowley, J. N., Herrmann, H., Jenkin, M. E., McNeill, V. F., Mellouki, A., Troe, J., and Wallington, T. J.: Evaluated kinetic and photochemical data for atmospheric chemistry: Volume VII – Criegee intermediates, Atmos. Chem. Phys., 20, 13497-13519, 10.5194/acp-20-13497-2020, 2020.

Crounse, J. D., Nielsen, L. B., Jørgensen, S., Kjaergaard, H. G., and Wennberg, P. O.: Autoxidation of Organic Compounds in the Atmosphere, The Journal of Physical Chemistry Letters, 4, 3513-3520, 10.1021/jz4019207, 2013.

D'Ambro, E. L., Lee, B. H., Liu, J., Shilling, J. E., Gaston, C. J., Lopez-Hilfiker, F. D., Schobesberger, S., Zaveri, R. A., Mohr, C., Lutz, A., Zhang, Z., Gold, A., Surratt, J. D., Rivera-Rios, J. C., Keutsch, F. N., and Thornton, J. A.: Molecular composition and volatility of isoprene photochemical oxidation secondary organic aerosol under low- and high-NOx conditions, Atmos. Chem. Phys., 17, 159-174, 10.5194/acp-17-159-2017, 2017.

D'Ambro, E. L., Schobesberger, S., Gaston, C. J., Lopez-Hilfiker, F. D., Lee, B. H., Liu, J., Zelenyuk, A., Bell, D., Cappa, C. D., Helgestad, T., Li, Z., Guenther, A., Wang, J., Wise, M., Caylor, R., Surratt, J. D., Riedel, T., Hyttinen, N., Salo, V. T., Hasan, G., Kurtén, T., Shilling, J. E., and Thornton, J. A.: Chamber-based insights into the factors controlling epoxydiol (IEPOX) secondary organic aerosol (SOA) yield, composition, and volatility, Atmos. Chem. Phys., 19, 11253-11265, 10.5194/acp-19-11253-2019, 2019.

Darquenne, C.: Aerosol Deposition in Health and Disease, Journal of Aerosol Medicine and Pulmonary Drug Delivery, 25, 140-147, 10.1089/jamp.2011.0916, 2012.

de Gouw, J.: In the Footsteps of My Countrymen: Atmospheric Chemistry in New England, Los Angeles, and the Southeast United States, Perspectives of Earth and Space Scientists, 2, e2021CN000151, https://doi.org/10.1029/2021CN000151, 2021.

DeCarlo, P. F., Slowik, J. G., Worsnop, D. R., Davidovits, P., and Jimenez, J. L.: Particle Morphology and Density Characterization by Combined Mobility and Aerodynamic Diameter Measurements. Part 1: Theory, Aerosol Science and Technology, 38, 1185-1205, 10.1080/027868290903907, 2004.

DeCarlo, P. F., Kimmel, J. R., Trimborn, A., Northway, M. J., Jayne, J. T., Aiken, A. C., Gonin, M., Fuhrer, K., Horvath, T., Docherty, K. S., Worsnop, D. R., and Jimenez, J. L.: Field-Deployable, High-Resolution, Time-of-Flight Aerosol Mass Spectrometer, Analytical Chemistry, 78, 8281-8289, 10.1021/ac061249n, 2006.

Dekermenjian, M.: FTIR analysis of aerosol formed in the ozone oxidation of sesquiterpenes, Aerosol Science & Technology, 30, 349-363, 1999.

DePalma, J. W., Horan, A. J., Hall Iv, W. A., and Johnston, M. V.: Thermodynamics of oligomer formation: implications for secondary organic aerosol formation and reactivity, Physical Chemistry Chemical Physics, 15, 6935-6944, 10.1039/C3CP44586K, 2013.

DeRieux, W. S. W., Li, Y., Lin, P., Laskin, J., Laskin, A., Bertram, A. K., Nizkorodov, S. A., and Shiraiwa, M.: Predicting the glass transition temperature and viscosity of secondary organic material using molecular composition, Atmos. Chem. Phys., 18, 6331-6351, 10.5194/acp-18-6331-2018, 2018.

Docherty, K. S., Wu, W., Lim, Y. B., and Ziemann, P. J.: Contributions of Organic Peroxides to Secondary Aerosol Formed from Reactions of Monoterpenes with O3, Environmental Science & Technology, 39, 4049-4059, 10.1021/es050228s, 2005.

Dockery, D. W., Schwartz, J., and Spengler, J. D.: Air pollution and daily mortality: Associations with particulates and acid aerosols, Environmental Research, 59, 362-373, https://doi.org/10.1016/S0013-9351(05)80042-8, 1992.

Donahue, N. M., Robinson, A. L., Stanier, C. O., and Pandis, S. N.: Coupled Partitioning, Dilution, and Chemical Aging of Semivolatile Organics, Environmental Science & Technology, 40, 2635-2643, 10.1021/es052297c, 2006.

Donahue, N. M., Robinson, A. L., and Pandis, S. N.: Atmospheric organic particulate matter: From smoke to secondary organic aerosol, Atmospheric Environment, 43, 94-106, https://doi.org/10.1016/j.atmosenv.2008.09.055, 2009.

Donahue, N. M., Epstein, S. A., Pandis, S. N., and Robinson, A. L.: A two-dimensional volatility basis set: 1. organic-aerosol mixing thermodynamics, Atmos. Chem. Phys., 11, 3303-3318, 10.5194/acp-11-3303-2011, 2011.

Donahue, N. M., Kroll, J. H., Pandis, S. N., and Robinson, A. L.: A two-dimensional volatility basis set – Part 2: Diagnostics of organic-aerosol evolution, Atmos. Chem. Phys., 12, 615-634, 10.5194/acp-12-615-2012, 2012.

Drewnick, F., Hings, S. S., DeCarlo, P., Jayne, J. T., Gonin, M., Fuhrer, K., Weimer, S., Jimenez, J. L., Demerjian, K. L., Borrmann, S., and Worsnop, D. R.: A New Time-of-Flight Aerosol Mass Spectrometer (TOF-AMS)—Instrument Description and First Field Deployment, Aerosol Science and Technology, 39, 637-658, 10.1080/02786820500182040, 2005.

Duhl, T. R., Helmig, D., and Guenther, A.: Sesquiterpene emissions from vegetation: a review, Biogeosciences, 5, 761-777, 10.5194/bg-5-761-2008, 2008.

Ehn, M., Thornton, J. A., Kleist, E., Sipilä, M., Junninen, H., Pullinen, I., Springer, M., Rubach, F., Tillmann, R., Lee, B., Lopez-Hilfiker, F., Andres, S., Acir, I.-H., Rissanen, M., Jokinen, T., Schobesberger, S., Kangasluoma, J., Kontkanen, J., Nieminen, T., Kurtén, T., Nielsen, L. B., Jørgensen, S., Kjaergaard, H. G., Canagaratna, M., Maso, M. D., Berndt, T., Petäjä, T., Wahner, A., Kerminen, V.-M., Kulmala, M., Worsnop, D. R., Wildt, J., and Mentel, T. F.: A large source of low-volatility secondary organic aerosol, Nature, 506, 476-479, 10.1038/nature13032, 2014.

Ehn, M., Berndt, T., Wildt, J., and Mentel, T.: Highly Oxygenated Molecules from Atmospheric Autoxidation of Hydrocarbons: A Prominent Challenge for Chemical Kinetics Studies, International Journal of Chemical Kinetics, 49, 821-831, https://doi.org/10.1002/kin.21130, 2017.

Eichler, P., Müller, M., D'Anna, B., and Wisthaler, A.: A novel inlet system for online chemical analysis of semi-volatile submicron particulate matter, Atmos. Meas. Tech., 8, 1353-1360, 10.5194/amt-8-1353-2015, 2015.

Epstein, S. A., Riipinen, I., and Donahue, N. M.: A Semiempirical Correlation between Enthalpy of Vaporization and Saturation Concentration for Organic Aerosol, Environmental Science & Technology, 44, 743-748, 10.1021/es902497z, 2010.

Francisco, M. A., and Krylowski, J.: Chemistry of Organic Nitrates: Thermal Chemistry of Linear and Branched Organic Nitrates, Industrial & Engineering Chemistry Research, 44, 5439-5446, 10.1021/ie049380d, 2005.

Gao, Y., Hall, W. A., and Johnston, M. V.: Molecular Composition of Monoterpene Secondary Organic Aerosol at Low Mass Loading, Environmental Science & Technology, 44, 7897-7902, 10.1021/es101861k, 2010.

Geron, C. D., and Arnts, R. R.: Seasonal monoterpene and sesquiterpene emissions from Pinus taeda and Pinus virginiana, Atmospheric Environment, 44, 4240-4251, https://doi.org/10.1016/j.atmosenv.2010.06.054, 2010.

Ghan, S. J., and Schwartz, S. E.: Aerosol Properties and Processes: A Path from Field and Laboratory Measurements to Global Climate Models, Bulletin of the American Meteorological Society, 88, 1059-1084, 10.1175/bams-88-7-1059, 2007.

Gkatzelis, G. I., Tillmann, R., Hohaus, T., Müller, M., Eichler, P., Xu, K. M., Schlag, P., Schmitt, S. H., Wegener, R., Kaminski, M., Holzinger, R., Wisthaler, A., and Kiendler-Scharr, A.: Comparison of three

aerosol chemical characterization techniques utilizing PTR-ToF-MS: a study on freshly formed and aged biogenic SOA, Atmos. Meas. Tech., 11, 1481-1500, 10.5194/amt-11-1481-2018, 2018.

Gliß, J., Mortier, A., Schulz, M., Andrews, E., Balkanski, Y., Bauer, S. E., Benedictow, A. M. K., Bian, H., Checa-Garcia, R., Chin, M., Ginoux, P., Griesfeller, J. J., Heckel, A., Kipling, Z., Kirkevåg, A., Kokkola, H., Laj, P., Le Sager, P., Lund, M. T., Lund Myhre, C., Matsui, H., Myhre, G., Neubauer, D., van Noije, T., North, P., Olivié, D. J. L., Rémy, S., Sogacheva, L., Takemura, T., Tsigaridis, K., and Tsyro, S. G.: AeroCom phase III multi-model evaluation of the aerosol life cycle and optical properties using ground- and space-based remote sensing as well as surface in situ observations, Atmos. Chem. Phys., 21, 87-128, 10.5194/acp-21-87-2021, 2021.

Goldstein, A. H., and Galbally, I. E.: Known and unexplored organic constituents in the earth's atmosphere, Environmental science & technology, 41, 1514-1521, 2007.

Griffin, R. J., Cocker III, D. R., Flagan, R. C., and Seinfeld, J. H.: Organic aerosol formation from the oxidation of biogenic hydrocarbons, Journal of Geophysical Research: Atmospheres, 104, 3555-3567, 1999.

Grosjean, D., Williams, E. L., Grosjean, E., Andino, J. M., and Seinfeld, J. H.: Atmospheric oxidation of biogenic hydrocarbons: reaction of ozone with. beta.-pinene, D-limonene and trans-caryophyllene, Environmental Science & Technology, 27, 2754-2758, 1993.

Gross, J. H.: Mass spectrometry: a textbook, Springer Science & Business Media, 2006.

Guenther, A. B., Jiang, X., Heald, C. L., Sakulyanontvittaya, T., Duhl, T., Emmons, L. K., and Wang, X.: The Model of Emissions of Gases and Aerosols from Nature version 2.1 (MEGAN2.1): an extended and updated framework for modeling biogenic emissions, Geosci. Model Dev., 5, 1471-1492, 10.5194/gmd-5-1471-2012, 2012.

Hakola, H., Tarvainen, V., Bäck, J., Ranta, H., Bonn, B., Rinne, J., and Kulmala, M.: Seasonal variation of mono- and sesquiterpene emission rates of Scots pine, Biogeosciences, 3, 93-101, 10.5194/bg-3-93-2006, 2006.

Hallquist, M., Wenger, J. C., Baltensperger, U., Rudich, Y., Simpson, D., Claeys, M., Dommen, J., Donahue, N. M., George, C., Goldstein, A. H., Hamilton, J. F., Herrmann, H., Hoffmann, T., Iinuma, Y., Jang, M., Jenkin, M. E., Jimenez, J. L., Kiendler-Scharr, A., Maenhaut, W., McFiggans, G., Mentel, T. F., Monod, A., Prévôt, A. S. H., Seinfeld, J. H., Surratt, J. D., Szmigielski, R., and Wildt, J.: The formation, properties and impact of secondary organic aerosol: current and emerging issues, Atmos. Chem. Phys., 9, 5155-5236, 10.5194/acp-9-5155-2009, 2009.

Hansen, U., and Seufert, G.: Temperature and light dependence of β-caryophyllene emission rates, Journal of Geophysical Research: Atmospheres, 108, 2003.

Haque, M. M., Kawamura, K., and Kim, Y.: Seasonal variations of biogenic secondary organic aerosol tracers in ambient aerosols from Alaska, Atmospheric Environment, 130, 95-104, 2016.

Hartonen, K., Parshintsev, J., Vilja, V.-P., Tiala, H., Knuuti, S., Lai, C. K., and Riekkola, M.-L.: Gas chromatographic vapor pressure determination of atmospherically relevant oxidation products of β-caryophyllene and α-pinene, Atmospheric Environment, 81, 330-338, https://doi.org/10.1016/j.atmosenv.2013.09.023, 2013.

Hearn, J. D., and Smith, G. D.: A Chemical Ionization Mass Spectrometry Method for the Online Analysis of Organic Aerosols, Analytical Chemistry, 76, 2820-2826, 10.1021/ac049948s, 2004.

Heinritzi, M., Dada, L., Simon, M., Stolzenburg, D., Wagner, A. C., Fischer, L., Ahonen, L. R., Amanatidis, S., Baalbaki, R., Baccarini, A., Bauer, P. S., Baumgartner, B., Bianchi, F., Brilke, S., Chen, D., Chiu, R., Dias, A., Dommen, J., Duplissy, J., Finkenzeller, H., Frege, C., Fuchs, C., Garmash, O., Gordon, H., Granzin, M., El Haddad, I., He, X., Helm, J., Hofbauer, V., Hoyle, C. R., Kangasluoma, J., Keber, T., Kim, C., Kürten, A., Lamkaddam, H., Laurila, T. M., Lampilahti, J., Lee, C. P., Lehtipalo, K., Leiminger, M., Mai, H., Makhmutov, V., Manninen, H. E., Marten, R., Mathot, S., Mauldin, R. L., Mentler, B., Molteni, U., Müller, T., Nie, W., Nieminen, T., Onnela, A., Partoll, E., Passananti, M., Petäjä, T., Pfeifer, J., Pospisilova, V., Quéléver, L. L. J., Rissanen, M. P., Rose, C., Schobesberger, S., Scholz, W., Scholze, K., Sipilä, M., Steiner, G., Stozhkov, Y., Tauber, C., Tham, Y. J., Vazquez-Pufleau, M., Virtanen, A., Vogel, A. L., Volkamer, R., Wagner, R., Wang, M., Weitz, L., Wimmer, D.,

Xiao, M., Yan, C., Ye, P., Zha, Q., Zhou, X., Amorim, A., Baltensperger, U., Hansel, A., Kulmala, M., Tomé, A., Winkler, P. M., Worsnop, D. R., Donahue, N. M., Kirkby, J., and Curtius, J.: Molecular understanding of the suppression of new-particle formation by isoprene, Atmos. Chem. Phys., 20, 11809-11821, 10.5194/acp-20-11809-2020, 2020.

Helmig, D., Daly, R. W., Milford, J., and Guenther, A.: Seasonal trends of biogenic terpene emissions, Chemosphere, 93, 35-46, https://doi.org/10.1016/j.chemosphere.2013.04.058, 2013.

Hu, D., Bian, Q., Li, T. W., Lau, A. K., and Yu, J. Z.: Contributions of isoprene, monoterpenes, β-caryophyllene, and toluene to secondary organic aerosols in Hong Kong during the summer of 2006, Journal of Geophysical Research: Atmospheres, 113, 2008.

Hu, Z., and Rao, K. R.: Particulate air pollution and chronic ischemic heart disease in the eastern United States: a county level ecological study using satellite aerosol data, Environmental Health, 8, 26, 10.1186/1476-069X-8-26, 2009.

Huang, W., Li, H., Sarnela, N., Heikkinen, L., Tham, Y. J., Mikkilä, J., Thomas, S. J., Donahue, N. M., Kulmala, M., and Bianchi, F.: Measurement report: Molecular composition and volatility of gaseous organic compounds in a boreal forest – from volatile organic compounds to highly oxygenated organic molecules, Atmos. Chem. Phys., 21, 8961-8977, 10.5194/acp-21-8961-2021, 2021.

Huey, L. G., Hanson, D. R., and Howard, C. J.: Reactions of SF6- and I- with Atmospheric Trace Gases, The Journal of Physical Chemistry, 99, 5001-5008, 10.1021/j100014a021, 1995.

Hyttinen, N., Pullinen, I., Nissinen, A., Schobesberger, S., Virtanen, A., and Yli-Juuti, T.: Comparison of saturation vapor pressures of α-pinene + O3 oxidation products derived from COSMO-RS computations and thermal desorption experiments, Atmos. Chem. Phys., 22, 1195-1208, 10.5194/acp-22-1195-2022, 2022.

Jaoui, M., Leungsakul, S., and Kamens, R.: Gas and particle products distribution from the reaction of β-caryophyllene with ozone, Journal of Atmospheric Chemistry, 45, 261-287, 2003a.

Jaoui, M., Leungsakul, S., and Kamens, R. M.: Gas and Particle Products Distribution from the Reaction of β-Caryophyllene with Ozone, Journal of Atmospheric Chemistry, 45, 261-287, 10.1023/A:1024263430285, 2003b.

Jaoui, M., Lewandowski, M., Kleindienst, T. E., Offenberg, J. H., and Edney, E. O.: β-caryophyllinic acid: An atmospheric tracer for β-caryophyllene secondary organic aerosol, Geophysical Research Letters, 34, 2007.

Jaoui, M., Kleindienst, T. E., Docherty, K. S., Lewandowski, M., and Offenberg, J. H.: Secondary organic aerosol formation from the oxidation of a series of sesquiterpenes: α-cedrene, β-caryophyllene, α-humulene and α-farnesene with O3, OH and NO3 radicals, Environmental Chemistry, 10, 178-193, 2013.

Jardine, K., Yañez Serrano, A., Arneth, A., Abrell, L., Jardine, A., van Haren, J., Artaxo, P., Rizzo, L. V., Ishida, F. Y., Karl, T., Kesselmeier, J., Saleska, S., and Huxman, T.: Within-canopy sesquiterpene ozonolysis in Amazonia, Journal of Geophysical Research: Atmospheres, 116, https://doi.org/10.1029/2011JD016243, 2011.

Jayne, J. T., Leard, D. C., Zhang, X., Davidovits, P., Smith, K. A., Kolb, C. E., and Worsnop, D. R.: Development of an Aerosol Mass Spectrometer for Size and Composition Analysis of Submicron Particles, Aerosol Science and Technology, 33, 49-70, 10.1080/027868200410840, 2000.

Jenkin, M., Wyche, K., Evans, C., Carr, T., Monks, P., Alfarra, M., Barley, M., McFiggans, G., Young, J., and Rickard, A.: Development and chamber evaluation of the MCM v3. 2 degradation scheme for β-caryophyllene, Atmospheric Chemistry & Physics Discussions, 12, 2012.

Jenkin, M. E.: Modelling the formation and composition of secondary organic aerosol from α- and β-pinene ozonolysis using MCM v3, Atmos. Chem. Phys., 4, 1741-1757, 10.5194/acp-4-1741-2004, 2004.

Jenkin, M. E., Young, J. C., and Rickard, A. R.: The MCM v3.3.1 degradation scheme for isoprene, Atmos. Chem. Phys., 15, 11433-11459, 10.5194/acp-15-11433-2015, 2015.

Jimenez, J. L., Jayne, J. T., Shi, Q., Kolb, C. E., Worsnop, D. R., Yourshaw, I., Seinfeld, J. H., Flagan, R. C., Zhang, X., Smith, K. A., Morris, J. W., and Davidovits, P.: Ambient aerosol sampling using the

Aerodyne Aerosol Mass Spectrometer, Journal of Geophysical Research: Atmospheres, 108, https://doi.org/10.1029/2001JD001213, 2003.

Jimenez, J. L., Canagaratna, M. R., Donahue, N. M., Prevot, A. S. H., Zhang, Q., Kroll, J. H., DeCarlo, P. F., Allan, J. D., Coe, H., Ng, N. L., Aiken, A. C., Docherty, K. S., Ulbrich, I. M., Grieshop, A. P., Robinson, A. L., Duplissy, J., Smith, J. D., Wilson, K. R., Lanz, V. A., Hueglin, C., Sun, Y. L., Tian, J., Laaksonen, A., Raatikainen, T., Rautiainen, J., Vaattovaara, P., Ehn, M., Kulmala, M., Tomlinson, J. M., Collins, D. R., Cubison, M. J., Dunlea, J., Huffman, J. A., Onasch, T. B., Alfarra, M. R., Williams, P. I., Bower, K., Kondo, Y., Schneider, J., Drewnick, F., Borrmann, S., Weimer, S., Demerjian, K., Salcedo, D., Cottrell, L., Griffin, R., Takami, A., Miyoshi, T., Hatakeyama, S., Shimono, A., Sun, J. Y., Zhang, Y. M., Dzepina, K., Kimmel, J. R., Sueper, D., Jayne, J. T., Herndon, S. C., Trimborn, A. M., Williams, L. R., Wood, E. C., Middlebrook, A. M., Kolb, C. E., Baltensperger, U., and Worsnop, D. R.: Evolution of Organic Aerosols in the Atmosphere, Science, 326, 1525-1529, doi:10.1126/science.1180353, 2009.

Jokinen, T., Kausiala, O., Garmash, O., Peräkylä, O., Junninen, H., Schobesberger, S., Yan, C., Sipilä, M., and Rissanen, M. P.: Production of highly oxidized organic compounds from ozonolysis of beta-caryophyllene: laboratory and field measurements, Boreal Environment Research, 2016.

Jordan, A., Haidacher, S., Hanel, G., Hartungen, E., Märk, L., Seehauser, H., Schottkowsky, R., Sulzer, P., and Märk, T. D.: A high resolution and high sensitivity proton-transfer-reaction time-of-flight mass spectrometer (PTR-TOF-MS), International Journal of Mass Spectrometry, 286, 122-128, https://doi.org/10.1016/j.ijms.2009.07.005, 2009.

Kammer, J., Flaud, P. M., Chazeaubeny, A., Ciuraru, R., Le Menach, K., Geneste, E., Budzinski, H., Bonnefond, J. M., Lamaud, E., Perraudin, E., and Villenave, E.: Biogenic volatile organic compounds (BVOCs) reactivity related to new particle formation (NPF) over the Landes forest, Atmospheric Research, 237, 104869, https://doi.org/10.1016/j.atmosres.2020.104869, 2020.

Kanakidou, M., Seinfeld, J. H., Pandis, S. N., Barnes, I., Dentener, F. J., Facchini, M. C., Van Dingenen, R., Ervens, B., Nenes, A., Nielsen, C. J., Swietlicki, E., Putaud, J. P., Balkanski, Y., Fuzzi, S., Horth, J., Moortgat, G. K., Winterhalter, R., Myhre, C. E. L., Tsigaridis, K., Vignati, E., Stephanou, E. G., and Wilson, J.: Organic aerosol and global climate modelling: a review, Atmos. Chem. Phys., 5, 1053-1123, 10.5194/acp-5-1053-2005, 2005.

Kari, E., Miettinen, P., Yli-Pirilä, P., Virtanen, A., and Faiola, C. L.: PTR-ToF-MS product ion distributions and humidity-dependence of biogenic volatile organic compounds, International Journal of Mass Spectrometry, 430, 87-97, https://doi.org/10.1016/j.ijms.2018.05.003, 2018.

Katrib, Y., Martin, S. T., Rudich, Y., Davidovits, P., Jayne, J. T., and Worsnop, D. R.: Density changes of aerosol particles as a result of chemical reaction, Atmos. Chem. Phys., 5, 275-291, 10.5194/acp-5-275-2005, 2005.

Keeling, C. I., and Bohlmann, J.: Genes, enzymes and chemicals of terpenoid diversity in the constitutive and induced defence of conifers against insects and pathogens*, New Phytologist, 170, 657-675, https://doi.org/10.1111/j.1469-8137.2006.01716.x, 2006.

Kesselmeier, J., and Staudt, M.: Biogenic Volatile Organic Compounds (VOC): An Overview on Emission, Physiology and Ecology, Journal of Atmospheric Chemistry, 33, 23-88, 10.1023/A:1006127516791, 1999.

Khamaganov, V. G., and Hites, R. A.: Rate Constants for the Gas-Phase Reactions of Ozone with Isoprene, α- and β-Pinene, and Limonene as a Function of Temperature, The Journal of Physical Chemistry A, 105, 815-822, 10.1021/jp002730z, 2001.

Kiendler-Scharr, A., Wildt, J., Maso, M. D., Hohaus, T., Kleist, E., Mentel, T. F., Tillmann, R., Uerlings, R., Schurr, U., and Wahner, A.: New particle formation in forests inhibited by isoprene emissions, Nature, 461, 381-384, 10.1038/nature08292, 2009.

Kiendler-Scharr, A., Mensah, A. A., Friese, E., Topping, D., Nemitz, E., Prevot, A. S. H., Äijälä, M., Allan, J., Canonaco, F., Canagaratna, M., Carbone, S., Crippa, M., Dall Osto, M., Day, D. A., De Carlo, P., Di Marco, C. F., Elbern, H., Eriksson, A., Freney, E., Hao, L., Herrmann, H., Hildebrandt, L., Hillamo, R., Jimenez, J. L., Laaksonen, A., McFiggans, G., Mohr, C., O'Dowd, C., Otjes, R., Ovadnevaite, J.,

Pandis, S. N., Poulain, L., Schlag, P., Sellegri, K., Swietlicki, E., Tiitta, P., Vermeulen, A., Wahner, A., Worsnop, D., and Wu, H.-C.: Ubiquity of organic nitrates from nighttime chemistry in the European submicron aerosol, Geophysical Research Letters, 43, 7735-7744, https://doi.org/10.1002/2016GL069239, 2016.

Kim, M. J., Zoerb, M. C., Campbell, N. R., Zimmermann, K. J., Blomquist, B. W., Huebert, B. J., and Bertram, T. H.: Revisiting benzene cluster cations for the chemical ionization of dimethyl sulfide and select volatile organic compounds, Atmos. Meas. Tech., 9, 1473-1484, 10.5194/amt-9-1473-2016, 2016.

Kim, S., Karl, T., Helmig, D., Daly, R., Rasmussen, R., and Guenther, A.: Measurement of atmospheric sesquiterpenes by proton transfer reaction-mass spectrometry (PTR-MS), Atmos. Meas. Tech., 2, 99-112, 10.5194/amt-2-99-2009, 2009.

Kirkby, J., Duplissy, J., Sengupta, K., Frege, C., Gordon, H., Williamson, C., Heinritzi, M., Simon, M., Yan, C., Almeida, J., Tröstl, J., Nieminen, T., Ortega, I. K., Wagner, R., Adamov, A., Amorim, A., Bernhammer, A.-K., Bianchi, F., Breitenlechner, M., Brilke, S., Chen, X., Craven, J., Dias, A., Ehrhart, S., Flagan, R. C., Franchin, A., Fuchs, C., Guida, R., Hakala, J., Hoyle, C. R., Jokinen, T., Junninen, H., Kangasluoma, J., Kim, J., Krapf, M., Kürten, A., Laaksonen, A., Lehtipalo, K., Makhmutov, V., Mathot, S., Molteni, U., Onnela, A., Peräkylä, O., Piel, F., Petäjä, T., Praplan, A. P., Pringle, K., Rap, A., Richards, N. A. D., Riipinen, I., Rissanen, M. P., Rondo, L., Sarnela, N., Schobesberger, S., Scott, C. E., Seinfeld, J. H., Sipilä, M., Steiner, G., Stozhkov, Y., Stratmann, F., Tomé, A., Virtanen, A., Vogel, A. L., Wagner, A. C., Wagner, P. E., Weingartner, E., Wimmer, D., Winkler, P. M., Ye, P., Zhang, X., Hansel, A., Dommen, J., Donahue, N. M., Worsnop, D. R., Baltensperger, U., Kulmala, M., Carslaw, K. S., and Curtius, J.: Ion-induced nucleation of pure biogenic particles, Nature, 533, 521-526, 10.1038/nature17953, 2016.

Kleist, E., Mentel, T. F., Andres, S., Bohne, A., Folkers, A., Kiendler-Scharr, A., Rudich, Y., Springer, M., Tillmann, R., and Wildt, J.: Irreversible impacts of heat on the emissions of monoterpenes, sesquiterpenes, phenolic BVOC and green leaf volatiles from several tree species, Biogeosciences, 9, 5111-5123, 10.5194/bg-9-5111-2012, 2012.

Kolb, C. E., and Worsnop, D. R.: Chemistry and Composition of Atmospheric Aerosol Particles, Annual Review of Physical Chemistry, 63, 471-491, 10.1146/annurev-physchem-032511-143706, 2012.

Kołodziejczyk, A., Pyrcz, P., Pobudkowska, A., Błaziak, K., and Szmigielski, R.: Physicochemical Properties of Pinic, Pinonic, Norpinic, and Norpinonic Acids as Relevant α-Pinene Oxidation Products, The Journal of Physical Chemistry B, 123, 8261-8267, 10.1021/acs.jpcb.9b05211, 2019.

Koppmann, R.: Volatile organic compounds in the atmosphere, John Wiley & Sons, 2008.

Koss, A. R., Warneke, C., Yuan, B., Coggon, M. M., Veres, P. R., and de Gouw, J. A.: Evaluation of NO+ reagent ion chemistry for online measurements of atmospheric volatile organic compounds, Atmos. Meas. Tech., 9, 2909-2925, 10.5194/amt-9-2909-2016, 2016.

Kristensen, K., Watne, Å. K., Hammes, J., Lutz, A., Petäjä, T., Hallquist, M., Bilde, M., and Glasius, M.: High-molecular weight dimer esters are major products in aerosols from α-pinene ozonolysis and the boreal forest, Environmental Science & Technology Letters, 3, 280-285, 2016.

Kroll, J. H., Donahue, N. M., Jimenez, J. L., Kessler, S. H., Canagaratna, M. R., Wilson, K. R., Altieri, K. E., Mazzoleni, L. R., Wozniak, A. S., Bluhm, H., Mysak, E. R., Smith, J. D., Kolb, C. E., and Worsnop, D. R.: Carbon oxidation state as a metric for describing the chemistry of atmospheric organic aerosol, Nature Chemistry, 3, 133-139, 10.1038/nchem.948, 2011.

Langford, B., Cash, J., Acton, W. J. F., Valach, A. C., Hewitt, C. N., Fares, S., Goded, I., Gruening, C., House, E., Kalogridis, A. C., Gros, V., Schafers, R., Thomas, R., Broadmeadow, M., and Nemitz, E.: Isoprene emission potentials from European oak forests derived from canopy flux measurements: an assessment of uncertainties and inter-algorithm variability, Biogeosciences, 14, 5571-5594, 10.5194/bg-14-5571-2017, 2017.

Lanz, V. A., Alfarra, M. R., Baltensperger, U., Buchmann, B., Hueglin, C., and Prévôt, A. S. H.: Source apportionment of submicron organic aerosols at an urban site by factor analytical modelling of aerosol mass spectra, Atmos. Chem. Phys., 7, 1503-1522, 10.5194/acp-7-1503-2007, 2007.

Larsen, B., Lahaniati, M., Calogirou, A., and Kotzias, D.: Atmospheric oxidation products of terpenes: A new nomenclature, Chemosphere, 37, 1207-1220, 1998.

Law, K. S., and Stohl, A.: Arctic Air Pollution: Origins and Impacts, Science, 315, 1537-1540, doi:10.1126/science.1137695, 2007.

Lee, A., Goldstein, A. H., Keywood, M. D., Gao, S., Varutbangkul, V., Bahreini, R., Ng, N. L., Flagan, R. C., and Seinfeld, J. H.: Gas-phase products and secondary aerosol yields from the ozonolysis of ten different terpenes, Journal of Geophysical Research: Atmospheres, 111, 2006a.

Lee, A., Goldstein, A. H., Keywood, M. D., Gao, S., Varutbangkul, V., Bahreini, R., Ng, N. L., Flagan, R. C., and Seinfeld, J. H.: Gas-phase products and secondary aerosol yields from the ozonolysis of ten different terpenes, Journal of Geophysical Research: Atmospheres, 111, https://doi.org/10.1029/2005JD006437, 2006b.

Lee, A., Goldstein, A. H., Kroll, J. H., Ng, N. L., Varutbangkul, V., Flagan, R. C., and Seinfeld, J. H.: Gas-phase products and secondary aerosol yields from the photooxidation of 16 different terpenes, Journal of Geophysical Research: Atmospheres, 111, https://doi.org/10.1029/2006JD007050, 2006c.

Lee, A., Goldstein, A. H., Kroll, J. H., Ng, N. L., Varutbangkul, V., Flagan, R. C., and Seinfeld, J. H.: Gas-phase products and secondary aerosol yields from the photooxidation of 16 different terpenes, Journal of Geophysical Research: Atmospheres, 111, 2006d.

Lee, B. H., Lopez-Hilfiker, F. D., Mohr, C., Kurtén, T., Worsnop, D. R., and Thornton, J. A.: An Iodide-Adduct High-Resolution Time-of-Flight Chemical-Ionization Mass Spectrometer: Application to Atmospheric Inorganic and Organic Compounds, Environmental Science & Technology, 48, 6309-6317, 10.1021/es500362a, 2014.

Lee, B. H., Mohr, C., Lopez-Hilfiker, F. D., Lutz, A., Hallquist, M., Lee, L., Romer, P., Cohen, R. C., Iyer, S., Kurtén, T., Hu, W., Day, D. A., Campuzano-Jost, P., Jimenez, J. L., Xu, L., Ng, N. L., Guo, H., Weber, R. J., Wild, R. J., Brown, S. S., Koss, A., Gouw, J. d., Olson, K., Goldstein, A. H., Seco, R., Kim, S., McAvey, K., Shepson, P. B., Starn, T., Baumann, K., Edgerton, E. S., Liu, J., Shilling, J. E., Miller, D. O., Brune, W., Schobesberger, S., D'Ambro, E. L., and Thornton, J. A.: Highly functionalized organic nitrates in the southeast United States: Contribution to secondary organic aerosol and reactive nitrogen budgets, Proceedings of the National Academy of Sciences, 113, 1516-1521, doi:10.1073/pnas.1508108113, 2016.

Lee, E., Chan, C. K., and Paatero, P.: Application of positive matrix factorization in source apportionment of particulate pollutants in Hong Kong, Atmospheric Environment, 33, 3201-3212, https://doi.org/10.1016/S1352-2310(99)00113-2, 1999.

Lee, S., and Kamens, R. M.: Particle nucleation from the reaction of α-pinene and O3, Atmospheric Environment, 39, 6822-6832, 2005.

Li, Y., Chen, Q., Guzman, M., Chan, C. K., and Martin, S.: Second-generation products contribute substantially to the particle-phase organic material produced by [beta]-caryophyllene ozonolysis, Atmospheric Chemistry and Physics, 11, 121, 2011a.

Li, Y., Pöschl, U., and Shiraiwa, M.: Molecular corridors and parameterizations of volatility in the chemical evolution of organic aerosols, Atmos. Chem. Phys., 16, 3327-3344, 10.5194/acp-16-3327-2016, 2016.

Li, Y., Day, D. A., Stark, H., Jimenez, J. L., and Shiraiwa, M.: Predictions of the glass transition temperature and viscosity of organic aerosols from volatility distributions, Atmos. Chem. Phys., 20, 8103-8122, 10.5194/acp-20-8103-2020, 2020.

Li, Y. J., Chen, Q., Guzman, M. I., Chan, C. K., and Martin, S. T.: Second-generation products contribute substantially to the particle-phase organic material produced by β-caryophyllene ozonolysis, Atmos. Chem. Phys., 11, 121-132, 10.5194/acp-11-121-2011, 2011b.

Li, Z., Buchholz, A., Ylisirniö, A., Barreira, L., Hao, L., Schobesberger, S., Yli-Juuti, T., and Virtanen, A.: Evolution of volatility and composition in sesquiterpene-mixed and α-pinene secondary organic aerosol particles during isothermal evaporation, Atmos. Chem. Phys., 21, 18283-18302, 10.5194/acp-21-18283-2021, 2021.

Lin, Y.-H., Zhang, H., Pye, H. O. T., Zhang, Z., Marth, W. J., Park, S., Arashiro, M., Cui, T., Budisulistiorini, S. H., Sexton, K. G., Vizuete, W., Xie, Y., Luecken, D. J., Piletic, I. R., Edney, E. O., Bartolotti, L. J., Gold, A., and Surratt, J. D.: Epoxide as a precursor to secondary organic aerosol formation from isoprene photooxidation in the presence of nitrogen oxides, Proceedings of the National Academy of Sciences, 110, 6718-6723, 10.1073/pnas.1221150110, 2013.

Liu, P., Ziemann, P. J., Kittelson, D. B., and McMurry, P. H.: Generating Particle Beams of Controlled Dimensions and Divergence: II. Experimental Evaluation of Particle Motion in Aerodynamic Lenses and Nozzle Expansions, Aerosol Science and Technology, 22, 314-324, 10.1080/02786829408959749, 1995.

Liu, P. S. K., Deng, R., Smith, K. A., Williams, L. R., Jayne, J. T., Canagaratna, M. R., Moore, K., Onasch, T. B., Worsnop, D. R., and Deshler, T.: Transmission Efficiency of an Aerodynamic Focusing Lens System: Comparison of Model Calculations and Laboratory Measurements for the Aerodyne Aerosol Mass Spectrometer, Aerosol Science and Technology, 41, 721-733, 10.1080/02786820701422278, 2007.

Liu, X., Day, D. A., Krechmer, J. E., Ziemann, P. J., and Jimenez, J. L.: Determining Activity Coefficients of SOA from Isothermal Evaporation in a Laboratory Chamber, Environmental Science & Technology Letters, 8, 212-217, 10.1021/acs.estlett.0c00888, 2021.

Lopez-Hilfiker, F. D., Mohr, C., Ehn, M., Rubach, F., Kleist, E., Wildt, J., Mentel, T. F., Lutz, A., Hallquist, M., Worsnop, D., and Thornton, J. A.: A novel method for online analysis of gas and particle composition: description and evaluation of a Filter Inlet for Gases and AEROsols (FIGAERO), Atmos. Meas. Tech., 7, 983-1001, 10.5194/amt-7-983-2014, 2014.

Lopez-Hilfiker, F. D.: A Molecular Characterization of Biogenic Secondary Organic Aerosol by High-Resolution Time-of-Flight Mass Spectrometry: Composition and Volatility, 2015.

Lopez-Hilfiker, F. D., Mohr, C., Ehn, M., Rubach, F., Kleist, E., Wildt, J., Mentel, T. F., Carrasquillo, A. J., Daumit, K. E., Hunter, J. F., Kroll, J. H., Worsnop, D. R., and Thornton, J. A.: Phase partitioning and volatility of secondary organic aerosol components formed from α-pinene ozonolysis and OH oxidation: the importance of accretion products and other low volatility compounds, Atmos. Chem. Phys., 15, 7765-7776, 10.5194/acp-15-7765-2015, 2015.

Lopez-Hilfiker, F. D., Iyer, S., Mohr, C., Lee, B. H., D'Ambro, E. L., Kurtén, T., and Thornton, J. A.: Constraining the sensitivity of iodide adduct chemical ionization mass spectrometry to multifunctional organic molecules using the collision limit and thermodynamic stability of iodide ion adducts, Atmos. Meas. Tech., 9, 1505-1512, 10.5194/amt-9-1505-2016, 2016.

Lopez-Hilfiker, F. D., Pospisilova, V., Huang, W., Kalberer, M., Mohr, C., Stefenelli, G., Thornton, J. A., Baltensperger, U., Prevot, A. S. H., and Slowik, J. G.: An extractive electrospray ionization time-of-flight mass spectrometer (EESI-TOF) for online measurement of atmospheric aerosol particles, Atmos. Meas. Tech., 12, 4867-4886, 10.5194/amt-12-4867-2019, 2019.

Maclean, A. M., Butenhoff, C. L., Grayson, J. W., Barsanti, K., Jimenez, J. L., and Bertram, A. K.: Mixing times of organic molecules within secondary organic aerosol particles: a global planetary boundary layer perspective, Atmos. Chem. Phys., 17, 13037-13048, 10.5194/acp-17-13037-2017, 2017.

Mahilang, M., Deb, M. K., and Pervez, S.: Biogenic secondary organic aerosols: A review on formation mechanism, analytical challenges and environmental impacts, Chemosphere, 262, 127771, https://doi.org/10.1016/j.chemosphere.2020.127771, 2021.

Marshall, F. H., Berkemeier, T., Shiraiwa, M., Nandy, L., Ohm, P. B., Dutcher, C. S., and Reid, J. P.: Influence of particle viscosity on mass transfer and heterogeneous ozonolysis kinetics in aqueous–sucrose–maleic acid aerosol, Physical Chemistry Chemical Physics, 20, 15560-15573, 2018.

McFiggans, G., Mentel, T. F., Wildt, J., Pullinen, I., Kang, S., Kleist, E., Schmitt, S., Springer, M., Tillmann, R., Wu, C., Zhao, D., Hallquist, M., Faxon, C., Le Breton, M., Hallquist, Å. M., Simpson, D., Bergström, R., Jenkin, M. E., Ehn, M., Thornton, J. A., Alfarra, M. R., Bannan, T. J., Percival, C. J., Priestley, M., Topping, D., and Kiendler-Scharr, A.: Secondary organic aerosol reduced by mixture of atmospheric vapours, Nature, 565, 587-593, 10.1038/s41586-018-0871-y, 2019.

McNeill, V. F., Wolfe, G. M., and Thornton, J. A.: The Oxidation of Oleate in Submicron Aqueous Salt Aerosols: Evidence of a Surface Process, The Journal of Physical Chemistry A, 111, 1073-1083, 10.1021/jp066233f, 2007.

Mohr, C., Lopez-Hilfiker, F. D., Zotter, P., Prévôt, A. S. H., Xu, L., Ng, N. L., Herndon, S. C., Williams, L. R., Franklin, J. P., Zahniser, M. S., Worsnop, D. R., Knighton, W. B., Aiken, A. C., Gorkowski, K. J., Dubey, M. K., Allan, J. D., and Thornton, J. A.: Contribution of Nitrated Phenols to Wood Burning Brown Carbon Light Absorption in Detling, United Kingdom during Winter Time, Environmental Science & Technology, 47, 6316-6324, 10.1021/es400683v, 2013.

Moise, T., Flores, J. M., and Rudich, Y.: Optical Properties of Secondary Organic Aerosols and Their Changes by Chemical Processes, Chemical reviews, 115, 4400-4439, 10.1021/cr5005259, 2015.

Moller, B., Rarey, J., and Ramjugernath, D.: Estimation of the vapour pressure of non-electrolyte organic compounds via group contributions and group interactions, Journal of Molecular Liquids, 143, 52-63, https://doi.org/10.1016/j.molliq.2008.04.020, 2008.

Müller, L., Reinnig, M. C., Warnke, J., and Hoffmann, T.: Unambiguous identification of esters as oligomers in secondary organic aerosol formed from cyclohexene and cyclohexene/α-pinene ozonolysis, Atmos. Chem. Phys., 8, 1423-1433, 10.5194/acp-8-1423-2008, 2008.

Müller, M., Eichler, P., D'Anna, B., Tan, W., and Wisthaler, A.: Direct Sampling and Analysis of Atmospheric Particulate Organic Matter by Proton-Transfer-Reaction Mass Spectrometry, Analytical Chemistry, 89, 10889-10897, 10.1021/acs.analchem.7b02582, 2017.

Nannoolal, Y., Rarey, J., Ramjugernath, D., and Cordes, W.: Estimation of pure component properties: Part 1. Estimation of the normal boiling point of non-electrolyte organic compounds via group contributions and group interactions, Fluid Phase Equilibria, 226, 45-63, https://doi.org/10.1016/j.fluid.2004.09.001, 2004.

Nannoolal, Y., Rarey, J., and Ramjugernath, D.: Estimation of pure component properties: Part 3. Estimation of the vapor pressure of non-electrolyte organic compounds via group contributions and group interactions, Fluid Phase Equilibria, 269, 117-133, https://doi.org/10.1016/j.fluid.2008.04.020, 2008.

Nguyen, T. L., Winterhalter, R., Moortgat, G., Kanawati, B., Peeters, J., and Vereecken, L.: The gas-phase ozonolysis of β-caryophyllene (C 15 H 24). Part II: A theoretical study, Physical Chemistry Chemical Physics, 11, 4173-4183, 2009.

Odum, J. R., Hoffmann, T., Bowman, F., Collins, D., Flagan, R. C., and Seinfeld, J. H.: Gas/Particle Partitioning and Secondary Organic Aerosol Yields, Environmental Science & Technology, 30, 2580-2585, 10.1021/es950943+, 1996.

Owen, S. M., MacKenzie, A. R., Stewart, H., Donovan, R., and Hewitt, C. N.: BIOGENIC VOLATILE ORGANIC COMPOUND (VOC) EMISSION ESTIMATES FROM AN URBAN TREE CANOPY, Ecological Applications, 13, 927-938, https://doi.org/10.1890/01-5177, 2003.

Paatero, P., and Tapper, U.: Positive matrix factorization: A non-negative factor model with optimal utilization of error estimates of data values, Environmetrics, 5, 111-126, https://doi.org/10.1002/env.3170050203, 1994.

Paatero, P., and Hopke, P. K.: Discarding or downweighting high-noise variables in factor analytic models, Analytica Chimica Acta, 490, 277-289, https://doi.org/10.1016/S0003-2670(02)01643-4, 2003.

Pandis, S. N., Harley, R. A., Cass, G. R., and Seinfeld, J. H.: Secondary organic aerosol formation and transport, Atmospheric Environment. Part A. General Topics, 26, 2269-2282, https://doi.org/10.1016/0960-1686(92)90358-R, 1992.

Pankow, J. F.: An absorption model of the gas/aerosol partitioning involved in the formation of secondary organic aerosol, Atmospheric Environment, 28, 189-193, https://doi.org/10.1016/1352-2310(94)90094-9, 1994a.

Pankow, J. F.: An absorption model of gas/particle partitioning of organic compounds in the atmosphere, Atmospheric Environment, 28, 185-188, https://doi.org/10.1016/1352-2310(94)90093-0, 1994b.

Parshintsev, J., Nurmi, J., Kilpeläinen, I., Hartonen, K., Kulmala, M., and Riekkola, M.-L.: Preparation of β-caryophyllene oxidation products and their determination in ambient aerosol samples, Analytical and bioanalytical chemistry, 390, 913-919, 2008.

Piccot, S. D., Watson, J. J., and Jones, J. W.: A global inventory of volatile organic compound emissions from anthropogenic sources, Journal of Geophysical Research: Atmospheres, 97, 9897-9912, https://doi.org/10.1029/92JD00682, 1992.

Piel, F., Müller, M., Winkler, K., Skytte af Sätra, J., and Wisthaler, A.: Introducing the extended volatility range proton-transfer-reaction mass spectrometer (EVR PTR-MS), Atmospheric Measurement Techniques, 14, 1355-1363, 2021.

Pöschl, U.: Atmospheric Aerosols: Composition, Transformation, Climate and Health Effects, Angewandte Chemie International Edition, 44, 7520-7540, https://doi.org/10.1002/anie.200501122, 2005.

Prospero, J. M., Charlson, R. J., Mohnen, V., Jaenicke, R., Delany, A. C., Moyers, J., Zoller, W., and Rahn, K.: The atmospheric aerosol system: An overview, Reviews of Geophysics, 21, 1607-1629, https://doi.org/10.1029/RG021i007p01607, 1983.

Quéléver, L. L. J., Kristensen, K., Normann Jensen, L., Rosati, B., Teiwes, R., Daellenbach, K. R., Peräkylä, O., Roldin, P., Bossi, R., Pedersen, H. B., Glasius, M., Bilde, M., and Ehn, M.: Effect of temperature on the formation of highly oxygenated organic molecules (HOMs) from alpha-pinene ozonolysis, Atmos. Chem. Phys., 19, 7609-7625, 10.5194/acp-19-7609-2019, 2019.

Reff, A., Eberly, S. I., and Bhave, P. V.: Receptor Modeling of Ambient Particulate Matter Data Using Positive Matrix Factorization: Review of Existing Methods, Journal of the Air & Waste Management Association, 57, 146-154, 10.1080/10473289.2007.10465319, 2007.

Reid, J. P., Bertram, A. K., Topping, D. O., Laskin, A., Martin, S. T., Petters, M. D., Pope, F. D., and Rovelli, G.: The viscosity of atmospherically relevant organic particles, Nature Communications, 9, 956, 10.1038/s41467-018-03027-z, 2018.

Ren, Y., Grosselin, B., Daële, V., and Mellouki, A.: Investigation of the reaction of ozone with isoprene, methacrolein and methyl vinyl ketone using the HELIOS chamber, Faraday Discussions, 200, 289-311, 10.1039/C7FD00014F, 2017.

Richters, S., Herrmann, H., and Berndt, T.: Gas-phase rate coefficients of the reaction of ozone with four sesquiterpenes at 295 ± 2 K, Physical Chemistry Chemical Physics, 17, 11658-11669, 10.1039/C4CP05542J, 2015.

Richters, S., Herrmann, H., and Berndt, T.: Different pathways of the formation of highly oxidized multifunctional organic compounds (HOMs) from the gas-phase ozonolysis of β-caryophyllene, Atmos. Chem. Phys., 16, 9831-9845, 10.5194/acp-16-9831-2016, 2016a.

Richters, S., Herrmann, H., and Berndt, T.: Different pathways of the formation of highly oxidized multifunctional organic compounds (HOMs) from the gas-phase ozonolysis of β-caryophyllene, Atmos. Chem. Phys, 16, 9831-9845, 2016b.

Riemer, D. D., Apel, E. C., Orlando, J. J., Tyndall, G. S., Brune, W. H., Williams, E. J., Lonneman, W. A., and Neece, J. D.: Unique isoprene oxidation products demonstrate chlorine atom chemistry occurs in the Houston, Texas urban area, Journal of Atmospheric Chemistry, 61, 227-242, 10.1007/s10874-009-9134-5, 2008.

Rinne, H. J. I., Guenther, A. B., Greenberg, J. P., and Harley, P. C.: Isoprene and monoterpene fluxes measured above Amazonian rainforest and their dependence on light and temperature, Atmospheric Environment, 36, 2421-2426, https://doi.org/10.1016/S1352-2310(01)00523-4, 2002.

Riva, M., Budisulistiorini, S. H., Zhang, Z., Gold, A., Thornton, J. A., Turpin, B. J., and Surratt, J. D.: Multiphase reactivity of gaseous hydroperoxide oligomers produced from isoprene ozonolysis in the presence of acidified aerosols, Atmospheric Environment, 152, 314-322, https://doi.org/10.1016/j.atmosenv.2016.12.040, 2017.

Riva, M., Rantala, P., Krechmer, J. E., Peräkylä, O., Zhang, Y., Heikkinen, L., Garmash, O., Yan, C., Kulmala, M., Worsnop, D., and Ehn, M.: Evaluating the performance of five different chemical ionization techniques for detecting gaseous oxygenated organic species, Atmos. Meas. Tech., 12, 2403-2421, 10.5194/amt-12-2403-2019, 2019.

Roberts, G. C., Andreae, M. O., Zhou, J., and Artaxo, P.: Cloud condensation nuclei in the Amazon Basin: "marine" conditions over a continent?, Geophysical Research Letters, 28, 2807-2810, https://doi.org/10.1029/2000GL012585, 2001.

Rodriguez-Saona, C., Crafts-Brandner, S. J., ParÉ, P. W., and Henneberry, T. J.: EXOGENOUS METHYL JASMONATE INDUCES VOLATILE EMISSIONS IN COTTON PLANTS, Journal of Chemical Ecology, 27, 679-695, 10.1023/A:1010393700918, 2001.

Rothfuss, N. E., and Petters, M. D.: Influence of Functional Groups on the Viscosity of Organic Aerosol, Environmental Science & Technology, 51, 271-279, 10.1021/acs.est.6b04478, 2017.

Saathoff, H., Naumann, K., Möhler, O., Jonsson, A., Hallquist, M., Kiendler-Scharr, A., Mentel, T. F., Tillmann, R., and Schurath, U.: Temperature dependence of yields of secondary organic aerosols from the ozonolysis of α-pinene and limonene, Atmos. Chem. Phys, 9, 1551-1577, 2009a.

Saathoff, H., Naumann, K. H., Möhler, O., Jonsson, Å. M., Hallquist, M., Kiendler-Scharr, A., Mentel, T. F., Tillmann, R., and Schurath, U.: Temperature dependence of yields of secondary organic aerosols from the ozonolysis of α-pinene and limonene, Atmos. Chem. Phys., 9, 1551-1577, 10.5194/acp-9-1551-2009, 2009b.

Salo, K., Jonsson, A., Andersson, P., and Hallquist, M.: Aerosol Volatility and Enthalpy of Sublimation of Carboxylic Acids, The journal of physical chemistry. A, 114, 4586-4594, 10.1021/jp910105h, 2010.

Sanadze, G., and Kursanov, A.: On certain conditions of the evolution of the diene C5H8 from poplar leaves, Soviet Plant Physiology, 13, 184-189, 1966.

Sanadze, G.: Light-dependent excretion of molecular isoprene, Prog Photosynth Res, 2, 701-707, 1969.

Schervish, M., and Donahue, N. M.: Peroxy radical chemistry and the volatility basis set, Atmos. Chem. Phys., 20, 1183-1199, 10.5194/acp-20-1183-2020, 2020.

Schmale, J., Zieger, P., and Ekman, A. M. L.: Aerosols in current and future Arctic climate, Nature Climate Change, 11, 95-105, 10.1038/s41558-020-00969-5, 2021.

Sharkey, T. D., and Yeh, S.: Isoprene emission from plants, Annual review of plant biology, 52, 407-436, 2001.

Sharkey, T. D., Wiberley, A. E., and Donohue, A. R.: Isoprene Emission from Plants: Why and How, Annals of Botany, 101, 5-18, 10.1093/aob/mcm240, 2007.

Shiraiwa, M., Ammann, M., Koop, T., and Pöschl, U.: Gas uptake and chemical aging of semisolid organic aerosol particles, Proceedings of the National Academy of Sciences, 108, 11003-11008, 10.1073/pnas.1103045108, 2011.

Shiraiwa, M., and Seinfeld, J. H.: Equilibration timescale of atmospheric secondary organic aerosol partitioning, Geophysical Research Letters, 39, https://doi.org/10.1029/2012GL054008, 2012.

Shiraiwa, M., Li, Y., Tsimpidi, A. P., Karydis, V. A., Berkemeier, T., Pandis, S. N., Lelieveld, J., Koop, T., and Pöschl, U.: Global distribution of particle phase state in atmospheric secondary organic aerosols, Nature Communications, 8, 15002, 10.1038/ncomms15002, 2017.

Shrivastava, M., Easter, R. C., Liu, X., Zelenyuk, A., Singh, B., Zhang, K., Ma, P.-L., Chand, D., Ghan, S., Jimenez, J. L., Zhang, Q., Fast, J., Rasch, P. J., and Tiitta, P.: Global transformation and fate of SOA: Implications of low-volatility SOA and gas-phase fragmentation reactions, Journal of Geophysical Research: Atmospheres, 120, 4169-4195, https://doi.org/10.1002/2014JD022563, 2015.

Shrivastava, M., Cappa, C. D., Fan, J., Goldstein, A. H., Guenther, A. B., Jimenez, J. L., Kuang, C., Laskin, A., Martin, S. T., Ng, N. L., Petaja, T., Pierce, J. R., Rasch, P. J., Roldin, P., Seinfeld, J. H., Shilling, J., Smith, J. N., Thornton, J. A., Volkamer, R., Wang, J., Worsnop, D. R., Zaveri, R. A., Zelenyuk, A., and Zhang, Q.: Recent advances in understanding secondary organic aerosol: Implications for global climate forcing, Reviews of Geophysics, 55, 509-559, https://doi.org/10.1002/2016RG000540, 2017.

Shu, Y., and Atkinson, R.: Rate constants for the gas-phase reactions of O3 with a series of terpenes and OH radical formation from the O3 reactions with sesquiterpenes at 296±2 K, International Journal of Chemical Kinetics, 26, 1193-1205, 1994a.

Shu, Y., and Atkinson, R.: Rate constants for the gas-phase reactions of O3 with a series of Terpenes and OH radical formation from the O3 reactions with Sesquiterpenes at 296 ± 2 K, International Journal of Chemical Kinetics, 26, 1193-1205, https://doi.org/10.1002/kin.550261207, 1994b.

Shu, Y., and Atkinson, R.: Atmospheric lifetimes and fates of a series of sesquiterpenes, Journal of Geophysical Research: Atmospheres, 100, 7275-7281, https://doi.org/10.1029/95JD00368, 1995.

Sindelarova, K., Granier, C., Bouarar, I., Guenther, A., Tilmes, S., Stavrakou, T., Müller, J. F., Kuhn, U., Stefani, P., and Knorr, W.: Global data set of biogenic VOC emissions calculated by the MEGAN model over the last 30 years, Atmos. Chem. Phys., 14, 9317-9341, 10.5194/acp-14-9317-2014, 2014.

Smith, L. D., Allan, J., Coe, H., Reyes-Villegas, E., Johnson, M. P., Crayford, A., Durand, E., and Williams, P. I.: Examining chemical composition of gas turbine-emitted organic aerosol using positive matrix factorisation (PMF), Journal of Aerosol Science, 159, 105869, https://doi.org/10.1016/j.jaerosci.2021.105869, 2022.

Spanel, P., and Smith, D.: SIFT studies of the reactions of H3O+, NO+ and O2+ with a series of alcohols, International Journal of Mass Spectrometry and Ion Processes, 167-168, 375-388, https://doi.org/10.1016/S0168-1176(97)00085-2, 1997.

Stark, H., Yatavelli, R. L. N., Thompson, S. L., Kang, H., Krechmer, J. E., Kimmel, J. R., Palm, B. B., Hu, W., Hayes, P. L., Day, D. A., Campuzano-Jost, P., Canagaratna, M. R., Jayne, J. T., Worsnop, D. R., and Jimenez, J. L.: Impact of Thermal Decomposition on Thermal Desorption Instruments: Advantage of Thermogram Analysis for Quantifying Volatility Distributions of Organic Species, Environmental Science & Technology, 51, 8491-8500, 10.1021/acs.est.7b00160, 2017.

Stewart, D. J., Almabrok, S. H., Lockhart, J. P., Mohamed, O. M., Nutt, D. R., Pfrang, C., and Marston, G.: The kinetics of the gas-phase reactions of selected monoterpenes and cyclo-alkenes with ozone and the NO3 radical, Atmospheric Environment, 70, 227-235, https://doi.org/10.1016/j.atmosenv.2013.01.036, 2013.

Sun, Y., Zhang, Q., Macdonald, A. M., Hayden, K., Li, S. M., Liggio, J., Liu, P. S. K., Anlauf, K. G., Leaitch, W. R., Steffen, A., Cubison, M., Worsnop, D. R., van Donkelaar, A., and Martin, R. V.: Size-resolved aerosol chemistry on Whistler Mountain, Canada with a high-resolution aerosol mass spectrometer during INTEX-B, Atmos. Chem. Phys., 9, 3095-3111, 10.5194/acp-9-3095-2009, 2009.

Tasoglou, A., and Pandis, S.: Formation and chemical aging of secondary organic aerosol during the β-caryophyllene oxidation, Atmospheric Chemistry & Physics, 15, 2015a.

Tasoglou, A., and Pandis, S. N.: Formation and chemical aging of secondary organic aerosol during the β-caryophyllene oxidation, Atmos. Chem. Phys., 15, 6035-6046, 10.5194/acp-15-6035-2015, 2015b.

Theloke, J., and Friedrich, R.: Compilation of a database on the composition of anthropogenic VOC emissions for atmospheric modeling in Europe, Atmospheric Environment, 41, 4148-4160, https://doi.org/10.1016/j.atmosenv.2006.12.026, 2007.

Tikkanen, O. P., Buchholz, A., Ylisirniö, A., Schobesberger, S., Virtanen, A., and Yli-Juuti, T.: Comparing secondary organic aerosol (SOA) volatility distributions derived from isothermal SOA particle evaporation data and FIGAERO–CIMS measurements, Atmos. Chem. Phys., 20, 10441-10458, 10.5194/acp-20-10441-2020, 2020.

Tillmann, R., Hallquist, M., Jonsson, Å. M., Kiendler-Scharr, A., Saathoff, H., Iinuma, Y., and Mentel, T. F.: Influence of relative humidity and temperature on the production of pinonaldehyde and OH radicals from the ozonolysis of α-pinene, Atmos. Chem. Phys., 10, 7057-7072, 10.5194/acp-10-7057-2010, 2010.

Tsigaridis, K., Daskalakis, N., Kanakidou, M., Adams, P. J., Artaxo, P., Bahadur, R., Balkanski, Y., Bauer, S. E., Bellouin, N., Benedetti, A., Bergman, T., Berntsen, T. K., Beukes, J. P., Bian, H., Carslaw, K. S., Chin, M., Curci, G., Diehl, T., Easter, R. C., Ghan, S. J., Gong, S. L., Hodzic, A., Hoyle, C. R., Iversen, T., Jathar, S., Jimenez, J. L., Kaiser, J. W., Kirkevåg, A., Koch, D., Kokkola, H., Lee, Y. H., Lin, G., Liu, X., Luo, G., Ma, X., Mann, G. W., Mihalopoulos, N., Morcrette, J. J., Müller, J. F., Myhre, G., Myriokefalitakis, S., Ng, N. L., O'Donnell, D., Penner, J. E., Pozzoli, L., Pringle, K. J., Russell, L. M., Schulz, M., Sciare, J., Seland, Ø., Shindell, D. T., Sillman, S., Skeie, R. B., Spracklen, D., Stavrakou, T., Steenrod, S. D., Takemura, T., Tiitta, P., Tilmes, S., Tost, H., van Noije, T., van Zyl, P. G., von

Salzen, K., Yu, F., Wang, Z., Wang, Z., Zaveri, R. A., Zhang, H., Zhang, K., Zhang, Q., and Zhang, X.: The AeroCom evaluation and intercomparison of organic aerosol in global models, Atmos. Chem. Phys., 14, 10845-10895, 10.5194/acp-14-10845-2014, 2014.

Tuet, W. Y., Chen, Y., Xu, L., Fok, S., Gao, D., Weber, R. J., and Ng, N. L.: Chemical oxidative potential of secondary organic aerosol (SOA) generated from the photooxidation of biogenic and anthropogenic volatile organic compounds, Atmos. Chem. Phys., 17, 839-853, 10.5194/acp-17-839-2017, 2017.

Ulbrich, I. M., Canagaratna, M. R., Zhang, Q., Worsnop, D. R., and Jimenez, J. L.: Interpretation of organic components from Positive Matrix Factorization of aerosol mass spectrometric data, Atmos. Chem. Phys., 9, 2891-2918, 10.5194/acp-9-2891-2009, 2009.

van Eijck, A., Opatz, T., Taraborrelli, D., Sander, R., and Hoffmann, T.: New tracer compounds for secondary organic aerosol formation from β-caryophyllene oxidation, Atmospheric Environment, 80, 122-130, 2013.

Veres, P., Roberts, J. M., Warneke, C., Welsh-Bon, D., Zahniser, M., Herndon, S., Fall, R., and de Gouw, J.: Development of negative-ion proton-transfer chemical-ionization mass spectrometry (NI-PT-CIMS) for the measurement of gas-phase organic acids in the atmosphere, International Journal of Mass Spectrometry, 274, 48-55, https://doi.org/10.1016/j.ijms.2008.04.032, 2008.

Verma, S. K., Kawamura, K., Deshmukh, D. K., Haque, M. M., and Pavuluri, C. M.: Seasonal Characteristics of Biogenic Secondary Organic Aerosols Over Chichijima Island in the Western North Pacific: Impact of Biomass Burning Activity in East Asia, Journal of Geophysical Research: Atmospheres, 126, e2020JD032987, https://doi.org/10.1029/2020JD032987, 2021.

Vespermann, K. A. C., Paulino, B. N., Barcelos, M. C. S., Pessôa, M. G., Pastore, G. M., and Molina, G.: Biotransformation of α- and β-pinene into flavor compounds, Applied Microbiology and Biotechnology, 101, 1805-1817, 10.1007/s00253-016-8066-7, 2017.

Von Hessberg, C., Von Hessberg, P., Pöschl, U., Bilde, M., Nielsen, O., and Moortgat, G.: Temperature and humidity dependence of secondary organic aerosol yield from the ozonolysis of β-pinene, Atmos. Chem. Phys, 9, 3583-3599, 2009.

Waked, A., Favez, O., Alleman, L. Y., Piot, C., Petit, J. E., Delaunay, T., Verlinden, E., Golly, B., Besombes, J. L., Jaffrezo, J. L., and Leoz-Garziandia, E.: Source apportionment of PM₁₀ in a north-western Europe regional urban background site (Lens, France) using positive matrix factorization and including primary biogenic emissions, Atmos. Chem. Phys., 14, 3325-3346, 10.5194/acp-14-3325-2014, 2014.

Wang, K. Y., and Shallcross, D. E.: Modelling terrestrial biogenic isoprene fluxes and their potential impact on global chemical species using a coupled LSM–CTM model, Atmospheric Environment, 34, 2909-2925, https://doi.org/10.1016/S1352-2310(99)00525-7, 2000.

Wang, Y., Zhao, Y., Li, Z., Li, C., Yan, N., and Xiao, H.: Importance of Hydroxyl Radical Chemistry in Isoprene Suppression of Particle Formation from α-Pinene Ozonolysis, ACS Earth and Space Chemistry, 5, 487-499, 10.1021/acsearthspacechem.0c00294, 2021.

Warneke, C., Roberts, J. M., Veres, P., Gilman, J., Kuster, W. C., Burling, I., Yokelson, R., and de Gouw, J. A.: VOC identification and inter-comparison from laboratory biomass burning using PTR-MS and PIT-MS, International Journal of Mass Spectrometry, 303, 6-14, https://doi.org/10.1016/j.ijms.2010.12.002, 2011.

Williams, L. R., Gonzalez, L. A., Peck, J., Trimborn, D., McInnis, J., Farrar, M. R., Moore, K. D., Jayne, J. T., Robinson, W. A., Lewis, D. K., Onasch, T. B., Canagaratna, M. R., Trimborn, A., Timko, M. T., Magoon, G., Deng, R., Tang, D., de la Rosa Blanco, E., Prévôt, A. S. H., Smith, K. A., and Worsnop, D. R.: Characterization of an aerodynamic lens for transmitting particles greater than 1 micrometer in diameter into the Aerodyne aerosol mass spectrometer, Atmos. Meas. Tech., 6, 3271-3280, 10.5194/amt-6-3271-2013, 2013.

Winterhalter, R., Herrmann, F., Kanawati, B., Nguyen, T. L., Peeters, J., Vereecken, L., and Moortgat, G. K.: The gas-phase ozonolysis of β-caryophyllene (C 15 H 24). Part I: an experimental study, Physical Chemistry Chemical Physics, 11, 4152-4172, 2009a.

Winterhalter, R., Herrmann, F., Kanawati, B., Nguyen, T. L., Peeters, J., Vereecken, L., and Moortgat, G. K.: The gas-phase ozonolysis of β-caryophyllene (C15H24). Part I: an experimental study, Physical Chemistry Chemical Physics, 11, 4152-4172, 10.1039/B817824K, 2009b.

Witkowski, B., and Gierczak, T.: Early stage composition of SOA produced by α-pinene/ozone reaction: α-Acyloxyhydroperoxy aldehydes and acidic dimers, Atmospheric Environment, 95, 59-70, 2014.

Wu, C., Bell, D. M., Graham, E. L., Haslett, S., Riipinen, I., Baltensperger, U., Bertrand, A., Giannoukos, S., Schoonbaert, J., El Haddad, I., Prevot, A. S. H., Huang, W., and Mohr, C.: Photolytically induced changes in composition and volatility of biogenic secondary organic aerosol from nitrate radical oxidation during night-to-day transition, Atmos. Chem. Phys., 21, 14907-14925, 10.5194/acp-21-14907-2021, 2021.

Yasmeen, F., Vermeylen, R., Szmigielski, R., Iinuma, Y., Böge, O., Herrmann, H., Maenhaut, W., and Claeys, M.: Terpenylic acid and related compounds: precursors for dimers in secondary organic aerosol from the ozonolysis of α- and β-pinene, Atmos. Chem. Phys., 10, 9383-9392, 10.5194/acp-10-9383-2010, 2010.

Yatavelli, R. L. N., Lopez-Hilfiker, F., Wargo, J. D., Kimmel, J. R., Cubison, M. J., Bertram, T. H., Jimenez, J. L., Gonin, M., Worsnop, D. R., and Thornton, J. A.: A Chemical Ionization High-Resolution Time-of-Flight Mass Spectrometer Coupled to a Micro Orifice Volatilization Impactor (MOVI-HRToF-CIMS) for Analysis of Gas and Particle-Phase Organic Species, Aerosol Science and Technology, 46, 1313-1327, 10.1080/02786826.2012.712236, 2012.

Ye, Q., Wang, M., Hofbauer, V., Stolzenburg, D., Chen, D., Schervish, M., Vogel, A., Mauldin, R. L., Baalbaki, R., Brilke, S., Dada, L., Dias, A., Duplissy, J., El Haddad, I., Finkenzeller, H., Fischer, L., He, X., Kim, C., Kürten, A., Lamkaddam, H., Lee, C. P., Lehtipalo, K., Leiminger, M., Manninen, H. E., Marten, R., Mentler, B., Partoll, E., Petäjä, T., Rissanen, M., Schobesberger, S., Schuchmann, S., Simon, M., Tham, Y. J., Vazquez-Pufleau, M., Wagner, A. C., Wang, Y., Wu, Y., Xiao, M., Baltensperger, U., Curtius, J., Flagan, R., Kirkby, J., Kulmala, M., Volkamer, R., Winkler, P. M., Worsnop, D., and Donahue, N. M.: Molecular Composition and Volatility of Nucleated Particles from α-Pinene Oxidation between −50 °C and +25 °C, Environmental Science & Technology, 53, 12357-12365, 10.1021/acs.est.9b03265, 2019.

Yli-Juuti, T., Pajunoja, A., Tikkanen, O.-P., Buchholz, A., Faiola, C., Väisänen, O., Hao, L., Kari, E., Peräkylä, O., Garmash, O., Shiraiwa, M., Ehn, M., Lehtinen, K., and Virtanen, A.: Factors controlling the evaporation of secondary organic aerosol from α-pinene ozonolysis, Geophysical Research Letters, 44, 2562-2570, https://doi.org/10.1002/2016GL072364, 2017.

Ylisirniö, A., Barreira, L. M. F., Pullinen, I., Buchholz, A., Jayne, J., Krechmer, J. E., Worsnop, D. R., Virtanen, A., and Schobesberger, S.: On the calibration of FIGAERO-ToF-CIMS: importance and impact of calibrant delivery for the particle-phase calibration, Atmos. Meas. Tech., 14, 355-367, 10.5194/amt-14-355-2021, 2021.

Zarnetske, P. L., Gurevitch, J., Franklin, J., Groffman, P. M., Harrison, C. S., Hellmann, J. J., Hoffman, F. M., Kothari, S., Robock, A., Tilmes, S., Visioni, D., Wu, J., Xia, L., and Yang, C.-E.: Potential ecological impacts of climate intervention by reflecting sunlight to cool Earth, Proceedings of the National Academy of Sciences, 118, e1921854118, 10.1073/pnas.1921854118, 2021.

Zhang, C., Park, S.-H., Seral‐Ascaso, A., Barwich, S., McEvoy, N., Boland, C. S., Coleman, J. N., Gogotsi, Y., and Nicolosi, V.: High capacity silicon anodes enabled by MXene viscous aqueous ink, Nature Communications, 10, 849, 10.1038/s41467-019-08383-y, 2019.

Zhang, H., Yee, L. D., Lee, B. H., Curtis, M. P., Worton, D. R., Isaacman-VanWertz, G., Offenberg, J. H., Lewandowski, M., Kleindienst, T. E., Beaver, M. R., Holder, A. L., Lonneman, W. A., Docherty, K. S., Jaoui, M., Pye, H. O. T., Hu, W., Day, D. A., Campuzano-Jost, P., Jimenez, J. L., Guo, H., Weber, R. J., de Gouw, J., Koss, A. R., Edgerton, E. S., Brune, W., Mohr, C., Lopez-Hilfiker, F. D., Lutz, A., Kreisberg, N. M., Spielman, S. R., Hering, S. V., Wilson, K. R., Thornton, J. A., and Goldstein, A. H.: Monoterpenes are the largest source of summertime organic aerosol in the southeastern United States, Proceedings of the National Academy of Sciences, 115, 2038-2043, 10.1073/pnas.1717513115, 2018.

Zhang, Q., Alfarra, M. R., Worsnop, D. R., Allan, J. D., Coe, H., Canagaratna, M. R., and Jimenez, J. L.: Deconvolution and Quantification of Hydrocarbon-like and Oxygenated Organic Aerosols Based on Aerosol Mass Spectrometry, Environmental Science & Technology, 39, 4938-4952, 10.1021/es048568l, 2005.

Zhang, Q., Jimenez, J. L., Canagaratna, M. R., Allan, J. D., Coe, H., Ulbrich, I., Alfarra, M. R., Takami, A., Middlebrook, A. M., Sun, Y. L., Dzepina, K., Dunlea, E., Docherty, K., DeCarlo, P. F., Salcedo, D., Onasch, T., Jayne, J. T., Miyoshi, T., Shimono, A., Hatakeyama, S., Takegawa, N., Kondo, Y., Schneider, J., Drewnick, F., Borrmann, S., Weimer, S., Demerjian, K., Williams, P., Bower, K., Bahreini, R., Cottrell, L., Griffin, R. J., Rautiainen, J., Sun, J. Y., Zhang, Y. M., and Worsnop, D. R.: Ubiquity and dominance of oxygenated species in organic aerosols in anthropogenically-influenced Northern Hemisphere midlatitudes, Geophysical Research Letters, 34, https://doi.org/10.1029/2007GL029979, 2007.

Zhang, X., Smith, K. A., Worsnop, D. R., Jimenez, J. L., Jayne, J. T., Kolb, C. E., Morris, J., and Davidovits, P.: Numerical Characterization of Particle Beam Collimation: Part II Integrated Aerodynamic-Lens–Nozzle System, Aerosol Science and Technology, 38, 619-638, 10.1080/02786820490479833, 2004.

Zhang, X., McVay, R. C., Huang, D. D., Dalleska, N. F., Aumont, B., Flagan, R. C., and Seinfeld, J. H.: Formation and evolution of molecular products in α-pinene secondary organic aerosol, Proceedings of the National Academy of Sciences, 112, 14168-14173, 10.1073/pnas.1517742112, 2015.

Zhang, X., Lambe, A. T., Upshur, M. A., Brooks, W. A., Gray Bé, A., Thomson, R. J., Geiger, F. M., Surratt, J. D., Zhang, Z., Gold, A., Graf, S., Cubison, M. J., Groessl, M., Jayne, J. T., Worsnop, D. R., and Canagaratna, M. R.: Highly Oxygenated Multifunctional Compounds in α-Pinene Secondary Organic Aerosol, Environmental Science & Technology, 51, 5932-5940, 10.1021/acs.est.6b06588, 2017.

Zhao, Y., Zhang, R., Sun, X., He, M., Wang, H., Zhang, Q., and Ru, M.: Theoretical study on mechanism for O3-initiated atmospheric oxidation reaction of β-caryophyllene, Journal of Molecular Structure: THEOCHEM, 947, 68-75, 2010.

Ziemann, P. J., and Atkinson, R.: Kinetics, products, and mechanisms of secondary organic aerosol formation, Chemical Society Reviews, 41, 6582-6605, 2012.

Publications during the PhD study

[1] **Gao, L.**, Song, J., Mohr, C., Huang, W., Vallon, M., Jiang, F., Leisner, T., and Saathoff, H.: Kinetics, SOA yields, and chemical composition of secondary organic aerosol from β-caryophyllene ozonolysis with and without nitrogen oxides between 213 and 313 K, Atmos. Chem. Phys., 22, 6001–6020, https://doi.org/10.5194/acp-22-6001-2022, 2022.

[2] Vallon, M., **Gao, L.**, Jiang, F., Krumm, B., Nadolny, J., Song, J., Leisner, T., and Saathoff, H.: LED-based solar simulator to study photochemistry over a wide temperature range in the large simulation chamber AIDA, Atmos. Meas. Tech., 15, 1795–1810, https://doi.org/10.5194/amt-15-1795-2022, 2022.

[3] Song, J., Saathoff, H., **Gao, L.**, Gebhardt, R., Jiang, F., Vallon, M., Bauer, J., Norra, S., and Leisner, T.: Variations of PM2.5 sources in the context of meteorology and seasonality at an urban street canyon in Southwest Germany, Atmos. Envi., 282 (2022), 119147, https://doi.org/10.1016/j.atmosenv.2022.119147.

Appendix A: Supplement for Results and Discussion

Note: Part of the figures in Appendix A are reprinted with permission from: Gao, L., Song, J., Mohr, C., Huang, W., Vallon, M., Jiang, F., Leisner, T., and Saathoff, H.: Kinetics, SOA yields, and chemical composition of secondary organic aerosol from β-caryophyllene ozonolysis with and without nitrogen oxides between 213 and 313 K, Atmos. Chem. Phys., 22, 6001–6020, https://doi.org/10.5194/acp-22-6001-2022, 2022.

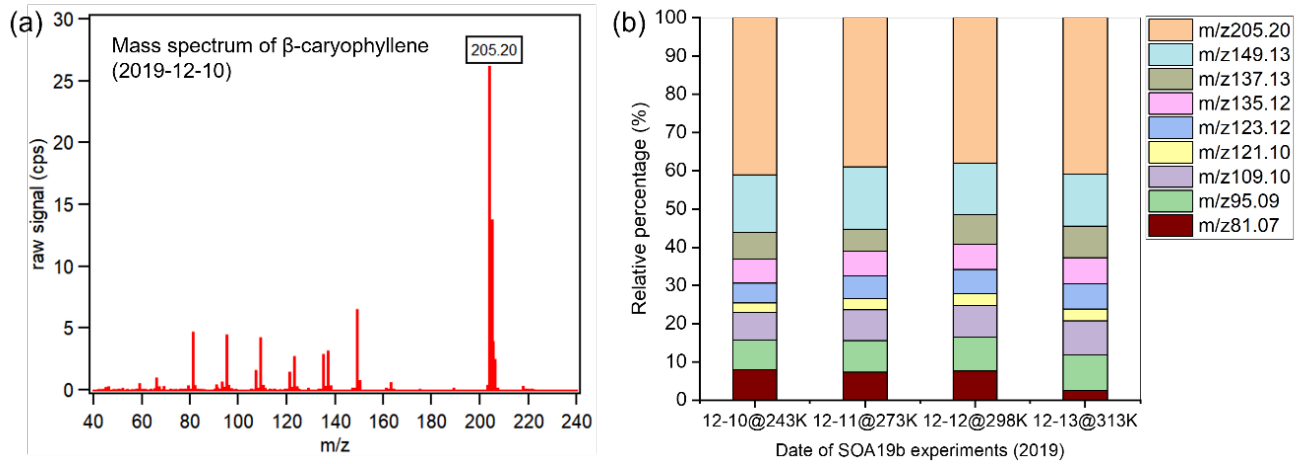

Figure S1. (a) Example of the 5-min average mass spectrum of β-caryophyllene with chamber background subtracted when the β-caryophyllene ion (m/z 205.20) shows relatively stable signal intensity in the chamber and (b) relative contribution of β-caryophyllene related ions detected by the PTR-MS in this study.

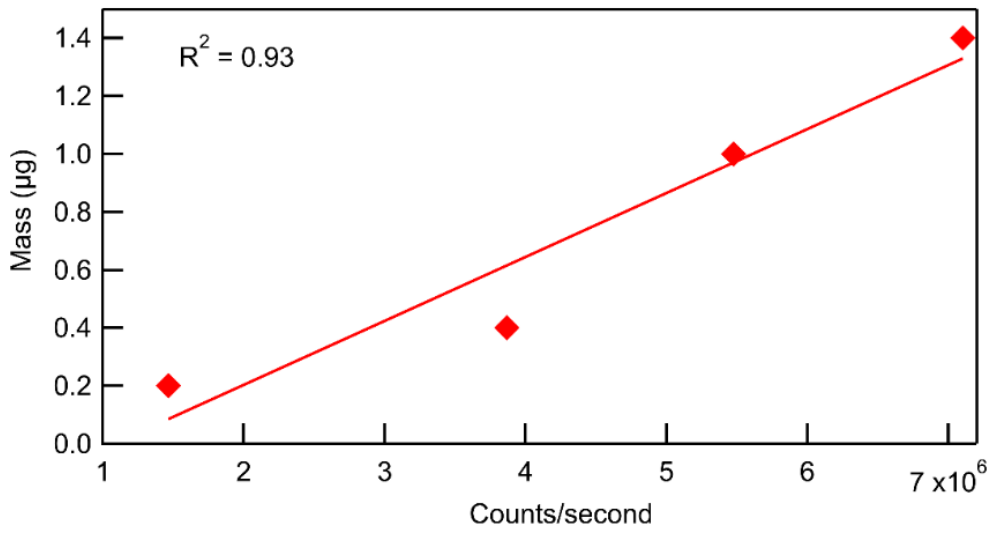

Figure S2. Calibration of the FIGAERO-CIMS with BCA. The β-caryophyllinic acid was dissolved into methanol to 0.2 ng m^{-3} as a standard BCA solution. Different volume of the standard BCA solution was deposited on a PTFE filter and then the deposited filter was heated by FIGAERO -CIMS carried by ultra-high purity nitrogen following a thermal desorption, as described in Section 2.1. The sensitivity of CIMS to β-caryophyllinic acid was calculated as $\left(\mathbf{2.4}\ ^{+0.96}_{-0.63}\right)$ cps ppt^{-1}.

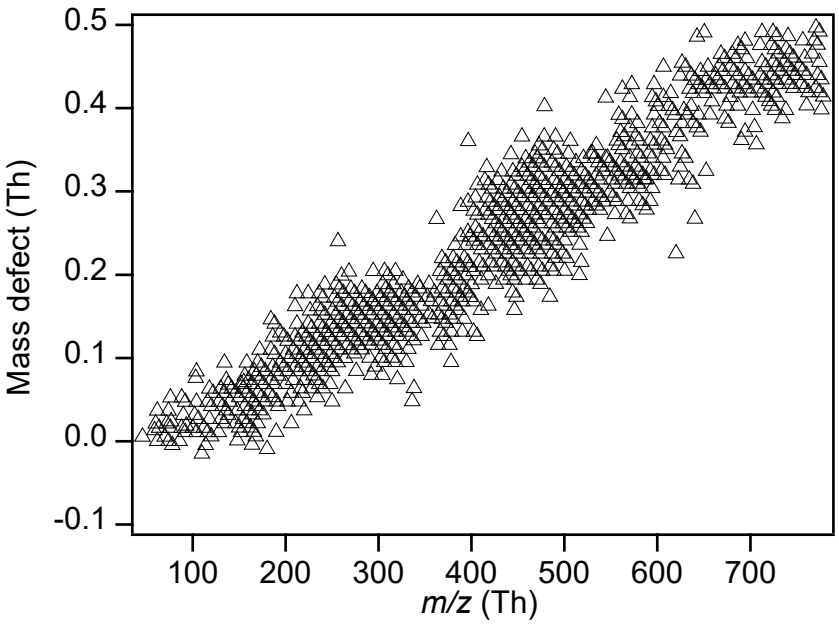

Figure S3. Plot of mass defect corresponding to the mass of molecules assigned for the β-caryophyllene SOA in this work.

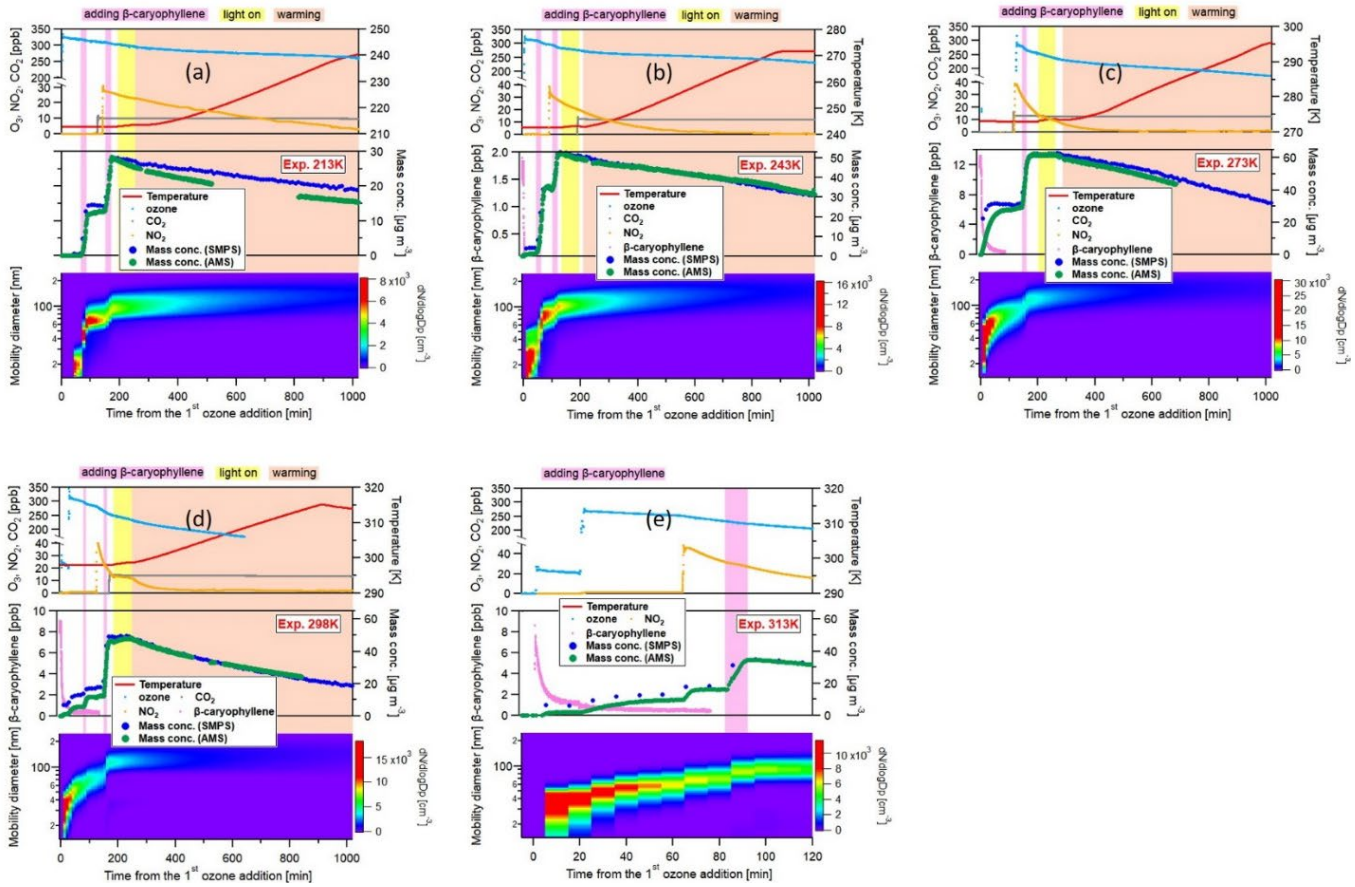

Figure S4. Time evolution of chamber ambient temperature, O_3, NO_2, CO_2, mass concentration, and particle size distribution in the five experiments which the β-caryophyllene SOA was formed at 213K (panel (a)), 243K (panel (b)), 273K (panel (c)), 298K (panel (d)), and 313K (panel (e)). In each panel, the pink, yellow, and orange shadow present the β-caryophyllene addition periods, photochemical aging, and SOA warming stages.

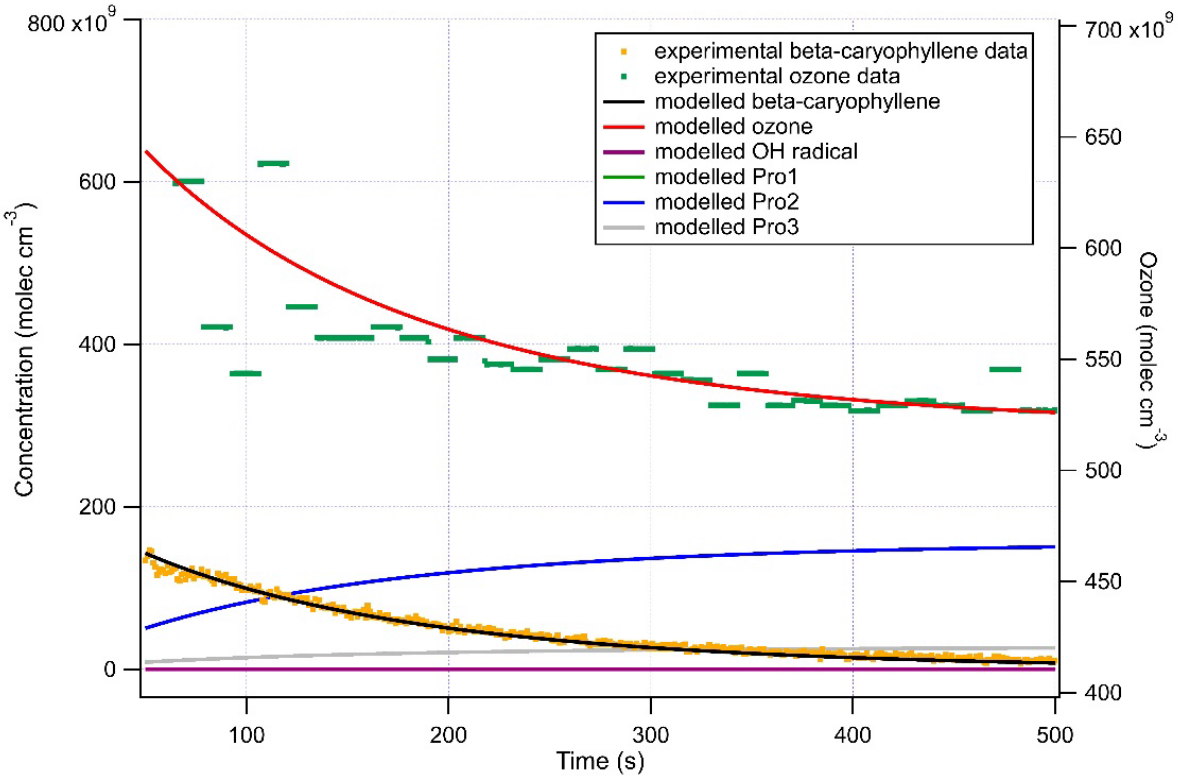

Figure S5. Example of the fit of the kinetic model to the observation for the experiment at 313K. Three main reactions were considered in the kinetic analysis to fit the observations:
Reaction1: β-caryophyllene + O_3 → Pro1 + ·OH, k_1;
Reaction2: β-caryophyllene + O_3 → Pro2, k_2;
Reaction3: β-caryophyllene + ·OH→ Pro3, k_3;
where β-caryophyllene is the beta-caryophyllene, Pro1, Pro2, and Pro3 represent different reaction products, and k_1, k_2, k_3 are the corresponding reaction rate constants.

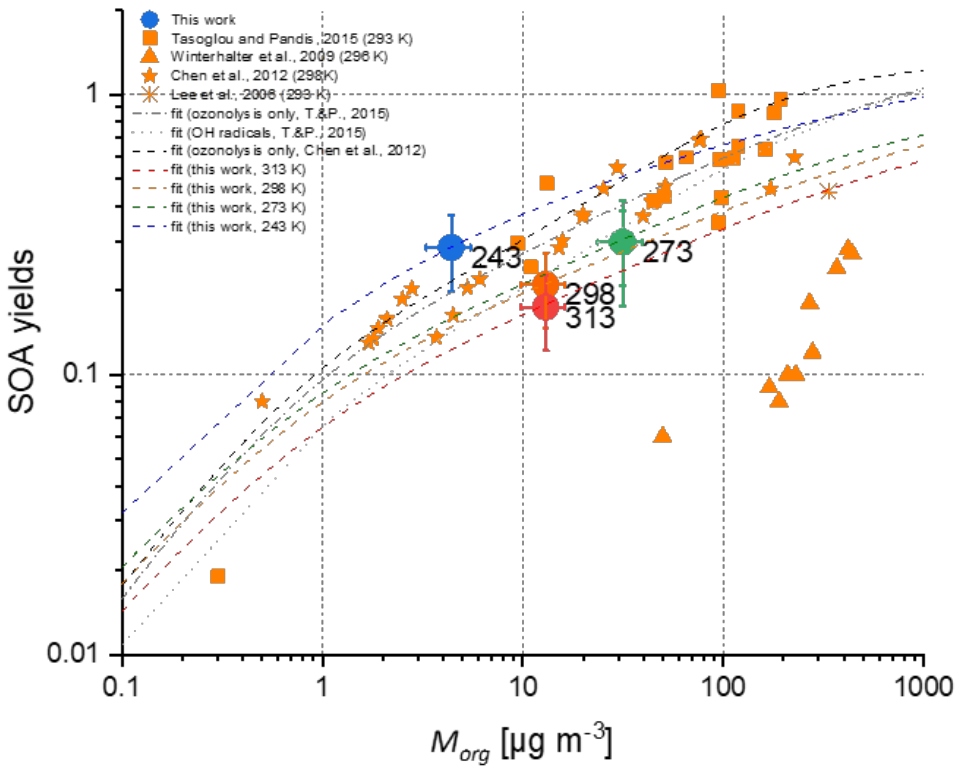

Figure S6. Temperature dependence of SOA yields as a function of the total organic particle mass concentration (M_{org}). Fitted lines are based on volatility distributions.

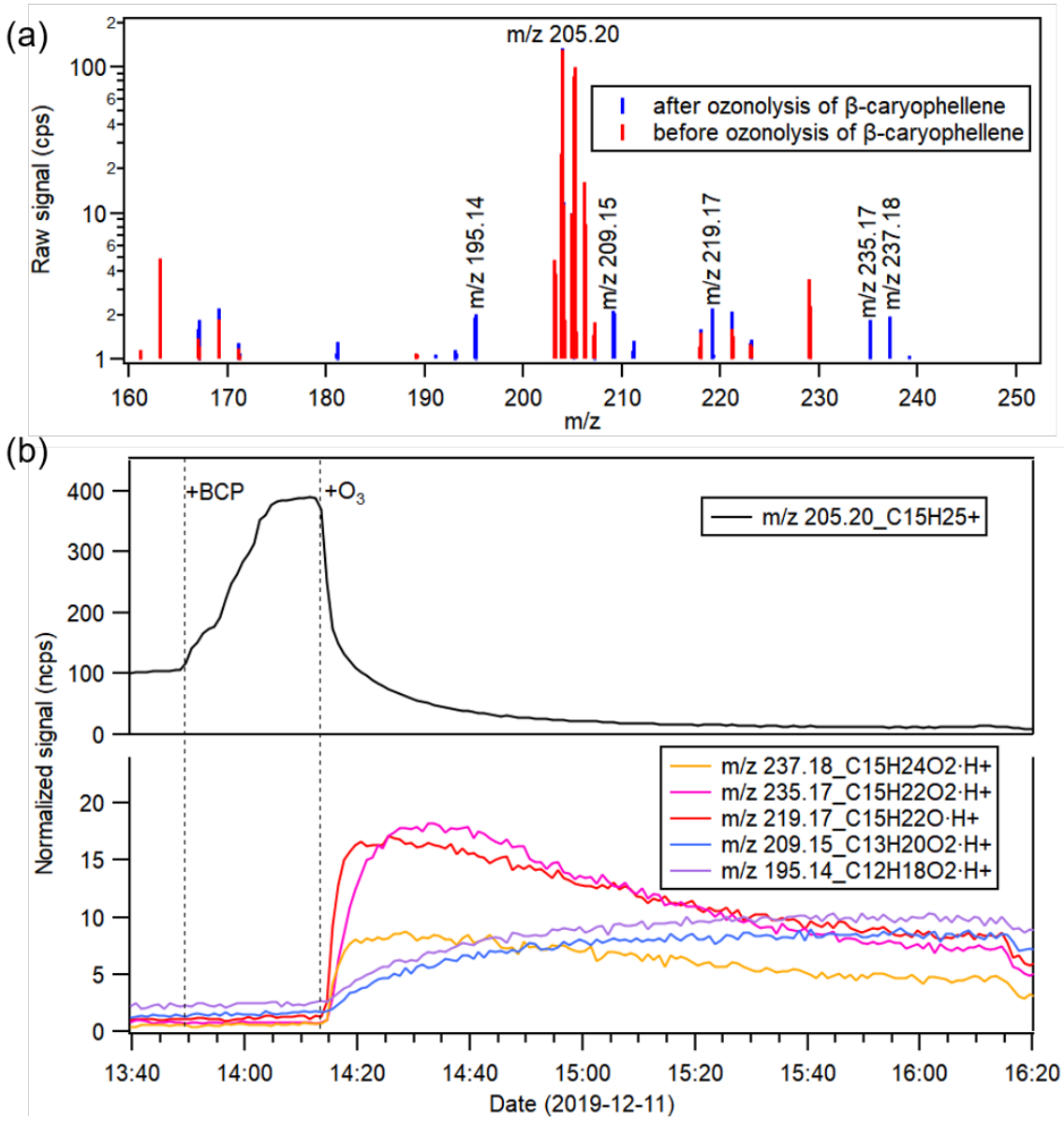

Figure S7. (a) Comparison between the average mass spectra detected by the PTR-MS over the 5 min before and after ozonolysis of β-caryophyllene in the experiment at 273 K on 12/11/2019. (b) Time series of β-caryophyllene (*m/z* 205.20) and several major gas phase product ions (*m/z* 237.18, *m/z* 235.17, *m/z* 219.17, *m/z* 209.15 and *m/z* 195.14) as labelled in (a). Two dashed line show the time points of β-caryophyllene addition and first O_3 addition to the chamber, respectively.

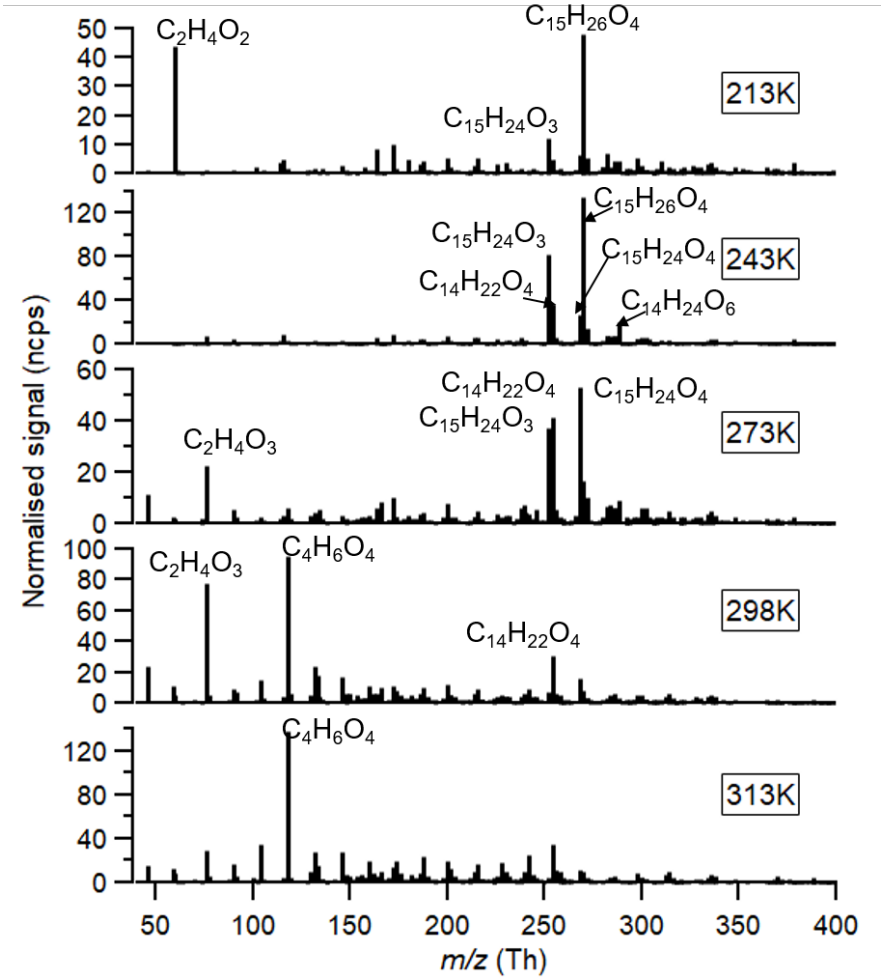

Figure S8. Averaged CIMS gas phase mass spectra (background subtracted) for all temperatures, with absolute normalized signal vs. mass to charge ratios (*m/z*).

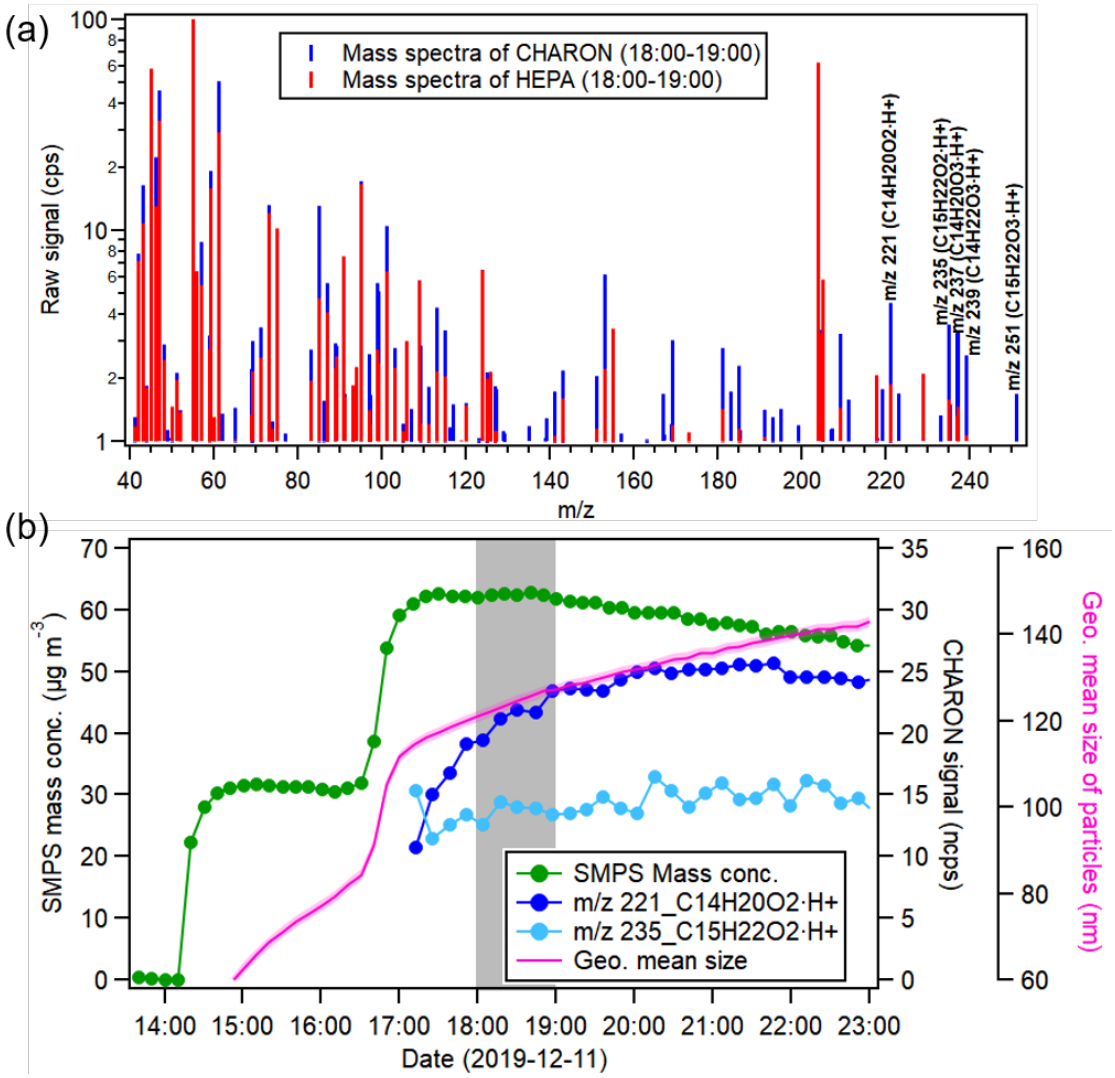

Figure S9. (a) Average mass spectra of particle phase by the CHARON (blue) and HEPA filter (red) measurement over the course of 1 hour (18:00-19:00 as shown in gray area in (b), aerosol mass concentration: 62 ± 0.3 µg m^{-3}) in the β-caryophyllene ozonolysis experiment at 273 K in 12/11/2019. Several major product ions (*m/z* 221, 235, 237, 239 and 251) are labelled. (b) time series of SMPS mass concentration of aerosol particles and two particle phase product ions (*m/z* 221 and 235) detected by the CHARON-PTR-MS. The time series of geometric mean size of aerosol particles is given to show the reduced transmission efficiency of CHARON inlet for smaller particles.

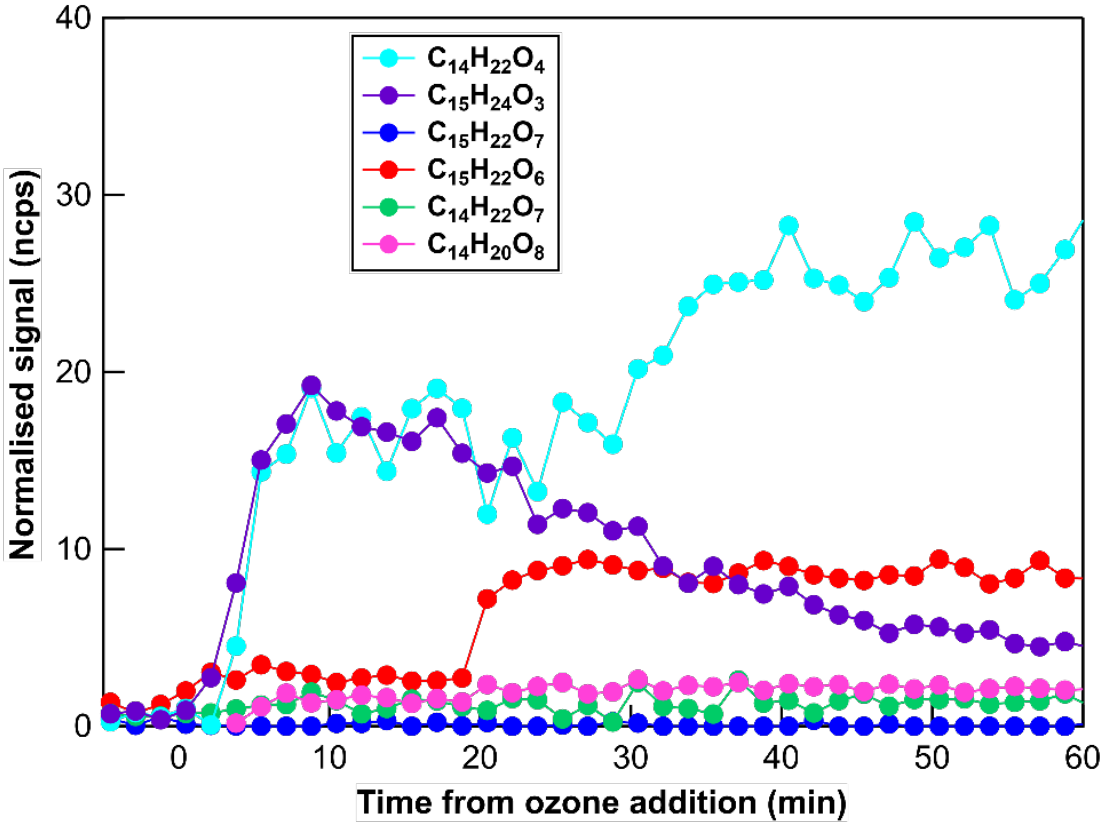

Figure S10. Evolution of major oxidation products detected by CIMS in the gas phase in the absence of NO_2. The time zero represents the timepoint when O_3 was added first.

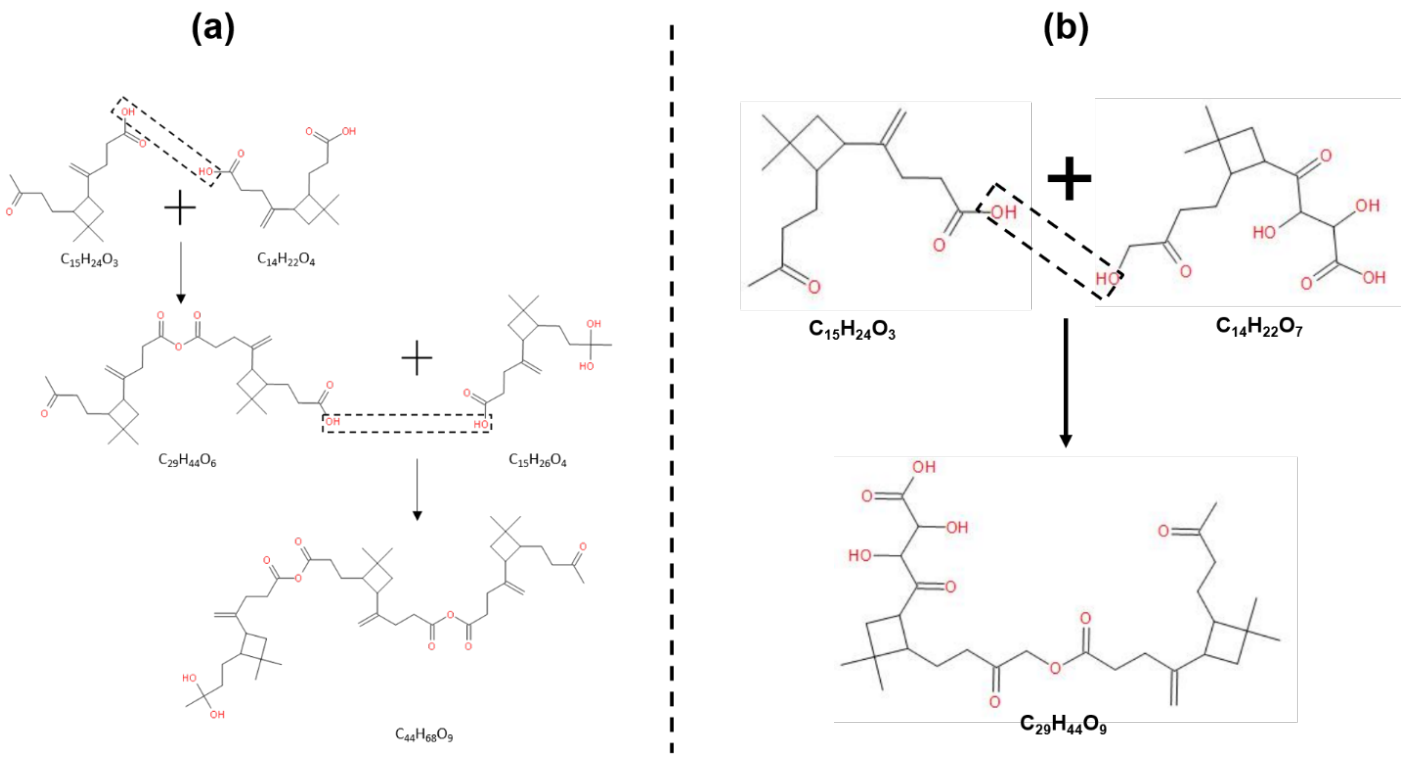

Figure S11. The potential esterification pathways of the formation of C_{29} and C_{44} compounds at 213 K. The structure of $C_{15}H_{24}O_3$, $C_{14}H_{22}O_4$, $C_{15}H_{26}O_4$, and $C_{14}H_{22}O_7$ were identified by (Li et al., 2011a; Chan et al., 2011a). Panel (a) shows the dimer ($C_{29}H_{44}O_6$) and trimer ($C_{44}H_{68}O_9$) formation at 213K; panel (b) represents the dimer ($C_{29}H_{44}O_9$) at 313K.

Similarly, the formation pathway of C_{30} and C_{35} compounds could be speculated as follows:

213K: $C_{15}H_{24}O_3 + C_{15}H_{26}O_3 \rightarrow C_{30}H_{48}O_5 + H_2O$

$C_{30}H_{48}O_5 + C_{14}H_{22}O_5 \rightarrow C_{44}H_{68}O_9 + H_2O$

313K: $C_{15}H_{24}O_4 + C_{20}H_{26}O_9 \rightarrow C_{35}H_{48}O_{12} + H_2O$

$C_{15}H_{24}O_4 + C_{15}H_{22}O_5 = C_{30}H_{44}O_8 + H_2O$

$C_{30}H_{44}O_8 + C_5H_7O_6N = C_{35}H_{49}O_{13}N + H_2O$

Note that we observed a short but significant increase of the dimer signal $C_{30}H_{48}O_5$ in the gas phase at 213K after the second addition of β-caryophyllene into the chamber. This suggests that the dimer formation could happen in the gas phase at 213K. However, no significant signal change of dimeric molecules was observed at 313K in the gas phase over the course of the experiments. One explanation could be the dimeric compounds (e.g. $C_{29}H_{44}O_9$) are quite highly oxygenated and extremely low volatile, resulting in a fast condensation process before being detected in the gas phase. The possibility cannot be excluded that the dimeric compounds could be formed in the

condensed phase as no dimeric signals could be detected visibly even with the time resolution of 1 s.

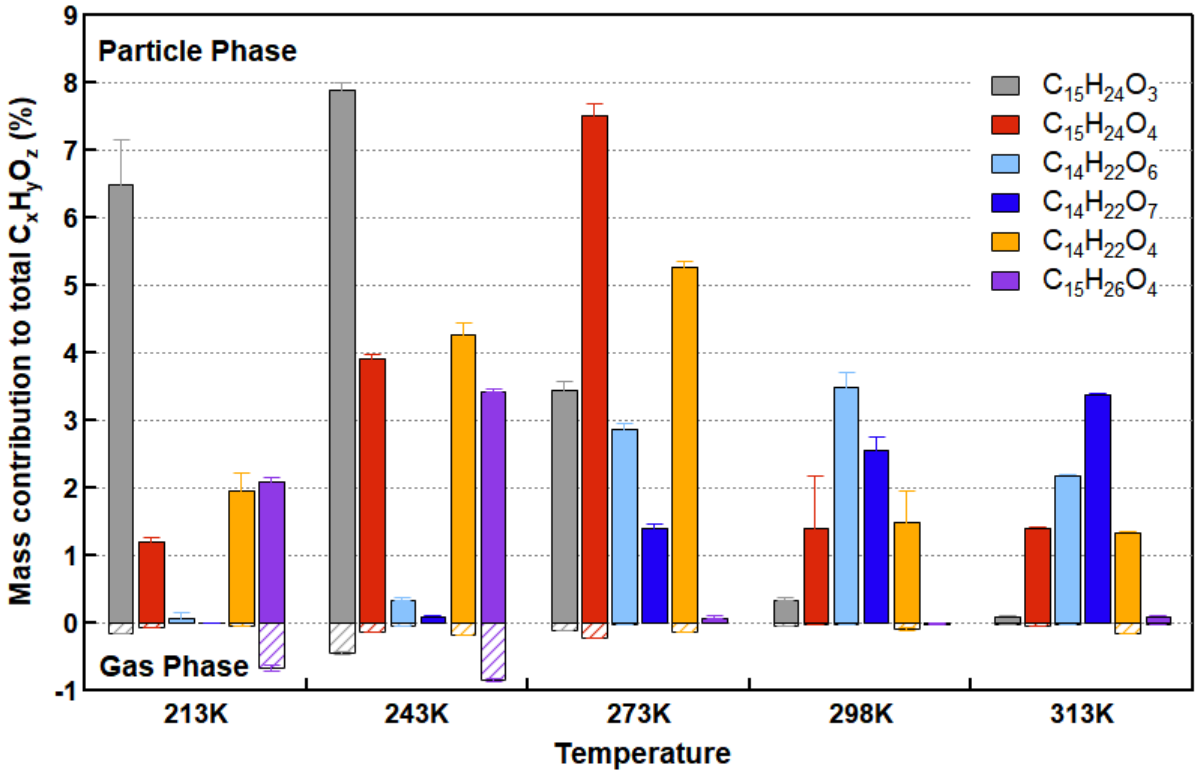

Figure S12. Fractions of six major particle phase compounds to the sum of all $C_xH_yO_z$ compounds as a function of temperature. The particle fraction (solid bars) and the gas fraction (dashed bars) of each compound are shown.

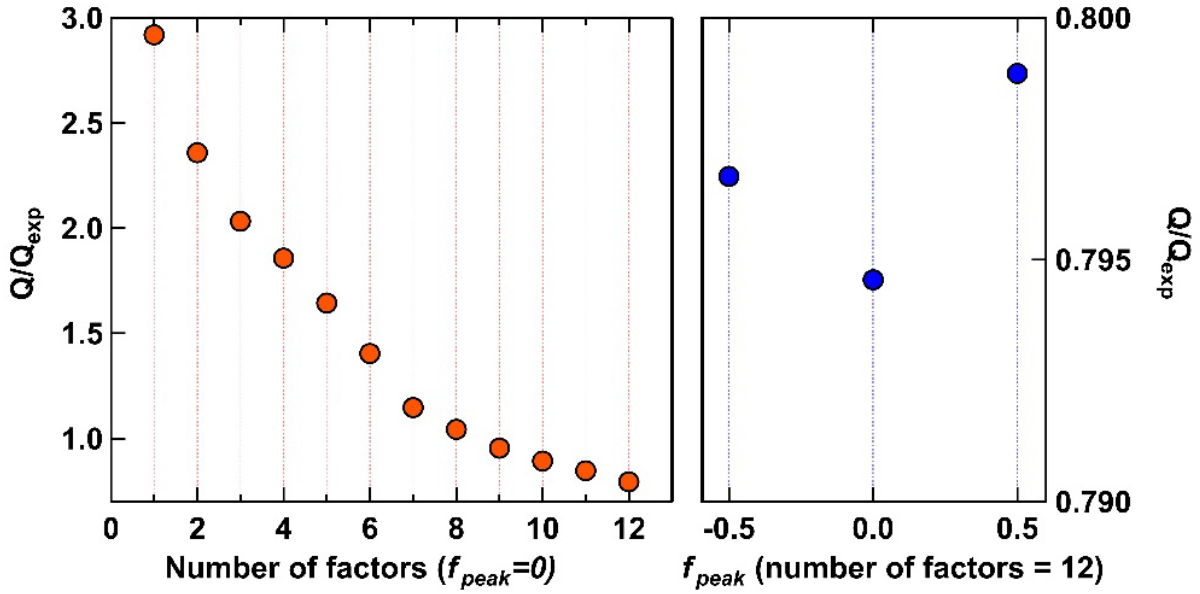

Figure S13. Q/Q_{exp} values for the varying number of factors in PMF solutions (left), and varying fpeak position in a 12-factor PMF solution (right).

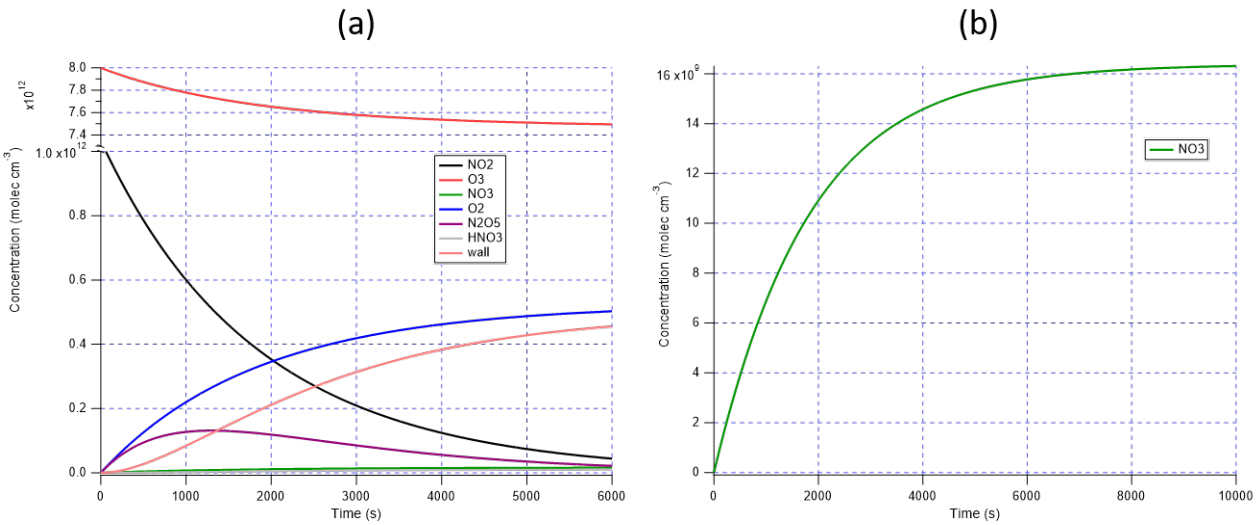

Figure S14. Modelling the NO_3 radical formation at 298K before the last β-caryophyllene addition. Time evolution of all reactants are modelled (left panel), including NO_2 (black line), O_3 (red line), NO_3 (green line), O_3 (blue line), N_2O_5 (purple line), HNO_3 (grey line) and wall loss (orange line). The right panel shows the NO_3 concentration evolution alone. Time zero is marked as the start of NO_2 addition.

Because of an excess of O_3 in the chamber over the course of the whole experiment, the following reactions were considered to estimate the potential NO_3 radical levels before the addition of another portion of β-caryophyllene:

$NO_2 + O_3 \rightarrow NO_3 + O_2$, k1

$NO_3 + NO_2 \rightarrow N_2O_5$, k2

$N_2O_5 \rightarrow NO_2 + NO_3$, k3

$N_2O_5 + H_2O \rightarrow HNO_3$, k4

$N_2O_5 \rightarrow$ wall, k5

All the rate constants used at all temperatures are listed below (IUPAC Task Group on Atmospheric Chemical Kinetic Data Evaluation (ipsl.fr), https://iupac-aeris.ipsl.fr/#):

Please note that we did not include the reactions of NO_3 radicals with β-caryophyllene or its oxidation products in our box model calculations used to estimate the NO_3 radical concentrations. Therefore, these NO_3 radical concentrations must be considered as upper limits.

	k_1	k_2	k_3	k_4	k_5*
213K	1.3E-18	3.5E-10	8.3E-07	1.00E-22	1.00E-03
243K	5.4E-18	2.0E-10	5.5E-04	1.00E-22	1.00E-03
273K	1.6E-17	1.3E-10	0.09	1.00E-22	1.00E-03
298K	3.5E-17	8.9E-11	2.9	1.00E-22	1.00E-03
313K	5.2E-17	7.3E-11	17.8	1.00E-22	1.00E-03

*Estimated from previous experiments with N_2O_5 measured inside the AIDA chamber by FTIR.

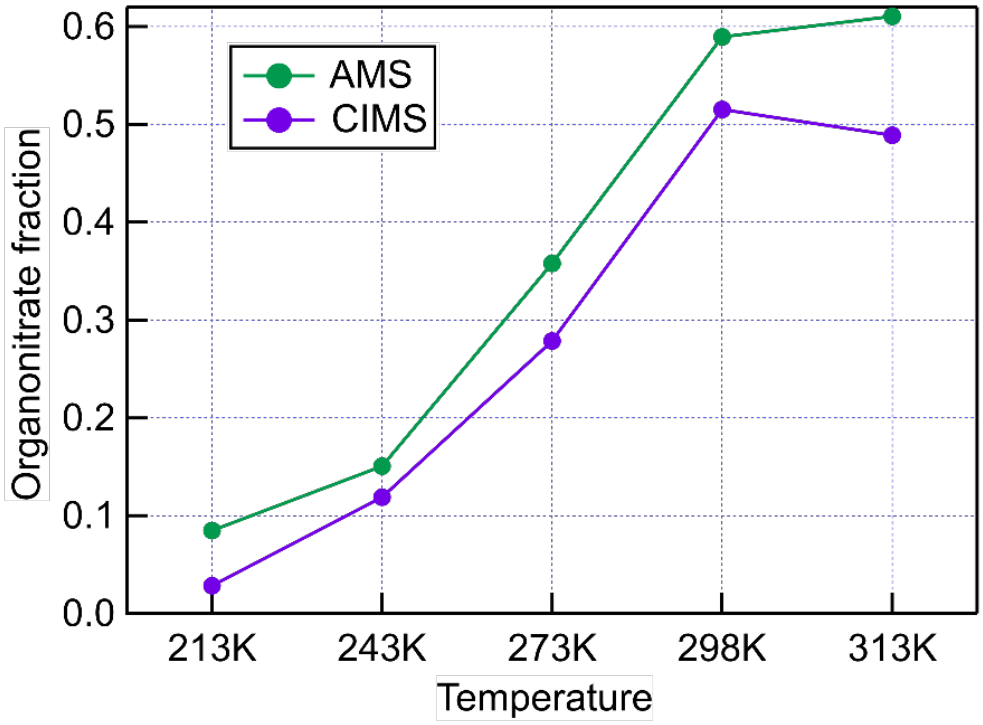

Figure S15. Comparison of the temperature dependence on the organonitrate fraction formed. The green dots represent the fraction of the organonitrate concentrated detected by HR-AMS, while the blue dots show the signal fraction of organonitrate assigned by FIGAERO-CIMS.

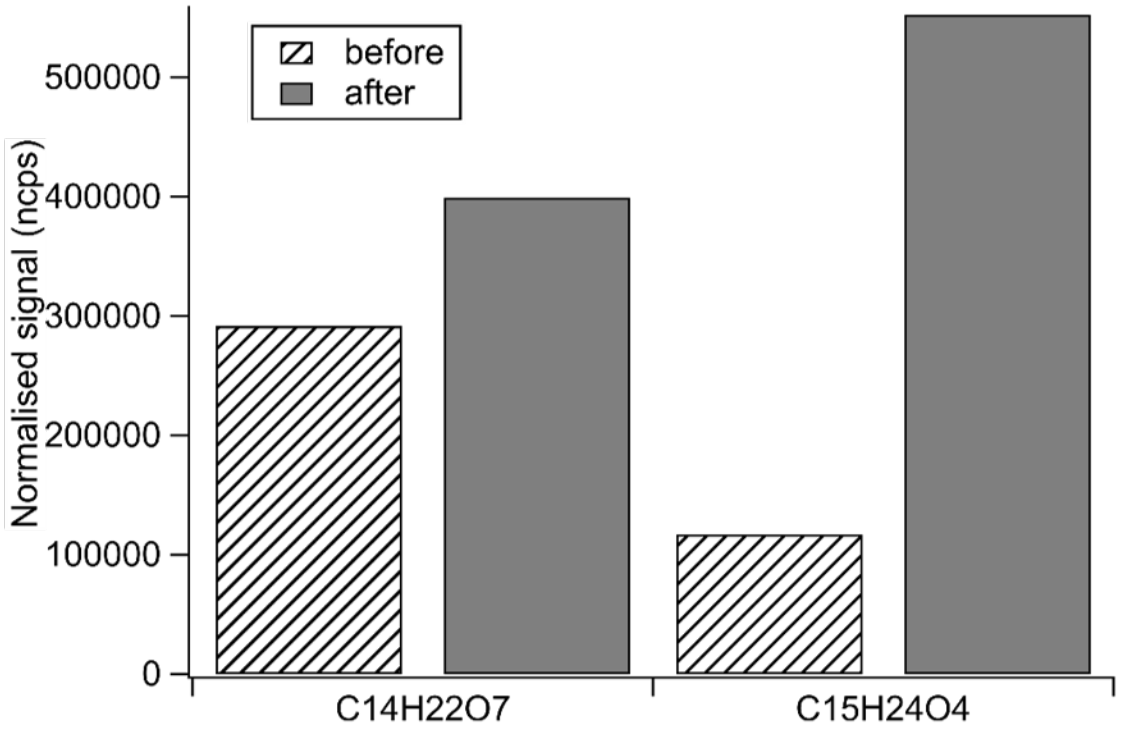

Figure S16. Comparison of the CIMS signals of $C_{14}H_{22}O_7$ and $C_{15}H_{24}O_4$ before (dashed) and after (solid) the last β-caryophyllene addition.

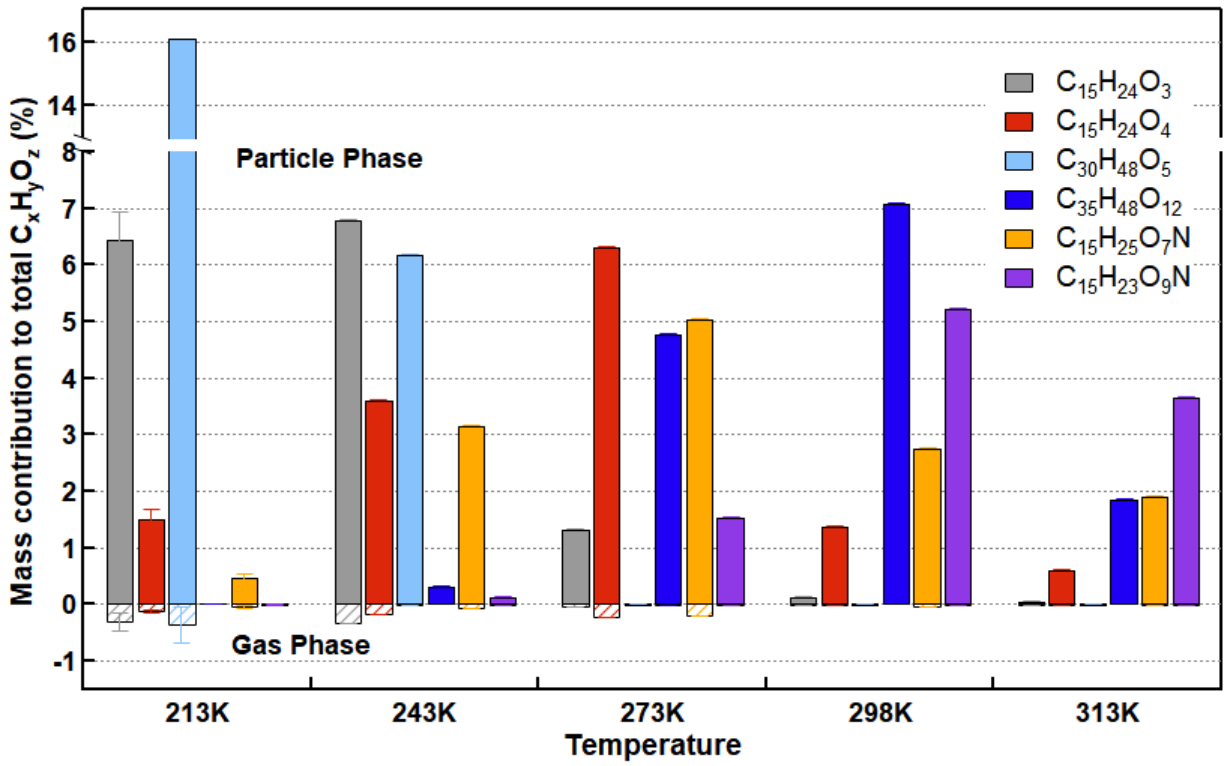

Figure S17. Mass fractions of major particle phase compounds to the sum of all detected molecues as a function of temperature. The particle fraction (solid bars in the top) and the gas fraction (dashed bars in the bottom) of each compound are shown.

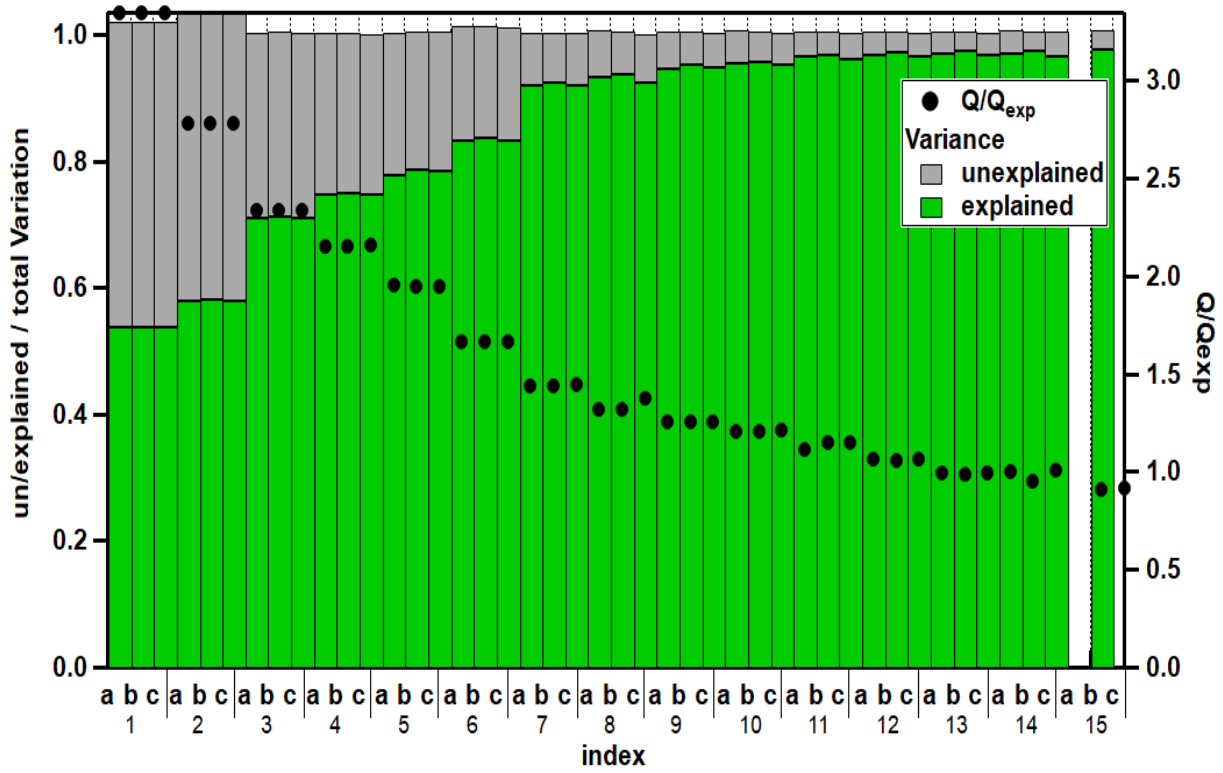

Figure S18. Q/Q_{exp} values for the varying number of factors in PMF solutions for the no-N-containing species (left axis), and varying f_{peak} position in a 11-factor PMF solution (right axis). The number in the x-axis index correspond to the number of factors, wherein a,b,c refers to f_{peak}=-0.5,0,+0.5, respectively.

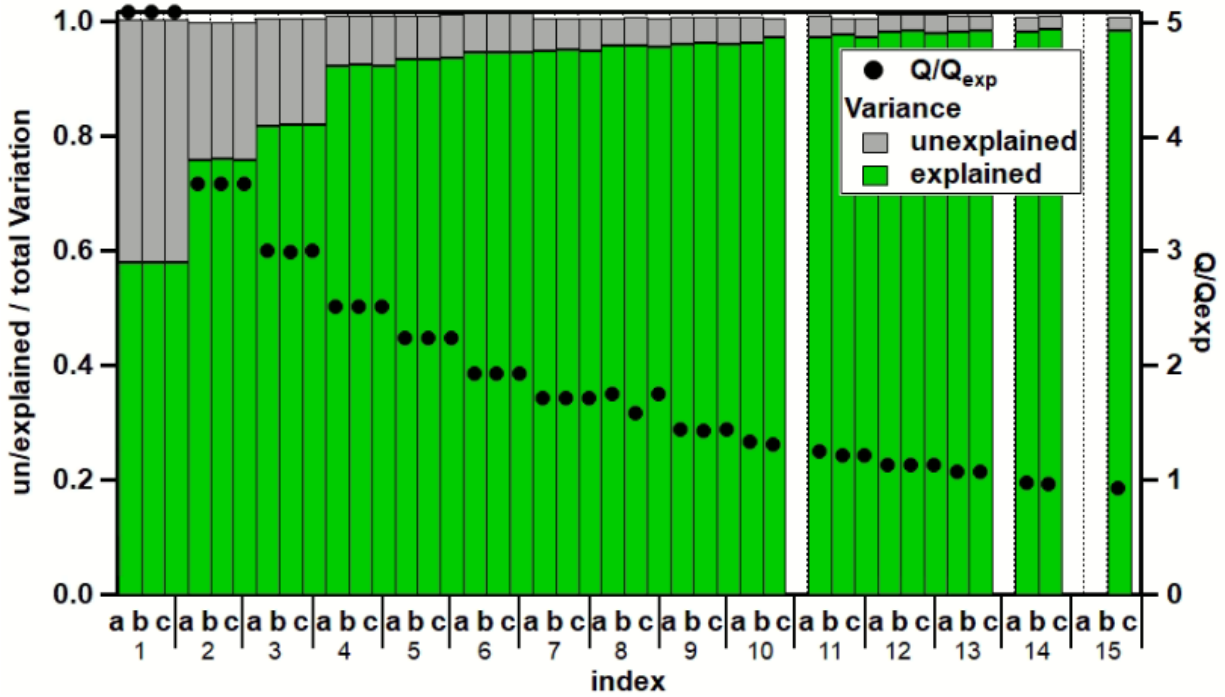

Figure S19. Q/Q_{exp} values for the varying number of factors in PMF solutions for the N-containing species (left axis), and varying f_{peak} position in an 8-factor PMF solution (right axis). The number in the x-axis index means the number of factors, wherein a,b,c refers to fpeak=-0.5,0,+0.5, respectively.

Table S1. Compilation of experimental conditions and particle mass yields reported in the literature for β-caryophyllene ozonolysis

Reference	Temperature [K]	ΔMorg [μg m-3]	RH [%]	Scavenger for OH or CI	Seed	Yield [%]
(Tasoglou and Pandis, 2015a)	293	0.3-194	<10	2-butanol	None	1.9-104
Winterhalter et al. (2009a)	296	50-370	dry	none	None	6-24
Jaoui et al. (2003b)	287-290	-	80-85	none	None	39
Lee et al. (2006b)	293	336 ± 3	6.2	Cyclohexane	None	45 ± 2
Lee et al. (2006c)	295	212	56	None	None	68
Chen et al. (2012b)	298	0.5-230	40	Cyclohexane	AS	8-70

Table S2. Fitted reaction rates kO_3 and OH radical yields for temperatures between 243K to 313K

Temperature [K]	k_{O3} [cm^3 $molecule^{-1}$ s^{-1}]	OH yields
313	(1.01±0.09) E-14	0.15±0.02
298	(1.09±0.21) E-14	0.08±0.01
258	(1.05±0.25) E-14	0.05±0.03
243	(1.99±0.28) E-14	0.05±0.02

Table S3. Main β-caryophyllene oxidation products and their phase partitioning

Formula	*m/z* (Th)	Compound assignment from literature	Ref.	Potential dimer
C2-C4 fragments				
$C_4H_6O_4$	118.0			
$C_2H_4O_3$	76.0			
C14-15 monomers				
$C_{14}H_{22}O_3$	238.2	β-nocaryophyllon aldehyde	a, b, c, d	
$C_{15}H_{24}O_3$	252.2	β-hydroxycaryophyllon aldehyde; β-caryophyllonic acid	a, b, c, d	$C_{30}H_{48}O_6$
$C_{14}H_{22}O_4$	254.2	β-hydroxynocaryophyllon aldehyde; β-nocaryophyllonic acid; β-caryophyllinic acid	a, b, c, d	$C_{28}H_{44}O_8$
$C_{15}H_{24}O_4$	268.2	β-hydroxycaryophyllonic acid	a, d	
$C_{15}H_{26}O_4$	270.2	Hydrated β-caryophyllonic acid	a	
$C_{14}H_{22}O_6$	286.1	Hydrated β-oxocaryophyllonic acid	a	$C_{28}H_{44}O_{12}$
$C_{14}H_{22}O_7$	302.1		b	
$C_{14}H_{24}O_7$	304.2			
$C_{15}H_{26}O_5$	286.2	Hydrated β-hydroxycaryophyllonic acid	a	$C_{30}H_{52}O_{10}$
$C_{15}H_{22}O_6$	298.1			
$C_{15}H_{22}O_7$	314.1		a	
$C_{14}H_{20}O_8$	316.1			
$C_{14}H_{22}O_8$	318.1			
$C_{15}H_{22}O_8$	330.1			
$C_{14}H_{22}O_9$	334.1			
$C_{15}H_{24}O_9$	348.1			
$C_{15}H_{30}O_9$	354.2			
$C_{15}H_{25}NO_8$	347.2		a	$C_{30}H_{50}N_2O_{16}$
$C_{14}H_{23}NO_9$	349.1		a	$C_{28}H_{46}N_2O_{18}$
$C_{15}H_{27}NO_8$	349.2		a	
$C_{15}H_{25}NO_9$	363.2		a	$C_{30}H_{50}N_2O_{18}$
C28-30 dimers				
$C_{28}H_{44}O_5$	460.3			
$C_{30}H_{48}O_5$	488.3			
$C_{29}H_{46}O_6$	490.3			

Formula	*m/z* (Th)	Compound assignment from literature	Ref.	Potential dimer
$C_{28}H_{44}O_7$	492.3			
$C_{30}H_{48}O_6$	504.3			
$C_{29}H_{46}O_7$	506.3			
$C_{28}H_{44}O_8$	504.3			
$C_{30}H_{48}O_7$	520.3			
$C_{29}H_{46}O_8$	552.3			
$C_{30}H_{48}O_8$	536.3			
$C_{29}H_{44}O_9$	536.3			
$C_{29}H_{46}O_9$	538.3			
$C_{29}H_{44}O_{10}$	552.3			
$C_{28}H_{42}O_{11}$	554.3			
$C_{29}H_{44}O_{11}$	568.3			
Others				
$C_{11}H_{18}O_3$	198.1	3,3-dimethyl-2-(3-oxobutyl) cyclobutanecarboxylic acid	b	
$C_{13}H_{20}O_5$	256.1	β-hydroxynornocaryophyllonic acid	a	$C_{26}H_{40}O_{10}$
$C_{35}H_{48}O_{12}$	660.3			
$C_{44}H_{68}O_9$	740.5			

[a] (Chan et al., 2011a); [b] (Li et al., 2011a); [c] (Winterhalter et al., 2009a); [d] (Jaoui et al., 2003b)